Characterising the Tumour Suppression Function of Folliculin

Rachael Preston

0740708

Thesis submitted for the degree of Doctor of Philosophy

Abstract

Birt–Hogg–Dubé (BHD) syndrome is a rare inherited autosomal dominant disorder first described by Birt, Hogg and Dube in 1977 (Birt et al,. 1977). BHD affects approximately 100 families worldwide. Approximately one third of diagnosed BHD patients also develop renal cell carcinoma (RCC) (Schmidt et al., 2005). BHD arises as a result of loss of function of the Folliculin protein expressed from the BHD gene, suggesting than Folliculin serves as a tumour suppressor (Vocke et al., 2005). Although it is considered that FLCN represses cell growth, the role that FLCN plays in cancer progression and/or initiation is currently unresolved. It has been observed that tumours taken from BHD patients have reduced levels of mitochondria (Yang et al., 2008). Previous studies have also suggested that aberrant levels of mTOR activity are observed in Folliculin-deficient cell lines (Baba et al., 2006; Baba et al., 2008). Aberrant levels of mTORC1 activity have been associated with increased levels of Hypoxia inducible factor transcriptional activity, decreased autophagic activity (Land and Tee, 2007; Hands et al., 2009). There are several genes within the mTOR pathways which act as Tumour Suppressors. Mutations within these genes result in inherited genetic disorders, including Tuberous, Sclerosis complex (TSC). Loss of function of TSC1/TSC2 results in TSC which is clinically similar to BHD (Gomez et al., 1999). Arbarrant levels of mitochondrial biogeneisis and HIF activity have been observed in cells deficient in TSC1 ad TSC2 (Land and Tee, 2007; Chen et al., 2008). Increased levels of mTORC1 activity have also been shown to result in decreased levels of autophagic activity in TSC2 deficient cells (Parkhitko et al., 2011). In order to characterise the tumour suppression function of Folliculin, the effects of loss of function of Folliculin on mitochondrial biogenesis and mitochondrial function, hypoxia inducible factor (HIF) transcriptional activity, and autophagic activity were investigated using multiple cell lines. The results from this study suggest that loss of function of FLCN results in increased production of ROS species. This leads to compromised mitochondrial membrane potential and decreased ATP production as a result of increased expression of uncoupling proteins in order to try and reduce the increased levels of ROS. FLCN is also phosphorylated at multiple residues by both mTORC1 and AMPK and activity of both mTORC1 and AMPK is increased in response to the depleted ATP levels as a result of increased UCP production in response to the increased ROS production observed upon loss of functional FLCN. This results in increased levels of mitochondrial biogenesis and increased levels of glycolytic activity via increased activation of HIFα proteins in order to compensate for this energy deficit. Furthermore, it appears that both mTORC1 and AMPK could drive HIF transcription and mitochondrial biogenesis through modulation of FLCN phosphorylation. ULK-mediated autophagy also appears to be upregulated upon loss of functional FLCN, possibly as a result of the increased levels of AMPK activation in order to provide a protection for these cells. This may be via the catabolising the dysfunctional mitochondria observed in cells upon loss of BHD, a process which may be exploited as a potential therapeutic target for BHD patients. Further investigations into these cellular processes may also provide clues to potential therapeutic targets for treatment of BHD patients.

Contents

Table of Figures

Acknowledgements

I would like to thank the Myrovlytis trust for their financial support and continued interest in this work, Dr. Andrew Tee for his advice and support as a supervisor throughout this project, Dr. Elaine Dunlop, Dr. Mark Davies, Dr. Kayleigh Dodd and all the other members of the Tee Lab.

I would also like to thank Mr. Chris Von Ruhland for his help with the Electron microscopy work in this project.

I would also like to thank David Hunt and Katy Harper for making me laugh and being a constant source of support throughout this project.

Last but not least I would like to thank my family, especially my parents, my partner Mark and his family, for their unconditional love and support and for being there for me every step of the way. I could not have done this without you.

Chapter 1
Introduction

1 Introduction

1.1 Birt-Hogg-Dube Syndrome.

The inherited autosomal dominant disorder Birt–Hogg–Dubé (BHD) syndrome was first described by Birt, Hogg and Dubé in 1977 (Birt *et al,.* 1977*).* BHD is a rare disorder, affecting approximately 100 families worldwide, and is characterised by trichiodomas, acrochordons and fibrofolliculomas of the face, neck and trunk. However, only fibrofolliculomas are a specific characteristic of BHD patients (Toro *et al.,* 1999). 89% of patients also present with bilateral lung cysts and 24% have a history of spontaneous pneumothoraces (Toro *et al*., 2007). Approximately one third of diagnosed BHD patients also develop renal cell carcinoma (RCC) (Schmidt *et al.,* 2005). These renal tumours may display multiple histological types of RCCs, which include chromophobe RCCs, clear cell papillary RCCs oncocytomas, and a hybrid of chromophobe RCC and oncocytoma is unique to BHD patients. Patients have also been reported to present with benign renal angiomyolipomas (AML) (Yang *et al.,* 2008; Byrne *et al*,. 2011). Work conducted by Cocciolone *et al.* has suggested that BHD patients may also be susceptible to melanomas (Cocciolone *et al.,* 2010). It has also been reported that BHD patients may present with colorectal neoplasias (Nahorski *et al.,* 2010).

1.2 Folliculin

Folliculin (FLCN) is a 66 kDa protein containing 579 amino acid residues and is expressed from the *BHD* gene. The function of FLCN is, as yet, unknown; however it has been found to be highly expressed in tissues from the skin, ovaries, testis, lungs, pancreas, prostate and

distal nephrons of the kidney (Hasumi *et al.*, 2009; Hartman *et al.*, 2009; Warren *et al.*, 2004). While it has been suggested that FLCN represses the growth of cells, the function of FLCN has in cancer initiation and development is as yet unknown.

1.3 Animal models of BHD

1.3.1 The Rat model of BHD

A rat model of hereditary renal carcinoma containing a single nucleotide insertion within the *BHD* gene has also been discovered in a Nihon rat model. This germline mutation within *BHD* produces a frameshift mutation which results in a premature stop codon approximately 26 amino acids downstream of the initial mutation. Data obtained from the Nihon rat model showed that homozygous mutations in *BHD* results in early embryonic lethality in rats as well as mice (Okimoto *et al.*, 2003).

1.3.2 The Dog model of BHD

A mutation in exon 7 of the canine homologue of *BHD* has been linked to a kidney cancer syndrome which naturally occurs in German shepherd dogs known as renal cystadenocarcinoma and nodular dermatofibrosis (RCND). RCND is characterised by bilateral renal tumours and nodules of the skin (Lingaas *et al.*, 2003). Furthermore, data obtained from work conducted using this model also suggests that mutations in the canine orthalog of the *BHD* gene are also homozygous lethal in a manner analogous to the Nihon rat model (Lingaas *et al.*, 2003).

These animal models are a valuable research tool as they provide models which help to determine the tumour suppressor function of FLCN, and may provide a means for testing drugs which provide a potential therapeutic benefit for BHD patients.

1.3.3 The Drosophila melanogaster model of BHD

A *D. melanogaster* model of BHD which exhibits decreased expression of the Drosophila homologue of FLCN (dBHD) has also been created by Singh *et al.* using *si*RNA (Sing *et al.,* 2006).

1.3.4 The S. pombe model of BHD

A *S. pombe* strain containing deletion of the *S. pombe* FLCN homologue, LST7, has also been created by van Slegtenhorst *et al*. As the results from experiments conducted using this model suggest that LST7 may activate Tor2 in yeast *(*van Slegtenhorst *et al.*, 2007), this model may be important for determining how FLCN may function in the mTOR pathway in mammals.

1.3.5 Mouse models of BHD

Work conducted on several mouse models of BHD has shown that homozygous deletion of *BHD* is lethal in mouse embryos (Chen *et al.*, 2008; Baba *et al.*, 2008). This notion is supported by data obtained from a mouse model containing a neomycin /β- galactosidase (β geo) cassette insertion in between exons 8 and exon 9 of *BHD,* which revealed that embryonic lethality was induced by day 8.5 of embryonic development upon homozygous deletion of *BHD* (Hudon *et al.,* 2010). These data are further supported by work conducted by Hasumi *et al.,* which revealed that *BHD* homozygous null mice die by day 6.5 of

embryonic development (Hasumi *et al.*, 2009). However, mouse models which have kidney targeted *BHD* knockout have been developed.

The first, developed by Baba *et al.*, contains a deletion of exon 7 of *BHD* and kidney specific conditional homozygous inactivation of *BHD* (Baba *et al.*, 2008). The second was developed by Chen *et al.* and has a deletion within the *BHD* gene that incorporates exons 3 and 4 of the *BHD* gene and results in kidney specific homozygous inactivation of *BHD* (Chen *et al.*, 2008). Hartman *et al.* also created a kidney specific knockout mouse model with of BHD by integrating a neomycin/β-galactosidase (β-geo) cassette in between exon 8 and exon 9 of *BHD*, resulting in the FLCN protein being truncated (Hartman *et al.*, 2009).

These mouse models are particularly useful as they are genetically modified in such a way that, as a direct result of the genetic modifications, they do not exhibit any additional genetic mutations other than those within the *BHD* gene, whereas the animal model systems of BHD may contain mutations other than those observed in the *BHD* gene. These mouse models therefore allow researchers to observe changes occurring that directly result from the mutations within the *BHD* gene.

1.4 The UOK257 cell line

The initial experiments in this thesis were conducted using either the UOK257 cell line or the UOK257-2 cell line (a kind gift from Laura Schmidt). The UOK257 cell line is a FLCN-deficient kidney tumour cell line derived from a BHD patient. The UOK257-2 cells are the UOK27 cells with *BHD* stably transfected and expressed (Yang *et al.*, 2008).

1.5 Genetic studies of BHD

1.5.1 Mutations of the BHD gene in BHD patients

Work conducted by Voke *et al.* has revealed germ-line and somatic mutations of the *BHD* gene on chromosome 17p11.2, and loss of heterozygosity in tumour tissue from BHD patients. *BHD* is highly conserved across species. These data suggest that it is the loss of functional FLCN which is the foundation of tumour formation in BHD patients; and supports the notion that FLCN serves as a tumour suppressor (Vocke *et al.*, 2005). Further genetic analyses conducted by Schmidt *et al*. identified several different mutations within the *BHD* gene which result in the FLCN protein being truncated. Mutation analyses performed on families of BHD patients revealed that the most common mutations are a duplication or deletion of a C nucleotide in a polycytosine tract located on exon 11 of *BHD*. This was found in approximately 53% of the families tested (Schmidt *et al*., 2005). However, work conducted has suggested that BHD patients can exhibit mutations throughout the coding region of BHD. Work conducted by Kunogi *et al.* detected a large genomic deletion in 2 BHD patients, one with a deletion within exon 14 of *BHD* and one with a deletion which included exons 9 to 14 of the *BHD* gene. These data suggested that BHD also arises as a result of large deletions in the *BHD* gene as well as small nucleotide alterations (Kunogi *et al.*, 2010). Benhammou *et al.* also identified 6 unique deletions in the *BHD* gene in nine BHD patients from 6 families. Six mutations involve deletions, where four of these deletions can occur in exon 1. The other two deletions in *BHD* encompassed exons 2 to 5, and exons 7 to 14. A duplication mutation involving exons 10 and 11 was also identified. This work supported the notion that large deletions or duplication within the *BHD* gene can result in BHD and that the 5'-noncoding-exon 1 may be a deletion hotspot for BHD patients (Benhammou *et al.*, 2011). Molecular analysis of BHD patients conducted by Palmirotta *et*

al. also highlighted the importance of mutations within exon 9 of the *BHD* gene in predisposition for cancer in BHD patients (Palmirotta *et al.,* 2008).

1.5.2 Geneotype – phenotype correlation studies in BHD patients

Several studies have been conducted in order to determine whether there is any correlation between mutations in the *BHD* gene and the phenotype exhibited. As BHD patients can also present with polycystic kidneys and RCCs, work has also been conducted in order to determine whether there is any correlation between mutations in the *BHD* gene and these phenotypes.

1.5.2.1 Mutations within the BHD gene and Renal Cell Carcinomas

Studies have suggested that although mutations within the BHD gene are rare in sporadic renal tumours, BHD is involved in all histological types of RCCs (Khoo *et al.*, 2002). Work conducted by Baba *et al.* and Chen *et al.* has revealed that conditional homozygous kidney specific inactivation of *BHD* in mice resulted in enlarged polycystic kidneys, which lead to kidney failure and fatality by the time they are 3 weeks old (Chen *et al.,* 2008; Baba *et al.,* 2008). Work conducted on a kidney targeted mouse model of BHD, also revealed that heterozygous *BHD* mutant mice develop renal cysts and neoplasia by the time they are 6 months old. After 10 months these heterozygous *BHD* knockout mice also spontaneously developed both solid tumours and cysts in their kidneys in a manner analogous to BHD patients (Hartman *et al.,* 2009). These data are also supported by work conducted by Hudon *et al.* which revealed that heterozygous *BHD* knockout mice develop tumours and cysts in their kidneys upon loss of *BHD* (Hudon *et al.,* 2010). Collectively, these data imply that FLCN has a crucial function in the initiation and/or development of kidney tumourigenesis

Work conducted by Vocke *et al.* revealed that 70% of renal tumours taken from BHD patients had a somatic mutation within the *BHD* gene or loss of heterozygosity of the *BHD* gene. 75% of the somatic mutations detected within the *BHD* gene were frameshift mutations which occurred within the open reading frame of *BHD*. One nonsense mutation was detected on exon 12 of the *BHD* gene. 2 other nonsense mutations were detected within exon 14 of the BHD gene (Vocke *et al.,* 2005). These differences in the mutations observed might influence which type of RCCs occurs in BHD patients (Yang *et al.,* 2008). However, this might also be explained by 'secondary hits' of additional genes or different genetic backgrounds of the patients. Work conducted by Chen *et al.* demonstrated that there was a correlation between kidney targeted loss of BHD and RCC in mice (Chen *et al.,* 2008). Work conducted by Hudon *et al.* also showed that heterozygous mice devoid of functional FLCN develop early preneoplastic kidney lesions which progress to malignant tumours. Knockdown of FLCN in the human kidney cancer cell line ACHN via short hairpin (sh) RNA was also shown to result in large tumours being formed. Furthermore, a decrease in tumour growth was observed in another kidney cancer cell line, 786-0, when FLCN was re-expressed (Hudon *et al.*, 2010). Okimoto *et al.* also observe that the primary RCCs within the Nihon rat model often exhibit loss of heterozygosity of *BHD*. Second hits within the canine orthologue of the human *BHD* gene were also observed in a large proportion of kidney tumours from dogs with RCND. These mutations were thought to result in loss of functional FLCN (Bønsdorff *et al.,* 2008). Cysts found on the surface of the kidneys in 6-8 week old puppies with RCND also display loss of heterozygosity of the *BHD* gene has also been observed in. Collectively, these data support the notion of FLCN functioning as a Knudson tumour suppressor in the kidney (Bønsdorff *et al.,* 2009; Khoo *et al.*, 2002)

1.5.2.2 Mutations within the BHD gene and Spontaneous pneumothoraces

As BHD patients can also present with spontaneous pneumothorax and air filled lung cysts, work has also been conducted in order to determine whether there is any correlation between mutations within the *BHD* gene and the spontaneous pneumothorax phenotype. Work conducted by Painter *et al.,* on the genotype-phenotype analysis of BHD patients revealed that patients which exhibit the dominantly inherited spontaneous pneumothorax have sporadic mutations within exon 4 of the *BHD* gene (Painter *et al.,* 2005). Further work conducted by Graham *et al.* revealed that patients which exhibit the isolated pneumothorax phenotype have germline mutations within exons 9 and 12 of the *BHD* gene (Graham *et al.,* 2005). Germline mutations in exons 6, 12 and 13 of the *BHD* gene have also been detected in patients that exhibit spontaneous pneumothoraces and lung cysts (Gunji *et al.,* 2007). Two further mutations in *BHD* which gave rise to spontaneous pneumothorax were identified by Fröhlich *et al*. (Fröhlich *et al.,* 2008). Genetic analysis conducted of a family with a history of spontaneous lung cysts and pneumothoraces also revealed a deletion mutation within exon 10 (Sundaram *et al.,* 2009). Collectively, these studies suggested that there is an association between mutations in the BHD gene and spontaneous pneumothorax, and that BHD patients may present with spontaneous pneumothoraces and an isolated phenotype with none of the other characteristics of BHD present. As there are mutations within the *BHD* gene that are associated with the isolated pneumothorax phenotype and lung cysts, it was hypothesised by Cho *et al.* that loss of function of FLCN may also contribute to chronic obstructive pulmonary disease (emphysema). However, no association was found between mutations in the *BHD* gene and chronic obstructive pulmonary disease (Cho *et al.,* 2008).

1.5.2.3 Mutations within the BHD gene are associated with Colorectal Cancer

Work conducted by Fernandes da Silva *et al.* also resulted in the detection of somatic and germline and missense mutations within primary colorectal cancer tumours (Fernandes da Silva *et al.,* 2003). In some tumours, frequent deletion and insertion mutations occur in the microsatellite repeats within the genome, resulting in microsatellite instability (MSI). Work conducted by Shin *et al.* revealed that mutations within the mononucleotide tract of eight cytosines (poly(C)8-tract) in exon 11of the *BHD* gene, previously identified by Schmidt *et al.* as a mutation hotspot for BHD patients, are associated with MSI sporadic colon cancer (Shin *et al.,* 2003). Analysis of genotype-phenotype correlations for *BHD* mutations conducted by Nahorski *et al.* revealed that carriers of a germline c.1285dupC mutation on the poly(C)8-tract in exon 11 of the *BHD* gene have an increased risk of developing colorectal neoplasias. 23% of sporadic colorectal cancers analysed also had somatic frameshift mutations within the poly(C)8-tract in exon 11 of the *BHD* gene (Nahorski *et al.*, 2010). These data suggested that loss of heterozygosity of *BHD* is also implicated in colorectal tumourigenesis.

1.5.2.3 BHD may be a MSI target gene

Work has also been conducted by Jiang *et al.* in order to determine whether mutations in the *BHD* gene gave rise to gastric cancer. Somatic mutations in the poly(C)(8)-tract of the *BHD* gene were detected in 15.8% of gastric cancer patients MSI, suggesting that mutations in the *BHD* gene rarely give rise to MSI gastric cancer. Work conducted by Fujii *et al.* also suggested that mutations within the poly(C)8 tract of the BHD gene are associated with sporadic endometrial carcinoma with MSI (Fujii *et al*., 2006). It may be possible that *BHD* is a MSI target gene. Alternatively, it may be equally possible that *BHD* is targeted downstream of other MSI target genes (Jiang *et al.,* 2007).

1.6 Signalling pathways which are regulated by FLCN

1.6.1 The Raf-MEK-Erk pathway

Work conducted by Baba *et al.* using a mouse model with kidney-specific loss of function of FLCN has also revealed that kidney specific knockdown of *BHD* results in activation of the Raf- mitogen-activated protein kinase (MAPK)/ERK kinase (MEK)- extracellular signal-regulated kinase (Erk) pathway (Baba *et al.,* 2008). The Raf-MEK-Erk pathway involves the MEK1/2 kinases being activated by Raf resulting in subsequent activation of ERK1/2, and regulates cell proliferation. Elevated activity levels of this pathway are exhibited in many cancers. (Roberts and Der, 2007). These data suggest that loss of functional FLCN may result in activation of an upstream effector of the Raf-MEK-ERK pathway, resulting in increased levels of cell growth and proliferation (Baba *et al.,* 2008).

1.6.2 JAK/STAT signalling

Work conducted by Singh *et al.* revealed that the FLCN may modulate tumourigenesis by regulating stem cells. Increased levels of the *D. melanogaster* homolog of the *BHD* gene (*dBhd*) were observed in early stage germline stem cells (GSCs). Suppression of *dBhd* and unpaired via shRNA lead to decreased numbers of GSCs, suggesting that it may be possible that *dBhd* may function downstream or in parallel to unpaired, an activator of the JAK/STAT pathway. This in turn controls the ability for GSCs to renew themselves (Singh *et al.,* 2006). If stem cells are not regulated properly this may lead to premature aging, tissue degeneration and the development of cancer (Okimoto *et al.,* 2003). It may be possible that the

misregulation of renal stem cells due to increased levels of the JAK/STAT pathway may provide a mechanism for renal tumourigenesis in BHD patients.

1.6.3 TGF-β signalling and transcriptional control

Transcription factor E3 (TFE3) and Transcription factor EB (TFEB) belong to the MiTF/TFE transcription factor family, and have been linked to RCC development including juvenile renal cancer. Work conducted by Hong *et al.* revealed that loss of functional FLCN leads to increased nuclear localisation of TFE3 and elevated levels of TFE3 activity. These results suggest that increased levels of TFE3 activity may be crucial part in the development of RCC in BHD patients (Hong *et al.,* 2010b). Studies conducted by Hong *et al.* using xenograph models and gene-expression profiles suggested that FLCN also functions as a tumour suppressor by regulating TGF-β signalling, essential in the regulation of a range of cellular functions (Hong *et al.,* 2010a). Another study also suggested that apoptosis is regulated by FLCN via TGF-β-dependent transcription. These data also suggested that autophagy inhibitors (such as chloroquine), and HDAC inhibitors, which are used to treat other cancer types, may provide potential therapeutic benefit for BHD patients (Cash *et al.,* 2011).

1.7 FLCN-binding proteins

Two FLCN-binding proteins have also been identified. These are known as FLCN-binding protein 1 (FNIP1) and FLCN-binding protein 2 (FNIP2). FNIP1 is an evolutionarily conserved 130 kDa protein which interacts with and facilitates the phosphorylation of FLCN (Baba *et al.,* 2006). FNIP2 is also evolutionarily conserved and has approximately 49% identity and 74% similarity to FNIP1 (Hasumi *et al.,* 2008). Work conducted by Komori *et*

al. has revealed that FNIP2 is involved the induction of apoptosis in response to DNA mispairing caused by O(6)-methylguanine (Komori *et al.,* 2009). Binding of both FNIP1 and FNIP2 to FLCN has been shown to be mediated through the C-terminus of FLCN. Truncation of the FLCN protein via mutations in the *BHD* gene reduces FLCN's ability to interact and form complexes with FNIP1 and FNIP2; suggesting that these interactions are of functional importance and are necessary for the tumour suppressor function of FLCN (Hasumi *et al.,* 2008; Baba *et al.,* 2006; Takagi *et al.,* 2008).

1.8 Tumour suppressors

Tumour suppressors modulate pathways within cells which are involved in processes such as autophagy, apoptosis, protein synthesis and metabolism which, if unregulated could lead to cancer. Tumour suppressors are therefore often mutated in cancers (Lowe *et al.,* 2004).

1.8.1 Tumour suppressors and apoptosis

One way in which tumour suppressors prevent uncontrolled cellular proliferation is via regulation of apoptosis, the process of programmed cell death. Pro-apoptotic effectors such as cytochrome C are contained within the intermembrane space of mitochondria. BH3 (Bcl-2 homologous 3) only proteins regulate the activity of pro-apoptotic proteins such as Bad and Bim and anti-apoptotic proteins such as Bcl2 which regulate mitochondrial membrane permeability. When expression of pro-apoptotic proteins is greater than the expression of anti-apoptotic proteins, mitochondrial membrane permeability is increased and the pro-

apoptotic factors contained within the intermembrane space of the mitochondria, such as cytochrome C are released. In the case of cytochrome C, this leads to the activation of the caspase cascade via the initiator capase, caspase 9. Proteins essential to cellular integrity are cleaved by caspases, resulting in cell death and engulfment of the cell. The apoptotic pathway may be regulated by tumour suppressor proteins at different levels, including regulating the transcription of members of the Bcl2/BH3 only family and modulating the transcription and expression of inhibitors of apoptosis which inhibit caspases.

1.8.2 Tumour suppressors and cellular senescence

Cellular senescence is a state of permanent cell-cycle arrest and can be induced by oncogenes, DNA damage and cellular stress. Cellular senescence is regulated by tumour suppressors such as Rb and p53 (Lowe *et al.*, 2004).

1.8.3 Tumour suppressor genes regulate pathways which promote cell growth and survival

When a cell is proliferating, the cell must generate enough energy to meet the demands of proliferation. The ability of a cell to proliferate is therefore regulated by its ability to obtain the energy and oxygen required in order to meet the energy demands of proliferation. In cancer cells, changes occur in pathways involved in nutrient uptake and energy metabolism. Many tumour suppressors regulate pathways which promote cell growth and survival. An example of this is phosphatidylinositol 3-kinase (PI3K). Activation of PI3K results in activation of Akt and mTOR which plays a part in the modulation of many metabolic processes which support cell growth and proliferation (Jones and Thompson, 2009).

1.9 The mTOR signalling pathway.

mTOR functions as serine/threonine kinase and belongs to the phosphoinositide 3-kinase related kinase (PIKK) family (Abraham, 2004). mTOR functions as two complexes, known as mTOR complex 1 (mTORC1) (comprised of the lethal with sec13 protein 8 (LST8 or GβL), proline-rich Akt substrate 40 kDa (PRAS40), and regulatory associated protein of mTOR (Raptor)) and mTOR complex 2 (mTORC2) (comprised of GβL, the stress-activated protein kinase-interacting protein (Sin1), and the rapamycin-insensitive companion of mTOR (rictor)) (Rosner *et al.,* 2008). PRAS40 inhibits mTORC1 activity, an effect which is relieved upon phosphorylation of PRAS40 by Akt (Nascimento and Ouwens, 2009). Raptor binds to mTOR and recruits eukaryotic initiation factor 4E binding protein-1 (4E-BP1) and ribosomal p70S6 kinase (p70S6K) which play a part in the regulation of protein translation (Nojima *et al.,* 2003). mTORC1 phosphorylates p70S6K and 4E-BP1, thus promoting protein synthesis (Watanabe *et al.,* 2011). S6K1 is known to phosphorylate ribsosomal protein S6 (rpS6), which modulates ribosomes (Rosner *et al.,* 2008). The FRB domain of mTOR binds the FKBP12/rapamycin complex and is required for mTORC1 inhibition (Chen *et al.,* 1995).. The interaction between mTOR and rictor is not inhibited by rapamycin. Both mTORC2, and phosphoinositide-dependent kinase-1 (PDK1), phosphorylate and activate Akt.

The mTOR signalling pathway is stimulated by the growth factors insulin and insulin like growth factor 1 (IGF1), glucose, and amino acids, and inhibited by stresses such as starvation, DNA damage and hypoxia. In response to these signals, mTOR regulates

translation, ribosome biogenesis, metabolism, proliferation, and autophagy in order to promote cell growth and survival (Figure 1) (Watanabe *et al.,* 2011).

mTOR signalling is activated by amino acids (Figure 1). When amino acids are present, Rag small G-proteins bind to Raptor, resulting in mTORC1 being translocated to the membrane and the binding of mTORC1 to Rheb. This interaction results in mTORC1 being activated (Sancak *et al.,* 2010).

The mTORC1 signalling pathway is inhibited in the presence of reactive oxygen species (ROS). This is due to the activation of TSC2 via LKB1 being activated by the cellular damage sensor Ataxia-telangiectasia mutated (ATM) and phosphorylation of AMPK. This results in increased autophagic activity (Figure 1) (Alexander *et al.,* 2010). AMPK is also known to phosphorylate Raptor and inhibit mTORC1 (Gwinn *et al.,* 2008).

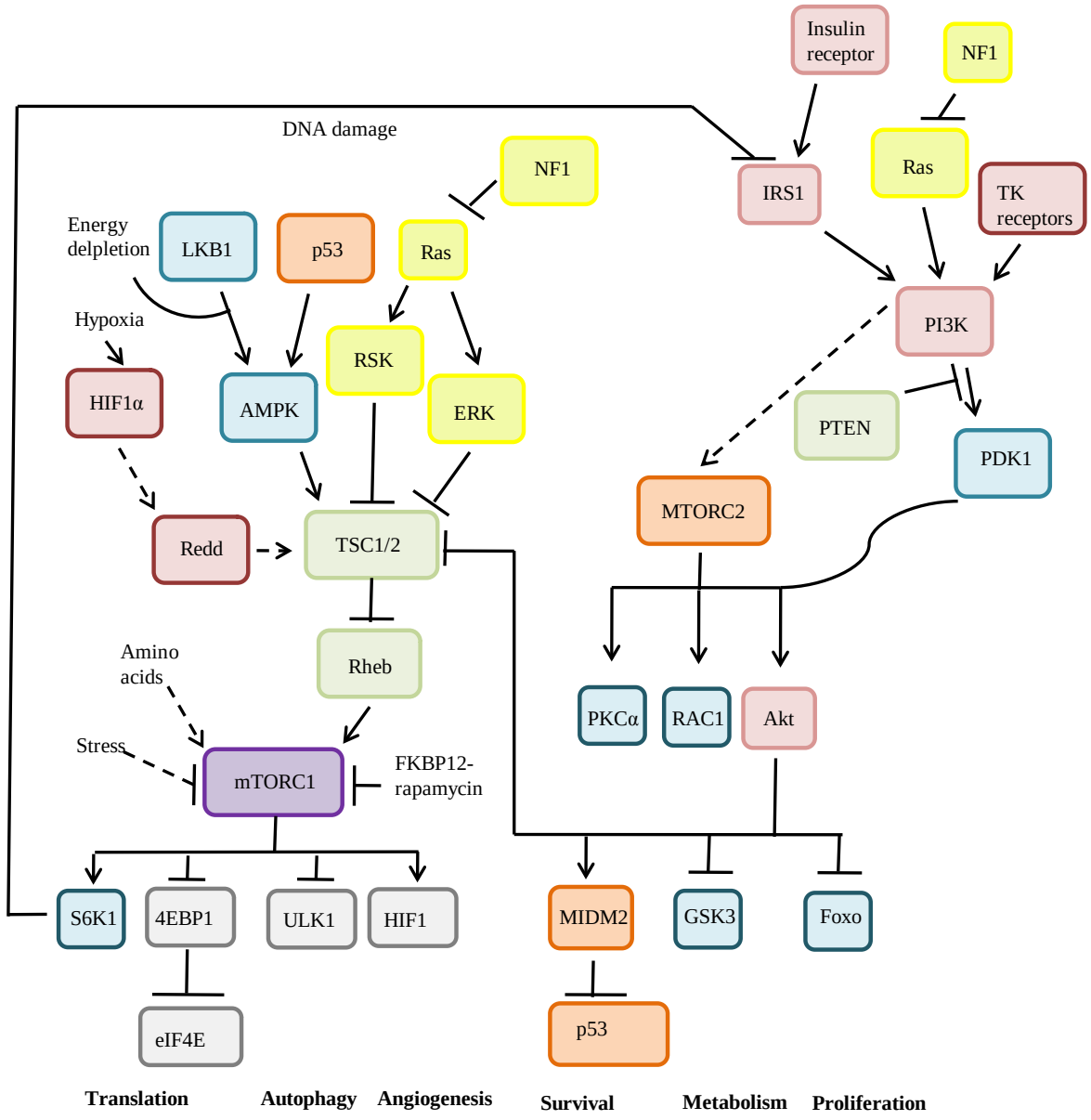

Figure 1. The mTORC1 and mTORC2 pathways. mTORC1 is involved in Angiogenesis, Autophagy and Translation through the regulation of S6K1, 4EBP1/eIF4E, ULK1 and HIF1α. mTORC2 is involved in cell survival, metabolism and proliferation through the regulation of MDM2, GSK3, and FOXO (Sabatini, 2006).

mTORC1 signalling is known to be inhibited under conditions of hypoxia. Hypoxia triggers dephosphorylation of mTORC1 and the downstream targets 4E-BP1, p70S6 kinase, and rpS6 (Figure 1). Hypoxic inhibition of these targets is dominant to activation via insulin or amino acids and may be independent of AMPK phosphorylation. This response was also thought to be dependent on Hypoxia inducible factor 1 (HIF1α) (Arsham *et al.*, 2003) and likely involves Redd1 and Redd2. HIF is known to promote expression of Redd1/2 which activates TSC2 via competitive binding for 14-3-3 proteins; leading to inhibition of mTORC1, even when Akt is constitutively active (Figure 1) (reviewed in (Dunlop and Tee, 2009)). Work conducted by Li *et al.* has also suggested that Bcl-2/adenovirus E1B 19-kDa interacting protein 3 (BNIP3), a downstream target of HIF1α, inhibits mTORC1 activation by binding to Rheb (Li *et al.*, 2007).

mTORC1 signalling is also inhibited under conditions of reduced ATP levels in order to reduce the levels of cellular processes, such as protein synthesis, which are energy demanding. This occurs via activation of AMP-dependent protein kinase (AMPK) via LKB1, which phosphorylates and activates TSC2 on Ser1345 and Thr1227, resulting in inhibition of mTORC1 (Inoki *et al.*, 2003). Work conducted by Gwinn *et al.* has shown that AMPK phosphorylates Raptor at Ser792 and Ser722. This results in induction of the binding of 14-3-3 proteins to Raptor and is essential for mTORC1 signalling being inhibited (Gwinn *et al.*, 2008).

1.10 mTOR signalling and cancer.

The PI3K/Akt/mTOR pathway has been shown to be upregulated in a number of human cancers. Studies conducted by Park *et al.* have also shown that an increased level of mTOR signalling is important in the tumourigenesis of bladder cancer. Furthermore, the phosphorylation status of rpS6 (an indicator of mTORC1 activity) has been shown to highly correlate with the recurrence, cancer progression and survival of bladder cancer patients (Park *et al*. 2011).

The PI3K/Akt/mTOR pathway signalling is upregulated in over half of pancreatic cancers. Activation of the PI3K/Akt/mTOR pathway reported within pancreatic cancers is associated with a poor prognosis (Schlieman *et al.,* 2003; Chadha *et al.,* 2006). A positive relationship between increased phosphorylation of p70S6K which indicates increased levels of mTORC1 activity, and poor prognosis in patients with breast cancer has also been observed (Shaw and Cantley, 2006).

Results from studies conducted on prostate cancer cells have shown mTORC1 inhibition via treatment with the rapalogue, RAD001, may provide potential therapeutic benefit for prostate cancer patients when used in combination with other reagents (Wedel *et al.,* 2011).

Increased levels of the PI3K/Akt/mTOR signalling have also been implicated in the development of RCCs, and a correlation has been observed between phosphorylation of mTOR and poor prognosis of patients with RCC (Elfiky *et al.,* 2011). Inhibitors of mTOR have been shown to have some effect on the development of RCCs, inhibiting angiogenesis and cell proliferation. Clinical trials investigating whether derivatives of rapamycin may

provide therapeutic benefit for patients with RCC have shown that treatment with the rapamycin derivatives, temsirolimus and everolimus, significantly inhibited tumour progression and prolonged overall survival in metastatic RCC patients with poor prognosis. However, there were some RCC patients for whom inhibitors of mTOR did not provide therapeutic benefit, revealing that there are variable outcomes with drug treatment (Wysoki, 2009). mTORC1 may be a therapeutic target for RCC (Husseinzadeh and Garcia, 2011). However work conducted by Elfiky *et al.* has suggested that targeting both mTOR and PI3K has a synergistic effect on the development of RCC, implying that inhibitors which target both PI3K and mTOR may provide greater therapeutic benefit for patients with RCC (Elfiky *et al.*, 2011).

PI3K may itself function as an oncogene or be activated by mutations in upstream effectors of PI3K such as insulin-like growth factor receptors. Increased PI3K activity has been shown to contribute to tumour development in ovarian and gastrointestinal cancer (Guertin and Sabatini, 2007; Chiang and Abraham, 2007; Wullschleger *et al.*, 2006; Jiang and Liu, 2008). Akt has also been shown to be upregulated in breast and ovarian cancer (Wullschleger *et al.*, 2006; Manning and Cantley, 2007; Guertin and Sabatini, 2007).

1.11 Tumour suppressor genes within the mTOR pathway

There are several other genes within the mTOR pathway which act as Tumour Suppressors. Mutations within these genes result in inherited genetic disorders. These include VHL, LKB1, TSC1 and TSC2, NF1 and PTEN. Mutations in these genes give rise to Von Hippel-Lindau, Peutz-Jeghers Syndrome, Tuberous sclerosis complex (TSC), Neurofibromatosis and Cowden Syndrome, respectively (Figure 2). mTORC1 signalling is upregulated within these

syndromes as a result of loss of function of these upstream tumour suppressor proteins; causing aberrant levels of cell proliferation and growth. Examining the similarities and differences between BHD and these other inherited genetic disorders which arise as a result of mutations within these genes may prove useful for determining the function of FLCN.

1.11.1 Tuberous Sclerosis Complex.

BHD patients present with symptoms which are clinically similar to TSC. TSC arises due to mutations within the *TSC1* or *TSC2* genes which code for the proteins hamartin (TSC1) and tuberin (TSC2), which function as tumour suppressors (Figure 2) (Green *et al.,* 1994a; Green *et al.,* 1994b). These mutations within the *TSC1* or *TSC2* genes result in hamartomas in the kidneys, and skin, and pulmonary cysts in a similar manner to that observed in BHD patients; as well as hamartomas of the brain, heart and eyes (Gomez *et al.*, 1999). The TSC1 and TSC2 inhibit mTORC1 signalling by acting as a GTPase activating protein (GAP) and reverting Rheb (Ras homolog enriched in brain); a potent activator of mTORC1 when bound to GTP, to its inactive GDP-bound form (reviewed in Dunlop and Tee, 2009). The TSC1-TSC2 complex also activates mTORC2 and thus promotes Akt activation. Work conducted by Tee *et al.* has revealed that tumours from patients with TSC may arise due to abnormally elevated levels of mTORC1 signalling (Tee *et al.*, 2002). Increased phosphorylation levels of ribosomal protein S6 kinase 1 and 4E-BP1 have also been observed in *TSC1* and *TSC2* deficient cells which is inhibited by rapamycin; consistent with constitutive activation of mTORC1 (Kwiatkowski *et al.,* 2002). TSC2, along with PTEN and LKB1, is thought to regulate HIF and VEGF. It has therefore been suggested that increased HIF and VEGF levels may be a regular feature of inherited hamartoma syndromes. It has even been suggested that

part of the tumour suppression function of TSC2 may be it's regulation of HIF transcriptional activity (Brugarolas and Kaelin, 2004).

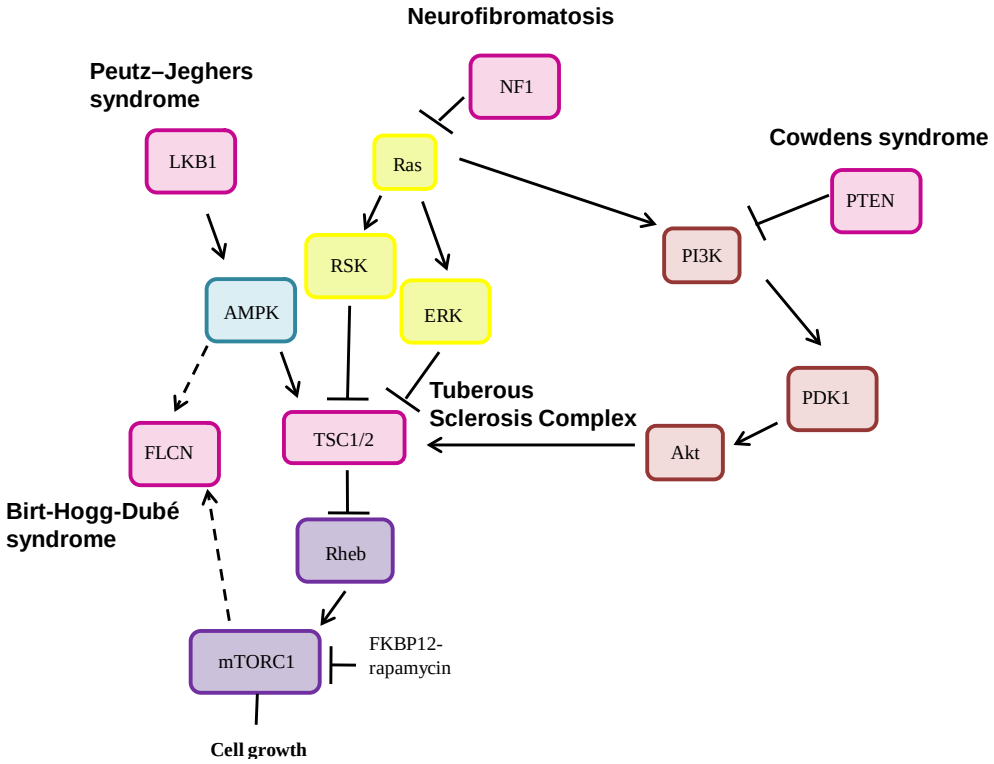

Figure 2. Tumour suppressors in the mTORC1 signalling pathway

mTORC1 is regulated by a number of tumour suppressors, including LKB1, NF1, PTEN, and TSC1/2. Loss of function of these tumour suppressors results in the cancer syndromes Peutz-Jeghers syndrome, Neurofibromatosis, Cowden syndrome, and Tuberous Sclerosis complex respectively. It may be possible that FLCN is another tumour suppressor which regulates the mTORC1 signalling pathway, where loss of FLCN function results in Birt-Hogg-Dubé syndrome.

1.11.5 Von-Hippel-Lindau disease

Von-Hippel-Lindau disease (VHL) arises due to mutations within the VHL tumour suppressor gene and subsequent loss of function of the VHL protein; resulting in increased

stability of HIFα proteins and heightened expression of their gene targets (Krieg *et al.,* 2000). VHL is characterised by tumours in the brain, the retina of the eyes, kidneys (clear cell carcinomas), adrenal glands, and the pancreas (Rosner *et al.,* 2008).

1.12 Constitutive activation of mTORC1 may also contribute to the development of tumours in BHD patients.

Work conducted by van Slegtenhorst *et al.* has suggested that loss of the yeast *BHD* homologue, LST7, results in inhibition of Tor2 in an opposing manner to that described upon loss of *TSC*, suggesting that LST7 may activate Tor2 and thus be important in the regulation of amino acid homeostasis in yeast (van Slegtenhorst *et al.,* 2007). However, work conducted by Baba *et al.* has shown that the phosphorylation status of downstream mTORC1 substrates is enhanced upon loss of functional FLCN, indicating that the Akt/mTOR pathway is elevated in cells deficient of FLCN (Baba *et al.,* 2008; Baba *et al.,* 2006). Work conducted by Hasumi *et al.* also suggested that levels of mTORC1 and mTORC2 activity are elevated along with increased expression levels of Rictor (a component of mTORC2) in tumours from *Bhd*$^{d/+}$ mice and human BHD patients (Hasumi *et al.,* 2009). mTORC2 has been shown to phosphorylate and stabilise Akt (Facchinetti *et al.,* 2008), suggesting that it is the activation of mTORC2 which is the primary mechanism by which Akt is activated in BHD-deficient tumours. Collectively, these results of these studies imply that FLCN may be part of a negative feedback loop which suppresses PI3K-Akt-mTOR signalling (Hasumi *et al.,* 2009). Loss of functional FLCN therefore results in increased levels of mTORC2 activity which in turn activates Akt and thus mTORC1 signalling. Results obtained from work conducted by Hartman *et al.* suggested that the increased levels of mTORC1 activation observed in BHD-

deficient cell lines was not a primary effect of loss of BHD, but mTOR may later be activated due to activation of Akt or other upstream kinases which regulate the TSC/Rheb/mTOR signalling pathway; in a manner analogous to TSC-deficient cell lines (Hartman *et al.*, 2009). These results suggest that FLCN regulates mTORC1 signalling in a context-dependent manner, and that the relationship between FLCN and mTOR is highly complicated and presumably involves negative feedback mechanisms and cell adaption to loss of FLCN function (Piao *et al.*, 2009).

The mTOR signalling pathway is also associated with pathways which have been implicated in the development of benign and malignant tumours. The increased levels of mTOR activity observed upon loss of function of FLCN have therefore been implicated in the development of melanomas in BHD patients (Cocciolone *et al.*, 2010). Treatment with rapamycin has also been shown to extend survival and inhibit further development of cysts in kidney-specific BHD knockout mice exhibiting polycystic kidneys, hyperplasia, and cystic RCC. These results suggest that the phenotypes exhibited by these mice arose as a result of activation of the mTOR pathway upon loss of FLCN (Chen *et al.*, 2008). These data suggest that BHD is another tumour suppressor in the mTOR pathway and that abnormally high levels of mTOR-mediated signalling may contribute to the development of tumours in BHD patients. Furthermore FLCN-mTOR signalling may regulate cell growth/proliferation.

1.13 FLCN is differentially phosphorylated by AMPK and mTOR.

Data from work conducted by Baba *et al.* revealed that phosphorylation of FLCN was partially blocked by rapamycin and amino acid starvation (Baba *et al.*, 2006). Further work conducted by Piao *et al.* identified Ser62 and Ser302 as phosphorylation sites of FLCN that

were differentially regulated by mTORC1. Downstream kinases of mTORC1, such as S6K1, appear to enhance phosphorylation of FLCN at Ser302 (Piao *et al.,* 2009). Work conducted by Piao *et al.* has revealed that loss of *TSC2* via shRNA resulted in phosphorylation of FLCN. Increased phosphorylation of FLCN at Ser62 and Ser302, was observed upon expression of Rheb, suggesting that tuberin signalling regulates the phosphorylation of FLCN (Piao *et al.,* 2009). These data suggest that the mTORC1 signalling pathway regulates the phosphorylation status FLCN and most likely its tumour suppression function.

Baba *et al.* revealed that inhibition of AMPK by adenine 9-β-D-arabinofuranoside (AraA) inhibited the phosphorylation of FLCN in UOK257-2 cells and they observed phosphorylation of GST-tagged FLCN *in vitro* AMPK kinase assays. It is possible that FLCN is phosphorylated at multiple, as yet unidentified, residues, by both mTORC1 and AMPK. Further work conducted by Wang *et al.* also revealed that the phosphorylation status of FLCN at the Ser62 site is enhanced by an AMPK-related pathway (Wang *et al.,* 2010). AMPK has also been shown to bind to both FNIP1 and FNIP2 (Takagi *et al.,* 2008; Baba *et al.,* 2006), and enhance the phosphorylation status of FNIP2 (Takagi *et al.,* 2008). Work conducted by Piao *et al.* also suggested that phosphorylation of FLCN regulates the formation of the FLCN/AMPK complex (Piao *et al.,* 2009). As AMPK is known to inhibit mTORC1 signalling by phosphorylating and activating TSC2, and FLCN has been shown to be phosphorylated by AMPK and mTOR, it has been suggested that phosphorylation of FLCN may be associated with feedback mechanisms which mTOR signalling pathways (Piao *et al.,* 2009).

1.14 AMPK and cancer

AMPK functions as an energy sensor and provides metabolic changes in order to adapt to conditions of depleted ATP (Yun *et al.,* 2005). AMPK modulates activity of acetyl CoA carboxylase (ACC), involved in fatty acid synthesis, and mTOR under conditions of elevated AMP levels in order to reduce the levels of cellular processes which are energy demanding, thus conserving ATP for survival. AMPK has therefore been shown to be upregulated in a number of cancers (Chhipa *et al.,* 2011), and has been shown to inhibit apoptosis under conditions of glucose deprivation in cancer cells (Luo *et al.,* 2005). However, it has also been suggested that arberrant levels of AMPK activity may inhibit the growth and survival of cancer cells due to the inhibition of mTOR and fatty acid synthesis (Luo *et al.,* 2005).

1.15 Both AMPK and mTOR positively regulate mitochondrial biogenesis

Mitochondria are fundamental to cellular metabolism and energy production. Oxidation of fatty acids and glucose produces high-energy electrons that subsequently enter the electron transport chain within the intermembrane space of the mitochondria. Energy from these reduced electrons is converted into a proton gradient which is used by the mitochondrion to generate ATP (Moiseeva *et al.,* 2009). Mitochondria also play a part in cell death pathways such as apoptosis and play a critical role in cellular senescence in response to oncogenic genes. It has been shown that the activation of oncogenic genes results in increased levels of mitochondrial DNA, mitochondrial mass and mitochondrial superoxide production. These changes subsequently lead to further elevated levels of ROS production, decreased mitochondrial membrane potential and the activation of AMPK (Moiseeva *et al.,* 2009). It

has been shown that elevated levels of AMPK activity results in increased levels of mitochondrial biogenesis due to activation of peroxisome proliferator-activated receptor gamma, coactivator 1 alpha (PGC1α) (Zong *et al.,* 2002). PGC1α interacts with and coactivates many nuclear and nonnuclear receptors directly responsible for the transcription and replication of mitochondrial DNA (Bogacka *et al.,* 2005). PGC1α is therefore able to enhance mitochondrial biogenesis and oxidative function.

It has also been shown that mTOR and Raptor associate with ying yang 1 (YY1) and mTOR has been shown to regulate mitochondrial oxidative function by regulating the YY1 –PGC1α transcriptional complex (Cunningham *et al.*, 2007).

1.16 Both AMPK and mTOR positively regulate Hypoxia Inducible Factor transcriptional activity

Another way in which AMPK provides changes to cellular metabolism in order for cells to be able to adapt to low cellular ATP levels is by enhancing the transcriptional activity of HIF-mediated transcription through a signalling pathway independent of the PI3K/Akt (Lee *et al.,* 2003). HIF1α subsequently increases the transcription of several genes in order to provide adaptations which enhance metabolism under hypoxic conditions. HIF is also able to enhance expression of genes which regulate cell survival and proliferation (Maxwell, 2005). Aberrant HIF activity levels have therefore been found to contribute to tumour development in several inherited diseases that give rise to RCCs (Maxwell, 2005).

mTOR has also been shown to positively regulate HIF transcriptional activity. This may be via modulation of the interaction between HIF1α and Raptor (Land and Tee, 2007).

However, it may also be possible that mTORC1 regulates HIF indirectly via activation of S6K (Jefferies *et al.,* 1994). mTORs ability to activate HIF is considered an important part of mTORs role in the tumourigenesis of RCCs due to HIFs ability to enhance transcription of genes involved in cellular processes such as angiogenesis (Elfiky *et al.,* 2011). This has lead to investigation into the effects of inhibitors of mTOR and VEGF, a HIF transcriptional target involved in angiogenesis, however the results of these investigations have not confirmed this as a viable therapeutic target for patients with RCC (Husseinzadeh and Garcia, 2011).

1.17 AMPK activation results in increased autophagic activity.

Autophagy is a process by which cells adapt to stress via the catabolism of unnecessary structures such as organelles and proteins, and has been shown to provide a protective function for tumour cells when moderately elevated (Schönthal *et al.,* 2009). AMPK may conserve ATP for survival via activation of autophagy, as amino acids are recycled from organelles catabolised during the autophagic process. Work conducted by Chhippa *et al.* has shown that autophagy induced by activation of AMPK is a cell survival mechanism within androgen-dependent prostate cancer cells (Chhipa *et al.,* 2011). AMPK has been shown to bind to UNC-51-like kinase 1 (ULK1) at the proline-serine rich (PS) domain; which is necessary for ULK1-mediated autophagy. When energy levels are depleted in a cell, activated AMPK has also been shown to recruit 14-3-3 proteins to Raptor. This interaction between 14-3-3 proteins and Raptor results in inhibition of mTORC1 and thus its activity in the ULK1 complex (Lee *et al.,* 2010), resulting in activation of autophagy. mTORC1 has been show to negatively regulate autophagy via the ULK1–Atg13–FIP200 complex (Figure 3) (Hosokawa *et al.,* 2009). Increased levels of mTORC1 activity have been shown to result in decreased levels of autophagic activity in TSC2-deficient cells (Parkhitko *et al.,* 2011) and

inhibition of mTORC1 via treatment with rapamycin has been shown to result in elevated levels of autophagic activity (Turcotte and Giaccia, 2010). Treatment with a combination of rapamycin and the reagent Chloroquine has been shown to have a synergistic effect on decreasing tumour size in TSC2-deficient tumours (Parkhitko *et al.*, 2011).

AMPK is also able to activate autophagy by increasing the transcriptional activity of HIF1α. HIF1α is able to mediate autophagy via the induction of BNIP3 (Bellot *et al.*, 2009). Multiple studies have shown that BNIP3 induces autophagy in response to elevated levels of reactive oxygen species and decreased mitochondrial membrane potential and which would result in cell death (Burton *et al*., 2009).

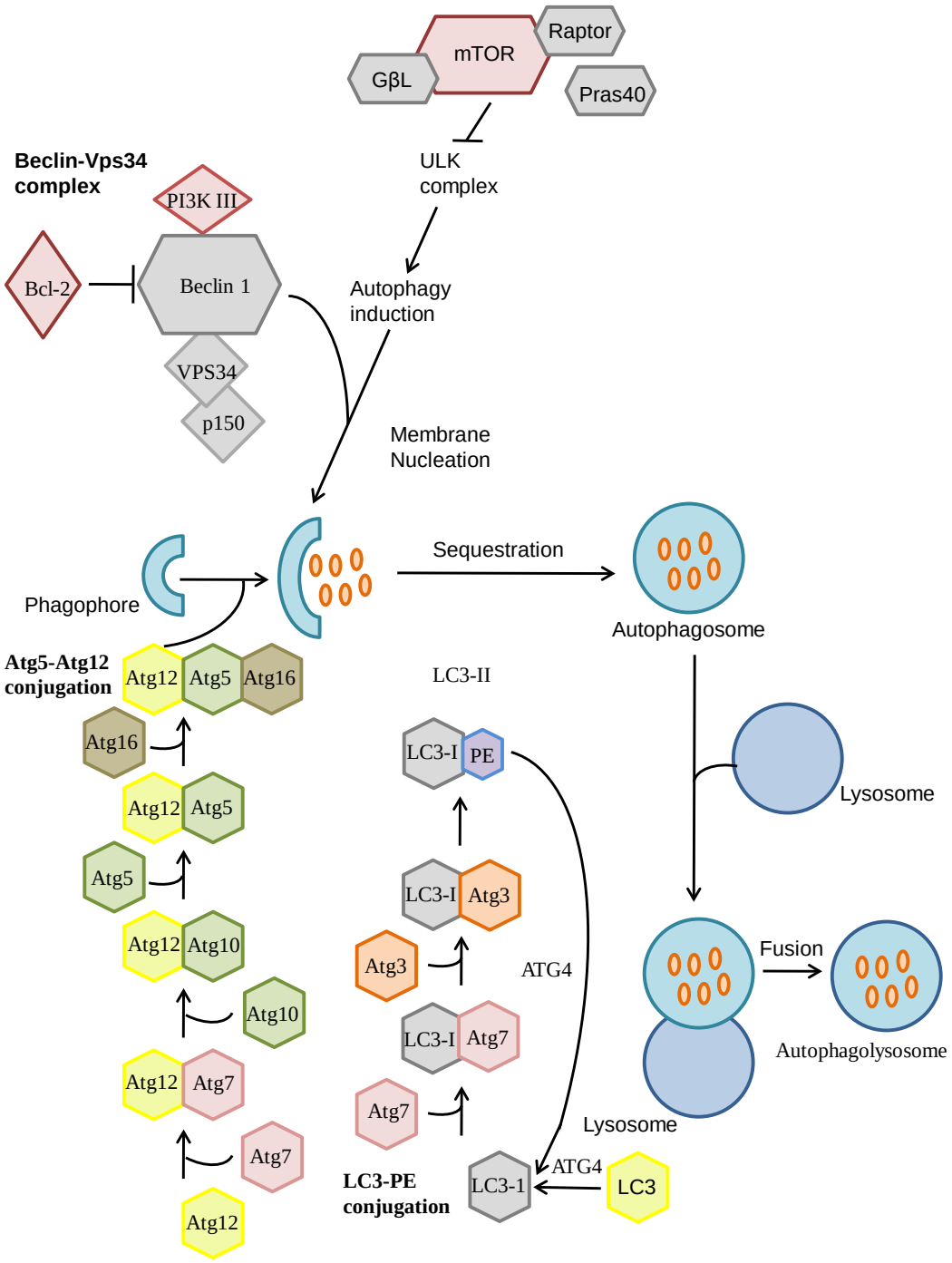

Figure 3. Inhibition of the autophagic pathway via mTORC1 inhibition of the ULK1 complex

mTORC1 has been show to negatively regulate autophagy via the UNC-51-like kinase 1 (ULK1) –Atg13–FIP200 complex resulting in reduced formation of Autophagosomes and lysosomes (Ravikumar *et al.* 2010).

1.18 Renal cell carcinomas.

RCCs can be divided into various subcategories. These are clear cell carcinomas, chromophobe carcinomas, oncocytomas, type 1 papillary or hybrids of the various categories (Stec *et al.,* 2009), where all these subtypes can occur in BHD patients.

1.18.1 Clear cell renal cell carcinomas

Clear cell RCC typically derive from the proximal tubular epithelium of the kidney and is characterised by a clear cytoplasm with a large prominent nucleus. Clear cell RCCs are the most common subtype of malignant RCCs (Störkel *et al.,* 1997). Clear cell RCCs are also often exhibited by VHL patients (Clark, 2009).

1.18.2 Chromophobe renal cell carcinomas.

Chromophobe RCCs are rarer than either clear cell or papillary RCCS, accounting for approximately 5% of RCCs, and typically derive from cells of the collecting duct. Chromophobe RCCs are characterised by abundant cytoplasm and binucleation (Amin *et al*., 1997).

1.18.3 Papillary renal cell carcinomas

Papillary RCCs are the second most common type of RCC, with approximately 10-15% of RCC patients presenting with this subtype. Papillary RCCs are usually derived from the distal convoluted tubules. Work conducted by Schmidt *et al.* observed that papillary RCCs have mutations within the MET proto-oncogene, resulting in activation of C-MET (Schmidt *et al.,* 1997).

1.18.4 Oncocytomas

Renal oncocytomas are benign tumours within the kidney and are characterized by dense accumulation of mitochondria. It has been observed that mitochondrial DNA levels and the activity of complexes which form the electron transport chain (oxidative phosphorylation) of the mitochondria are increased in renal oncocytomas as a result of this accumulation of mitochondria (Simonet *et al.*, 2003).

1.18.5 Renal cell carcinoma syndromes, mitochondrial dysfunction and aberrant HIF signalling.

Many cancer syndromes which give rise to RCCs exhibit decreased mitochondrial function, aberrant levels of HIF activity, or a combination of both. An example of this is Hereditary Leiomyomatosis Renal Cell Carcinoma (HLRCC), which arises due to mutations within the gene coding for Fumarate hydratase (FH), an enzyme involved in the Tricarboxylic acid (TCA) cycle (otherwise known as the Krebs cycle). Patients with HLRCC may develop type 2 papillary and clear cell RCCs. Loss of function of FH results in mitochondrial dysfunction due to lack of ability to generate ATP via aerobic respiration involving the Krebs cycle and the electron transport chain within the mitochondria. Kidney tumour cells from HLRCC patients also exhibit aberrant HIF signalling (Isaacs *et al.*, 2005; Sudarshan *et al.*, 2011).

If cells are unable to generate ATP through the electron transport chain, a shift in their metabolism towards ATP generation by glycolysis occurs, thus resulting in cells exhibiting the Warburg effect (Fosslein, 2008). The term Warburg effect refers to a metabolic shift towards increased glucose uptake, lactate production and decreased levels of respiration that occurs in some cancer cells even when oxygen supplies are adequate (Semenza, 2007). In clear cell renal carcinoma, aberrant levels HIF activity have also been shown to result in

increased transcription of genes involved in glucose uptake, glycolysis and the production of lactate; thus mediating the Warburg effect (Semenza, 2007).

1.19 Cyst formation

1.19.1 Polycystic kidney disease

Autosomal dominant polycystic kidney disease (ADPKD), the most widespread type of polycystic kidney disease, occurs due to mutations within the PKD1 gene encoding for polycystin 1 (PC1), and is characterised by renal cysts in a similar manner to TSC. ADPKD patients can also exhibit mutations in *TSC2* as well as *PKD1* due to the fact that the two genes are next to each other (contiguous gene syndrome). It has been suggested that *PKD1* and *TSC2* may have a synergistic effect as patients that exhibit mutations in both genes present with a more severe form of ADPKD at an earlier age than patients which only exhibit mutations in *PKD1*. It has been revealed that the localisation of PC1 to the plasma membrane is dependent on TSC2 (Kleymenova *et al.*, 2001) and PC1 is able to regulate mTORC1 signalling via interaction with TSC2 and mTOR (Shillingford *et al.*, 2006).

As previously discussed, BHD patients present with lungs cysts and polycystic kidneys (Baba *et al.*, 2008). A study conducted by Torres *et al.* also suggested that elevated levels of proliferation, apoptosis and loss of polarity within the cystic epithelia all contribute to cystogenesis and development (Torres, 2010).

1.19.1 Ciliopathy and renal cyst formation

Cilia are hair-like organelles which are involved in the detection and management of external signals (Hildebrandt *et al.,* 2011). They are also key co-ordinators of cellular signalling functions within a cell during development and the maintenance of homeostasis in normal tissue (Satir *et al.,* 2010; Goetz and Anderson, 2010). Primary cilia regulate several signalling pathways (Simons *et al.,* 2005; Christiensen *et al.,* 2008). Primary cilia are also thought to regulate mTORC1 signalling (Boehlke *et al.,* 2010). Mutations within proteins such as polycystin 1 and polycystin 2, which are located in the primary cilia and are involved in Ca^{2+} uptake, are observed in many diseases which present with cyst formation (Pazour *et al.,* 2002; Yoder *et al.*, 2002). Data produced by Thoma *et al* revealed that VHL, involved in oxygen sensing, and GSK3β may function together to maintain cilia, and that loss of function of these genes results in disruption of the maintenance of the cilia, thus promoting cyst formation (Thoma *et al.,* 2007). Given that cysts also occur in the lungs and kidneys of BHD patients, it is possible that BHD might also be a ciliopathy.

1.19.2 mTOR signalling and cystogenesis.

Aberrant mTOR signalling is observed in many diseases which present with renal cyst formation, including BHD. It has been shown that aberrant mTOR signalling results in changes in the activity levels of processes within a cell which promote cystogenesis such as protein synthesis. Polycystin 1 has been shown to interact with TSC2 which, when complexed with TSC1, regulates mTORC1 activity. Furthermore, it has been shown that TSC1 localises to the basal body of the primary cilium (Hartman *et al.,* 2009). TSC1, TSC2, and polycystin 1 have also been shown be involved in the maintenance of cell polarity in pre-cystic renal and hepatic cells, and important for the prevention of cystogenesis (Bonnet *et al.,*

2009). LKB1, another tumour suppressor protein in the mTOR signalling pathway, is also localised to the primary cilia.

Renal primary cilia monitor urinary flow through the tubules of the kidney via polycystin 1 and polycystin 2 (Boehlke *et al.*, 2010). Work conducted by Boehlke *et al.* has also shown that bending of the cilia by urine flow results in inhibition of mTORC1 (Boehlke *et al.*, 2010). As aberrant levels of mTORC1 signalling appears to be involved in the tumourigenesis exhibited in BHD patients, and BHD patients present with polycystic kidneys, it may be possible that ciliopathy also occur upon loss of functional FLCN (*Baba et al.*, 2008; Baba, *et al.*, 2006).

1.20 Aims and Objectives of this Project

There are 3 main aims of this project:

(i) To examine the effect of FLCN on mitochondrial biogenesis

(ii) To investigate the effect of FLCN on HIF.

(iii) To examine autophagy in the context of BHD

Chapter 2

The effect of loss of functional Folliculin on HIF transcriptional activity

2 The effect of loss of functional Folliculin on HIF transcriptional activity

2.1 Introduction

Hypoxia inducible factor (HIF) exists as a complex containing α and β subunits. HIF1α and HIF2α function as heterodimers and are activated under conditions of low oxygen. Under normoxic conditions, the HIFα subunits are hydroxylated at three sites; an asparagine residue which is located in the C-terminal transactivation domain (C-TAD) and two proline residues that are located in the oxygen dependent degradation domain (ODDD). The ODDD of HIF contains proline residues which are hydroxylated by prolyl hydroxylases. This provides the recognition signal to allow for capture of HIF by a specific E3 ligase protein, VHL. This leads to the polyubiquitylation of the HIFα proteins and their subsequent degradation by the proteasome. The asparagine residue on the C-terminus is hydroxylated by a HIF asparagine hydroxylase. It is this modification which prevents the recruitment of CBP/P300 and controls HIF transcriptional activity (Figure 4) (Maxwell, 2005). Loss of functional VHL protein leads to the HIFα proteins being stabilised and subsequent increased levels of HIF mediated gene expression (Semenza, 2004).

HIF1α and HIF2α function as transcription factors and enhance the expression of over 100 genes involved in processes such as angiogenesis; as well as glucose uptake and metabolism. HIF activation also plays an important part in cell proliferation and survival (Maxwell, 2005). HIF1α is known to enhance the gene expression of BNIP3 involved in autophagy and cell death, Beclin-1 which is involved in autophagy, and vascular endothelial growth factor (VEGF) which is involved in angiogenesis (Figure 5).

HIF-1α is over-expressed in a number of tumour types, including breast, pancreatic, colon, lung, gastric, prostate, ovarian, and skin cancers. HIF also appears to have a crucial role in several inherited diseases that give rise to RCCs (Maxwell, 2005) including VHL, HLRCC and TSC (Krieg *et al.*, 2000). HLRCC is another hereditary disorder which gives rise to RCC. HLRCC arises as a result of mutations in the Fumarate Hydratase (FH) gene which results in inhibition of prolyl hydroxylases and the stabilisation of HIF1α protein (Pollard *et al.*, 2005). Further work conducted by Sudarshan *et al.* has also suggested that aberrant HIF signalling may also occur upon loss of FH via a VHL-independent mechanism (Sudarshan *et al.*, 2011). HLRCC patients also exhibit skin lesions similar to those observed in BHD patients.

HIF is also thought to play a part in the growth of tumours in Tuberous Sclerosis Complex (TSC) patients (Liu *et al.*, 2003). TSC arises from mutations in either the *TSC1* or *TSC2* genes. The proteins encoded by these genes form a complex which negatively regulates mTORC1 (Brugarolas *et al.*, 2003). Activation of mTORC1 results in increased transcription of HIF target proteins and increased HIF-mediated transcriptional activity (Land and Tee, 2007). TSC2-deficient cells exhibit increased levels of mTORC1 activity and increased HIF activity compared to those expressing functional TSC2 which was reversed upon treatment with the mTOR inhibitor rapamycin (Land and Tee, 2007). TSC patients exhibit overlapping characteristics to BHD patients; including benign tumours (called harmatomas) in the skin, kidneys and lung.

mTOR inhibition has been shown to significantly reduce expression levels of HIFα protein in most cell types (Knaup *et al.*, 2009). However; the exact mechanism as to how HIF is

regulated by mTOR remains unclear. Studies conducted by Land and Tee revealed that HIF1α interacts with Raptor. This interaction requires an mTOR signaling (TOS) motif which is located in the N-terminus of HIF1α. HIF1α is unable to bind to its co activator CBP/p300 when this TOS motif is absent; resulting in decreased levels of HIF activity under hypoxic conditions (Land and Tee, 2007). This work implies that HIF1α is a direct mTORC1 substrate. However it has also been suggested that mTORC1 regulates HIF indirectly via S6K; a well characterised mTORC1 substrate (Dunlop and Tee, 2009).

It has also been shown that the translation of mRNAs containing a 5′-terminal tract of polypyrimidines (5′-TOP) and the phosphorylation of ribosomal protein S6 is selectively repressed upon treatment with rapamycin. Therefore, it was hypothesised that 40S ribosomes containing rpS6 may selectively recognise these terminal pyrimidine tract mRNA motifs or proteins which bind to it and mediate their translation. Phosphorylation of rpS6 by S6K1 would therefore result in increased translation of 5'TOP mRNAs (Jefferies *et al.*, 1994). The 5′-untranslated region (UTR) of HIF-1α has pyrimidine tracts downstream of nucleotide + 32; suggesting that translation of HIF1α may also be regulated as a 5'TOP message (Iyer *et al.*, 1998). However work conducted by Stolovich *et al.* suggested that S6K1 activation is not required for the translation of 5'TOP mRNAs (Stolovich *et al.*, 2002). The mechanism as to how 5′-TOP mRNA translation is regulated by mTORC1 and whether HIF-1α mRNA is regulated by mTORC1 as a 5′-TOP message therefore remains unclear (Dunlop and Tee, 2009).

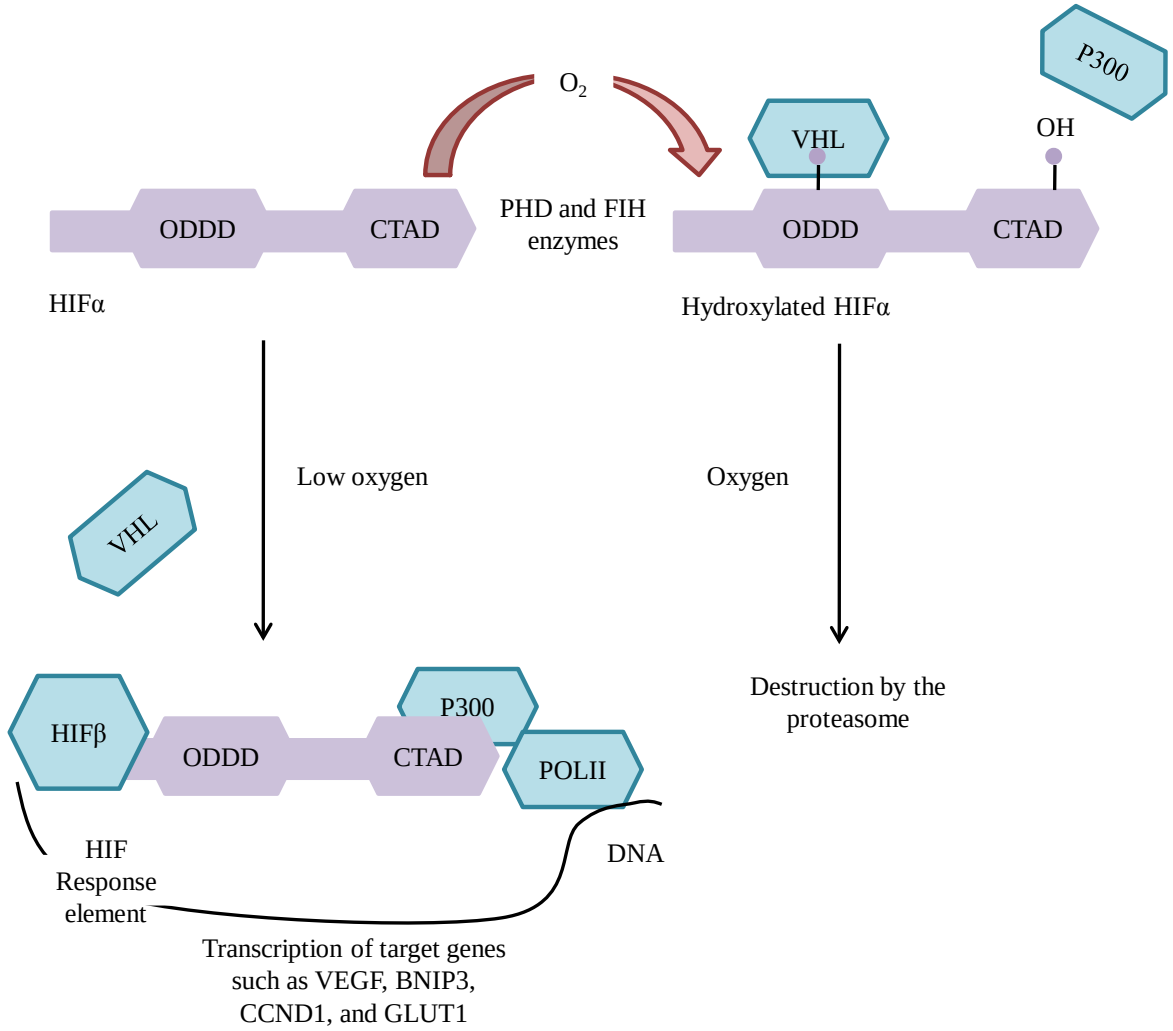

Figure 4. The regulation of the HIF complex by oxygen through hydroxylation of the HIFα subunit

In the presence of oxygen, the asparagine residue in the C terminal transactivation domain (CTAD) and the prolyl residues in the ODDD are hydroxylated. This allows the HIF protein to be captured by VHL resulting in subsequent ubiquitylation and proteosomal degradation of HIF (Maxwell, 2005).

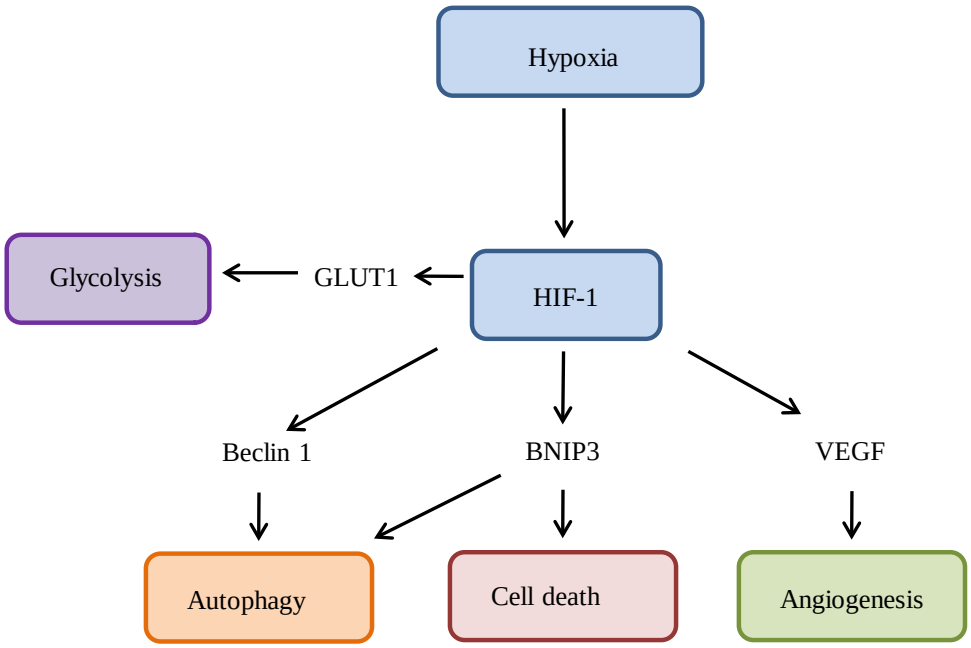

Figure 5. HIF-1 regulates the transcription of genes involved in autophagy, cell death and angiogenesis.

Under conditions of hypoxia, HIF-1 regulates the transcription of BNIP3 which is involved in the regulation of cell death and autophagy, Beclin 1 which is involved in the regulation of autophagy while VEGF is involved in angiogenesis and Glut 1 is involved in glycolysis (Melillo, 2010).

Given that HIF appears to have a crucial role in the pathology associated with other inherited cancer syndromes which give rise to RCC, and have overlapping or similar clinical symptoms to those exhibited in BHD patients, I wanted to examine whether FLCN deficient cells had increased levels of HIF-mediated gene expression that would result in a cancer phenotype. In this chapter, HIF-mediated signalling events are analysed within cell lines deficient in functional BHD.

2.2 Results

2.2.1 Cells lacking functional FLCN have increased levels of HIF-mediated transcription.

In order to determine whether HIF-mediated gene-expression was upregulated within cells deficient in FLCN, the mRNA levels of downstream transcriptional targets of HIF were compared within the UOK257 cell line and the UOK257-2 cell line. The mRNA levels of BNIP3 (a HIF1α transcriptional target, (Figure 6A) (Guo *et al*., 2001)), CCND1 (a HIF2α transcriptional target (Figure 6B) (Maxwell, 2005)) and VEGF-A (a transcriptional target of both HIF1α and HIF2α (Figure 6C) (Maxwell, 2005)) were measured using RT-PCR. The results suggested that, under conditions of normoxia and hypoxia, there is a significant increase in the transcription of genes which are regulated by HIF1α and HIF2α in the FLCN-deficient UOK257 cells compared to the UOK257-2 cells. I also observed increased expression of HIF1α and HIF2α transcriptional targets in the presence of normal levels of oxygen. The results also suggested that the mRNA levels of BNIP3 (Figure 6B) and CCND1 (Figure 6C) were inhibited under hypoxic conditions in the FLCN-deficient UOK257 cells when treated with the specific mTORC1 inhibitor, rapamycin. Therefore mTORC1 may play a role in the upregulation of HIF-mediated transcription in FLCN-deficient UOK257 cells. However, treatment of FLCN-deficient UOK257 cells with rapamycin did not appear to result in a decrease in the mRNA levels of VEGF-A (Figure 6C). Interestingly, under conditions of both normoxia and hypoxia, only very low mRNA levels were observed for BNIP3, CCND1 and VEGF-A (Figure 6A, Figure 6B, and Figure 6C respectively) were detected in the UOK257-2 cells under conditions of both normoxia and hypoxia. In fact, these data show no increase in the CCND1 and VEGF-A mRNA levels in the UOK257-2 cells under normoxic conditions compared to hypoxic conditions, suggesting that when FLCN is overexpressed, this hypoxic response is lost. No difference in VEGF-A mRNA

levels was observed under conditions of rapamycin treatment, suggesting that the elevated levels of VEGF-A gene transcripton in these cells lacking FLCN is rapamycin insensitive.

The mRNA levels of HIF transcriptional targets which regulate the metabolism of glucose were also analysed; glucose transporter 1 (GLUT1) (Figure 6D) and glucose-6-phosphate dehydrogenase 1 (G6PD1) (Figure 6E). GLUT1 is involved with the uptake of glucose into the cell while G6PD1 helps maintain cellular redox homeostasis via the pentose phosphate pathway**.** Increased levels of both GLUT1 and G6PD1 mRNA were observed in the FLCN-deficient UOK257 cells under conditions of both normoxia and hypoxia. Treatment of either cell line with rapamycin did not result in a difference in mRNA levels of GLUT1, suggesting that transcription of GLUT1 (like VEGF-A) is rapamycin insensitive. Higher levels of GLUT1 mRNA suggest that there are likely to be higher levels of glucose uptake in the UOK257 cells and that these cells may be more glucose dependent than the UOK257-2 cells.

To confirm that loss of functional FLCN causes increased protein expression of downstream HIF transcriptional targets, the total protein levels of CCND1, BNIP3, GLUT1, and VEGF-A were analysed via western blot (Figure 6F). I observed an increase in BNIP3, VEGF-A and GLUT1 protein levels in the UOK257 cells under conditions of normoxia and hypoxia when compared to the UOK257-2 cells. Increased protein levels of CCND1were also observed in the FLCN-deficient UOK257 cells compared to the UOK257-2 cells under conditions of hypoxia.

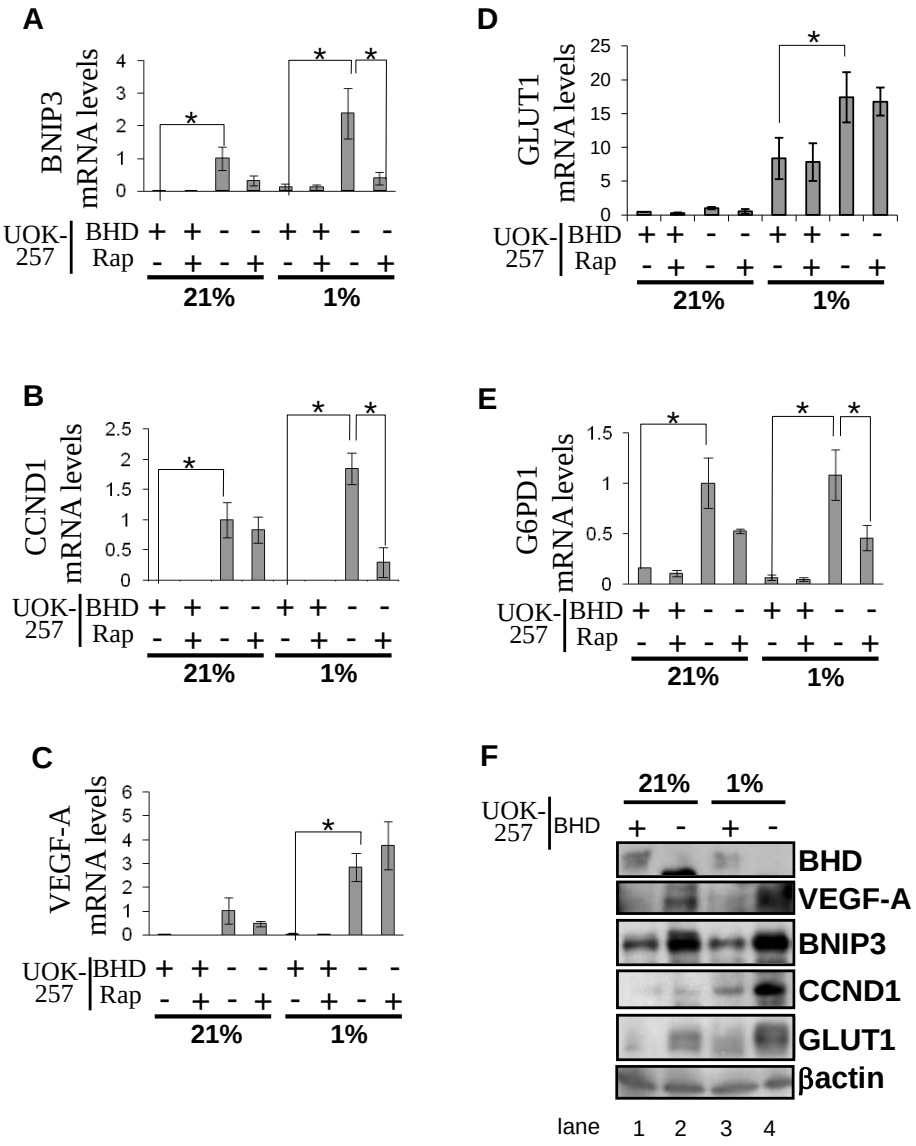

Figure 6. HIF transcriptional activity is negatively regulated upon expression of FLCN.

The levels of BNIP3 mRNA **(A)**, CCND1 mRNA **(B)**, VEGF mRNA **(c)**, GLUT1 mRNA **(D)**, and G6PD1 mRNA **(E)** were determined within UOK257 and UOK257-2 cell lines maintained in 21% or 1% oxygen and treated with 50nm rapamycin where indicated by RT-PCR. The levels of mRNA for each of the genes were standardised against β-Actin mRNA. n = 3. * = significant at the 0.05 significance level. ** = significant at the 0.01 significance level. **(F)** Western blot analyses were performed on cell lysates prepared from UOK257 and UOK257-2 cells maintained in 21% or 1% oxygen where indicated. Protein levels of Folliculin, BNIP3, VEGF-A, GLUT1, CCND1, and β-Actin were determined.

2.2.2 Loss of functional FLCN in UOK257 cells does not affect HIF1α or HIF2α protein or mRNA levels

To establish if HIF1α and HIF2α are regulated by BHD at the gene-expression level, HIF1α mRNA levels (Figure 7A) and HIF2α mRNA levels (Figure 7B) were compared within the UOK257 and UOK257-2 cell lines using RT-PCR. Under conditions of both normoxia and hypoxia no significant difference in the mRNA levels of HIF1α was observed between the UOK257 and UOK257-2 cell lines. A significant increase in HIF2α mRNA levels was observed when cells were subjected to hypoxia; however FLCN did not appear to regulate this increase. Li *et al.* also observed that hypoxic conditions resulted in an increase in HIF2α mRNA levels in glioma stem cells but HIF1α mRNA levels were unaffected (Li *et al.*, 2009). When the protein levels of both HIF1α and HIF2α were analysed under normoxic and hypoxic conditions via western blot, an accumulation of HIF1α and HIF2α protein under conditions of hypoxia was observed in the UOK257 and UOK257-2 cells (Figure 7C). In both of the cell lines, the accumulation of HIF1α protein was to a similar level; however there was an increased level of HIF2α protein in the UOK257-2 cells under hypoxic conditions.

The effect of over-expression of FLCN on HIF activity was further analysed by transfecting FLCN-deficient UOK257 cells with a luciferase reporter construct containing 7x HIF response elements (HRE), together with either Flag-tagged *BHD* or pRK7 empty vector. A higher level of HIF activity was observed in the FLCN-deficient cells (lane 1, Figure 7D) which was decreased when the cells were transfected with *BHD* (Lane 2, Figure 7D). Rapamycin did not appear to repress HIF activity to the same extent as FLCN (Lanes 3 and 4, Figure 7D). Together, these data imply that over-expression of FLCN results in impaired HIF transcriptional activity rather than affecting the protein levels of HIF1α or HIF2α either through protein stability or gene-expression.

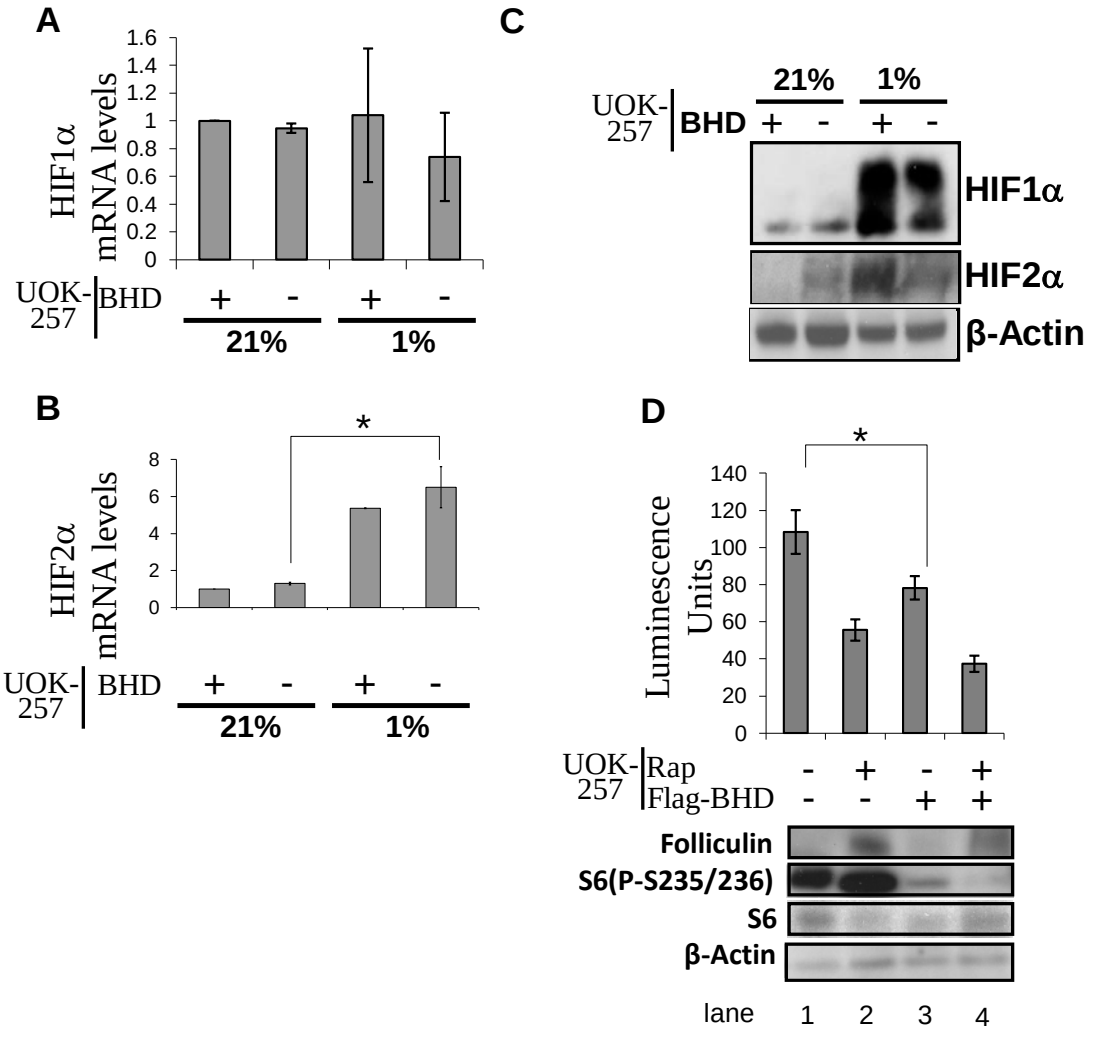

Figure 7. Increased levels of HIF1α and HIF2α – mediated transcription in FLCN-deficient cells

(A) HIF1α and **(B)** HIF2α mRNA levels were compared within UOK257 and UOK257-2 cells maintained under normoxic (21%) and hypoxic conditions (1%) overnight, where indicated, by RT-PCR. mRNA levels were standardised against β-Actin mRNA. n = 3. **(C)** Western blot analyses were performed on cell lysates obtained from UOK257 and UOK257-2 cells maintained under normoxic (21%) and hypoxic (1%) conditions and protein expression levels of HIF1α and HIF2α were determined. **(D)** BHD^- UOK257 cells transiently transfected with a HIF luciferase reporter construct containing 7x HIF response elements and either Flag-tagged *BHD* or pRK7 empty vector were maintained in hypoxia (1%) and treated with 50nm rapamycin for 24h where indicated. Levels of luminescence are representative of levels of luciferase and therefore HIF transcriptional activity. Western blot analyses were performed to determine protein levels of Folliculin, S6**,** and S6 (P-S235/236) were determined. n = 3.

2.2.3 HIF activity is enhanced upon BHD knockdown by small hairpin (sh)RNA under hypoxic conditons

To verify the results obtained from the experiments conducted in the UOK257 cell lines, another model was tested where endogenous *BHD* is knocked down by small hairpin (sh) RNA. The levels of HIF1α and HIF2α protein were determined along with HIF activity levels within the human kidney cancer cell line, ACHN, which had been stably transfected with either FLCN shRNA (BHD^-) or scrambled shRNA (BHD^+) (a kind gift from Arnim Pause). Protein levels of HIF1α and HIF2α within the ACHN BHD^+ and BHD^- cell lines under normoxic and hypoxic conditions were also analysed via western blot. These data showed that knockdown of *BHD* did not enhance the rise in HIF1α and HIF2α protein levels under hypoxic conditions (Figure 8a).

However, when HIF activity was determined by transfecting BHD^+ and BHD^- ACHN cells with a luciferase reporter construct containing 7x HIF response elements a threefold increase in HIF activity in the BHD^- ACHN cells was observed compared to those transfected with *BHD* (Figure 8B). Further confirmation that HIF transcriptional activity levels were upregulated in ACHN cells devoid of FLCN was obtained using RT-PCR by analysing VEGF-A mRNA levels within BHD^+ and BHD^- ACHN cells (Figure 8C). These results suggested that BHD^- ACHN cells have increased levels of VEGF-A mRNA when compared to the BHD^+ ACHN cells. Collectively, these data support the data from the UOK257 cells suggesting that HIF activity under hypoxic conditions is enhanced upon loss of *BHD*.

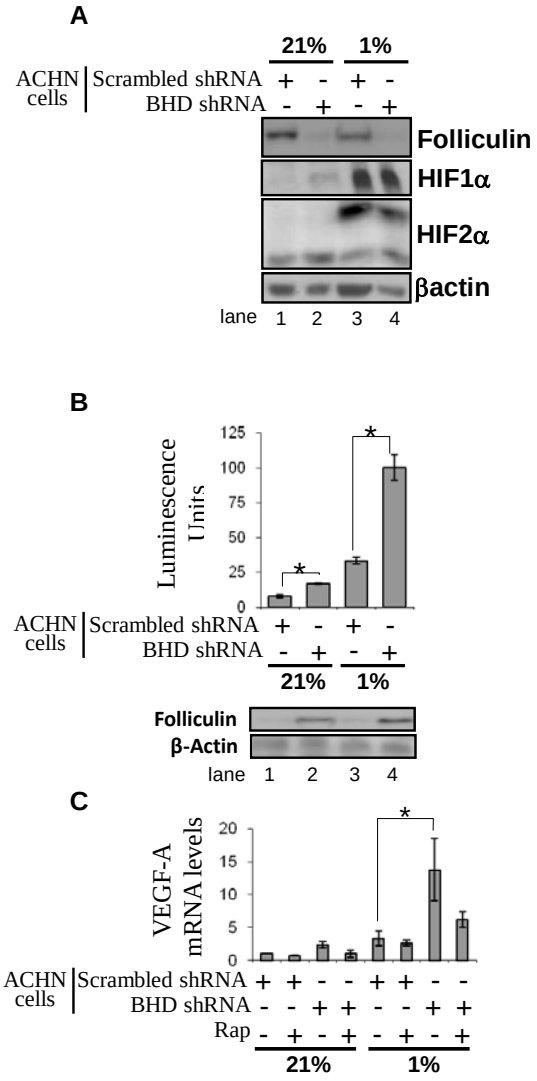

Figure 8. HIF transcriptional activity is upregulated in ACHN cells upon loss of *BHD* via shRNA.

(A) Western blot analyses were performed on cell lysates prepared from ACHN cells which have been stably transfected with *BHD* shRNA (*BHD*$^-$) or scrambled shRNA (*BHD*$^+$) and maintained under normoxic (21%) and hypoxic (1%) conditions. Protein expression levels of HIF1α and HIF2α were determined. **(B)** ACHN cells stably transfected with scrambled shRNA (*BHD*$^+$) or *BHD* shRNA (*BHD*$^-$) were transiently transfected with a HIF luciferase reporter construct containing 7x HIF response elements and a renilla control under normoxic (21%) and hypoxic (1%) conditions where indicated. Levels of luminescence are representative of levels of luciferase and therefore HIF transcriptional activity. Western blot analyses were performed and protein levels of Folliculin were determined. n = 3. **(C)** The mRNA levels of VEGF-A were compared within ACHN cells stably transfected with scrambled shRNA (*BHD*$^+$) or *BHD* shRNA (*BHD*$^-$), maintained under normoxic (21%) and hypoxic (1%) conditions overnight, and treated with 50nm rapamycin where indicated, by RT-PCR. mRNA levels were standardised against β-Actin mRNA. n = 3. * = significant at the 0.05 significance level. ** = significant at the 0.01 significance level.

To support the work conducted using the UOK257 and ACHN cell lines HIF activity and protein levels were analysed in two other cell lines. HIF activity was analysed within $BHD^{+/+}$ and $BHD^{-/-}$ Mouse Embryonic Fibroblasts (MEFs) (a kind gift from Prof. Arnim Pause) by transfecting $BHD^{+/+}$ and $BHD^{-/-}$ MEF cells with a luciferase reporter construct containing 7x HIF response elements. An increase in HIF activity was apparent in the $BHD^{-/-}$ MEF cell line (Figure 9a). The mRNA levels of BNIP3 (Figure 9B) within the $BHD^{+/+}$ and $BHD^{-/-}$ MEF cells were also analysed using RT-PCR. These results suggested that $BHD^{-/-}$ deficient MEF cells have increased levels of BNIP3 mRNA compared to the $BHD^{+/+}$ MEF cells. This data was consistent with increased HIF activity levels in the $BHD^{-/-}$ MEF cells observed in Figure 9a.

HIF activity was also analysed in Human Kidney 2 (HK2) cells (a kind gift from Prof. Maurice Van Steensel's lab) which had been stably transfected with either scrambled shRNA (BHD^{+}) or *BHD* shRNA (BHD^{-}). BHD^{+} and BHD^{-} HK2 cells were transfected with a luciferase reporter construct containing 7x HIF response elements. An increase in HIF activity in the BHD^{-} HK2 cells compared to the BHD^{+} HK2 cells was observed (Figure 10a). Protein levels of VEGF-A and BNIP3 (Figure 10B) were also analysed within BHD^{+} and BHD^{-} HK2 cells under hypoxic conditions via western blot. These results suggest that BHD-deficient HK2 cells have increased protein expression of VEGF-A and BNIP3 protein. These data supported the increased levels of HIF activity in the BHD^{-} HK2 cells observed in Figure 5a; and support the notion that HIF activity under hypoxic conditions is enhanced upon loss of FLCN.

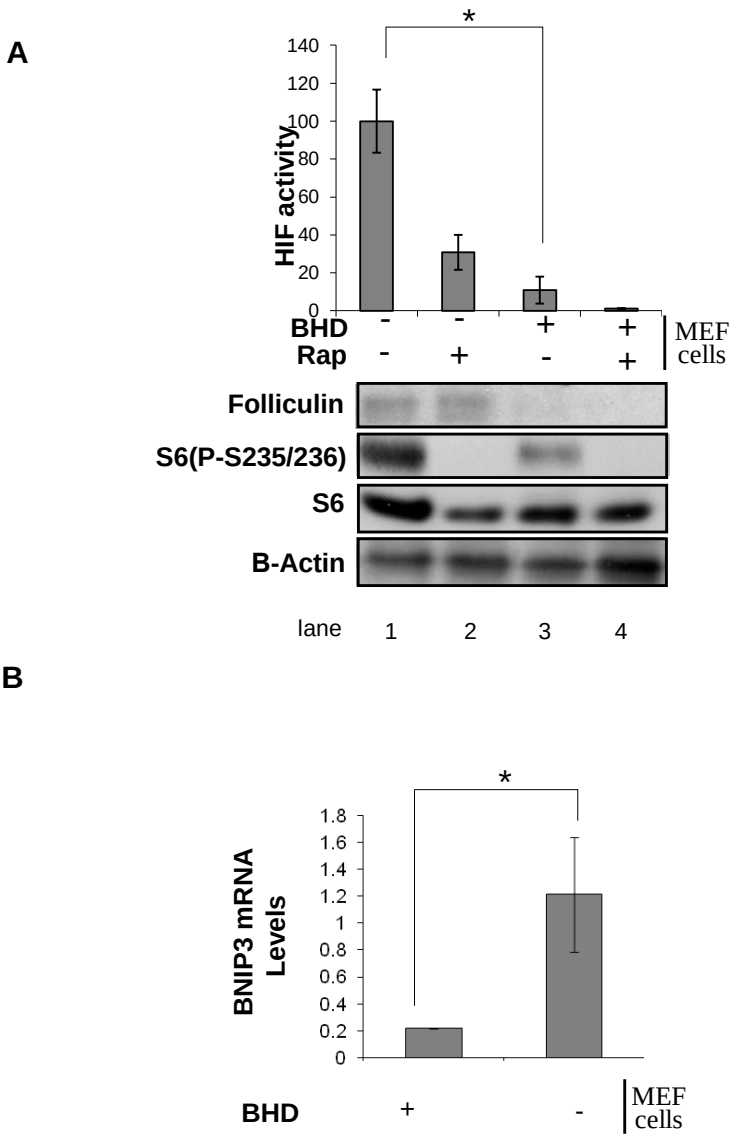

Figure 9. HIF1α transcriptional activity is upregulated in *BHD*$^{-/-}$ MEF cells.

(A) *BHD*$^{+/+}$ and *BHD*$^{-/-}$ MEF cells were transiently transfected with a HIF luciferase reporter construct containing 7x HIF response elements and a renilla control under hypoxic (1%) conditions and treated with 50nm rapamycin where indicated. Levels of luminescence are representative of levels of luciferase and therefore HIF transcriptional activity. Western blot analyses were performed and protein levels of Folliculin, S6**,** and S6 (P-S235/236) were determined. n = 3. **(B)** The mRNA levels of BNIP3 were compared within *BHD*$^{+/+}$ and *BHD*$^{-/-}$ MEF cells maintained in hypoxia (1%) overnight by RT-PCR. mRNA levels were standardised against β-Actin mRNA. n = 3. * = significant at the 0.05 significance level. ** = significant at the 0.01 significance level.

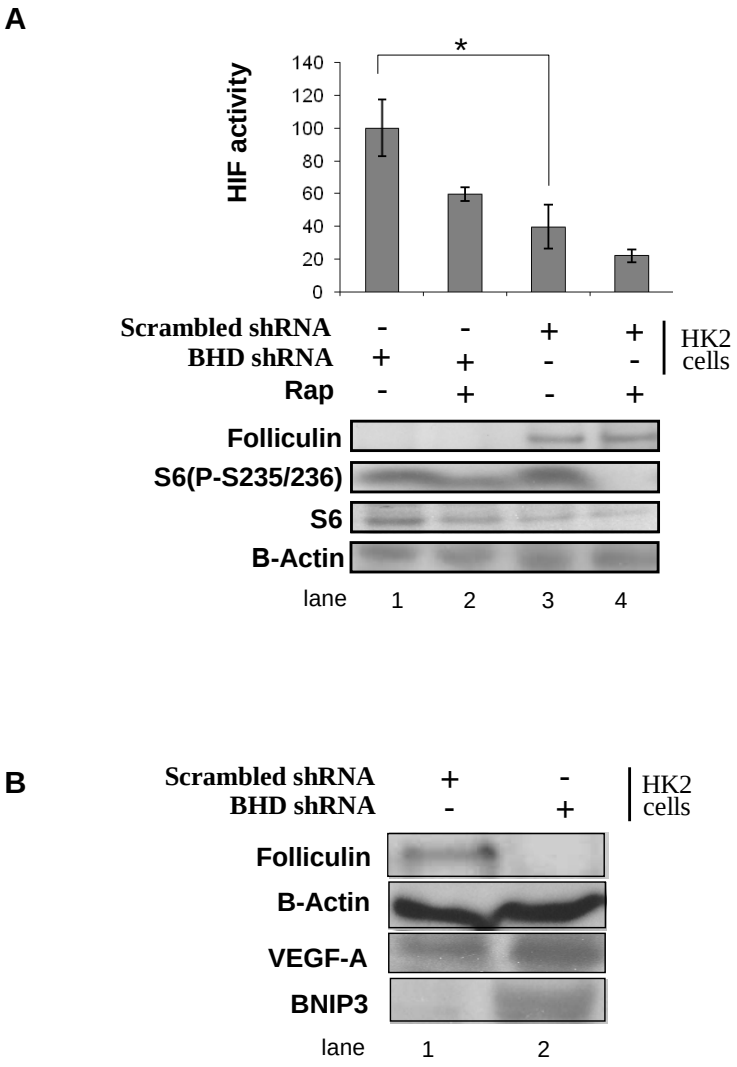

Figure 10. HIF transcriptional activity is upregulated in HK2 cells upon loss of *BHD*.

(A) HK2 cells stably transfected with *BHD* shRNA (*BHD*$^-$) or scrambled shRNA (*BHD*$^+$) were transiently transfected with a HIF luciferase reporter construct containing 7x HIF response elements and a renilla control under hypoxic (1%) conditions and treated with 50nm rapamycin where indicated. Levels of luminescence are representative of levels of luciferase and therefore HIF transcriptional activity. Western blot analyses were peformed and protein levels of Folliculin, S6**,** and S6 (P-S235/236) were determined. n = 3. * = significant at the 0.05 significance level. ** = significant at the 0.01 significance level. **(B)** Western blot analyses were performed on cell lysates prepared from HK2 cells which had been stably transfected with scrambled shRNA (*BHD*$^+$) or *BHD* shRNA (*BHD*$^-$) and maintained under hypoxic (1%) conditions. Protein expression levels of VEGF-A, BNIP3, Folliculin and β-Actin were determined.

2.2.4 UOK257 cells exhibit a metabolic profile which resembles the 'Warburg effect'

As the work conducted on multiple cell lines shows that loss of functional FLCN results in increased HIF activity, it was hypothesised that energy metabolism would also be modulated within these cells due to the increase in HIF activity. As part of this study, work was conducted by Dr. Andrew Tee into determining the activity levels of a series of metabolic enzymes (shown in Figure 11a) within the UOK257 cell lines. Enzymes analysed were involved in the Krebs cycle, fatty acid oxidation as well as glucose metabolism. These data revealed no significant differences in the activity of hexokinase between the UOK257, UOK257-2, and HEK293 cell lines (representative of a 'normal' human kidney cell line) (Figure 11B). However increased activity levels of the enzymes Pyruvate kinase (Figure 11C) and Lactate dehydrogenase (LDH) (Figure 11D) was observed in the FLCN-deficient UOK257 cell line. These increased levels of LDH and Pyruvate kinase activity within FLCN-deficient cells should lead to an increase in L-lactate production.

An increase in 3-hydroxy-acyl- CoA was also observed in the FLCN-deficient UOK257 cells (Figure 11E), implying that fatty acid oxidation may also be upregulated within the UOK257 cell line. No difference in the activity of citrate synthase (Figure 11F) and malate dehydrogenase (Figure 11G) (involved in the Krebs cycle) was observed between the UOK257, UOK257-2 and HEK293 cell lines. The term 'warburg effect' refers to the ability of tumour cell lines to break down glucose via glycolysis at an increased rate compared to normal cell lines, even in the presence of oxygen, resulting in glucose being converted to L-lactate (Warburg, 1956). These data collectively suggest that UOK257 cells lacking FLCN exhibit a metabolic profile that resembles the 'Warburg effect'.

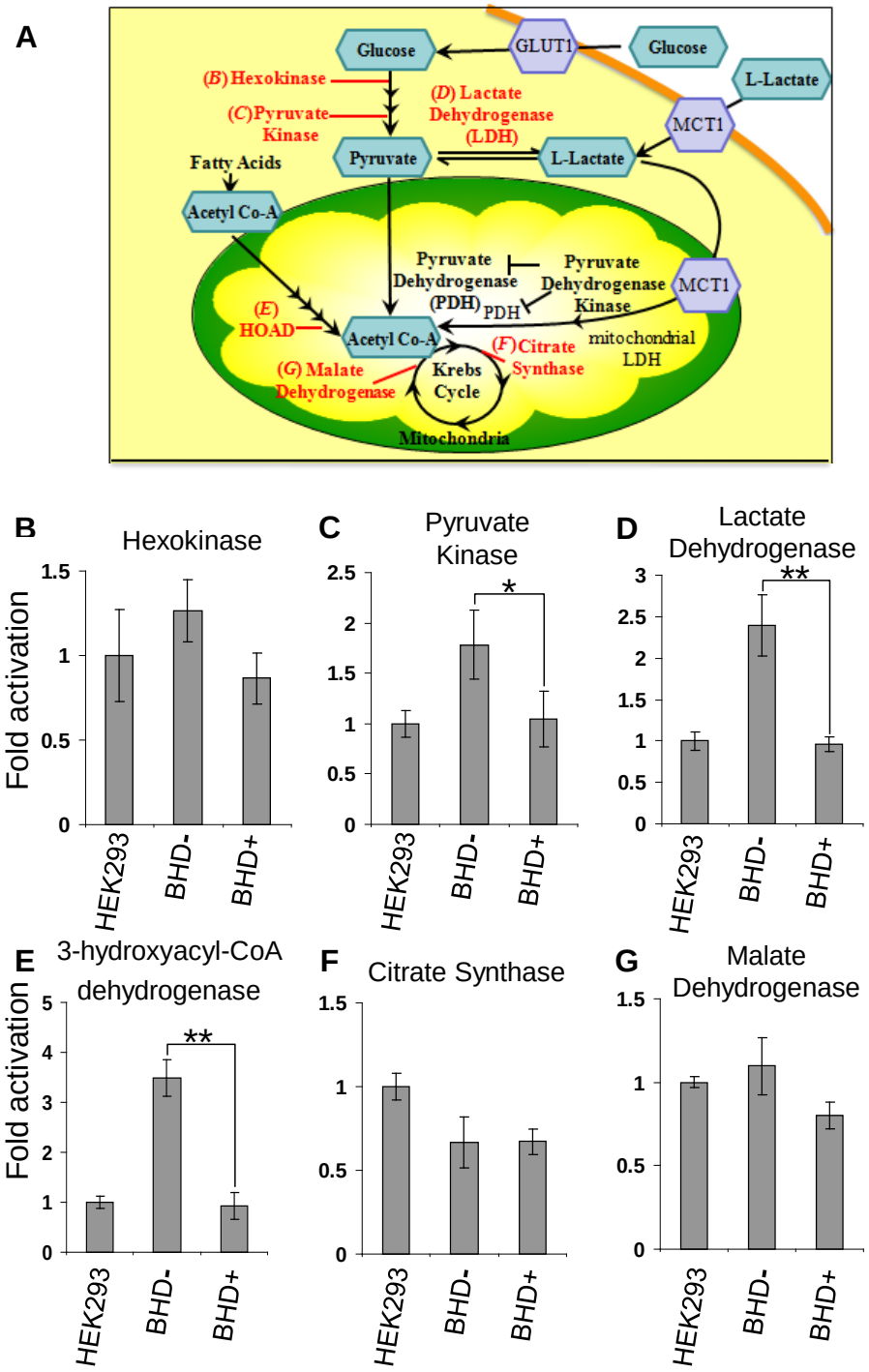

Figure 11. The levels of activity of the enzymes pyruvate kinase, HOAD and lactate dehydrogenase are increased in FLCN-deficient UOK257 cells.

(A) Diagram showing aerobic and anaerobic metabolism of glucose and fatty acids. Enzyme activity levels of **(B)** hexokinase, **(C)** pyruvate kinase, **(D)** lactate dehydrogenase, **(E)** 3-hydroxyacyl-CoA dehydrogenase, **(F)** citrate synthase, **(G)** malate dehydrogenase in BHD^- UOK257, $FLCN^+$ UOK257-2) and HEK-293 cells were determined by enzyme activity assays. (Work conducted by Dr. Andrew Tee). * = significant at the 0.05 significance level. ** = significant at the 0.01 significance level.

2.2.5 UOK257 cells lacking FLCN favour glycolysis

Pyruvate is a substrate for either LDH, which results in the production of L-lactate, or pyruvate dehydrogenase (PDH), which converts pyruvate to acetyl CoA which then goes into the Krebs cycle (shown in Figure 11a). Under conditions of low oxygen, PDH is phosphorylated and inhibited by pyruvate dehydrogenase kinase 1 (PDK1), resulting in more pyruvate being converted to L-lactate by LDH and the conversion of pyruvate to acetyl-coA being limited (Wigfield *et al*., 2008). Given that an increase in LDH activity was observed in the FLCN-deficient UOK257 cells, I wanted to analyse the phosphorylation status of PDH within the UOK257 cell line as an indication of PDH activity. Therefore, Western blot analyses were performed in order to analyse the protein expression of PDK1 and phosphorylated PDH (Figure 12). PDK1 protein levels were significant increased in the FLCN-deficient UOK257 cells compared to UOK257-2 cells under both normoxic (Figure 12, lanes 1 and 3) and hypoxic conditions (Figure 12, lanes 5 and 7). Increased levels of PDH phosphorylation in the FLCN-deficient UOK257 cells were also observed (Figure 12, lanes 3 and 7), suggesting that PDH is phosphorylated and inhibited by PDK1 in these cells. The protein levels of phosphorylated ribosomal protein S6 were also analysed as an indication of the levels of mTORC1 signalling. In line with previous reports by Hartman *et al.,* (2009) I observe an increase in the level of rpS6 phosphorylation in the FLCN-deficient UOK257 cells, suggesting that there is an increased basal level of mTOR signalling within the FLCN-deficient UOK257 cells. This increase in rpS6 phosphorylation was effectively repressed upon treatment with rapamycin (Figure 12, lane 4). Only low levels of rpS6 phosphorylation were detected within the FLCN-deficient UOK257 cells under hypoxic conditions (Figure 12, lane 7). This result was expected, as hypoxia is known to repress mTORC1 signalling (Liu *et al.,* 2003).

The western blot also revealed that there are increased levels of Thr308 phosphorylation of AKT within the FLCN-deficient UOK257 cells (figure 12, lanes 3 and 7). These data suggest that UOK257 cells exhibit increased levels of LDH activity and PDH phosphorylation; implying that UOK 257 cells may convert pyruvate to L-Lactate more readily.

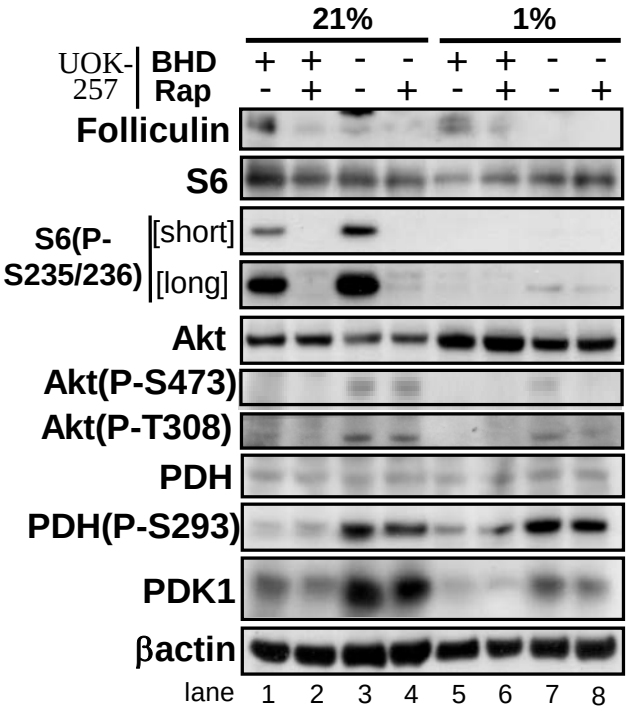

Figure 12. The Krebs cycle enzyme PDH is inhibited by enhanced expression of PDK1 upon loss of FLCN.

UOK257-2 and UOK257 cells growing in DMEM were washed with fresh DMEM and maintained in 21% oxygen or 1% oxygen and treated with rapamycin as indicated. Protein expression levels of PDK1, PDH, PDH (P-S293), Akt, Akt (P-T308), Akt (P-S473), S6, S6 (P-S2350236), Folliculin and β-Actin were determined.

2.2.6 L-lactate is used by FLCN-deficient UOK257 cells as a metabolic fuel

The next stage in determining whether glycolysis is increased in UOK257 cells was to examine whether there was increased L-Lactate production via facilitated diffusion within these cells. Interestingly, when extracellular acidification was measured as an indication of L-lactate production and glycolytic rate, no difference was observed between the UOK257 and the UOK257-2 cell lines (Figure 13a). However, monocarboxylate transporter 1 (MCT1), involved in L-Lactate influx, and MCT4, involved in the efflux of L-Lactate, revealed that the BHD^- UOK257 cells express more of the MCT1 but not of the MCT4 (Figure 13b lanes 1 and 4).

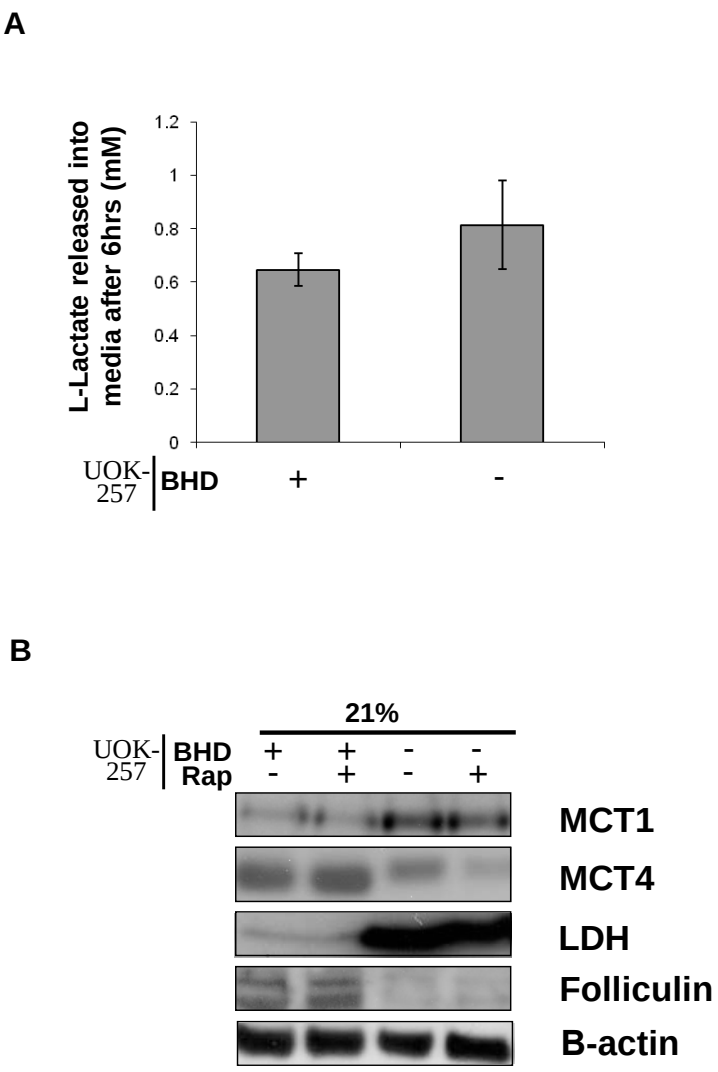

Figure 13. UOK257 cells are able to use L-lactate as a metabolic fuel.

(A) UOK257 and UOK257-2 cells growing in DMEM were washed with fresh DMEM and maintained in 21% oxygen. After 6 hours this media was removed. L-lactate levels within these samples were analysed using an EnzyChrom L-Lactate Assay Kit according to manufacturer's protocol. Level of absorbance is representative of the amount of L-lactate within the growth media of the cells after 6 hours. **(B)** Western blot analyses were performed on cell lysates prepared from UOK257 and UOK257-2 cells treated with and without 50 nm rapamycin as indicated. Protein expression levels of MCT1, MCT4, LDH, Folliculin and β-Actin were determined.

2.3 Discussion

2.3.1 Increased levels of HIF activation may be involved in cancer progression and the development of renal tumours and cyst formation in BHD patients

HIF plays a pivotal role in tumour development in a number of inherited genetic disorders which result in RCCs. These include VHL, HLRCC and TSC (Kaelin, 2005; Isaacs *et al.*, 2003; Liu *et al*., 2003). HIF promotes tumour progression by mediating the expression of genes involved in cellular metabolism, glucose transport, cell survival, angiogenesis and metastasis. The data presented suggests an abnormal level of HIF activation may be involved in cancer progression and the development of renal tumours and cyst formation in BHD patients (Tuder *et al.*, 2006). The fact that increased levels of HIF activity are observed across multiple FLCN-deficient cell lines suggests that these findings may be applicable to multiple types of tumours found in BHD patients. This notion is further supported by the immunohistochemical data provided by Prof Maurice Van Steensel's lab conducted on chromophobe carcinomas from patients with BHD; in which increased levels of BNIP3, VEGF-A and GLUT 1 are observed (Preston *et al.*, 2011).

2.3.2 Increased levels of BNIP3 mRNA levels may serve a protective function in BHD-deficient cells

Data obtained from multiple BHD cell line models revealed that cells deficient in BHD have increased levels of both BNIP3 mRNA and protein. Immunohistochemistry (provided by Prof Maurice Van Steensel) also showed elevated levels of BNIP3 staining in the BHD patient chromophobe carcinoma tissue. Although multiple studies have shown that cell death

via either necrosis or apoptosis is induced by BNIP3, contrasting results have also suggested that BNIP3 promotes cell survival; possibly via upregulation of autophagy (Burton *et al.*, 2009). Therefore, it may be possible that the change in expression pattern of BNIP3 is indicative of a protective function of BNIP3 in the chromophobe tumour. Furthermore, this work highlights the possibility that autophagy may be functioning as a protective mechanism within these tumour cells (further discussed in chapter 4).

2.3.3 HIF transcriptional activity rather than HIF protein stability is enhanced upon loss of functional FLCN.

The way that HIF signalling becomes disregulated varies between different inherited disorders. In VHL and HLRCC, Increased stability of HIFα proteins is considered a major factor in tumour development (Bratslavskey *et al.*, 2007; Issacs *et al.*, 2005). The data obtained from the ACHN cell line suggested that the BHD^- ACHN cells have an increased basal level of HIF1α protein under normoxic conditions compared to the ACHN cells expressing endogenous BHD. However no difference in the protein levels of HIF1α or HIF2α was observed between the BHD^- ACHN cells and the ACHN cells expressing endogenous BHD under hypoxic conditions. This is further supported by data obtained from the UOK257 cell line which revealed no significant difference in the mRNA or protein levels of HIF1α between the UOK257 (BHD^-) and UOK257-2 (BHD^+) cell lines under conditions of both normoxia and hypoxia. An increased level of HIF2α protein in the UOK257-2 (BHD^+) cell line compared to the UOK257 (BHD^-) cell line was also observed under hypoxic conditions. It is probably increased levels of HIFα activity rather than protein stability which result in the increased HIF-driven gene expression observed in the BHD deficient cell lines. However immunohistochemistry conducted by Prof Maurice Van Steensel's lab on

chromophobe carcinoma tissue from BHD patients showed elevated levels of HIF1α protein in the chromophobe carcinoma tissue of the BHD patient (Preston *et al.,* 2011). It is likely that the increased protein levels of HIF1α observed in the chromophobe carcinoma tissue is reflective of hypoxic tissue. It, therefore, cannot be ruled out that protein stability of HIF1α may be enhanced during tumour progression in BHD patients.

2.3.4 mTOR activity is enhanced upon loss of functional FLCN in BHD-deficient UOK257 cells.

The data obtained from the UOK257 cell line show that there are also increased levels of rpS6 phosphorylation within the BHD^- UOK257 cells compared to the UOK257-2 cells. These data suggest that mTORC1 activity is upregulated in UOK257 cells deficient in BHD which was inhibited upon rapamycin treatment or over-expression of BHD. Immunohistochemistry conducted by Prof Maurice Van Steensel's lab on chromophobe carcinoma tissue from BHD patients also showed increased staining for phosphorylated rpS6 in the chromophobe carcinoma tissue of the patient compared to normal tissue (Preston *et al.,* 2011). Work conducted by Baba *et al*. has also shown that Akt/mTOR pathway is hyperactivated in cells deficient in BHD (Baba *et al.,* 2008). This notion is supported by the observation of elevated levels of phosphorylation of Akt at Ser 473 (the mTORC2 phosphorylation site) in the BHD^- UOK257 cells; indicative of increased Akt activation by mTORC2. Hasumi *et al.* have also observed increased mTORC2 activity levels along with increased expression levels of rictor (a regulator of mTORC2) in tumours from $BHD^{d/+}$ mice (Hasumi *et al.,* 2009). mTORC2 has also been shown to phosphorylate and stabilise Akt (Facchinetti *et al.,* 2008); suggesting that it is the activation of mTORC2 which is the primary mechanism by which Akt is activated in FLCN-deficient tumours. Together with data from

work conducted by Baba *et al.* which suggest that phosphorylation of FLCN was partially blocked by rapamycin (an mTOR inhibitor) and thus mTOR regulates FLCN function (Baba *et al.,* 2006); these data suggested that FLCN is involved in a negative feedback loop which suppresses PI3K-Akt-mTOR signalling (Hasumi *et al.,* 2009). Increased phosphorylation levels of ribosomal protein S6 kinase 1 and 4E-BP1 have also been observed in *TSC1* and *TSC2* deficient cells which is inhibited by rapamycin; consistent with constitutive activation of mTORC1 (Kwiatkowski *et al.,* 2003). These data suggest that mTOR activity is elevated upon loss of functional FLCN in a manner analogous to *TSC1* and *TSC2*-deficient cells. This is quite the reverse to the results from work conducted by Hartmen *et al.,* which showed that mTOR is inactivated in BHD-deficient mice. The results obtained by Hartman *et al.* suggested that the increased levels of mTOR activation observed in cell lines such as the UOK257 cell line was not a primary effect as a result of loss of BHD, but mTOR is activated later in the cancer development due to increased activity levels of kinases such as Akt upstream of mTOR in a similar manner to that exhibited in TSC deficient cell lines (Hartman *et al.,* 2009). However, these diffences of opinion on the effects of loss of functional folliculin may be attributed to the differences in the models used in this study and that conducted by Hartman *et al.* and the length of time that functional folliculin has not been expressed.

2.3.5 HIF transcriptional activity may be regulated via mTORC1- dependent and independent mechanisms in BHD deficient cells.

In TSC, upregulation of mTORC1 signalling is known to mediate increased HIF activity (Land and Tee, 2007). Land and Tee observed increased levels of HIF activity in cells deficient of *TSC2*, which was reversed when *TSC2* was added back to the cells or mTOR was inhibited with rapamycin (Land and Tee, 2007). In fact, mTOR inhibition has been shown to

significantly reduce expression levels of HIFα protein in several types of cells (Knaup *et al.*, 2009). Given that increased levels of mTOR signalling are observed in the UOK257 cells it may be possible that increased mTORC1 signalling may also be promoting the activity of HIF within the FLCN-deficient UOK257 cells. This notion is supported by the fact that inhibition of mTOR via treatment with rapamycin impairs the accumulation of G6PD1, CCND1 and BNIP3 mRNA within the BHD$^-$ UOK257 cell line under hypoxic conditions. HIF activity within the BHD$^-$ UOK257 cell line and the *BHD*$^{-/-}$ MEF cell line, as analysed using a HIF luciferase reporter construct, is also significantly reduced upon treatment with rapamycin.

Elevated levels of rpS6 phosphorylation are observed under hypoxic conditions in the UOK257 cells compared to the UOK257-2 cells, suggesting that activation of mTOR may play a part in the regulation of HIF transcriptional activity under hypoxic conditions. This is supported by the fact that hypoxia-driven accumulation of G6PD1, CCND1 and BNIP3 within the BHD$^-$ UOK257 cell line is impaired when mTORC1 is inhibited via treatment with rapamycin. HIF activity within the BHD$^-$ UOK257 cell line and *BHD*$^{-/-}$ MEF cell line under hypoxic conditions, as analysed using a HIF luciferase reporter construct, is also reduced upon treatment with rapamycin. However, rpS6 phosphorylation is still decreased in the UOK257cells under hypoxia compared to normoxic conditions. Work conducted by Knaup *et al.* suggests that HIF represses rpS6 under hypoxic conditions and that stimulation of HIFα by mTORC1 may only be relevant under mildly hypoxic, or even normoxic conditions. Knaup *et al.* also observed that in the majority of cancer cells they studied, no influence of mTOR inhibitors on HIFα protein levels was observed under severe hypoxic conditions (Knaup *et al.*, 2009). Hypoxia triggers dephosphorylation of mTORC1 and the downstream targets 4E-BP1, p70S6 kinase, and rpS6. Hypoxic inhibition of these targets is dominant to

activation via insulin or amino acids. This response was also thought to be independent of HIF1α (Arsham *et al.,* 2003). However, HIF is also known to express Redd1/2 which activate TSC2 via competitive binding for 14-3-3 proteins; leading to inhibition of mTORC1 (reviewed in Dunlop and Tee, 2009). The elevated mRNA levels of GLUT1 and VEGF-A observed in BHD^- UOK257 cells also did not appear to be rapamycin sensitive under hypoxic conditions. This result may also be explained by the increased levels of BNIP3 mRNA and protein expression observed in the FLCN-deficient cell lines, as work conducted by Li *et al.* suggested that BNIP3 inhibits mTORC1 activation by binding to Rheb (Li *et al.*, 2007). Therefore it is probable that mTORC1 signalling is required for transient bursts of HIF activity in the cells, rather than long term activation.

2.3.6 The increased levels of HIF activity observed in BHD-deficient cells is resulting in a metabolic profile similar to the 'Warburg effect'.

HIF1α is able to alter the metabolic profile of a cell by enhancing the gene-expression of glycolytic genes such as glucose transporter 1 (GLUT1) allowing increased glucose uptake. Under hypoxia, glucose is converted to pyruvate and then subsequently to L-lactate. Activation of glycolytic genes is considered a crucial adaptation to hypoxia (Kim *et al*., 2006). The data obtained from the UOK257 cell line show that the BHD^- UOK257 cells have increased mRNA and protein levels of GLUT1 compared to the BHD^+ UOK257-2 cells. Immunohistochemistry work conducted by Prof Maurice Van Steensel also revealed increased level of GLUT1 staining in chromophobe carcinoma tissue compared to normal tissue from BHD patients (Preston *et al.,* 2011). Together these data suggest that the BHD^- UOK257 cells have increased levels of glucose uptake into the cell. Increased mRNA levels of another HIF1α transcriptional target, glucose-6-phosphate dehydrogenase 1 (G6PD1),

were also observed in the (BHD^-) UOK257 cell line when compared to the (BHD^+) UOK257-2 cell line under both normoxic and hypoxic conditions. G6PDH is a NADPH-generating enzyme of the oxidative pentose phosphate pathway (OPPP). These data imply that BHD-deficient UOK257 cells may be more dependent on glucose than UOK257-2 cells expressing BHD and therefore are increasing the amount of glucose uptake and metabolism into the cell in order to meet their energy demands.

HIF1α also actively suppresses metabolism through the Krebs cycle by activating the gene encoding PDK1. PDK1 phosphorylates and inhibits PDH, which normally converts pyruvate to acetyl-CoA which can then enter the Krebs cycle. This causes a metabolic switch resulting in pyruvate being converted to lactate via the enzyme lactate dehydrogenase. Data obtained from examining the phosphorylation status of PDH within the UOK257 cells revealed that there are increased levels of PDK1 protein and phosphorylated PDH in the UOK257 cells under conditions of both normoxia and hypoxia. These data suggested that PDH activity was inhibited in the BHD^- UOK257 cell line, which was rescued in the UOK257-2 cells expressing BHD.

Data obtained from work conducted by Dr. Andrew Tee on the metabolic profile of the UOK257 cell line also suggested that the BHD^- UOK257 cells exhibit increased levels of LDH activity, along with increased levels of 3-hydroxy-acyl-CoA; implying that fatty acid oxidation may also be upregulated within the UOK257 cell line. These data suggest that BHD^- UOK257 cells exhibit an altered metabolic profile that resembles the ‘Warburg effect' as these cells appear to break down glucose via glycolysis at an increased rate, even in the presence of adequate oxygen levels, resulting in more glucose being converted to L-lactate in a manner analogous to that described by Otto Warburg (Figure 14) (Warburg, 1956). It may

appear more disadvantageous for the UOK257 cell line to favour glycolysis over oxidative phosphorylation, even in an adequate oxygen environment, as approximately 18 times less ATP is generated by glycolysis compared to oxidative phosphorylation. However, the metabolic changes observed when a cell exhibits the 'warburg effect' result in glucose entering the pentose phosphate pathway more readily, leading to increased production of nucleotides, aromatic amino acids and fatty acids, all of which are essential for cell proliferation (Van der Heiden *et al.*, 2009). There is also growing evidence that some cancer cells use L-Lactate as a metabolic fuel. Oxygenated cells on the outside of the tumour may take up and oxidise the L-Lactate which is produced by the cells situated in the hypoxic conditions within the core of a tumour (Sonveaux *et al.*, 2008).

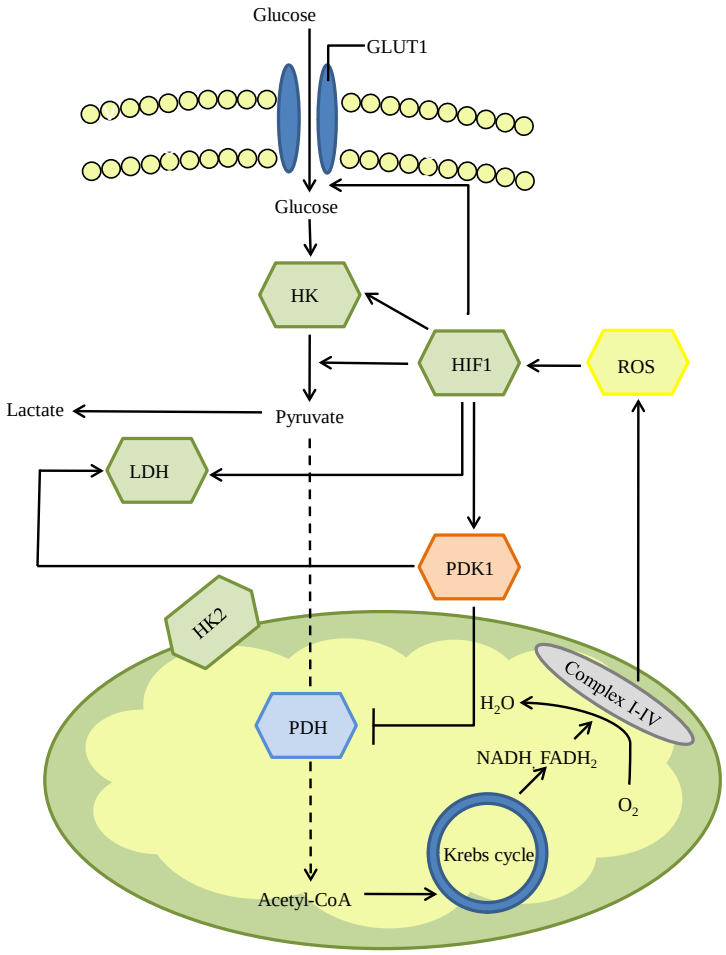

Figure 14. HIF activation and the Warburg effect.

HIF1 activates hexokinase 2 (HK2) and pyruvate dehydrogenase kinase 1 (PDK1), which results in inhibition of pyruvate dehydrogenase (PDH) and prevents glucose being converted from pyruvate to acetyl-CoA. As a consequence, pyruvate is instead preferentially converted to l-lactate. This is a contributing factor in the development of the 'Warburg effect' type metabolic profile (Dang*;* 2008).

Data from the UOK257 cell line suggest that although the BHD^- UOK257 cells exhibit increased LDH activity, which would increase L-Lactate production, no difference in L-Lactate secretion into culture media was observed between the BHD^- UOK257 and BHD^+ UOK257-2 cells.

This may be explained by the observation that BHD^- UOK257 cells exhibit elevated protein expression levels of the L-Lactate transporter MCT1, involved in the uptake of L-lactate into the cell. However no difference in another L-Lactate transporter, MCT4, involved in the export of L-Lactate from the cell was observed. Work conducted by Dr Keith Barr also revealed that the BHD^- UOK257 cells have a high capacity to oxidise L-Lactate (Preston *et al.*, 2011). Together these results imply that the BHD^- UOK257 cells are able to use L-Lactate as a metabolic fuel, and thus the ability for the UOK257 cells to readily convert glucose to lactate may provide a proliferative advantage. Data from immunohistochemistry conducted by Prof .Maurice van Steensel's lab on BHD patient tumour samples also revealed increased staining for LDH and MCT1 in the chromophobe carcinoma tissue compared to the normal tissue (data not shown); suggesting that this may be more broadly applicable to other BHD cell lines and tumour types, rather than just the UOK257 cell line.

Chapter 3

The effect of loss of functional Folliculin on mitochondrial biogenesis and mitochondrial function

3 The effect of loss of functional FLCN on mitochondrial biogenesis and mitochondrial function.

3.1 Introduction

In eukaryotic cells, mitochondria play a central role in cellular energy metabolism (Shadel, 2008). Contained within the intermembrane space of the mitochondria are mitochondrial enzymes, such as those involved in the Krebs cycle (Shadel, 2008). Mitochondria generate ATP via oxidative phosphorylation (oxPhos) of glycolysis and lipolysis products (Hock and Kralli, 2009). Many classic errors of metabolism result from genetic defects resulting in altered expression or activity of enzymes contained within the mitochondria which are involved in these processes. Some of these metabolic errors are caused by defects involving oxPhos complexes I-V. Common features of defects involving the oxPhos complexes include loss of ATP production, elevated levels of reactive oxygen species (ROS) production by complexes I and III of the electron transport chain, and irregular apoptosis. Mitochondrial function is also sensed and controlled by cell signalling pathways. Therefore disruption of the oxPhos complex may result in defective signal transduction (Shadel, 2008). Given their central roles in cellular metabolism and signalling, strict regulation of the mass and function of mitochondria is crucial (Hock and Kralli, 2009).

The growth and division of mitochondria is known as mitochondrial biogenesis and is upregulated under conditions of environmental stresses such as cell division, renewal and oxidative stress (Ventura-Clapier, 2008). The process of mitochondrial biogenesis requires the replication of mitochondrial DNA (mtDNA) as well as proteins and lipids being synthesised, imported, and incorporated into the mitochondria. Nuclear genes encode most of the proteins which are imported into the mitochondria as part of mitochiondrial biogenesis (Hock and Kralli, 2009). Human mtDNA is circular double stranded DNA which is

approximately 16.5 Kilobases in length and encodes 37 genes. 13 of these genes encode for integral components of the oxPhos complexes (Shadel 2008). It has been suggested that there is a significant correlation between mitochondrial mRNA levels and protein levels, implying that the mass of mitochondria in a cell is mostly regulated at the transcriptional level. Mitochondrial biogenesis requires the transcription of genes in the mitochondria and nucleus which are essential for the process to be coordinated (Hock and Kralli, 2009). This coordination is achieved via mitochondrial genes which are encoded in the nucleus, such as TFAM, that are induced in response to signalling pathways which promote mitochondrial biogenesis and regulate the replication and transcription of mtDNA (Hock and Kralli, 2009). This coordinates the activities of the nucleus and the mitochondria in order to regulate mitochondrial gene expression and oxPhos activity (Shadel, 2008).

During mitochondrial biogenesis, mitochondria undergo fission and fusion. This allows the existing mitochondria to divide and helps ensure that mitochondrial structures are organised correctly during biogenesis (Ventura-Clapier, 2008).

Peroxisome proliferator–activated receptors (PPARs) regulate genes located within the mitochondria which are involved in uncoupling and fatty acid oxidation (Hock and Kralli, 2009). PGC1α interacts with and coactivates many nuclear and nonnuclear receptors such as NRF1/NRF2 and mitochondrial transcription factor A (TFAM), which is directly responsible for the replication and transcription of mtDNA (Figure 15) (Bogacka *et al*., 2005). PGC1α is therefore able to enhance mitochondrial biogenesis and the oxidative function of a cell.

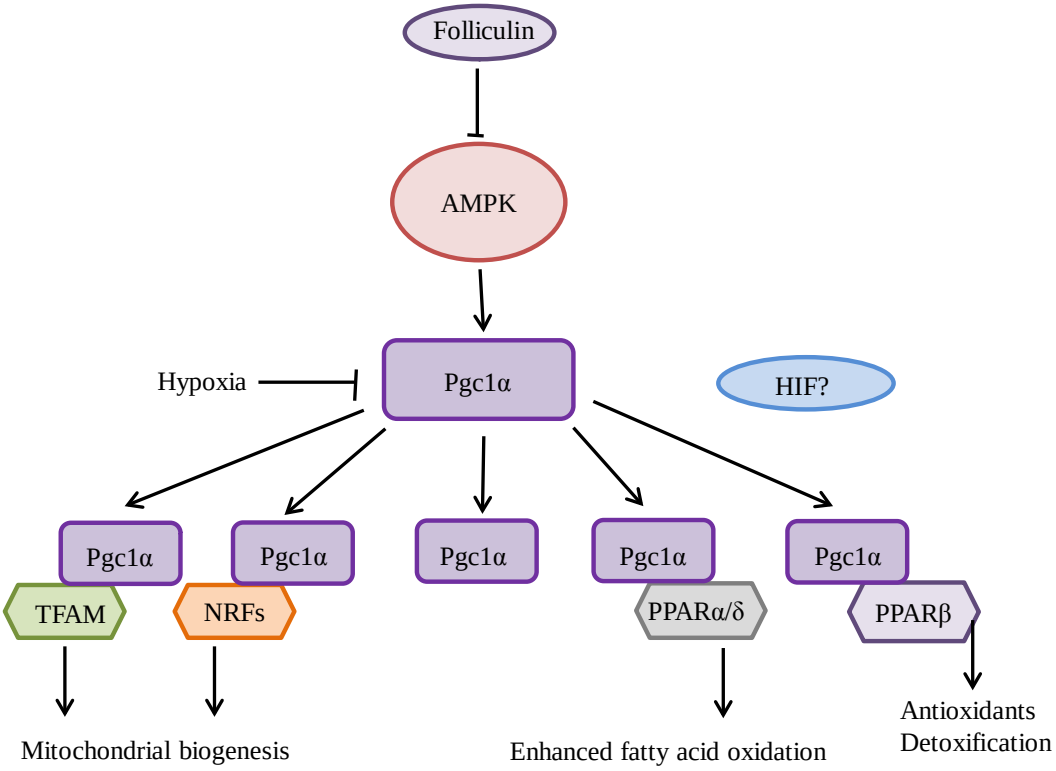

Figure 15. The PGC1α regulatory cascade.

PGC1α has been shown to be regulated by several signalling pathways including activation of adenosine-monophosphate-activated kinase (AMPK). PGC-1α then co-activates transcription factors involved in mitochondrial biogenesis such as TRβ1 and nuclear respiratory factors (NRFs), and PPARs, known to regulate fatty acid oxidation, and antioxidant detoxification (Ventura-Clapier, 2008).

Related coactivators such as PGC1β also functions similarly to PGC1α (Hock and Kralli, 2009). PGC1α may be activated via the cAMP/PKA cascade increasing PGC1α gene expression or by activation of the p38 MAPK and/or cAMP/p38 MAPK cascade which results in phosphorylation of the PGC1α protein (Bogacka *et al.*, 2005). Several transcription factors have been implied in the regulation of PGC1α gene expression. The transcription

factor CRE (CAMP response element) binding protein (CREB) is able to activate transcription of PGC1α. This occurs via binding of CREB to a functional CRE in the promoter region of PGC1α (Kelly and Scarpulla, 2004).

Expression of PGC1α in cultured white fat cells also results in a doubling of mitochondrial DNA content and an increase in mRNA for uncoupling protein 1 (UCP1), and several genes of the oxidative phosphorylation pathway. The uncoupling proteins (UCPs) are tissue specific intramembranous mitochondrial proteins and play an important role in thermogenesis. It has been shown that both UCP2 and UCP3 uncouple respiration when expressed in mammalian cells. Activating mitochondrial uncoupling is a major part of adaptive thermogenesis, a process that occurs primarily in the mitochondria of skeletal muscle and brown fat. During adaptive thermogenesis, elevated numbers of mitochondria and elevated levels of activity of the electron transport system in those mitochondria are observed in response to more energy being dispelled in the form of heat. This occurs in response to stimuli such as decreased external temperature. This may be due to the cells need to increase the overall levels of ATP production in order to preserve normal levels of ATP while so much energy is being dissipated as heat (Wu *et al.*, 1999).

It has been shown that the mTOR pathway is a key regulator for cellular metabolism. mTOR regulates several processes which are important to a cell, such as autophagy, protein synthesis, and nutrient uptake. It has also been shown that mitochondrial oxidative function is regulated by mTOR via alteration of the interaction of the YY1 – PGC1α transcriptional complex (Cunningham *et al.*, 2007).

TSC has also been shown to be an important regulator of cellular metabolism. Deletion of the *TSC1* gene in hematopoeitic stem cells (HSCs) drives them from quiescence, which is associated with their long-term function, into rapid cell cycling, resulting in increased

mitochondrial DNA content together with increased transcription of mitochondrial genes involved in oxidative phosphorylation, including Cox5a, Atp5a1 and Ucp3. This increase in the transcription of genes involved in oxidative phosphorylation subsequently leads to increased levels of ROS production in HSC cells deficient in *TSC1*. These results suggested that the TSC–mTOR pathway is involved in the maintenance of the quiescence and function in these cells via the repression of ROS production. When *TSC1* is deleted, increased level of ROS are observed, which is detrimental in metabolically active HSCs (Chen *et al.*, 2008).

Observations have also been made that chromophobe renal tumours from BHD patients had abnormally high levels of mitochondria; suggesting that loss of FLCN may result in an accumulation of mitochondria (Yang *et al.*, 2008). RCC syndromes are often associated with mitochondrial dysfunction. Cells within RCCs from HLRCC patients, which exhibit similar symptoms clinically to BHD patients, exhibit a decreased ability to generate ATP via the electron transport chain due to loss of function of the mitochondrial enzyme FH (Isaacs *et al.*, 2005; Sudarshan *et al.*, 2011). BHD patients also present with oncocytomas, known to exhibit defects within complex 1 of the mitochondria, along with increased mitochondrial DNA (mtDNA) content as a result of accumulation of mitochondria (Simonnet *et al.*, 2003).

As BHD-deficient cells also exhibit increased levels of mTOR activity in a similar manner to that observed in TSC-deficient cells (as discussed in Chapter 2), and both tumours from BHD and TSC patients, which exhibit overlapping clinical features to TSC patients, have been observed to have abnormal levels of mitochondria, I wanted to examine mitochondrial biogenesis in the UOK257 BHD patient cells line. In this chapter, I investigate the expression level of genes which regulate the transcription of mitochondrial genes and the replication of mitochondrial DNA in the context of loss of FLCN.

3.2 Results

3.2.1 Endogenous FLCN is localised to the Nucleus, Cytosol and Mitochondria.

Given that FLCN inhibits HIF activity, and HIF is a nuclear protein, I hypothesised that FLCN would also be localised to the nucleus. In order to investigate this, mitochondrial, nuclear and cytosolic fractions were prepared from fully confluent HEK293 cells, which express endogenous FLCN and are representative of a 'normal' kidney cell line. Levels of FLCN within these fractions were subsequently determined via western blot (Figure 16a). FLCN was detected in all three fractions; however the two isoforms of FLCN were differentially expressed in each fraction. The upper isoform of FLCN was detected in the nuclear fractions whereas the lower isoform of FLCN was detected in the mitochondrial fraction. Both of these isoforms were detected in the cytosolic fraction.

I next sought to determine whether the localisation of FLCN was altered under certain drug treatment conditions (Figure 16B). HEK293 cells were treated with 2-deoxyglucose (2DG); known to phosphorylate FLCN via activation of AMPK, and the mTORC1 inhibitor rapamycin, which is known to dephosphorylate FLCN (Baba *et al.*, 2006). Mitochondrial, cytosolic and nuclear fractions were prepared from these treated cells, together with untreated cells for comparison.

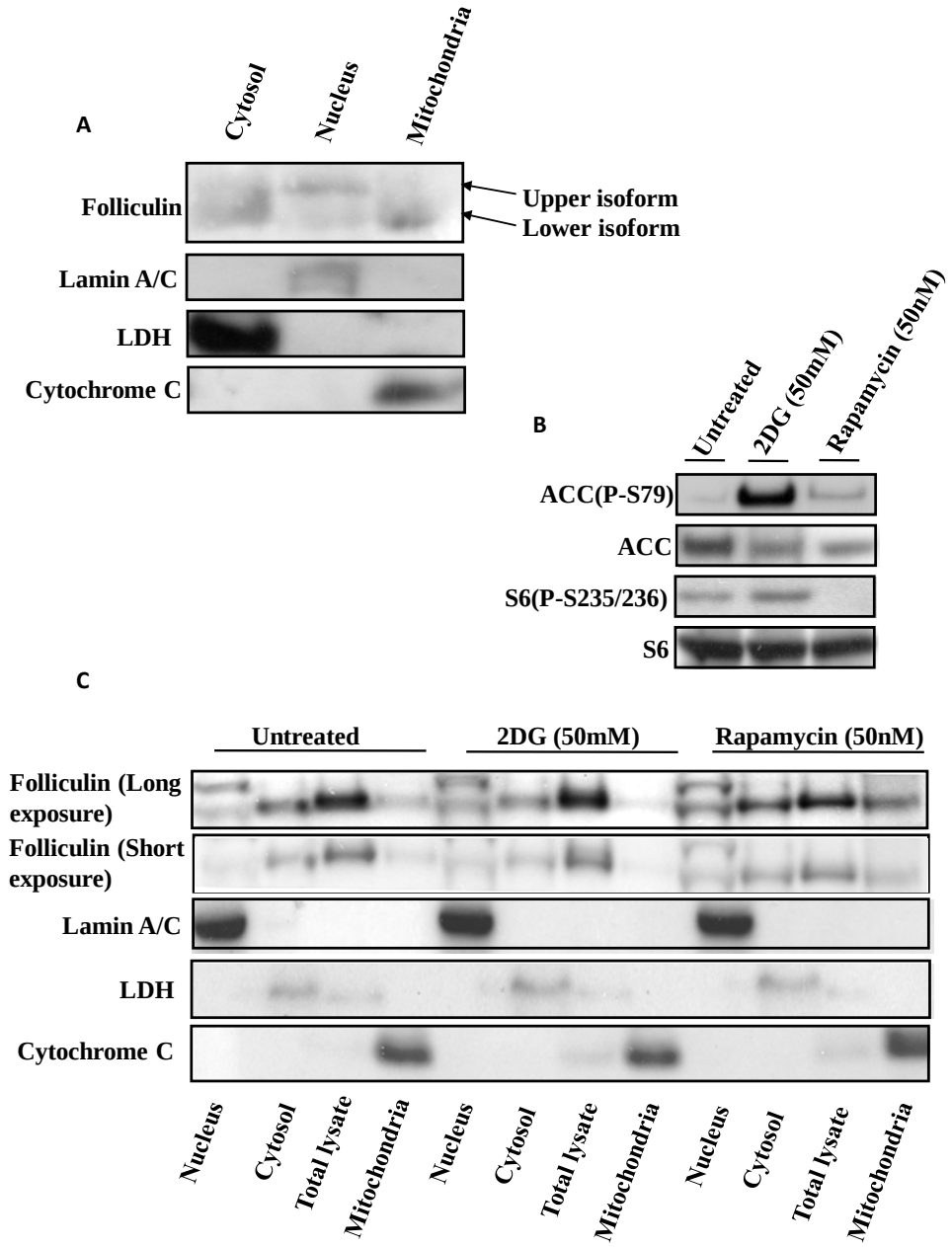

Figure 16. Cellular localisation of Folliculin.

(A) Mitochondrial, nuclear and cytosolic protein lysates were created from HEK293 cells grown to full confluency. Western blot analyses were then performed and the protein levels of BHD, lamin A/C, LDH and cytochrome C were determined. **(B)** Western blot analyses were performed on cell lysates prepared from HEK293 cells treated for 2 h with 50 nm rapamycin or 50 mM 2-deoxyglucose where indicated. Protein levels of ACC (P-S79), ACC, S6 (P-S235/236), and S6 were determined. **(C)** Mitochondrial, nuclear and cytosolic protein lysates were created from HEK293 cells grown to full confluency and treated for 2 h with 50 nm rapamycin or 50 mM 2-deoxyglucose where indicated. Western blot analyses were then performed and the protein levels of FLCN, lamin A/C, LDH and cytochrome C were determined.

The results suggested that, in untreated cells, most of the Folliculin in the nucleus exists in the upper isoform. However, when the cells were subjected to rapamycin treatment, both the upper and lower isoforms of FLCN are detected in the nucleus at approximately equal levels. The amount of FLCN expressed in the mitochondria is also increased upon rapamycin treatment, suggesting that dephosphorylated FLCN might translocate to mitochondria. A third isoform of FLCN was detected in the total lysate just above the lower isoform of FLCN when the cells were subjected to treatment with 2DG, which indicates FLCN phosphorylation that occurs in an AMPK-dependent manner.

3.2.2 Mitochondrial biogenesis is upregulated in UOK257 cells devoid of FLCN

It has been shown that tumours from BHD patients exhibit increased levels of mitochondria (Yang *et al.*, 2008). As data from the HEK293 cells revealed that FLCN can be localised to mitochondria (Figure 16a), I sought to confirm whether UOK257 cells deficient in FLCN have increased levels of mitochondria. The relative levels of mitochondrial and genomic DNA were compared within the BHD^- UOK257 and BHD^+ UOK257-2 cells using RT-PCR (Figure 17a). Levels of a mitochondrial gene (Cytochrome B) were compared to those of a genomic gene (Ribosomal protein L13 (RPL13)) in both cell lines under normoxic and hypoxic conditions. Cytochrome B is involved in the electron transport chain of mitochondria (Esposti *et al.*, 1993).

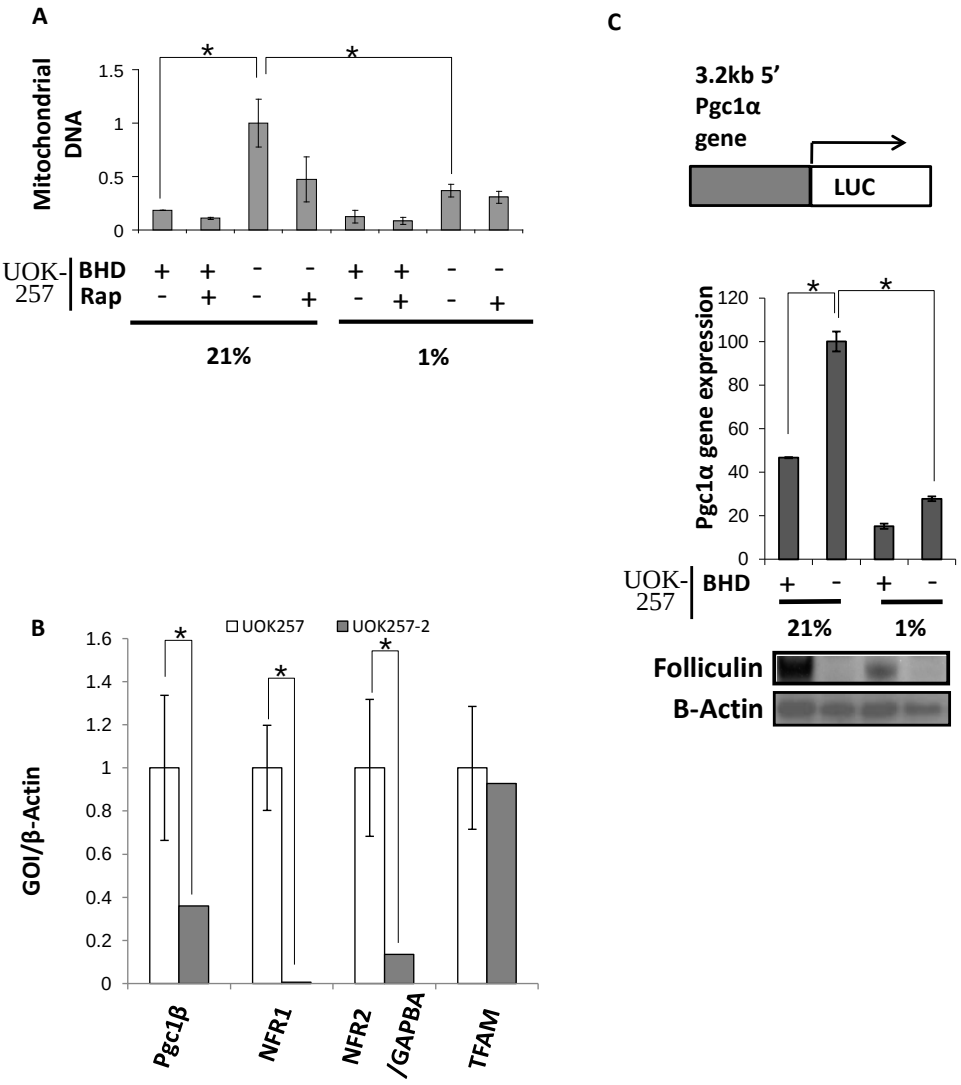

Figure 17. Mitochondrial Biogenesis is upregulated in UOK257 cells devoid of BHD.

(A) The DNA levels of cytochrome B were compared within BHD^+ and BHD^- cells treated with 50 nM rapamycin under normoxia (21%) and hypoxia (1%) overnight, where indicated, by RT-PCR. DNA levels were standardised against RPL13. n = 3. **(B)** The mRNA levels of PGC1β, NRF1, NRF2/GABPA and TFAM were compared within UOK257 and UOK257-2 cell lines by RT-PCR. mRNA levels were standardised against β-Actin mRNA. n = 3. **(C)** BHD^- UOK257 cells transiently transfected with a PGC1α luciferase reporter construct containing the PGC1α promoter region and either pRK7 empty vector or Flag-tagged BHD were maintained in normoxia (21%) or hypoxia (1%) for 24h where indicated. Levels of luminescence are representative of levels of luciferase and therefore PGC1α transcription. Western blot analyses were performed and protein levels of Folliculin were determined. n = 3. * = significant at the 0.05 significance level. ** = significant at the 0.01 significance level.

Approximately a 5 fold increase in the level of mitochondrial DNA was observed in the BHD^- UOK257 cells under normoxic conditions. This was significantly reduced upon treatment with rapamycin (Figure 17a). This finding suggests that cells lacking FLCN have heightened levels of mitochondria which is driven by mTORC1. A significant reduction in the level of mitochondrial DNA was also observed in the BHD^- UOK257 cells under hypoxic conditions (Figure 17a). These data support findings which suggest that decreased transcription of genes such as PGC1α is observed under hypoxic conditions, possibly in a HIF1α dependent manner (Gamboa and Andrade, 2009).

To determine whether the increased levels of mitochondrial DNA observed within the BHD^- UOK257 cells was as a result of enhanced transcription levels of genes involved in mitochondrial biogenesis in the UOK257 cell line RT-PCR was used to determine the mRNA levels of several genes involved in mitochondrial biogenesis. (Figure 17B). The mRNA levels of Nuclear respiratory factor 1(NRF1), Peroxisome proliferator-activated receptor-gamma coactivator 1 β (PGC1β), mitochondrial transcription factor A (TFAM) and Nuclear respiratory factor 2 (NRF2) were analysed under normoxic conditions in the BHD^- UOK257 and BHD^+ UOK257-2 cells. The results revealed that the BHD^- UOK257 cells exhibit significantly increased mRNA levels of the majority of mitochondrial biogenesis markers analysed. Approximately a 3 fold increase in PGC1β mRNA was observed in the UOK257 cells, together with approximately 10 fold increases in the mRNA levels of NRF1 and NRF2. However no significance in TFAM mRNA levels was observed. These data support the thought that mitochondrial biogenesis is upregulated in cells lacking FLCN. Upregulation of mitochondrial biogenesis may therefore be involved in cancer progression in BHD tumours.

In order to further investigate the effect of FLCN expression on the transcription of genes involved in mitochondrial biogenesis UOK257 cells were transfected with a luciferase reporter construct whose expression is regulated by the 5' Peroxisome proliferator-activated receptor-gamma coactivator 1 α (PGC1α) promoter region, together with either Flag-tagged BHD or pRK7 empty vector (Figure 17C). The level of PGC1α gene transcription in the BHD^- UOK257 cells was reduced by approximately 50% upon transfection of the Flag-tagged BHD vector. A further reduction in PGC1α gene transcription was also observed when the cells were subjected to hypoxia, a known suppressor of mitochondrial biogenesis (Zhang and Semenza, 2007). Collectively, these data suggest that mitochondrial biogenesis is upregulated within UOK257 cells upon loss of FLCN.

3.2.3 Mitochondrial biogenesis is enhanced upon BHD knockdown by short hairpin (sh)RNA.

In order to verify the results obtained from the UOK257 cell line, the mRNA and transcription levels of genes involved in mitochondrial biogenesis were analysed within two other cell lines; Mouse Embryonic Fibroblast cells and Human kidney 2 cells which had been stably transfected with either scrambled shRNA (BHD^+) or *BHD* shRNA (BHD^-). RT-PCR was used to analyse the mRNA levels of two genes involved in mitochondrial biogenesis (PGC1α, and ATP synthase H^+ transporting mitochondrial F0 complex subunit C1 (subunit 9) (ATP5G1)) within $BHD^{+/+}$ and $BHD^{-/-}$ MEF cells (Figure 18a). Approximately a 10 fold increase in the levels of ATP5G1 mRNA was observed within the $BHD^{-/-}$ MEFs, together with approximately a 6 fold increase in PGC1α mRNA levels. These data suggest that transcription of mitochondrial biogenesis genes is increased upon loss of FLCN.

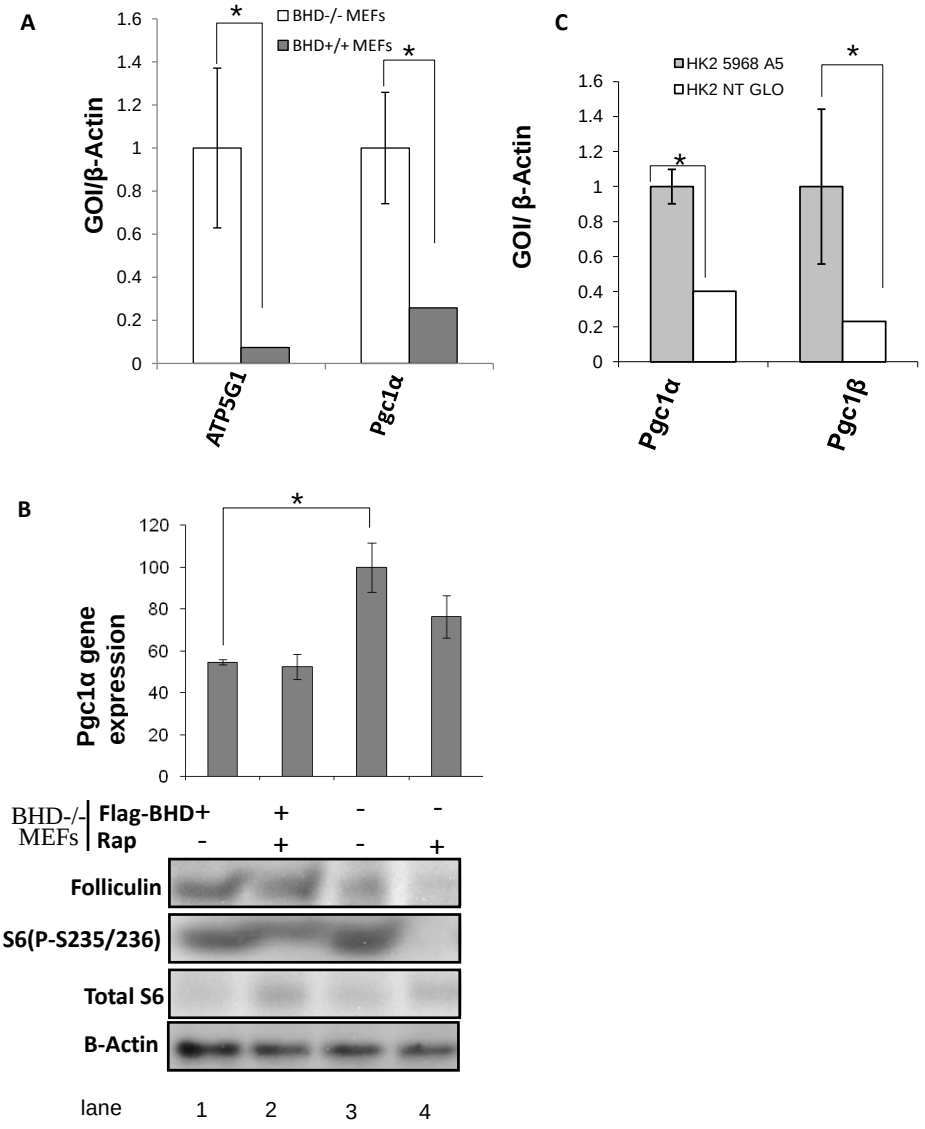

Figure 18. Mitochondrial Biogenesis is upregulated upon loss of BHD via shRNA.

(A) The mRNA levels of ATP5G1 and PGC1α were compared within $BHD^{+/+}$ and $BHD^{-/-}$ mouse embyonic fibroblast cell lines by RT-PCR. mRNA levels were standardised against β-Actin mRNA. n = 3. **(B)** $BHD^{-/-}$ MEF cells transiently transfected with a PGC1α luciferase reporter construct containing the PGC1α promoter region and either pRK7 empty vector or Flag-tagged BHD were treated with 50nm rapamycin where indicated and maintained in normoxia (21%) for 24h. Levels of Luminescence are representative of levels of Luciferase and therefore PGC1α transcription. Western blot analyses were performed and protein levels of Folliculin, S6 (P-S235/236), and S6 were determined. n = 3. **(C)** The mRNA levels of PGC1α and PGC1β were compared within HK2 5968A5 (BHD^{-}) and HK2 NT G10 (BHD^{+}) cell lines by RT-PCR. mRNA levels were standardised against β-Actin mRNA. n = 3. * = significant at the 0.05 significance level. ** = significant at the 0.01 significance level.

The level of PGC1α directed gene expression was then analysed by transfecting $BHD^{-/-}$ MEFs with a luciferase reporter construct containing the 3.2kb 5' PGC1α promoter region, together with either Flag-tagged BHD or pRK7 empty vector (Figure 18B). The results revealed that the level of transcription of the PGC1α gene was reduced by approximately 50% within the $BHD^{-/-}$ MEFs upon transfection with BHD. These data were consistent with increased level of transcription of genes involved in mitochondrial biogenesis exhibited by the FLCN-deficient UOK257 cells. The level of PGC1α transcription was also analysed after the cells had been subjected to treatment with the mTORC1 inhibitor rapamycin. mTORC1 signalling is known to drive mitochondrial biogenesis via a PGC1α- YY1 complex (Sengupta, 2010). Treatment with rapamycin did result in a decrease in the transcription of PGC1α in the $BHD^{-/-}$ MEFs of approximately 30%; however the reduction in the level of PGC1α transcription observed upon transfection with Flag-tagged *BHD* was not further enhanced upon treatment with rapamycin.

RT-PCR was also used to analyse the transcription levels of two genes involved in mitochondrial biogenesis (PGC1α and PGC1β) within HK2 cells (Figure 18C). A 2 fold increase in mRNA levels of PGC1α was observed in the HK2 cells upon loss of *BHD* via shRNA, together with approximately a 10 fold increase in PGC1β mRNA. These data were consistent with increased level of transcription of genes involved in mitochondrial biogenesis exhibited by the FLCN deficient UOK257 and MEF cell lines and support the notion that mitochondrial biogenesis is upregulated upon loss of FLCN.

3.2.4 ATP levels are depleted in UOK257 cells deficient in FLCN.

As the work conducted on multiple cell lines had clearly shown that mitochondrial biogenesis is upregulated upon loss of FLCN, resulting in increased numbers of mitochondria in

UOK257 cells; it was hypothesised that ATP levels might be higher in cells deficient in BHD. Therefore, an ATP assay was conducted in order to compare levels of ATP within the UOK257 (BHD^-) and UOK257-2 (BHD^+) cells (Figure 19). The results suggest that, despite the increased levels of mitochondria observed in the FLCN-deficient UOK257 cells, ATP production within these cells is decreased by approximately 40%; suggesting that the mitochondria within the BHD^- UOK257 cells do not respire efficiently. These results are supported by data from work conducted by Dr. Stephen Land using a JC1 monomer which revealed that the BHD^- UOK257 cells have reduced levels of healthy respiring mitochondria (Figure 20a). Of interest, Dr. Stephen Land also observed large foci of green JC1 monomer in the BHD^- UOK257 cells, indicative of swollen mitochondria. The decreased levels of ATP production may also explain the fact that BHD^- UOK257 cells exhibit increased levels of phosphorylated AMP-dependent protein kinase (AMPK), enhanced phosphorylation of raptor at S792 (an AMPK phosphorylation site) and phosphorylated Acetyl co-A carboxylase; indicative of AMPK activity (Figure 21). AMPK acts as an energy sensor when ATP levels are low, and provides metabolic adaptations to these conditions. These data suggest that levels of AMPK activity are increased within the BHD^- UOK257 cells in order to provide metabolic adaptations in response to the depleted ATP levels exhibited by these cells.

3.2.5 Compromised mitochondrial membrane potential in BHD^- UOK257 cells results in increased ROS production and subsequent over-expression of Uncoupling proteins.

Further analysis conducted by Dr. Stephen Land on the UOK257 cell line using treatment with a potent mitochondrial uncoupling agent, carbonyl cyanide m-chloro phenyl hydrazone (CCCP), also suggested that the mitochondrial membrane potential may be compromised in the BHD^- UOK257 cells (Figure 20B). Uncoupling proteins reduce mitochondrial membrane

potential within mammalian cells and inhibit the ability of a cell to generate ATP (Patanè, 2002).

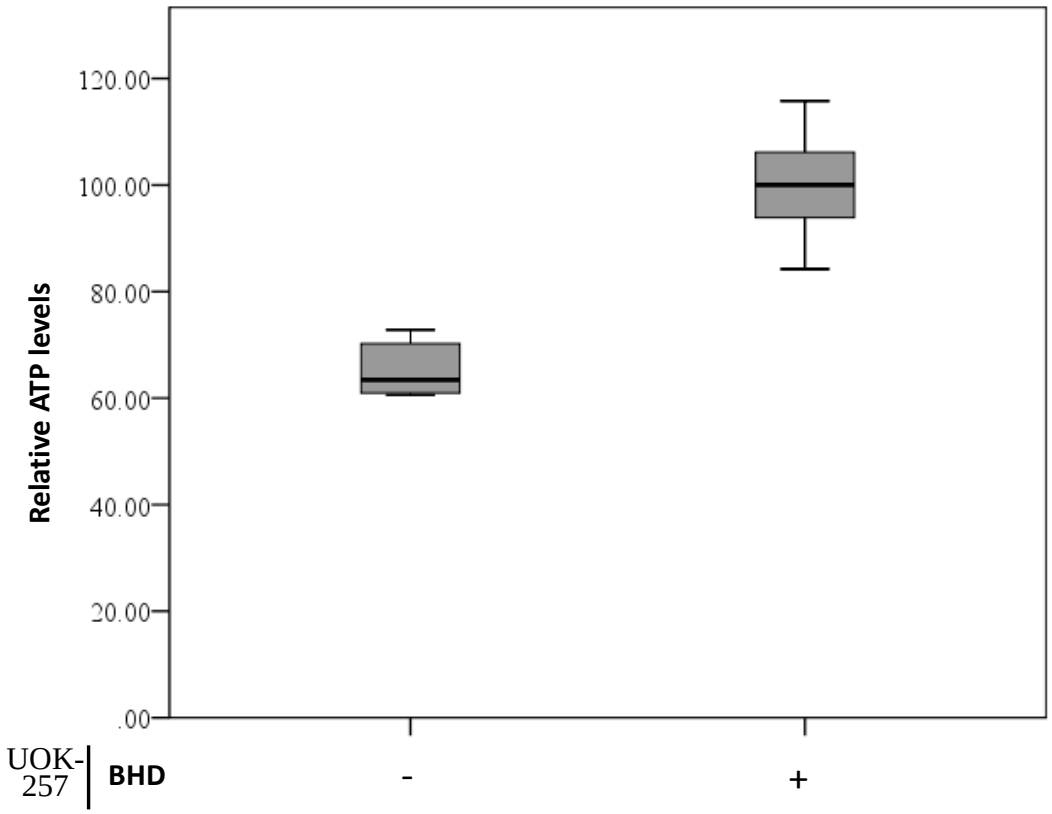

Figure 19. Decreased production of ATP in FLCN-deficient UOK257 cells.

The levels of ATP production were compared within UOK257 and UOK257-2 cells using a CellTiter-Glo Luminescent Cell Viability Assay. Cells were incubated with 150µl CellTiter Glo Reagent for 1 hour at room temperature before the luminesence was read. n = 3.

As decreased levels of ATP production and compromised mitochondrial membrane potential have been observed within the BHD$^-$ UOK257 cells, uncoupling protein 3 (UCP3) mRNA (Figure 22a) and protein levels (Figure 22B) were analysed within the UOK257 and UOK257-2 cell lines. The results showed that there was a significant increase in UCP3 mRNA and protein levels in the BHD$^-$ UOK257 cells. No UCP3 mRNA or protein was detected in the UOK257-2 cells over-expressing BHD. These data suggest that

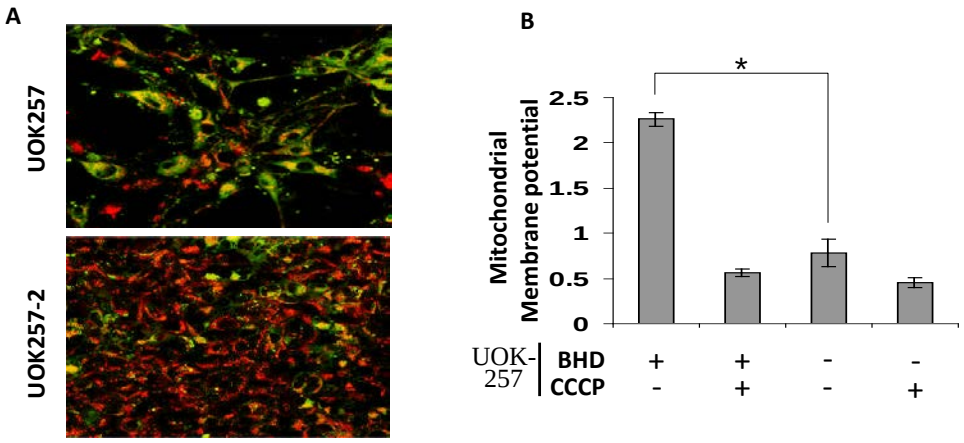

Figure 20. Decreased Mitochondrial Membrane Potential in FLCN-deficient UOK257 cells.

(A) BHD^+ UOK257-2 and BHD^- UOK257 cells maintained in normoxia (21%) were treated with a JC1 monomer and the amount of green JC1 monomer to red JC1 aggregate were determined. Amount of JC1 aggregate is representative of the amount of respiring mitochondria (work carried out by Dr Steven Land). **(B)** BHD^+ UOK257-2 and BHD^- UOK257 cells maintained in normoxia (21%) were treated with CCCP where indicated and the mitochondrial membrane potential was determined (work carried out by Dr Steven Land). * = significant at the 0.05 significance level. ** = significant at the 0.01 significance level.

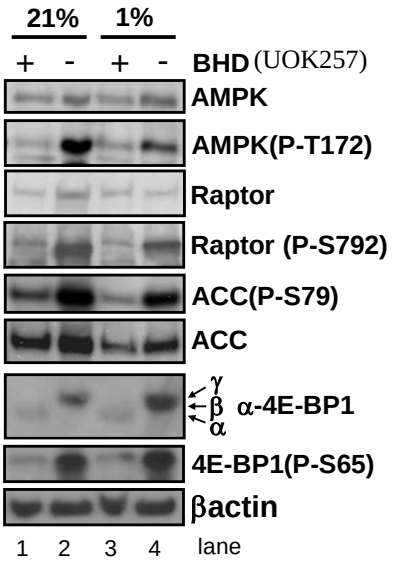

Figure 21. Levels of AMPK activity are increased in UOK257 cells devoid of BHD.

Western blot analyses were performed on cell lysates obtained from BHD^- (UOK257) and BHD^+ (UOK257-2) cells maintained in normoxic (21%) or hypoxic (1%) conditions where indicated. Protein levels of raptor, raptor (P-S792), acetyl-CoA carboxylase (ACC), AMPKa, AMPKa (P- Thr172), 4E-BP1, 4E-BP1 (P-S65), ACC (P-S79), and β-actin (used as a loading control) were determined.

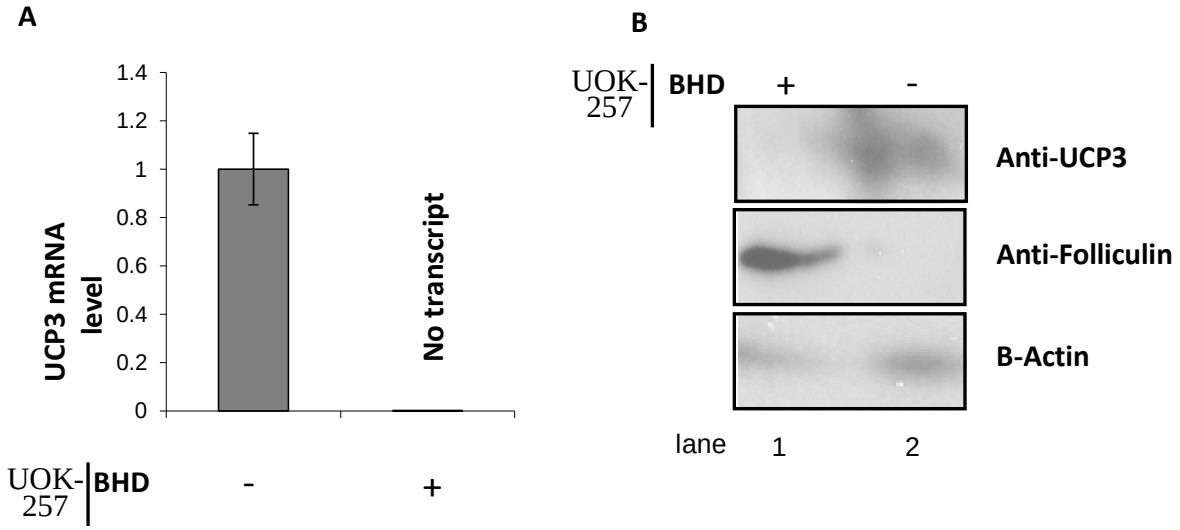

Figure 22. UOK257 cells deficient in BHD exhibit increased levels of Uncoupling protein 3.

(A) The mRNA levels of UCP3 were compared within BHD^- UOK257 and BHD^+ UOK257-2 cell lines by RT-PCR. mRNA levels were standardised against β-Actin mRNA. n = 3. **(B)** Western blot analyses were performed on mitochondrial fractions created from BHD^+ (UOK257-2) and BHD^- (UOK257) cells maintained in normoxia (21%). Protein levels of UCP3, Folliculin and β-actin (used as a loading control) were determined.

overexpression of uncoupling proteins may result in compromised mitochondrial membrane potential and decreased levels of ATP production within the BHD^- UOK257 cells.

UCPs are also produced by a cell in order to reduce ROS production (Patanè, 2002). However, mitochondria are the main source of ROS produced from the electron transport chain. A reduced mitochondrial membrane potential therefore often results in increased ROS production. Cells express antioxidants in order to effectively reduce the levels of ROS within a cell. Oxidative stress occurs as a result of a cell's inability to reduce ROS efficiently by expressing cellular antioxidants. This inability to reduce ROS may lead to cellular components being damaged by ROS, which includes mitochondria, and subsequently results in further mitochondrial dysfunction (Bellance *et al.*, 2009). Therefore, levels of hydrogen

peroxide (H_2O_2), one of many species of ROS, were analysed in order to determine the levels of ROS production within the BHD^- UOK257 and BHD^+ UOK257-2 cell line (Figure 23a). The results suggested that H_2O_2 production was increased by approximately 4-fold in the BHD^- UOK257 cells.

mRNA (Figure 23B) and protein levels (Figure 23C) of Superoxide dismutase 2 **(**SOD2**)** were also analysed within the BHD^- UOK257 and BHD^+ UOK257-2 cells via RT-PCR and western blot respectively. SOD2 converts superoxide anion radicals (O_2^-), a byproduct of mitochondrial respiration, into H_2O_2 and oxygen. The results showed that there was a significant increase in SOD2 mRNA and protein levels in the BHD^- UOK257 cells. Of interest; no SOD2 mRNA or protein was detected in the UOK257-2 cells over-expressing BHD. These data collectively suggest that ROS production is increased in the BHD^- UOK257 cells as a result of decreased mitochondrial membrane potential. Production of UCP and antioxidants such as SOD2 is subsequently increased within these cells in order to reduce the excess ROS.

3.2.6 A loss of mitochondrial cristae is observed in MEF cells upon loss of BHD.

As depleted ATP levels are observed in the UOK257 cells, together with decreased mitochondrial membrane potential, and increased levels of H_2O_2, I hypothesised that loss of BHD may result in a defect in the mitochondria. Therefore, electron microscopy work was conducted in order to examine the mitochondria in the $BHD^{+/+}$ and $BHD^{-/-}$ MEF cells. The results indicated a trend towards loss of cristae in the $BHD^{-/-}$ MEF cells (Figure 24), resulting in approximately a 30% decrease in the surface area of the inner mitochondrial membrane in these cells compared to $BHD^{+/+}$ MEF cells.

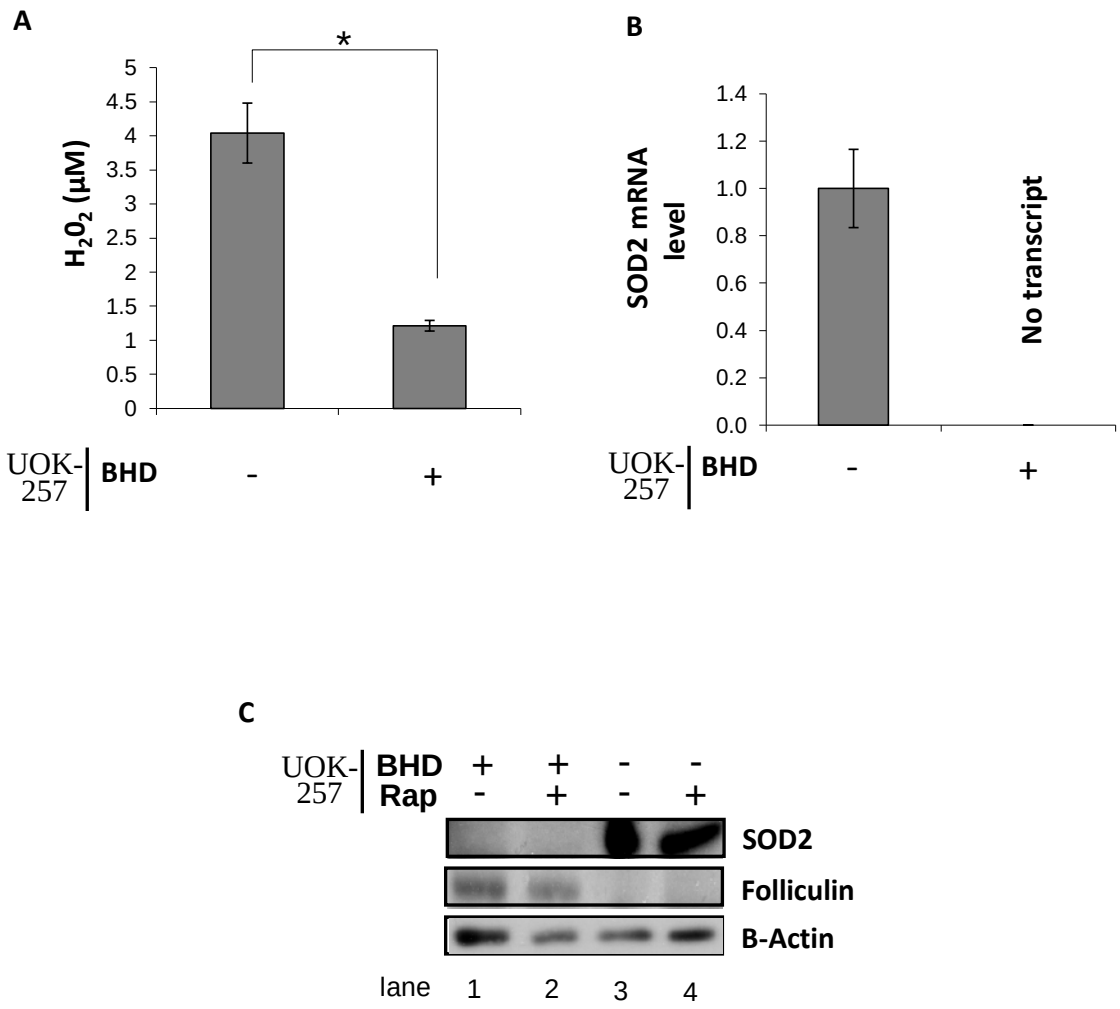

Figure 23. UOK257 cells deficient in FLCN exhibit increased levels of ROS production.

(A) The levels of H_2O_2 within the growth media of BHD^+ UOK257-2 and BHD^- UOK257 cells were analysed using an Amplex red H_2O_2 assay. Cells growing in DMEM were washed with Krebs ringer buffer before being incubated in Krebs ringer buffer for 30mins in normoxia (21%). Media was then taken from the cells and incubated with Amplex red reagent according to manufacturer's instructions before absorbance was read. Level of absorbance is representative of the amount of H_2O_2 within the growth media of the cells after 30mins. **(B)** The mRNA levels of SOD2 were compared within BHD^+ UOK257-2 and BHD^- UOK257 cell lines by RT-PCR. mRNA levels were standardised against β-Actin mRNA. n = 3. **(C)** Western blot analyses were performed on cell lysates obtained from BHD^- (UOK257) and BHD^+ (UOK257-2) cells maintained in normoxia (21%) and treated with 50nm rapamycin as indicated. Protein levels of SOD2, Folliculin and β-actin (used as a loading control) were determined. * = significant at the 0.05 significance level. ** = significant at the 0.01 significance level.

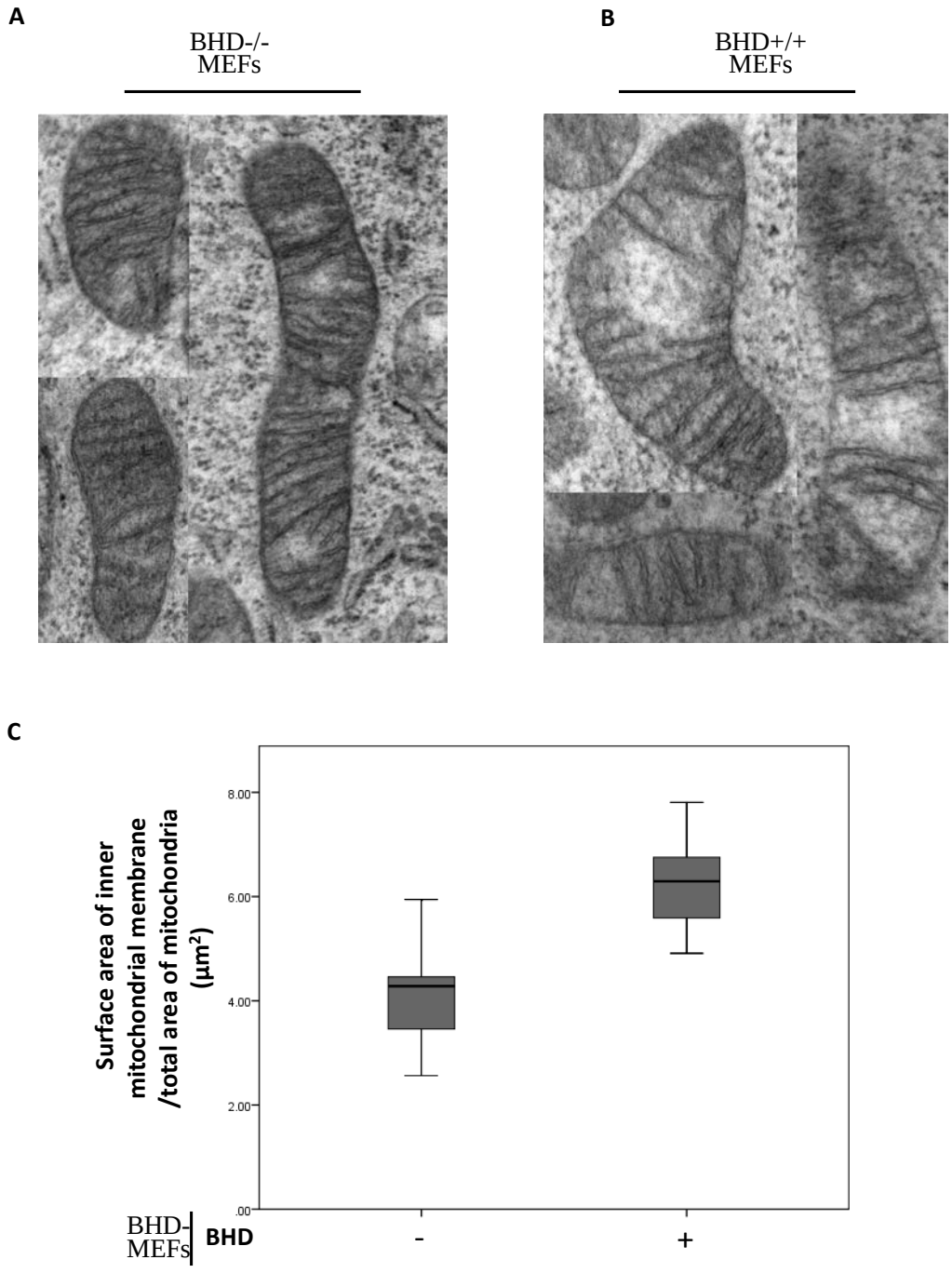

Figure 24. A trend towards loss of cristae and reduced surface area of the mitochondria is observed upon loss of FLCN.

Electron microscopy work was conducted looking at mitochondria of **(A)** $BHD^{-/-}$ MEFs and **(B)** $BHD^{+/+}$ MEFs maintained in 35 mm plates in DMEM and fixed in 1% glutaraldehyde. **(C)** The surface area of the inner mitochondrial membrane of the mitochondria in the images obtained from these cells was then measured and the ratio of surface area of inner membrane/total area of mitochondria was determined. (Work carried out by Mr. Chris Von Ruhland).

The electron transport chain synthesises ATP by generating a proton gradient via oxidation/reduction reactions, which is subsequently used by ATP synthase to produce ATP via the phosphorylation of ADP. The components of the electron transport chain are contained in the inner membrane of the mitochondria. Cristae are formed to increase the surface area of the inner membrane of the mitochondria in order to increase the ability of mitochondria to produce ATP via the electron transport chain (Paumard *et al.*, 2002). The trend towards loss of cristae and resulting loss of surface area of the inner membrane of the mitochondria in the $BHD^{-/-}$ MEF cells therefore may contribute to the depleted levels of ATP production observed upon loss of FLCN.

It has been observed that H_2O_2 induces a response in cardiac myocytes which results in the mitochondrial permeability transition pore (PTP) being opened. This results in the loss of mitochondrial membrane potential, and swelling of mitochondria (Akao *et al.*, 2006). Collectively these data suggest that a loss of FLCN may result in an increase in H_2O_2 production, resulting in morphological changes to the mitochondria (swelling and loss of cristae), increased UCP levels, a reduction in mitochondrial membrane potential, and depleted ATP levels. AMPK activity levels are subsequently elevated in these cells in order to provide metabolic adaptations in order to cope with the depleted levels of ATP as a result of this mitochondrial dysfunction.

3.3 Discussion

3.3.1 Different isoforms of FLCN are localised to the nucleus and the mitochondria.

This chapter provides information for the first time on the cellular localisation of endogenous FLCN. Data obtained from HEK293 cells reveal that FLCN localises to the nucleus, cytosol, and mitochondria. These data support work conducted by Baba *et al.* which suggested that transiently expressed HA-tagged FLCN is localised to the nucleus and mitochondria where it interacts with transiently expressed Flag-tagged FNIP1 (Baba *et al.*, 2006). The results from these data also reveal differential expression of FLCN isoforms between the cellular compartments. The upper isoform of FLCN was detected in the nuclear fractions whereas the lower isoform of FLCN was detected in the mitochondrial fraction. Both of these isoforms were detected in the cytosolic fraction. Work conducted by Baba *et al.* suggests that FLCN exists in several phosphorylated forms which are electrophoretically distinct; and that the slower migrating species of FLCN are phosphorylated forms of FLCN (Baba *et al.*, 2006). These data suggest that the FLCN isoform detected in the nucleus is a phosphorylated species of FLCN whereas the FLCN isoform detected in the mitochondria is a dephosphorylated species of FLCN. However it is also possible that the upper FLCN isoform could be as a result of another post-translation modification such as ubiquitination.

3.3.2 Differences in the localisation of FLCN are observed upon activation of AMPK and inhibition of mTOR

Data obtained from HEK293 cells also revealed that most of the endogenous FLCN expressed in the nucleus resolves as the upper isoform when cells are growing in serum.

However, when the cells are subjected to treatment with the mTORC1 inhibitor rapamycin, the lower isoform of FLCN becomes more apparent in the nuclear fraction. This suggests that rapamycin inhibits the phosphorylation status of the nuclear pool of FLCN. These support the work conducted by Baba *et al.* also who first showed that rapamycin treatment of the UOK257-2 cells led to dephosphorylated over-expressed FLCN in UOK257-2 cells, as observed by complete elimination of the upper phospho-FLCN band (Baba *et al.*, 2006). These data support the hypothesis by Baba *et al.* that implies that the mTORC1 signalling pathway plays a role in the modulation of FLCN phosphorylation and presumably its tumour suppression function. However it not known whether FLCN is a direct mTORC1 substrate or a substrate of a kinase activated downstream of mTOR. For instance, it is possible that FLCN could be directly phosphorylated by S6K1 or S6K2. Increased expression of the lower isoform of FLCN in the mitochondrial fraction was also observed when the HEK293 cells were treated with rapamycin, suggesting that dephosphorylated FLCN shuttles to the mitochondria. It is possible that FLCN might be involved in regulating or maintaining mitochondrial function to produce energy and control ROS production.

When the HEK293 cells were subjected to treatment with the AMP-dependent kinase (AMPK) activator 2-deoxyglucose (2-DG) a third isoform of FLCN was detected in the total lysate just above the lower isoform of FLCN. Decreased expression of the lower isoform of FLCN was also observed in the mitochondrial fraction upon treatment with 2-DG. Work conducted by Baba *et al.* also showed that inhibition of AMPK by AraA inhibited the phosphorylation of FLCN in the UOK257-2 cells and phosphorylation of GST-tagged FLCN by purified AMPK. Several phosphorylation sites of FLCN have been identified. Work conducted by Piao *et al.* identified Ser62 and Ser302 as phosphorylation sites of FLCN, and that mTORC1 differentially regulated the phosphorylation of these sites. In particular,

downstream kinases of mTORC1 appear to phosphorylate FLCN at Ser302 (Piao *et al.*, 2009). Further investigation revealed that Ser62 of FLCN is phosphorylated in the AMPK-related pathway, but is not directly phosphorylated by AMPK (Wang *et al.*, 2010). These data support the notion that both mTORC1 and AMPK phosphorylate FLCN at multiple residues.

Communication between mitochondria and the nucleus is important in the maintenance of energy homeostasis. Mitochondrial biogenesis requires coordination of the transcription of genes located in the mitochondria and in the nucleus which are essential to the process (Hock and Kralli, 2009). As FLCN localises to both the mitochondria and the nucleus, it may be possible that FLCN maintains a level of communication between the nucleus and the mitochondria involving energy homeostasis. Both mTORC1 and AMPK are also potent drivers of mitochondrial biogenesis and it is thought to be driven by transcriptional events. It is very likely that both mTORC1 and AMPK could drive mitochondrial biogenesis through modulation of FLCN phosphorylation.

3.3.3 Mitochondrial biogenesis is enhanced upon loss of function of FLCN

The data presented in this chapter reveal that mitochondrial biogenesis is upregulated in multiple FLCN-deficient cell lines. Of particular interest is the enhanced level of transcription of PGC1α observed in the FLCN-deficient UOK257 and MEF cell lines upon transfection with a PGC1α luciferase reporter construct. Results from RT-PCRs conducted on BHD-deficient MEF and HK2 cells also revealed that they exhibit increased mRNA levels of PGC1α. Increased mRNA levels of PGC1α have also been observed TSC2 deficient cells, in which mTORC1 is highly active, which was rescued upon inhibition with rapamycin

(Cunningham *et al.*, 2007). mTOR and Raptor associate with YY1 and mTOR has been shown to regulate the interaction between YY1 and PGC1α and thus alter how they function. mTORC1 is therefore able to enhance mitochondrial gene expression in an Akt independent manner (Cunningham *et al.*, 2007). The fact that PGC1α transcription in the $BHD^{-/-}$ MEF cells is reduced upon treatment with rapamycin suggests that mTORC1 activity may also be contributing to the increased levels of PGC1α transcription and thus mitochondrial biogenesis, observed upon loss of FLCN.

PGC1α interacts with nuclear respiratory factor 1 NRF1 and NRF2 thus enhancing mitochondrial biogenesis and oxidative function (Bogaka *et al.*, 2005). Increased mRNA levels of NRF1 and NRF2 are observed in the FLCN-deficient cell lines, as well as PGC1β and ATP5G1, in a similar manner to that observed in the TSC2-deficient cells (Cunningham *et al.*, 2007). However, although increased NRF1 mRNA levels are observed within the BHD^- UOK257 cells, no increase in the levels of TFAM mRNA was observed. This suggests that the increased mtDNA levels observed in the BHD^- UOK257 cells does not occur as a result of increased transcription of TFAM via increased levels of NRF1. However, increased mRNA levels of NRF2 are also observed in the BHD^- UOK257 cells. NRF2 sites have also been identified in genes encoding mitochondrial transcription factor A (TFAM) involved in mitochondrial transcription and DNA replication (Kelly and Scarpulla, 2004). Therefore it may be possible that increased transcription of mitochondrial transcription factors via the increased levels of NRF2 results in the increased mtDNA levels observed in the BHD^- UOK257 cells. The fact that increased levels of mitochondrial biogenesis genes are observed in multiple BHD-deficient cell lines suggests that this may be applicable to a number of BHD tumour types. The high levels of mitochondrial biogenesis observed in the BHD^- UOK257 cells is in line with observations made by Yang *et al.*, who revealed that chromophobe renal

tumours from BHD patients had abnormally high levels of mitochondria. This supports the notion that loss of FLCN may result in an accumulation of mitochondria (Yang *et al.*, 2008).

3.3.4 Decreased levels of ATP production are observed upon loss of functional FLCN

The FLCN-deficient cell lines exhibited increased mRNA levels of mitochondrial biogenesis genes together with elevated levels of mitochondrial DNA. Hence it was hypothesised that levels of ATP production would also be increased upon loss of FLCN as mitochondria generate ATP via oxidative phosphorylation (oxPhos) of glycolysis and lipolysis products (Hock and Kralli, 2009). When ATP levels were analysed within the BHD^- UOK257 and BHD^+ UOK257-2 cells the results revealed that ATP levels are depleted within the FLCN-deficient UOK257 cell line. These data, combined with work conducted by Dr. Steven Land (our collaborator from Dundee University) using a JC1 monomer, suggest that the mitochondria within the FLCN-deficient UOK257 cells do not respire efficiently, and that some of the mitochondria in the BHD^- UOK257 cells may be swollen, indicating morphological changes may occur in the UOK257 cells upon loss of FLCN. As discussed in Chapter 2 the FLCN-deficient UOK257 cells also appear to favour glycolysis over oxidative phosphorylation. Approximately 18 times less ATP is generated by glycolysis compared to oxidative phosphorylation (Van der Heiden *et al*., 2009); possibly contributing to the depleted ATP levels exhibited by the BHD^- UOK257 cells. Mitochondrial biogenesis may therefore be increased within the FLCN-deficient UOK257 cells as a compensatory mechanism in response to this energy deficit.

3.3.5 Compromised mitochondrial membrance potential and enhanced expression of uncoupling proteins is observed in response to increased levels of ROS production upon loss of functional FLCN.

Further analysis conducted on the UOK257 cell line by Dr. Stephen Land suggested that mitochondrial membrane potential may be compromised in the BHD^- UOK257 cells. In mammalian cells, mitochondrial membrane potential is reduced by UCPs that reduce the ability of mitochondria to generate ATP (Patanè, 2002). Results obtained from the BHD^- UOK257 cell line revealed elevated mRNA and protein levels of UCP3. These data suggest that increased levels of UCPs within the BHD^- UOK257 cells may also account for their compromised mitochondrial membrane potential and depleted ATP levels. UCPs are also produced by a cell in order to reduce production of ROS. Increased ROS production can lead to mitochondrial dysfunction as well as misregulation of cellular signalling and chromosomal instability. Therefore ROS production plays a critical role in cancer progression (Bellance *et al.,* 2009). The BHD^- deficient cells exhibit a 10- fold increase in ATP5G1 mRNA levels compared to a 5- fold increase in mitochondrial DNA content. These results suggest that loss of functional FLCN results in increased transcription of genes involved in oxidative phosphorylation in a similar manner to that observed in cells deficient in TSC1. This increase in mitochondrial oxidation in TSC1-deficient cells also results in increased levels of ROS production (Chen *et al.,* 2008). Therefore it was hypothesised that levels of ROS would also be increased in UOK257 cells deficient in FLCN. The results from Amplex Red Hydrogen peroxide assays reveal increased levels of H_2O_2 within the growth media of BHD^- UOK257 cells. Furthermore, increased mRNA and protein levels of SOD2 are also exhibited in the BHD^- UOK257 cell line. These data suggest that ROS production is increased in the UOK257 cell line upon loss of FLCN. The fact that the BHD^- UOK257 cells exhibit increased levels of ROS production together with increased levels of mitochondrial

biogenesis genes suggests that loss of functional FLCN results in the upregulation of ROS production and increased mitochondrial biogenesis in a similar manner to that observed in TSC1-deficient cells (Chen *et al,.* 2008).

PGC1α is also a powerful regulator of ROS metabolism and has been shown to induce transcription of UCPs in response to ROS (Valle *et al.,* 2005). It has also been shown that PGC1α is required for the induction of SOD2 and other ROS-detoxifying enzymes (St Pierre *et al.*, 2006). It may be possible that the enhanced level of transcription of PGC1α observed in FLCN-deficient cells contributes to the enhanced expression of SOD2 observed upon loss of BHD. Therefore the enhanced transcription of PGC1α may also serve to provide a protective function against elevated ROS production observed upon loss of FLCN.

3.3.6 Reduced numbers of mitochondrial cristae are observed upon loss of functional FLCN.

Electron microscopy conducted on the $BHD^{+/+}$ and $BHD^{-/-}$ MEF cells revealed a trend towards loss of cristae and thus decreased surface area of the inner mitochondrial membrane of $BHD^{-/-}$ MEF cells. This loss of cristae and resulting loss of surface area of the inner membrane of these mitochondria would reduce the ability of these mitochondria to produce ATP efficiently via the electron transport chain. Therefore, it appears that the increased levels of H_2O_2 production observed upon loss of FLCN result in loss of cristae as well as swelling of mitochondria, compromised mitochondrial membrane potential and decreased levels of ATP production (Akao *et al.*, 2006). This may explain the fact that the BHD^{-} UOK257 cells exhibit a metabolic profile that resembles the Warburg effect. HIF-mediated transcription of genes such as GLUT1 may be increased in order to elevate levels of glucose uptake and increase metabolism via glycolysis to compensate for the resulting energy deficit.

The ability of FLCN-deficient cells to take up and oxidise the excess L-lactate produced by glycolysis may also be a compensatory mechanism in order for these cells to meet their energy demands in spite of their lack of ability to produce ATP via the electron transport system due to loss of cristae.

3.3.7 Increased levels of mitochondrial biogenesis observed upon loss of functional FLCN may create a transiently hypoxic environment and enhance HIF activity levels.

Enhanced expression of PGC1α and subsequent increased levels of mitochondrial biogenesis leads to an increased demand for oxygen. This transiently creates a hypoxic environment within a cell resulting in the stabilisation of HIF1α protein and increased expression of HIF transcriptional target genes (Shoag and Arany, 2010). Increased mitochondrial biogenesis may be creating a transiently hypoxic environment within the FLCN-deficient cells and consequently reducing the levels of production of ATP within these cells. This may explain why increased levels of HIF transcriptional activity are observed in the FLCN deficient cell lines even under normoxic conditions.

3.3.8 Increased levels of AMPK activity upon loss of functional FLCN may also enhance expression of HIF transcriptional targets.

Data obtained revealed that UOK257 cells deficient in FLCN have increased levels of phosphorylated AMPK as well as increased levels of phosphorylated Acetyl CoA carboxylase (ACC); an indicator of AMPK activity. Under conditions of low ATP levels AMPK functions as an energy sensor and provides changes to cellular metabolism in order to adapt to these conditions (Yun *et al.*, 2005). AMPK has been shown to enhance HIF-1 transcriptional activity via a signalling pathway independent of the PI3K/Akt (Lee *et al.*, 2003). AMPK has also been shown to enhance VEGF and GLUT 1 mRNA levels in a HIF1α independent manner (Yun *et al.*, 2005). It may be possible that AMPK activity levels are

increased within the UOK257 cells in response to increased ROS production and subsequent depleted ATP levels. This may then lead to increased levels of VEGF expression, glucose uptake and fatty acid oxidation in a HIF1α-dependent and HIF1α-independent manner.

Activation of AMPK in response to oxidative stress is required for the activation of PGC1α in skeletal muscle cells and thus activation of mitochondrial biogenesis (Zong *et al.*, 2002). Although the levels of PGC1α gene expression within $BHD^{-/-}$ MEFs are reduced upon treatment with the mTORC1 inhibitor rapamycin, these levels are not reduced to the levels exhibited when the cells express FLCN. This suggests that PGC1α gene expression is being enhanced by multiple mechanisms.

Chapter 4

The effect of loss of function of Folliculin on autophagic activity

4 The effect of loss of function of FLCN on autophagic activity

4.1 Introduction

Autophagy is a process by which cells adapt to stress by catabolising unnecessary structures such as organelles and proteins. Macroautophagy is probably the best characterised form of autophagy in mammalian cells and involves the formation of autophagosomes (a double membrane vesicle). These autophagosomes engulf cytosolic substrates. The autophagosomes then fuse with lysosomes to form autophagolysosomes and the material that was engulfed within the lysosome is degraded; a process which requires proteases (Figure 3) (Hands *et al.*, 2009).

Evidence has been provided which suggests that at moderately elevated levels autophagy may provide protection for tumour cells. However when autophagic activity is increased to extremely high levels autophagy abandons its protective functions and instead initiates cell death (Schönthal, 2009). Autophagy is also reduced upon loss of several tumour suppressor proteins such as PTEN, TSC1 and TSC2, as well as LKB1/STK11 (Maiuri *et al.*, 2009).

Autophagy has also been shown to be negatively regulated by mTOR. Although the exact mechanism as to how mTOR controls autophagy is not well established. (Hands *et al.*, 2009). Studies have shown that mTORC1 also regulates autophagy through direct regulation of the UNC-51-like kinase 1 (ULK1) –Atg13–FIP200 complex (Figure 3) (Hosokawa *et al.,* 2009). Furthermore, work conducted by Dunlop *et al.* has also revealed that ULK1 inhibits mTORC1 by directly phosphorylating Raptor (Dunlop *et al*, 2011). Work conducted by Parkhitko *et al.* revealed that levels of autophagic activity in $Tsc2^{-/-}p53^{-/-}$ murine embryonic

fibroblasts (MEFs), which exhibit increased levels of mTORC1 activity, are decreased (Parkhitko *et al.*, 2011).

mTOR may also regulate autophagy by activating the class I PI3K/Akt -pathway (Ren *et al.*, 2009). Work conducted by Mortimore and Schworer has shown that amino acids inhibit autophagosome formation (Mortimore and Schworer, 1998), which is regulated by mTOR. mTOR is also a sensor for ATP (Dennis *et al.*, 2001). Autophagic sequestration and other post-sequestering events in the autophagic pathway have been shown to be sensitive to changes in cellular ATP levels (Schellens *et al.*, 1988; Plomp *et al.*, 1989).

Several reports have shown that targeting mTORC1 with rapamycin induces autophagy (Turcotte and Giaccia, 2010). Treatment with rapamycin has also been shown to result in increased levels of autophagic activity in yeast (Noda and Ohsumi, 1998) and rat hepatocytes (Blommaart *et al.*, 1995). When Parkhitko *et al.* examined the effects of a combined treatment of the autophagy inhibitor Chloroquine with the mTORC1 inhibitor rapamycin on TSC2-deficient tumours they observed that a combination of the two reagents resulted in a synergistic reduction in tumour size which was greater than that observed when the tumours were subjected to treatment with either reagent alone (Parkhitko *et al.*, 2011).

The unfolded protein response (otherwise known as the Endoplasmic Reticulum Stress (ERS) response) is another process by which cells adapt to stress (Tsutsumi, 2004). It has been shown that, although autophagy and the unfolded protein response function independently, when the activity of one of these processes is altered the activity of the other is also altered; suggesting that there are important connections between these systems. When activity of the ERS response is moderate to low it has also been shown to protect a cell. However when ERS activity is increased to high levels, it also abandons its protective functions and instead initiates cell death (Schönthal, 2009). Elevated levels of the protective components of the

ERS response have also been exhibited by tumour cells as an adaptive mechanism that promotes cell survival and the potential anti-cancer benefits of reagents which target autophagy by exploiting the ERS response are being explored (Schönthal, 2009).

FLCN-deficient cells also exhibit increased levels of mTOR activity in a similar manner to that observed in TSC-deficient cells (as discussed in Chapter 2) and autophagic activity is decreased upon loss of TSC1 or TSC2, which also results in overlapping clinical features to BHD patients. Hence I wanted to examine levels of autophagic activity in FLCN-deficient cell lines. In this chapter, I investigated the mRNA levels of genes involved in the regulation of autophagy and the expression of downstream autophagy markers in the context of loss of FLCN. The potential for autophagy to be exploited as a potential therapeutic target for BHD patients is also investigated.

4.2 Results

4.2.1 Autophagic activity is upregulated upon loss of FLCN.

In order to determine the effects of overexpression of FLCN on the regulation of autophagy, western blots probing for the downstream autophagy markers p62 and Microtuble-associated protein light chain 3 (LC3) were conducted on UOK257 (BHD^-) and UOK257-2 (BHD^+) cells treated with or without rapamycin (Figure 25a). It has been shown that protein levels of p62 may be indicative of autophagic activity as well as the conversion of LC3-I (Cytosolic) to LC3-II (lipidated) (Wang *et al.*, 2006). In the BHD^+ UOK257 cells; the ratio of LC3-I to LC3-II protein was approximately equal (Figure 25a). However, in the BHD^- cells the majority of LC3 was in the second isoform (LC3-II) and indicates that these cells generate more autophagosomes. A decrease in the protein levels of p62 was also observed in the

BHD$^-$ UOK257 cells. Together, these data suggest that autophagic activity is increased in UOK257 cells devoid of FLCN.

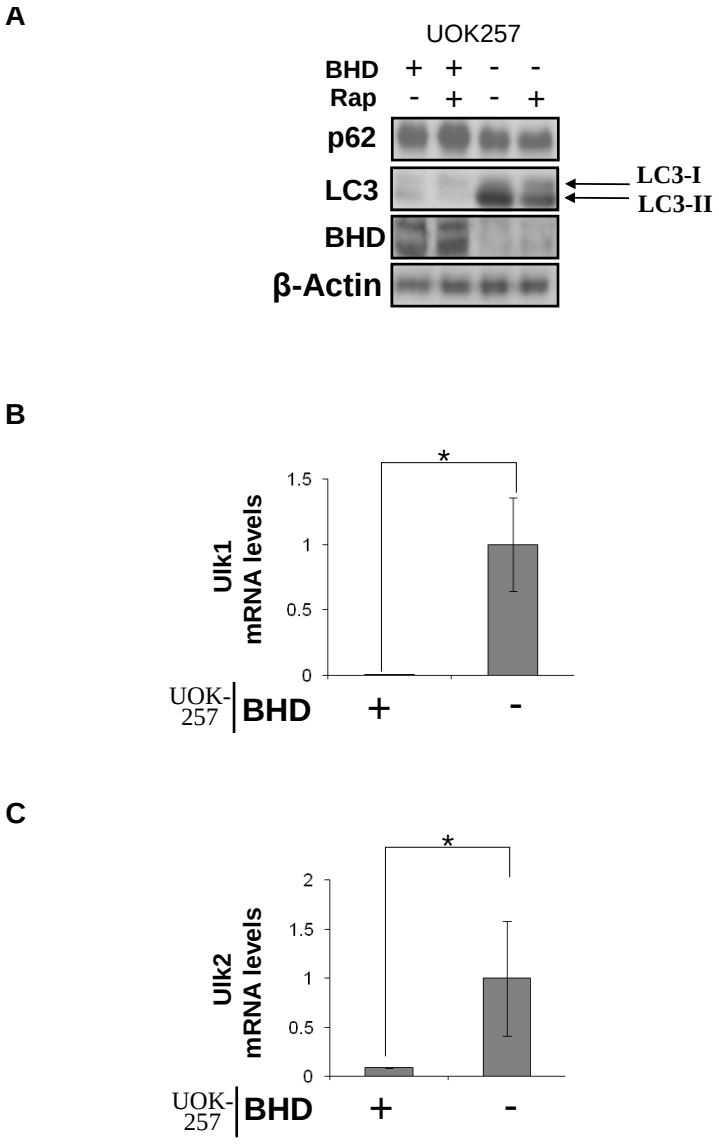

Figure 25. ULK-mediated autophagy is upregulated in UOK257 cells devoid of FLCN.

(A) Lysates were created from BHD$^-$ UOK257 and BHD$^+$ UOK257 cells maintained in normoxia (21%) and treated overnight with 50nm Rapamycin where indicated. Western blot analyses were then performed and protein levels of P62, LC3, Folliculin and β-actin were determined. **(B)** The mRNA levels of ULK1 were compared within the UOK257 and UOK257-2 cell lines by RT-PCR. mRNA levels were standardised against β-Actin mRNA. n = 3. **(C)** The mRNA levels of ULK2 were compared within UOK257 and UOK257-2 cell lines by RT-PCR. mRNA levels were standardised against β-Actin mRNA. n = 3. * = significant at the 0.05 significance level. ** = significant at the 0.01 significance level.

The effects of FLCN on the regulation of genes involved in the initiation of the autophagy pathway in the UOK257 cell line were then examined. Given that ULK1 and UNC-51-like kinase 2 (ULK2) are vital for initiation of autophagy and ULK1 has been shown to be regulated by AMPK (Lee *et al.*, 2010), I wanted to analyse ULK1 and ULK2 in the UOK257 cell line. RT-PCR was used to determine the mRNA levels of ULK1 (Figure 25B) and ULK2 (Figure 25C) in the UOK257 (BHD^-) and UOK257-2 (BHD^+) cell lines. Increased levels of AMPK activity have been observed in the UOK257 cell line and AMPK has been shown to activate ULK-mediated autophagy by binding to the PS domain of ULK1 (Lee *et al.*, 2010). Approximately a 10 fold increase in ULK1 mRNA levels was observed in the BHD- UOK257 cells together with a 5 fold increase in ULK2 mRNA. These data suggest that there is increased transcription of genes involved in the initiation of autophagy in the BHD^- UOK257 cell lines and support the notion that autophagic activity is increased upon loss of FLCN.

In order to confirm these results, the effects of loss of FLCN on the regulation of autophagy were examined in the $BHD^{-/-}$ and $BHD^{+/+}$ MEF cells lines. The expression levels of p62 and LC3-I versus LC3-II protein were determined via western blot analysis (Figure 26a). The mRNA levels of ULK1 were determined by RT-PCR in these cells (Figure 26B). In the $BHD^{+/+}$ MEF cells the ratio of LC3-I to LC3-II protein was approximately equal. However, in the $BHD^{-/-}$ MEF cells the majority of LC3 was in the second isoform (LC3-II). A decrease in the protein levels of p62 was also observed in the $BHD^{-/-}$ MEF cells. Approximately a 3 fold increase in ULK1 mRNA levels was also observed in the $BHD^{-/-}$ MEF cells. Collectively, these data supported the data obtained from the UOK257 cell lines and suggested that autophagic activity is upregulated upon loss of FLCN.

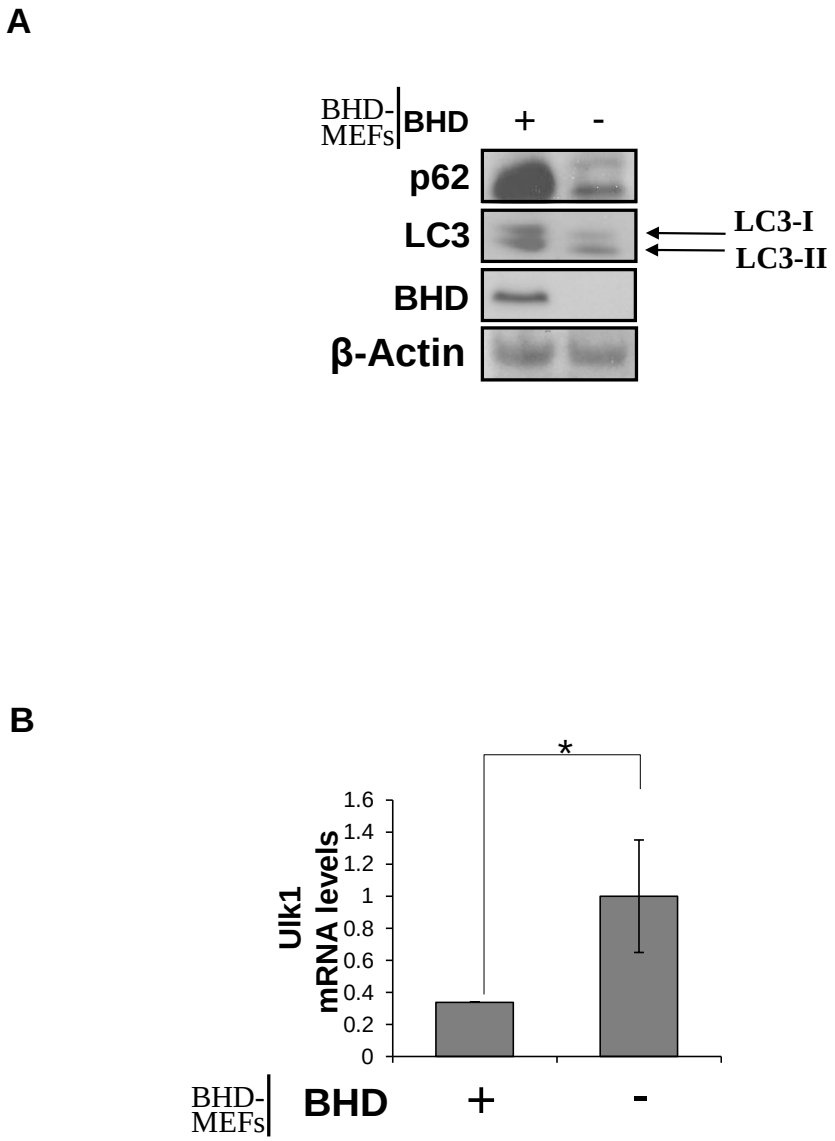

Figure 26. ULK-mediated autophagy is also upregulated in $BHD^{-/-}$ MEF cells.

(A) Lysates were created from $BHD^{-/-}$ and $BHD^{+/+}$ MEF cells maintained in normoxia (21%). Western blot analyses were then performed and protein levels of P62, LC3, Folliculin and β-actin were determined. **(B)** The mRNA levels of ULK1 were compared within $BHD^{-/-}$ and $BHD^{+/+}$ MEF cells by RT-PCR. mRNA levels were standardised against β-Actin mRNA. n = 3. * = significant at the 0.05 significance level. ** = significant at the 0.01 significance level.

4.2.2 Increased level of BNIP3 expression observed in BHD-deficient cells does not account for the increased levels of autophagic activity exhibited upon loss of BHD.

Several studies have shown that localisation of Bcl-2/adenovirus E1B 19-kDa-interacting protein 3 (BNIP3) to the mitochondria may result in decreased mitochondrial membrane potential and increased levels of ROS production, often resulting in necrosis or apoptotic cell death (Burton *et al*., 2009). It has also been suggested that BNIP3 is able to induce autophagy by competing with Beclin-1 for binding with Bcl-2. The binding of Bcl-2 to Beclin-1 inhibits the induction of autophagy, therefore it has been suggested that if there are increased levels of BNIP3 available to bind to Bcl-2, there is more Beclin-1 avalable to stimulate autophagy. BNIP3, by binding to and repressing Rheb, may also be able to initiate autophagy by inhibiting activation of mTORC1, a potent inhibitor of autophagy (Burton *et al.*, 2009) (Figure 27a). It has also been shown that dysfunctional mitochondria are turned over by autophagy during development and under pathological conditions such as cancer (termed mitophagy) (Tolkovsky, 2009). Studies conducted by Hamacher-Brady *et al.* have shown that BNIP3 mediates mitochondrial dysfunction and cell death, and that BNIP3-mediated autophagy is increased in HL-1 cardiac myocytes as a protective mechanism against the BNIP3-mediated cell death observed in these cells (Hamacher-Brady *et al.*, 2006). Further studies conducted by Rikka *et al.* revealed that mitochondrial autophagy is initiated in response to BNIP3-mediated mitochondrial dysfunction; resulting in increased mitochondrial turnover (Rikka *et al.*, 2011).

Work conducted by Dr. Stephen Land has suggested that the BHD$^-$ UOK257 cells have decreased mitochondrial membrane potential (as discussed in Chapter 3) and investigations into the expression levels of HIF transcriptional targets suggest that the BHD$^-$ UOK257 cells have increased protein levels of BNIP3 (as discussed in Chapter 2). I therefore wanted to

examine whether BNIP3 may be involved in the mitochondrial dysfunction observed in the UOK257 cells and whether autophagy was being activated in these cells in response to BNIP3-mediated activation of the mitochondrial cell death pathway.

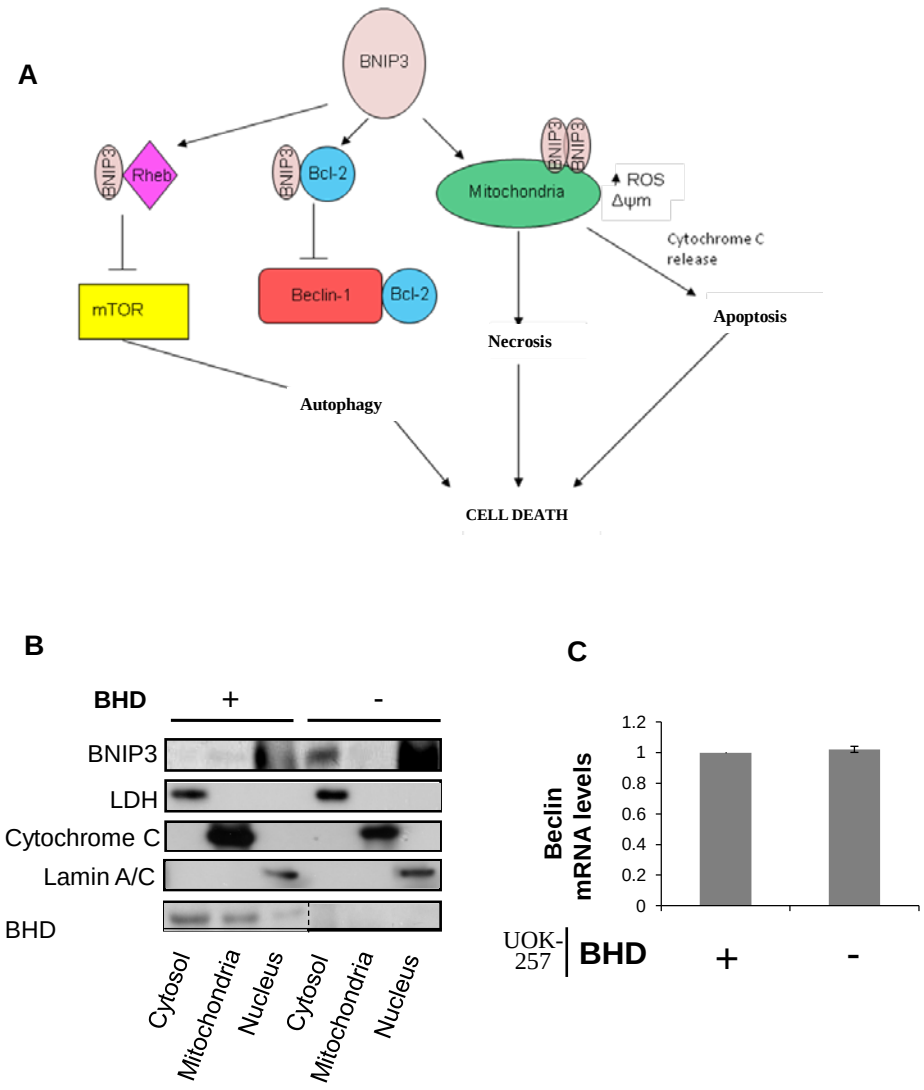

Figure 27 Increased BNIP3 mRNA levels do not account for the increased levels of autophagic activity observed in the UOK257 cells upon loss of FLCN.

(A) Several studies have shown that BNIP3 may induce all of the main types of cell death; necrosis, apoptosis and/or autophagy (Burton and Gibson, 2009). **(B)** Mitochondrial, nuclear and cytosolic protein lysates were created from BHD^- UOK257 and BHD^+ UOK257-2 cells maintained in normoxia (21%). Western blot analyses were then performed and protein levels of BNIP3, Folliculin, lamin A/C, LDH and cytochrome C were determined. **(C)** The mRNA levels of Beclin were compared within BHD^+ UOK257-2 and BHD^- UOK257 cells by RT-PCR. mRNA levels were standardised against β-Actin mRNA.

As BNIP3 initiates cell death and mitochondrial dysfunction when it is localised to the mitochondria, the first stage of investigating whether BNIP3 was involved in the mitochondrial dysfunction observed in the BHD^- UOK257 cells was to determine where BNIP3 was localised in the BHD^- UOK257 and BHD^+ UOK257-2 cells. Cytosolic, nuclear and mitochondrial fractions were created from UOK257 and UOK257-2 cell lines and western blots probing for BNIP3 were conducted (Figure 27B). The results revealed that in the BHD^- UOK257 cells, BNIP3 is localised to the nucleus whereas in the BHD^+ UOK257 cells, BNIP3 is localised to both the nucleus and the mitochondria. Therefore it appears that the increased levels of autophagic activity observed in these cells are not a response to BNIP3 mediated mitochondrial dysfunction and initiation of the mitochondrial cell death pathway. However, it may still be possible that increased levels of BNIP3 are contributing to the increased levels of autophagic activity observed in the UOK257 cells upon loss of FLCN, as mitochondrial autophagy initiated by BNIP3 is not dependent on the mitochondrial cell death pathway being initiated (Rikka *et al.*, 2011).

Beclin-1, a Bcl-2-interacting protein, has also been shown to induce autophagy in mammalian cells (Liang *et al.*, 1999). Beclin-1 is a member of the ATG family which is involved in autophagosome formation (Meijer and Codogno, 2004). A positive association has also been revealed between HIF1α protein expression and expression of Beclin 1 (Wan *et al.*, 2010). Therefore the mRNA levels of Beclin-1 in the BHD^- UOK257 and BHD^+ UOK257-2 cells were determined via RT-PCR (Figure 27C). The results revealed that no difference in the levels of Beclin-1 mRNA occured in the BHD^- UOK257 versus the BHD^+ UOK257-2 cells. These data suggest that increased levels of transcription of Beclin-1 do not account for the increased levels of autophagic activity observed within the BHD^- UOK257 cells.

4.2.3 Exploiting the increased levels of autophagy observed upon loss of BHD may provide a potential therapeutic target for BHD patients

Therapeutic strategies have been developed which seek to exploit the protective components of autophagy and the ERS response and activate apoptotic cell death in tumour cells (Schönthal, 2009). Nelfinavir was initially developed as a treatment for (HIV). It has been shown that Nelfinavir triggers the ERS response via inhibiting the proteasome which leads to subsequent accumulation of 'garbage' proteins which are bound for the Endoplasmic Reticulum Associated Protein Degradation (ERAD) pathway which targets these proteins for ubiquination and degradation by the proteasome (Schönthal, 2009). 3-Methyladenine (3MA) inhibits autophagy by inhibiting the maturation of autophagosomes (Castino *et al.*, 2005). Therefore I sought to examine the effects of these reagents on the levels of autophagy in the $BHD^{+/+}$ and $BHD^{-/-}$ MEFs. First of all, the $BHD^{+/+}$ and $BHD^{-/-}$ MEF cells were treated with 30 μM Nelfinavir and 5 mM 3MA where indicated and their effects on protein expression levels of LC3 were determined via western blot (figure 28a). The results suggested that the ratio of LC3-II to LC3-I exhibited by the $BHD^{+/+}$ MEF cells was increased to levels similar to those observed in the $BHD^{-/-}$ MEFs (figure 28a) when the cells were subjected to treatment with Nelfinavir. These data suggests that Nelfinavir induced autophagy in these cells. Treatment of the $BHD^{-/-}$ MEF cells with 3MA resulted in a reduction of the ratio of LC3-II to LC3-I so that both isoforms were expressed at approximately equal levels in a similar manner to that displayed in the $BHD^{+/+}$ MEF cells (Figure 28a).

As low to medium levels of autophagic activity are thought to provide an advantage to tumour cells by promoting cell survival a CyQUANT (R) cell proliferation assay was conducted to investigate the effects of Nelfinavir and 3MA on the proliferation of the $BHD^{+/+}$

and $BHD^{-/-}$ cells. 3MA appeared to have very little effect on the proliferation of either cell line. Although a general decrease in proliferation was observed when the cells were treated with 3MA in combination with Nelfinavir in a dose dependent manner, no difference between the proliferation of $BHD^{+/+}$ and $BHD^{-/-}$ cells was observed (Figure 28B).

As 3MA on its own did not appear to have a significant effect on the proliferation of either cell line, I decided to examine the effects of another drug which inhibits autophagy, Chloroquine. Chloroquine is a drug which was initially developed as an anti-malarial drug but has subsequently been shown to inhibit autophagy by inhibiting the degradative function of autolysosomes through altered lysosomal pH (Degtyarev *et al.*, 2008). First, the $BHD^{+/+}$ and $BHD^{-/-}$ MEF cells were treated with 30 µM Nelfinavir and 100 µM Chloroquine, where indicated, and their effects on protein levels of LC3 were determined via western blot analysis (Figure 29). These results also suggested that the ratio of LC3-II to LC3-I exhibited by the $BHD^{+/+}$ MEF cells was increased to levels similar to those observed in the $BHD^{-/-}$ MEFs (figure 29) when the cells were subjected to Nelfinavir treatment. No difference was observed in the ratio of LC3-II to LC3-I in the $BHD^{-/-}$ MEF cells upon treatment with Nelfinavir, however an accumulation of LC3-II was observed in both cell lines. Chloroquine treatment on its own did not appear to have an effect on the protein expression levels of p62 in the $BHD^{-/-}$ MEF cells and appeared to decrease p62 protein expression levels in the $BHD^{+/+}$ MEF cells. An increased ratio of LC3-II to LC3-I was also observed in both cell lines under conditions of Chloroquine treatment. However, in glioma cells treatment with

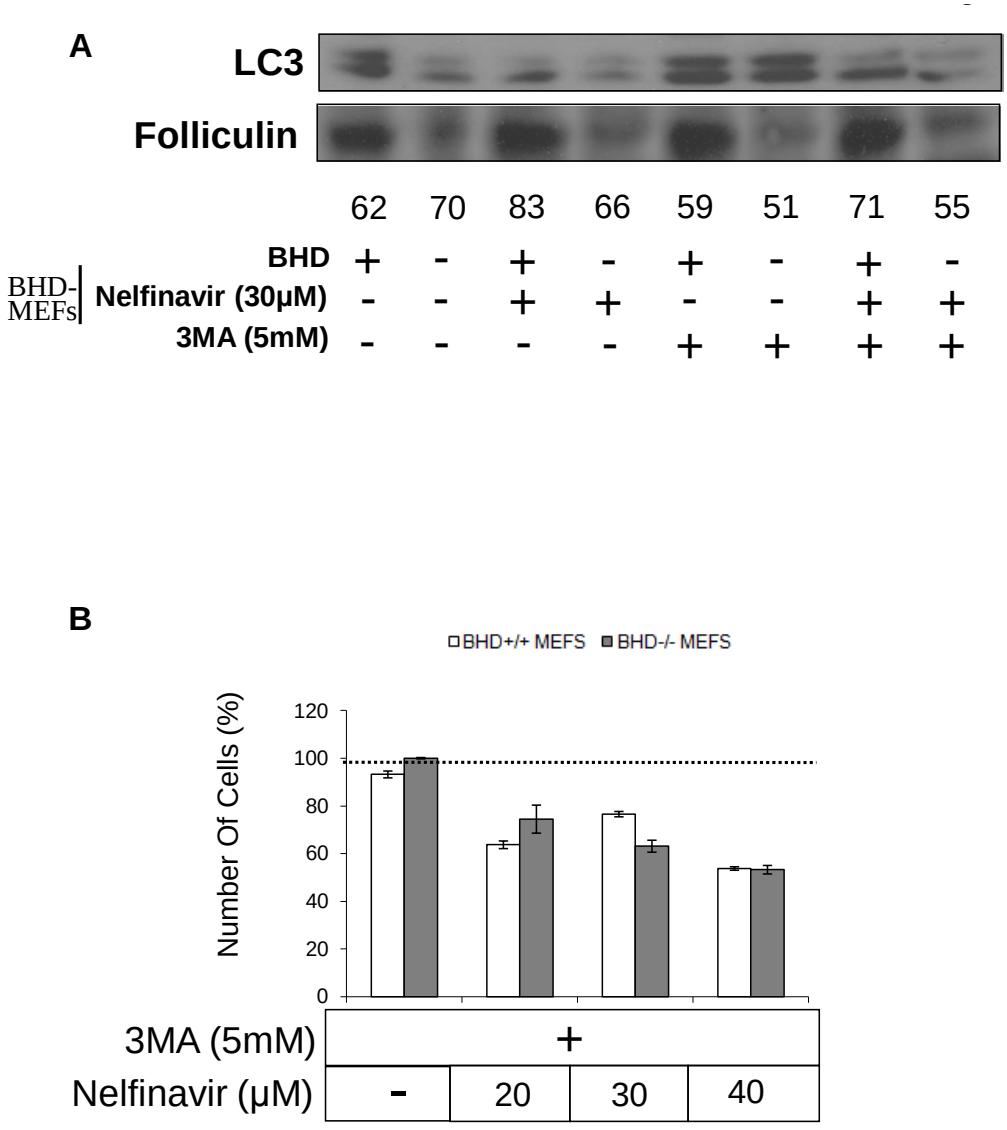

Figure 28. 3MA reduces autophagic activity in $BHD^{-/-}$ MEF cells but does not significantly affect cell proliferation.

(A) Lysates were created from $BHD^{-/-}$ and $BHD^{+/+}$ MEF cells maintained in normoxic conditions (21%) and treated overnight with 30μM Nelfinavir and 5mM 3MA where indicated. Western blot analyses were performed and protein levels of LC3 were determined. Densitometry analyses were performed in order to determine the ratio of LC3-II to LC3-I (level of LC3-II as a percentage of total LC3 shown). **(B)** CyQUANT (R) cell proliferation assays were carried out on $BHD^{-/-}$ and $BHD^{+/+}$ MEF cells maintained in normoxic conditions (21%) and treated overnight with 5mM 3MA and Nelfinavir at 20μM, 30μM, and 40μM concentrations where indicated and absorbance was read. Level of absorbance is representative of the amount of cells present and therefore the level of cell proliferation.

Chloroquine an accumulation of LC3-II and increased formation of autophagic vacuoles was observed which consequently induced cell death (Geng *et al.*, 2010). It may be possible that chloroquine is having a similar effect in these cells. Treatment of the $BHD^{+/+}$ and $BHD^{-/-}$ MEF cells with a combination of both Chloroquine and Nelfinavir resulted in a further decrease in p62 protein levels and an increased ratio of LC3-II to LC3-I in both cell lines; suggesting that a combination of Nelfinavir and Chloroquine results in the largest increase in autophagic activity in these cells. A CyQUANT (R) cell proliferation assay was then conducted in order to investigate the effects of Nelfinavir and Chloroquine on the proliferation of the $BHD^{+/+}$ and $BHD^{-/-}$ cells (Figure 30a). The results suggested that treatment with Nelfinavir selectively inhibited the proliferation of the $BHD^{-/-}$ MEF cells in a dose dependent manner both on its own and in combination with 100 μM Chloroquine. Treatment with 100 μM Chloroquine on its own also selectively inhibited the proliferation of $BHD^{-/-}$ MEF cells by approximately 40%.

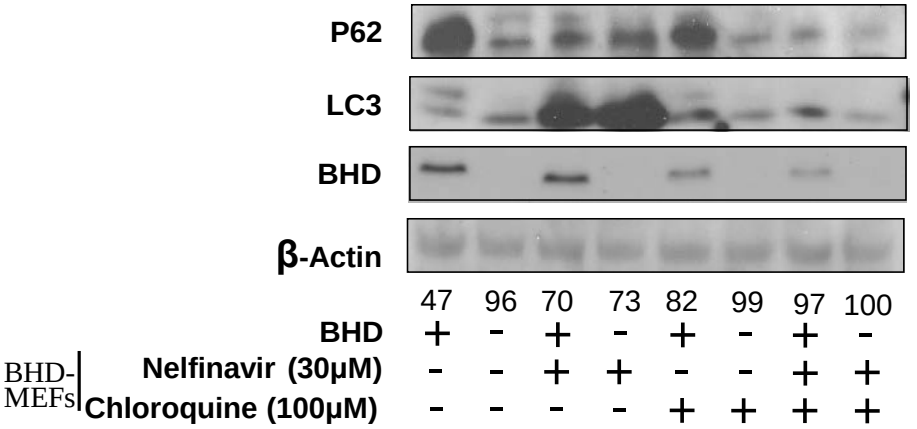

Figure 29. Treatment with Nelfinavir and Chloroquine results in an accumulation of LC3-II in $BHD^{-/-}$ MEF cells.

Lysates were created from $BHD^{-/-}$ and $BHD^{+/+}$ MEF cells maintained in normoxic conditions (21%) and treated overnight with 30μM Nelfinavir and 100μM Chloroquine where indicated. Western blot analyses were then carried out and protein levels of LC3, P62, Folliculin and β-actin were determined. Densitometry analyses were performed in order to determine the ratio of LC3-I to LC3-II (level of LC3-II as a percentage of total LC3 shown).

A combination of Nelfinavir and Chloroquine appeared to have a synergistic effect on the proliferation of $BHD^{-/-}$ MEF cells when compared to treatment with each reagent on its own.

I next sought to determine whether Nelfinavir and Chloroquine selectively induce cell death in the $BHD^{-/-}$ MEFs rather than simply inhibit proliferation. As the cell proliferation assay suggested that treatment with Nelfinavir at the 30 μM concentration produced the most significant difference in terms of cell proliferation between the $BHD^{+/+}$ and $BHD^{-/-}$ MEF cells, 30uM Nelfinavir was used. $BHD^{+/+}$ and $BHD^{-/-}$ MEF cells were treated with Chloroquine (100 μM) and Nelfinavir (30 μM) as indicated and an anti-histone based cell death ELISA assay was conducted (Figure 30B). Approximately a 4 fold increase in levels of cell death was observed in the $BHD^{-/-}$ MEF cells upon treatment with 30μM Nelfinavir both on its own and in combination with 100μM Chloroquine. Treatment with 100μM Chloroquine on its own increased levels of cell death in the $BHD^{-/-}$ MEF cells by approximately 3 fold.

Collectively, the results suggested treatment with Nelfinavir, Chloroquine, or a combination of both selectively induced cell death in the $BHD^{-/-}$ MEF cells at these concentrations.

In order to determine whether Chloroquine and Nelfinavir selectively induce cell death in the $BHD^{-/-}$ MEFs at slightly lower concentration levels, $BHD^{+/+}$ and $BHD^{-/-}$ MEF cells were treated with Chloroquine (50 μM) and Nelfinavir (20 μM), as indicated, and a cell death ELISA assay was conducted (Figure 31). Cells were also treated with a combination of 50 nm rapamycin and 50 μM Chloroquine where indicated for comparison. Treatment with 20 μM Nelfinavir still induced cell death selectively in the $BHD^{-/-}$ MEF cells, although this induction of cell death was to a lesser degree than that observed when the cells were treated with 30 μM Nelfinavir.

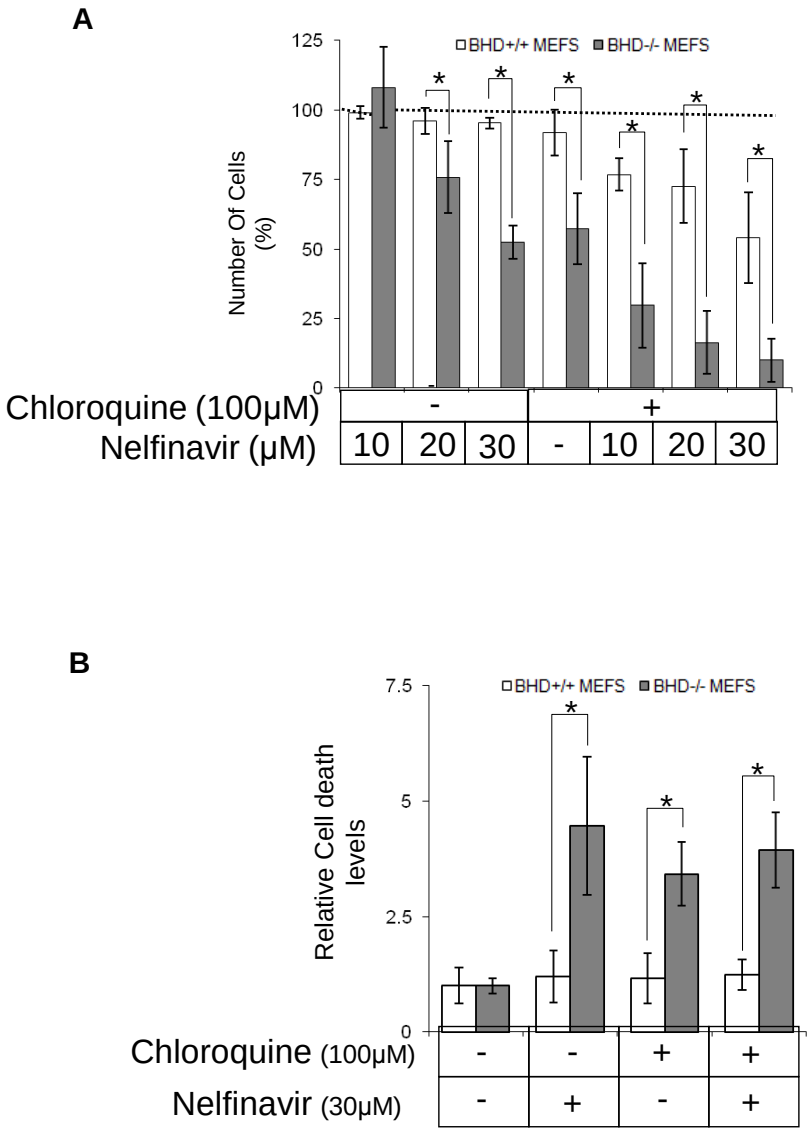

Figure 30. Treatment with Nelfinavir and Chloroquine selectively reduces proliferation of $BHD^{-/-}$ MEF cells and selectively induces cell death in $BHD^{-/-}$ MEF cells.

(A) CyQUANT (R) cell proliferation assays were carried out on $BHD^{-/-}$ and $BHD^{+/+}$ MEF cells maintained in normoxia (21%) and treated overnight with 100μM Chloroquine and Nelfinavir at 10μM, 20μM, and 30μM concentrations where indicated and absorbance was read. Level of absorbance is representative of the amount of cells present and therefore cell number n=3. **(B)** Cell death assays were carried out on $BHD^{-/-}$ and $BHD^{+/+}$ MEF cells maintained in normoxia (21%) and treated overnight with 100μM Chloroquine and 30μM Nelfinavir where indicated and absorbance was read. Level of absorbance is representative of the amount of histone and therefore level of cell death. n=3. * = significant at the 0.05 significance level. ** = significant at the 0.01 significance level.

Treatment with 50 μM Chloroquine did not induce cell death in either cell line; however a combination of 20 μM Nelfinavir and 50 μM Chloroquine resulted in an increase in cell death levels in the $BHD^{-/-}$ MEF cells of approximately 5.5 fold. Treatment with a combination of 50 nM rapamycin and 50 μM Chloroquine selectively induced cell death in the $BHD^{-/-}$ MEF cells by approximately 4.5 fold; however this effect was not as great as that observed after combined treatment with 50 μM Chloroquine and 20 μM Nelfinavir. These data support the notion that exploiting the increased levels of autophagy observed upon loss of FLCN may provide a potential therapeutic target for BHD patients.

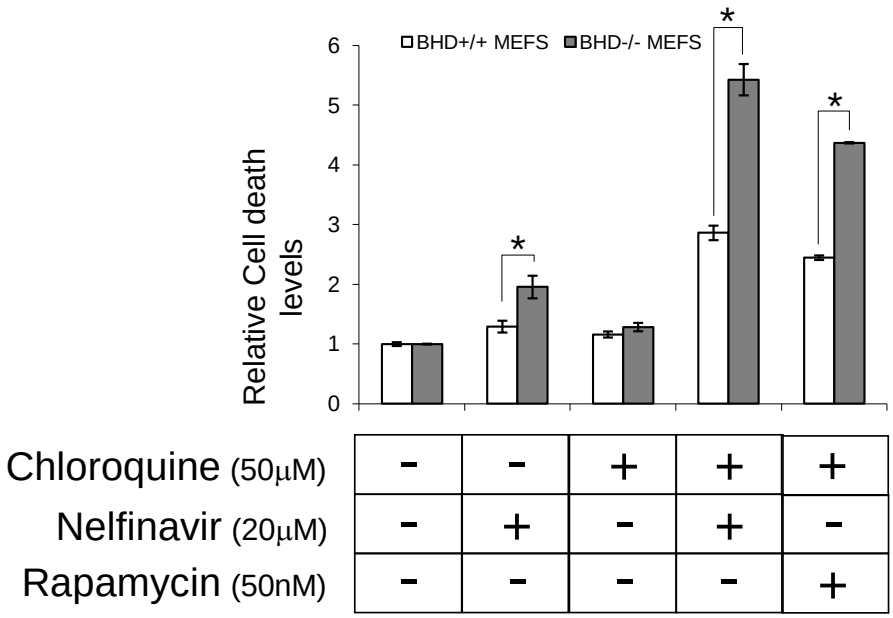

Figure 31 Treatment with Nelfinavir and Chloroquine at lower concentrations still selectively induces cell death in $BHD^{-/-}$ MEF cells.

(A) Cell death assays were carried out on $BHD^{-/-}$ and $BHD^{+/+}$ MEF cells maintained in normoxia (21%) and treated overnight with 50μM Chloroquine, 20μM Nelfinavir, and 50nm rapamycin where indicated and absorbance was read. Level of absorbance is representative of the amount of histone and therefore level of cell death. n=3. * = significant at the 0.05 significance level. ** = significant at the 0.01 significance level.

4.3 Discussion

4.3.1 ULK mediated autophagic activity is upregulated upon loss of function of FLCN

Autophagy may be reduced upon loss of several tumour suppressor proteins such as PTEN, TSC1 and TSC2, as well as LKB1/STK11 (Maiuri *et al.*, 2009). Although moderately elevated levels of autophagy may provide protection for tumour cells, apoptosis can be initiated when autophagic activity becomes extremely high. The protective functions of autophagy are abandoned when autophagy becomes too high and triggers cell death (Schönthal *et al.*, 2009). Data from this chapter provide evidence that autophagic activity is upregulated in cells deficient in FLCN. Further analysis into autophagy also suggests that exploitation of their high autophagic activity may provide a potential therapeutic target for BHD patients. Given that BHD$^-$ UOK257 cells exhibit decreased expression levels of p62 protein and an accumulation of LC3-II protein, it is likely that both ULK1 and ULK2 are driving the autophagic activity in the UOK257 cells deficient in FLCN. This may be due to increased levels of AMPK resulting in activation of ULK1. Of interest there is an accumulation of the second isoform of LC3 in the BHD$^-$ UOK257 cells.

4.3.2 Aberrant levels of mTORC1 activity do not appear to inhibit levels of autophagic activity upon loss of functional FLCN.

As discussed in Chapter 2; BHD$^-$ UOK257 cells exhibit increased levels of mTORC1 activity. Autophagy is suppressed by mTORC1 through direct regulation of the ~3-MDa ULK1–Atg13–FIP200 complex (Hosokawa *et al.*, 2009). mTORC1 inhibition has also been

shown to reduce phosphorylation of ULK1, suggesting that mTORC1 inhibits ULK1 by direct phosphosphorylation (Kim *et al.,* 2011). Thus, increased levels of mTORC1 activity should lead to inhibition of ULK1-mediated autophagy. However, RT-PCR data obtained from the UOK257 cell line suggested that BHD^- UOK257 cells exhibit increased levels of ULK1 and ULK2 mRNA. During autophagy, the cytosolic form of LC3 (LC3-I) is converted to LC3-II, at the same time as cytoplasmic components are being engulfed by autophagosomes. LC3-II, is subsequently recruited to autophagosomal membranes. Lysosomes then fuse with the autophagosomes to form autolysosomes and then degradation of the engulfed cytoplasmic components within the autophagosomes occur (Tanida *et al.,* 2008). The accumulation of LC3-II protein within the BHD^- UOK257 cells could also suggest that the autophagosomes may have difficulties fusing with lysosomes in these cells. The fact that increased levels of ULK1 mRNA are also exhibited in a $BHD^{-/-}$ MEF cell line, together with decreased levels of p62 protein and an accumulation of LC3-II protein, suggests that ULK-mediated autophagic activity is also upregulated in these cells. These data support the work conducted on the UOK257 cell line and suggest that increased autophagic activity can occur upon loss of FLCN.

4.3.3 Aberrant levels of AMPK activity may be contributing to the increased levels of autophagic activity upon loss of functional FLCN.

The mitochondrial dysfunction and subsequent reduction in mitochondrial membrane potential and ATP levels observed in the BHD^- UOK257 cells result in the increased levels of AMPK activity (as discussed in Chapter 3). The high levels of AMPK activity in these BHD null cells are most likely leading to ULK1 complex activation as AMPK has been shown to bind to, phosphorylate and activate ULK1 (Kim *et al.,* 2011). It is possible that the high

levels of AMPK induced phosphorylation of ULK1 lead to increased levels of autophagic activity in the UOK257 cells deficient in FLCN.

4.3.4 The elevated levels of autophagic activity observed in these cells are not a response to BNIP3 mediated mitochondrial dysfunction and initiation of the mitochondrial cell death pathway.

HIF is able to mediate autophagy via the induction of BNIP3 (Bellot *et al.,* 2009). Several studies have shown that BNIP3 is able to induce mitochondrial dysfunction and cell death, and that autophagy is upregulated in response to BNIP3-mediated mitochondrial dysfunction and cell death (Hamacher-Brady *et al.,* 2006). As I saw higher levels of BNIP3 mRNA and protein in the BHD^- UOK257 cells, I hypothesised that the observed reduction of mitochondrial membrane potential and high autophagic activity upon loss of functional FLCN could involve BNIP3. However, western blot analyses revealed that BNIP3 is not localised to the mitochondria in BHD^- UOK257 cells, suggesting that the elevated levels of autophagic activity observed in these cells are not a response to BNIP3 mediated mitochondrial dysfunction and initiation of the mitochondrial cell death pathway. However, it may still be possible that increased levels of BNIP3 are contributing to the increased levels of autophagic activity observed in the UOK257 cells upon loss of FLCN; as mitochondrial autophagy initiated by BNIP3 is not dependent on the mitochondrial cell death pathway being initiated (Rikka *et al.,* 2011). It could be possible that nuclear localised BNIP3 could also have a part to play in upregulation of gene-expression that drives autophagy.

RT-PCR analyses also revealed no difference in the mRNA levels of Beclin-1 between the UOK257 cell lines. This suggests that that increased levels of transcription of Beclin-1 do

not account for the increased levels of autophagic activity observed within the BHD^- UOK257 cells.

4.3.5 The increased levels of autophagic activity observed upon loss of function of FLCN may serve to protect against mitochondrial dysfunction and subsequent induction of apoptosis.

Work conducted by Xu *et al.* has also shown that production of H_2O_2 leads to mitochondrial dysfunction which induces apoptosis and autophagy (Xu *et al.*, 2010). It has also been shown that dysfunctional mitochondria are turned over by autophagy (Tolkovsky *et al.*, 2009). Investigations conducted on the UOK257 cell line revealed that BHD^- UOK257 cells are not respiring properly due to the presence of dysfunctional mitochondria. Further investigation has revealed that there are also elevated levels of H_2O_2 in the growth media of BHD^- cells. Combined with the increased levels of autophagic activity in the BHD^- UOK257 cells these data imply that increased H_2O_2 production may have resulted in mitochondrial dysfunction and that this may have led to subsequent induction of autophagy in the UOK257 cells upon loss of FLCN in order to try and catabolise these dysfunctional mitochondria.

4.3.6 Inhibition of autophagic activity via treatment with Chloroquine selectively induces cell death in BHD-deficient cells.

Therapeutic strategies have been developed which seek to exploit the protective components of autophagy and activate apoptotic cell death in tumour cells (Schönthal *et al.*, 2010). As elevated levels of autophagic activity are observed in the FLCN-deficient cell lines, I sought to investigate whether exploiting the protective components of autophagy may be a potential therapeutic strategy for treatment of BHD patients. Data obtained from the $BHD^{+/+}$ and $BHD^{-/-}$ MEF cells revealed that treatment with 3MA did not result in the selective inhibition

of proliferation of the $BHD^{-/-}$ MEF cells. However, treatment with Chloroquine at the 100 µM concentration did selectively inhibit cell proliferation and induce cell death in the $BHD^{-/-}$ MEFs. Treatment with Chloroquine has been shown to increase the formation of autophagic vacuoles and induces cell death in glioma cells (Geng *et al.*, 2010). An accumulation of LC3-II is also observed in the $BHD^{-/-}$ cells when treated with 100 µM Chloroquine. It is possible that Chloroquine at the 100 µM concentration induced cell death in these cells by impeding autophagic fluxing. These data support the notion that the elevated levels of autophagic activity exhibited by these cells is providing a protective function and suggests that inhibition of autophagic activity may provide a potential therapeutic treatment for BHD patients. It may be beneficial to investigate whether other autophagy inhibitors may provide therapeutic benefit for BHD patients.

4.3.7 Activation of the ERS response and autophagic activity selectively induces cell death in BHD-deficient cells

It has been shown that, although autophagy and the ERS response pathway function independently; when the activity of one of these processes is altered the activity of the other is also altered. Work conducted by Kang *et al.* also suggested that ER stress inducing reagents may be used to selectively kill TSC1 or TSC2 mutant cells and could provide therapeutic benefit for patients with TSC (Kang *et al.*, 2010). It may be possible that treatment with ER stress reagents increases the already elevated autophagic activity in the $BHD^{-/-}$ MEFs to a level which would selectively induce cell death in these cells. Evidence to support this notion was provided by data obtained from $BHD^{+/+}$ and $BHD^{-/-}$ MEF cells treated the reagent Nelfinavir. Data obtained from these cells revealed that treatment with Nelfinavir resulted in an accumulation of LC3-II protein in these cells; indicative of autophagic activity.

Cell death ELISAs revealed that treatment with Nelfinavir selectively inhibits cell proliferation and induces cell death in the $BHD^{-/-}$ cells (both at the 20 μM and 30 μM concentration). As Nelfinavir enhanced autophagy in these cells, this work suggests that further increases in autophagic activity can lead to cell death in BHD deficient cells. Another proteosomal inhibitor which induces ER stress is bortezomib (Velcade). Bortezomib is already clinically approved for treating other cancers and may selectively induce cell death in the $BHD^{-/-}$ MEFs by inducing autophagy in a similar manner to that observed under conditions of Nelfinavir treatment.

4.3.8 Treatment with a combination of Chloroquine and Nelfinavir appears to have a synergistic effect in selectively inducing cell death in BHD-deficient cells.

Several reports have shown that targeting mTORC1 with rapamycin induces autophagy (Turcotte and Giaccia, 2010). When Parkhitko *et al.* examined the effects of a combined treatment of Chloroquine with the mTORC1 inhibitor rapamycin on TSC2-deficient tumours they observed that a combination of the two reagents resulted in a reduction in tumour size which was greater than that observed when the tumours were subjected to treatment with each reagent individually. Data obtained from $BHD^{+/+}$ and $BHD^{-/-}$ MEF cells suggested that treatment with a combination of 50 nm rapamycin and 25 μM Chloroquine also selectively inhibited proliferation and induced cell death in $BHD^{-/-}$ MEF cells. However this induction of cell death in the $BHD^{-/-}$ cells was not as great as that observed when the $BHD^{-/-}$ cells were treated with a combination of 25 μm Nelfinavir and 50 μM Chloroquine. This work suggests that out of the combinations tested, treatment with both 25 μm Nelfinavir and 50 μM Chloroquine was the most effective at selectively inducing cell death in the $BHD^{-/-}$ cells. These data are supported by western blot analyses which revealed that treatment of $BHD^{-/-}$

cells with Chloroquine and Nelfinavir resulted in the largest decrease in p62 protein levels and the greatest accumulation of LC3-II protein. The fact that both of these reagents are currently administered to humans for treatment of malaria (Chloroquine) and HIV (Nelfinavir) enhances their potential as a therapeutic treatment for BHD as these reagents are safe to administer to humans. However further analysis will have to be conducted in order to confirm whether these drugs have therapeutic potential in the context of BHD. It may also be beneficial to investigate whether treatment with combinations of other ERS response inducers and autophagy inhibitors, such as those mentioned above, could inhibit proliferation and induce cell death in FLCN-deficient cells more effectively than the combination of Nelfinavir and Chloroquine, and so provide alternative drug combinations.

Chapter 5
Final discussion

5 Final discussion

Data presented in chapters 2, 3 and 4 revealed that loss of functional FLCN resulted in increased levels of mTOR signalling and AMPK activity. Aberrant levels of HIF transcriptional activity and transcription of genes involved in mitochondrial biogenesis are also observed within FLCN-deficient cells, including PGC1α. The elevated levels of mitochondrial biogenesis upon loss of functional FLCN have subsequently resulted in increased mitochondrial DNA levels. Mitochondrial dysfunction and reduction of mitochondrial cristae has also been observed in FLCN-deficient cells. Loss of functional FLCN results in increased levels of ROS production, depleted ATP levels and increased mitochondrial membrane permeability. These changes upon loss of functional FLCN result in BHD-deficient UOK257 cells exhibiting a metabolic profile resembling the Warburg effect. Elevated levels of ULK-mediated autophagic activity were also observed in cells deficient in functional FLCN. Furthermore, data obtained from $BHD^{-/-}$ MEF cells suggests that increased autophagic activity exhibited upon loss of functional FLCN may be exploited as a potential therapeutic target. Here I shall discuss my findings presented in these chapters that indicate how FLCN might function as a tumour suppressor. Furthermore, I will discuss how my findings might provide useful insight for potential therapeutic strategies to reduce tumour formation (cancer progression) in BHD patients.

5.1 Translocation of FLCN between the nucleus and mitochondria may be involved in sensing ROS, and the maintenance of energy homeostasis.

Data obtained from localisation studies conducted on HEK293 cells revealed that endogenous FLCN localised to the nucleus, cytoplasm and mitochondria. This localisation of FLCN is altered upon inhibition of mTOR and activation of AMPK, both of which are involved in mitochondrial biogenesis and are sensitive to changes in ATP levels. Given that increased levels of ROS production are also observed upon loss of functional FLCN, it may be possible that FLCN is involved in energy homeostasis and sensing ROS. In response to ROS and other DNA damage agents, the DNA damage response pathway is activated in order to repair the damage and/or initiate apoptosis. The signalling response initiated depends on the type of DNA damage present. For example ATM and ATR mediate repair of double strand breaks while members of the Poly(ADP-ribose) polymerase family mediate repair of double and single strand breaks. Mutations in genes involved in the DNA damage response pathway can also lead to defects within the immune, nervous and reproductive systems as well as premature aging and cancer (Ciccia and Elledge, 2010). It may be possible that FLCN and its complexes are involved in sensing DNA damage and subsequent initiation of the DNA damage response pathway and apoptotic response.

Data obtained by electron microscopy conducted on the $BHD^{+/+}$ and $BHD^{-/-}$ MEF cells suggests that increased ROS levels upon loss of FLCN may lead to loss of cristae. This subsequently results in decreased surface area of the inner mitochondrial membrane and reduced ability for these FLCN-deficient cells to produce ATP via the electron transport chain (Akao *et al.*, 2003). However, the mitochondrial damage exhibited and subsequent

decreased mitochondrial membrane potential may be increasing ROS production and thus causing DNA damage within FLCN-deficient cells. To determine whether increased levels of ROS result in loss of mitochondrial cristae upon loss of functional FLCN or whether the cristae remodelling results in increased levels of ROS, electron microscopy work may be undertaken after treating $BHD^{-/-}$ MEF cells with antioxidants (Blokhina, 2003). If increased numbers of cristae are observed after treating the cells with antioidants this may suggest that it is the increased levels of ROS which are causing the loss of cristae within the mitochondria of BHD-deficient cells.

Data obtained from the BHD-deficient cells suggest that levels of PGC1α gene transcription are upregulated upon loss of FLCN. The fact that the data presented in chapter 3 suggest that PGC1α is upregulated upon knockdown of *BHD* by shRNA suggests that FLCN may directly regulate PGC1α. Further interaction studies conducted on purified FLCN would be required in order to determine whether FLCN interacts and regulates PGC1α directly. For example Folliculin could be purified using immunoprecipitation and mass-spectrometry analyses performed in order to determine whether PGC1α is co-purified with Folliculin.

The data presented in chapter 3 reveals that increased levels of PGC1α transcription drives mitochondrial biogenesis and mitochondrial DNA content upon loss of functional FLCN. Collectively, these data support the notion that loss of BHD results in an accumulation of mitochondria. This accumulation of mitochondria may be as a compensatory mechanism in response to the depleted mitochondrial ATP levels and mitochondrial dysfunction observed upon loss of FLCN in order to try and increase the amount of mitochondria and thus ATP production in these cells.

PGC1α also increases the expression of genes involved in fatty acid oxidation and gluconeogenesis (Liang and Ward, 2006). Data presented in chapter 2 suggests that glucose uptake and fatty acid oxidation may also be upregulated in BHD-deficient cells as a result of increased activity of enzymes such as GLUT1 and HOAD in order to meet their energy demands. The increased levels of PGC1α observed upon loss of functional FLCN may contribute to the increased levels of glucose utilisation and fatty acid oxidation observed in FLCN-deficient cells in order to compensate for the decreased levels of ATP production. PGC1α expression therefore could enhance energy production within the BHD-deficient cells via multiple mechanisms.

Data presented in chapter 3 also suggests that the increased transcription of PGC1α observed upon loss of functional FLCN also increases the expression levels of antioxidant enzymes such as SOD2 as well as UCPs in response to the increased ROS production (Valle *et al.*, 2005; St Pierre *et al.*, 2006). This increase in UCP expression may contribute to the compromised mitochondrial membrane potential and subsequent decrease in ATP levels (Patanè, 2002). Overall, the data reflect that FLCN null cells are less capable at maintaining energy homeostasis.

It may be possible that, as well as reduced cristae, FLCN-deficient cells exhibit defects within the complexes of the electron transport chain. It has been documented that oncocytomas can exhibit defects within complex 1 of the electron transport chain along with accumulation of mitochondria (Simonnet *et al.*, 2003). It is possible that oncocytomas in BHD patients might have a similar mitochondrial complex 1 defect. Further electron microscopy work as well as measuring the activity of the mitochondrial respiratory chain complexes would be required to

determine whether FLCN null cells from BHD patients exhibit defects within the mitochondrial complexes.

5.2 FLCN modulates the transcriptional activity of HIF.

Data presented in chapter 2 imply that the activity of HIF is potently increased upon loss of FLCN. Increased HIF activity results in increased transcription of VEGF, BNIP3, and CCND1. It is likely that the increased levels of AMPK activity exhibited by the FLCN-deficient cells also contribute to the increased HIF1α activity levels observed upon loss of FLCN, as AMPK is able to regulate HIF via a signalling pathway independent of PI3K/Akt (Lee *et al.*, 2003).

Data presented in chapter 2 suggests that FLCN is translocated to the nucleus where it might modulate transcription factors such as HIF. It may be possible that the increased levels of HIF activity observed upon loss of functional FLCN may be as a result of the nuclear pool of FLCN modulating HIF transcriptional activity, possibly via VHL. FLCN patients are susceptible to developing cysts in the lungs and the kidneys in a in a manner analogous to TSC patients (Toro *et al.*, 2007; Baba *et al.*, 2008) and cilia are important in the regulation of cyst formation (Pazour *et al.*, 2002; Yoder *et al.*, 2002). It may be possible that FLCN could regulate ciliary function. Both TSC2 and VHL are known to localise to cilia. Given that loss of function of FLCN results in cyst formation, BHD might be a ciliopathy. Further localisation studies are needed to determine whether FLCN is localised to the cilia and whether it is a ciliopathy.

HIF transcriptional activity may also be enhanced upon loss of functional FLCN as a result of the increased levels of mitochondrial biogenesis causing an increased demand for oxygen and

a transient hypoxic environment within a cell (Shoag and Arany, 2010). Increased mitochondrial biogenesis may create a transiently hypoxic environment within a cell upon loss of BHD and contribute to HIF stabilisation under normoxic conditions within the FLCN-deficient cells. In order for these cells to restore normal function, HIF1α-mediated transcription of VEGF-A would promote angiogenesis and resupply these cells with oxygen.

Data presented in chapter 2 showed that FLCN-deficient UOK257 cells favour glycolysis over oxidative phosphorylation; thus exhibiting a metabolic profile which reflects the Warburg effect (Preston *et al.*, 2011). Via personal communication with Dr Arnim Pause (McGill University, Canada), it appears that $BHD^{-/-}$ MEFS also have increased glycolysis and l-lactate production. The metabolic changes observed in the BHD^{-} UOK257 cells may result in glucose entering the pentose phosphate pathway more readily, leading to increased production of nucleotides, aromatic amino acids and fatty acids. All of these are essential for cell proliferation (Van der Heiden *et al.*, 2009). FLCN-deficient UOK257 cells also appear to take up and oxidise the excess L-lactate produced and use it as a metabolic fuel. This is an important adaptation for tumour cells and may provide a proliferative advantage for these FLCN-deficient cells, particularly in the hypoxic environment of the core of a tumour where cells may be in energy defecit as a result of reduced ability to produce ATP via oxidative phosphorylation.

The elevated levels of glucose uptake and metabolism via glycolysis and increased ability for FLCN-deficient cells to take up and oxidise L-lactate may also function as a compensatory mechanism due to these cells being energy deficient. However, less ATP is generated by glycolysis compared to oxidative phosphorylation. This may further contribute to the depleted ATP levels exhibited by the BHD^{-} UOK257 cells (Van der Heiden *et al.*, 2009).

5.3 FLCN may be involved in a negative feedback loop which causes PI3K-Akt-mTOR signalling to be inhibited.

Data obtained from the FLCN-deficient UOK257 cell line also provides evidence that loss of functional FLCN results in increased levels of mTORC1 activity. This may be as a result of increased activation of Akt, as increased levels of Akt phosphorylation at Thr308 (a PDK1 phosphorylation site) and Ser473 (an mTORC2 phosphorylation site) are observed in the UOK257 cell line upon loss of FLCN. mTORC2 has also been shown to phosphorylate and stabilise Akt (Facchinetti *et al.*, 2008), and Hasumi *et al.* have observed increased mTORC2 activity levels along with increased expression levels of Rictor (a regulator of mTORC2) in tumours from $BHD^{d/+}$ mice (Hasumi *et al.*, 2009). Collectively, these data suggest that mTORC1 signalling levels are elevated in these BHD deficient cell lines as a result of increased mTORC2 signalling and subsequent Akt activation. These data also support the notion that FLCN might be involved in a negative feedback loop leading to inhibition of PI3K-Akt-mTOR signalling (Hasumi *et al.*, 2009)

5.4 Aberrant levels of AMPK and mTOR signalling may be contributing to the tumourigenesis observed upon loss of functional FLCN.

mTOR is involved in the regulation of cell proliferation, protein translation, and cell survival. Aberrant mTOR signalling observed in these FLCN-deficient cancer cell lines is therefore important for promoting their proliferation and survival (Watanabe *et al.*, 2011). However, these are processes which require a lot of energy (Chhipa *et al.*, 2011). In order to meet this

increased demand for energy, more mitochondria are required in order to generate more ATP. Aberrant levels of mTOR signalling have been shown to result in increased levels of PGC1α transcription and mitochondrial biogenesis in TSC-deficient cells (Cunningham *et al.*, 2007). Transcription of PGC1α could be further enhanced by mTOR in FLCN-deficient cells to increase the levels of mitochondrial biogenesis and mitochondrial levels. Data presented in chapter 3 revealed that the elevated level of PGC1α gene transcription was reduced upon treatment with the mTORC1 inhibitor rapamycin in these FLCN-null cells.

This constitutive activation of mTORC1 upon loss of functional FLCN also appears to contribute to the increased levels of HIF activity in a manner analogous to that observed in TSC2-deficient cells (Land and Tee, 2007). This is supported by data from chapter 2, revealing that the increased levels of HIF activity observed in both the UOK257 and MEF cell lines are reduced upon treatment with rapamycin. It is likely that mTORC1 enhances HIF transcriptional activity within FLCN-deficient cells.

Activation of the PI3K/Akt/mTOR pathway also contributes to increased ROS production in cells via increased glucose metabolism (Kim *et al.*, 2005). It may be possible that increased glycolytic activity exhibited by the BHD-deficient UOK257 cells as a result of the arberrent levls of mTOR activity observed in these cells also contribute to production of ROS species such as H_2O_2 observed in BHD-deficient cells.

The data presented suggest that in the BHD-deficient cells increased levels of Akt induce aberrant levels of mTOR signalling which may subsequently result in elevated levels of ROS production, increased levels of mitochondrial biogenesis, increased levels of HIF transcriptional activity and a metabolic profile which mimics the Warburg effect.

The data presented in chapter 3 provides evidence that endogenous FLCN located in the nucleus resolves as an upper isoform. However, when mTORC1 activity is inhibited upon treatment with rapamycin, the lower isoform of FLCN becomes more apparent in the nuclear fraction. These data suggests that the phosphorylation status of the nuclear pool of FLCN is reduced upon inhibition of mTORC1 signalling. Furthermore, rapamycin treatment results in increased expression of the lower isoform of FLCN in the mitochondrial fraction; suggesting that dephosphorylated FLCN shuttles to the mitochondria. Collectively, these data support the hypothesis proposed by Baba *et al.* that the mTORC1 pathway plays a role in the modulation of FLCN phosphorylation and presumably its tumour suppression function (Baba *et al.*, 2006; Baba *et al.*, 2008). However, further investigation is required in order to determine whether FLCN is a direct mTORC1 substrate or a substrate of a kinase activated downstream of mTOR. This may be achieved via conducting mTORC1 kinase assays on purified FLCN/FNIP protein complexes or purifying FLCN via immunoprecipitation and observing whether mTORC1 or S6K are co-purified.

Data provided in chapter 2 also suggest that levels of AMPK activity are increased upon loss of functional FLCN. AMPK may be upregulated upon loss of functional FLCN in response to the depleted ATP levels and mitochondrial dysfunction exhibited in BHD-deficient cells in order to inhibit processes which are energy demanding; thus conserving ATP within BHD-deficient cells and promoting their survival (Yun *et al.*, 2005; Chhipa *et al.*, 2011). AMPK has been shown to regulate PGC1α (Zong *et al.*, 2002). Therefore, FLCN may also regulate PGC1α through modulation of AMPK. AMPK has also been shown to enhance HIF-1 transcriptional activity (Lee *et al.*, 2003). It is therefore likely that the changes to the metabolic profile of cells upon loss of FLCN are also, at least in part, as a result of arberrent

levels of AMPK activity in response to the depleted ATP levels observed in BHD-deficient cells.

As AMPK has previously been shown to bind to FLCN and its binding partners, FNIP1 or FNIP2, it may also be possible that FLCN directly regulates AMPK (Baba *et al.*, 2006). Decreased expression of the lower isoform of FLCN was also observed in the mitochondrial fraction upon treatment with 2-DG. These data support the notion that FLCN is phosphorylated by AMPK (Baba *et al.*, 2006). It may be possible that FLCN expressed in the nucleus regulates transcription of PGC1α, and that both mTORC1 and AMPK drive mitochondrial biogenesis through modulation of FLCN phosphorylation.

5.5 Increased levels of autophagic activity observed upon loss of functional FLCN may provide a viable therapeutic target for BHD patients.

Autophagy is induced within cells as a stress response and catabolises unnecessary structures such as old/damaged organelles and proteins (Hands *et al*., 2009). Data presented in chapter 4 suggests that autophagy might be enhanced in the UOK257 cells upon loss of BHD. This may be via increased binding of AMPK to ULK, and direct phosphorylation of ULK via AMPK (Lee *et al.*, 2010). As it has been shown that dysfunctional mitochondria may be turned over by mitophagy (Tolkovsky *et al.*, 2009), it might be possible that mitophagy is upregulated upon loss of functional FLCN. Mitophagy may provide protection for these tumour cells via catabolising the dysfunctional mitochondria observed in FLCN-deficient cells. The enhanced level of autophagy in FLCN-deficient MEF cells is likely due to increased AMPK/ULK1 activity. FLCN could directly regulate ULK. However further investigation would be required to see whether FLCN regulates the kinase activity of ULK1.

The increased levels of autophagic activity exhibited by FLCN-deficient cells may also be as a result of the increased levels of HIF mediated transcription of BNIP3 observed, as BNIP3-mediated mitophagy has been shown to be upregulated in response to mitochondrial dysfunction and initiation of the mitochondrial cell death pathway (Rikka *et al.*, 2011).

It has been shown that increased permeability of the mitochondrial membrane results in the release of proapoptotic factors contained within the mitochondrial membrane and that BNIP3 can inhibit induction of apoptosis via Apoptosis Inducing Factor (AIF) (Akao *et al.*, 2006, Burton *et al.* 2009). It may be possible that the increased levels of BNIP3 observed upon loss of functional FLCN may be repressing apoptosis that would otherwise be induced as a result of the release of proapoptotic factors contained within the mitochondrial membrane. However this resistance to apoptosis observed may also be due to misregulation of TGFβ signalling upon loss of functional FLCN and subsequent downregulation of proapoptotic factors such as Bim (Cash *et al.*, 2011).

Data presented in chapter 4 suggests that autophagic activity is increased in FLCN-deficient cells in order to provide a protective function and that inhibition of autophagic activity via treatment with Chloroquine induced cell death. This notion is supported by the fact that treatment with autophagy inhibitors Chloroquine and 3MA rescues the death-resistance phenotype exhibited by $BHD^{-/-}$ embryonic stem cells (Cash *et al.*, 2011).

Data presented in chapter 4 also revealed that treatment with the reagent Nelfinavir results in autophagic activity within these cells being increased to a level at which autophagy abandons its protective function. This results in selective inhibition of cell proliferation and induction of cell death in these cells (both at the 20 μM and 30 μM concentration). These data suggest

that inducing autophagy via treatment with reagents which induce the ERS response such as Nelfinavir may be of therapeutic benefit to BHD patients.

Treatment with a combination of Nelfinavir and Chloroquine appears to have a synergistic effect in the selective inhibition of cell proliferation and promotion of cell death in the $BHD^{-/-}$ MEF cells when compared to treatment with either drug individually. Furthermore, combined treatment with Nelfinavir and Chloroquine was more effective at selectively inducing cell death in the $BHD^{-/-}$ MEF cells than combination treatment with rapamycin and Chloroquine. Both of these reagents are currently administered to humans for treatment of HIV (Nelfinavir) and malaria (Chloroquine). Therefore, these drugs might be suitable candidate drugs for treating BHD. However, further analysis will have to be conducted in order to confirm whether these drugs do indeed have therapeutic potential in BHD patients and whether the combination of these reagents at the concentrations required to have therapeutic benefit is safe to administer to patients.

Other combinations of ER stress activators and autophagy inhibitors may also provide therapeutic benefit for BHD patients. Further investigation would be required in order to determine whether treatment with any of these reagents, either individually or in combination, would selectively inhibit cell proliferation or induce cell death in FLCN-deficient cells.

5.6 FLCN may be required in order to relay negative feedback signals in order for AMPK and ULK1 to fully repress mTORC1signalling.

It is unusual for both AMPK and mTOR signalling to be constitutively active in a cell line, as AMPK potently inhibits mTORC1 signalling (Chen *et al.*, 2011; Gwinn *et al.*, 2008).

Data obtained with the UOK257 cells suggest that increased levels of phosphorylation of Raptor at Ser792 (AMPK site) are observed in the UOK257 cells deficient in functional FLCN. Work conducted by Li *et al.* has suggested that phosphorylation of Raptor at this site results in inhibition of mTOR (Li *et al.*, 2010). However although enhanced phosphorylation of Raptor by AMPK at this site is observed, this does not appear to result in inhibition of mTOR in cells deficient in functional FLCN. Work conducted by Gwinn *et al.* has shown that AMPK also phosphorylates Raptor at Ser722 as well as Ser792, resulting in inhibition of mTOR (Gwinn *et al.*, 2008). It may be possible that a phosphorylation event such as the phosphorylation of Raptor by AMPK at Ser722 may not occur upon loss of FLCN.

It has also been shown that ULK1 phosphorylates Raptor at multiple sites, including Ser855 and Ser859, resulting in inhibition of mTORC1 (Dunlop *et al.*, 2011). mTORC1 has also been shown directly regulate the ~3-MDa ULK1–Atg13–FIP200 complex (Hosokawa *et al.*, 2009), and further work conducted by Kim *et al.* has shown that mTORC1 inhibits ULK1 by direct phosphosphorylation (Kim *et al.*, 2011). However, although increased levels of ULK1 mediated autophagy are observed in BHD-deficient cells, ULK1 does not appear to be inhibiting mTOR via phosphorylation of Raptor within these cells. Furthermore, the increased level of mTOR activity observed within the FLCN-deficient cells does not appear to be resulting in inhibition of ULK1 in these cells. It may be possible that FLCN is also required to relay these negative feedback signals to fully repress mTORC1. Without FLCN, activation of AMPK and ULK1 does not result in the repression of mTORC1 (Figure 32a).

5.7 Aberrant levels of AMPK and mTOR signalling, HIF1α transcriptional activity and glycolytic activity upon loss of functional FLCN may provide potential therapeutic targets for BHD patients.

The fact that the BHD$^-$ UOK257 cells exhibit a metabolic profile that parallels the 'Warburg effect' may also provide some potential therapeutic targets for Birt-Hogg-Dubé patients. Several groups have explored the selective killing of cancer cells by developing compounds which inhibit glycolysis (Figure 33) (Chen *et al.*, 2007). Increased glycolytic activity is exhibited in the BHD$^-$ UOK257 cells, as shown by increased levels of GLUT1 mRNA and protein, which would result in increased glucose uptake within these cells.
Glycolytic activity within a cell can also be inhibited by inhibiting Hexokinase. Hexokinase is the first rate-limiting enzyme in the glycolysis pathway which converts glucose to glucose-6-phosphate. Inhibition of Hexokinase will have a significant effect on both glycolysis and the pentose phosphate pathways, as glucose 6 phosphate is an intermediate for both of these pathways (Chen *et al.*, 2007). Known inhibitors of hexokinase include 2-deoxyglucose (2DG) (Chen *et al.*, 2007).

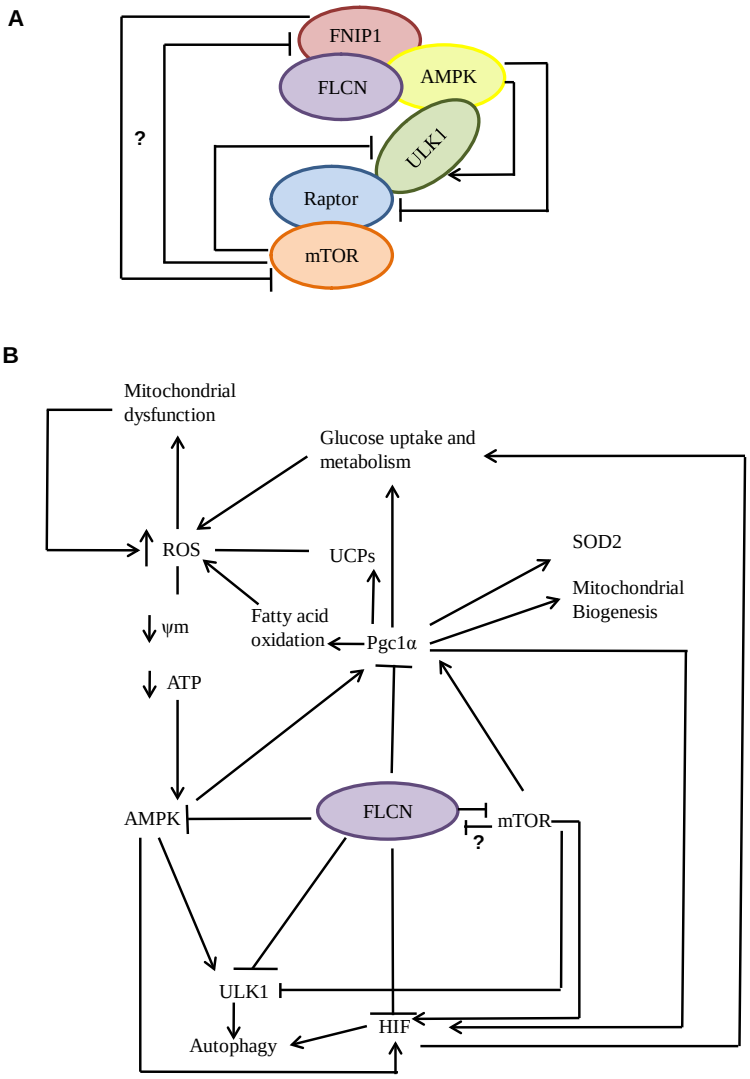

Figure 32. The tumour suppression function of FLCN

(A) FLCN may be required to relay negative feedback signals to fully repress mTORC1 via AMPK or ULK1. In the absence of FLCN, activation of AMPK and ULK1 does not result in the repression of mTORC1. (B) Loss of functional FLCN appears to result in increased HIF activity, increased mitochondrial biogenesis and increased autophagic activity via the regulation of AMPK and mTOR signalling.

Work conducted in Dr. Andrew Tee's lab suggested that treatment with 2-deoxyglucose selectively inhibits the proliferation of the BHD^- UOK257 cells (Preston *et al.*, 2011). These data imply that inhibition of Hexokinase may be a potential therapeutic target for Birt-Hogg-

Dubé patients. Further investigation would be required in order to determine whether glycolytic inhibitors which target hexokinase, either individually or in combination with other reagents such as rapamycin (Xu *et al.*, 2005a), would selectively inhibit cell proliferation or induce cell death in FLCN-deficient cells.

As data obtained from the UOK257 cells have shown that these cells exhibit increased levels of LDH activity and that L-lactate may be taken up and oxidised by these cells upon loss of FLCN, it may also be possible that reagents which inhibit LDH provide potential therapeutic benefit for BHD patients. The reagent oxamate inhibits LDH by competing with pyruvate as its substrate (Thornburg *et al.*, 2008). Further investigation would be required in order to determine whether glycolytic inhibitors which target LDH or Hexokinase would selectively inhibit cell proliferation or induce cell death in BHD-deficient cells without being highly toxic to BHD^+ cells, thus providing a potential therapeutic benefit for BHD patients (Figure 32).

Studies have also shown that inhibition of HIF1α, through treatment with different therapeutic agents, has significant effect on tumour growth in several cancer types. Data obtained from multiple cell lines have provided clear evidence that HIF1α transcriptional activity is increased in several cell lines deficient in FLCN. Inhibition of HIF1α may therefore provide more potential benefit for BHD patients. Sunitanib is a reagent which has been shown to inhibit HIF1α (Shin *et al*; 2010). Further investigation would be required in order to determine whether inhibition of HIF1α using reagents such as Sunitanib would be of therapeutic benefit for BHD patients.

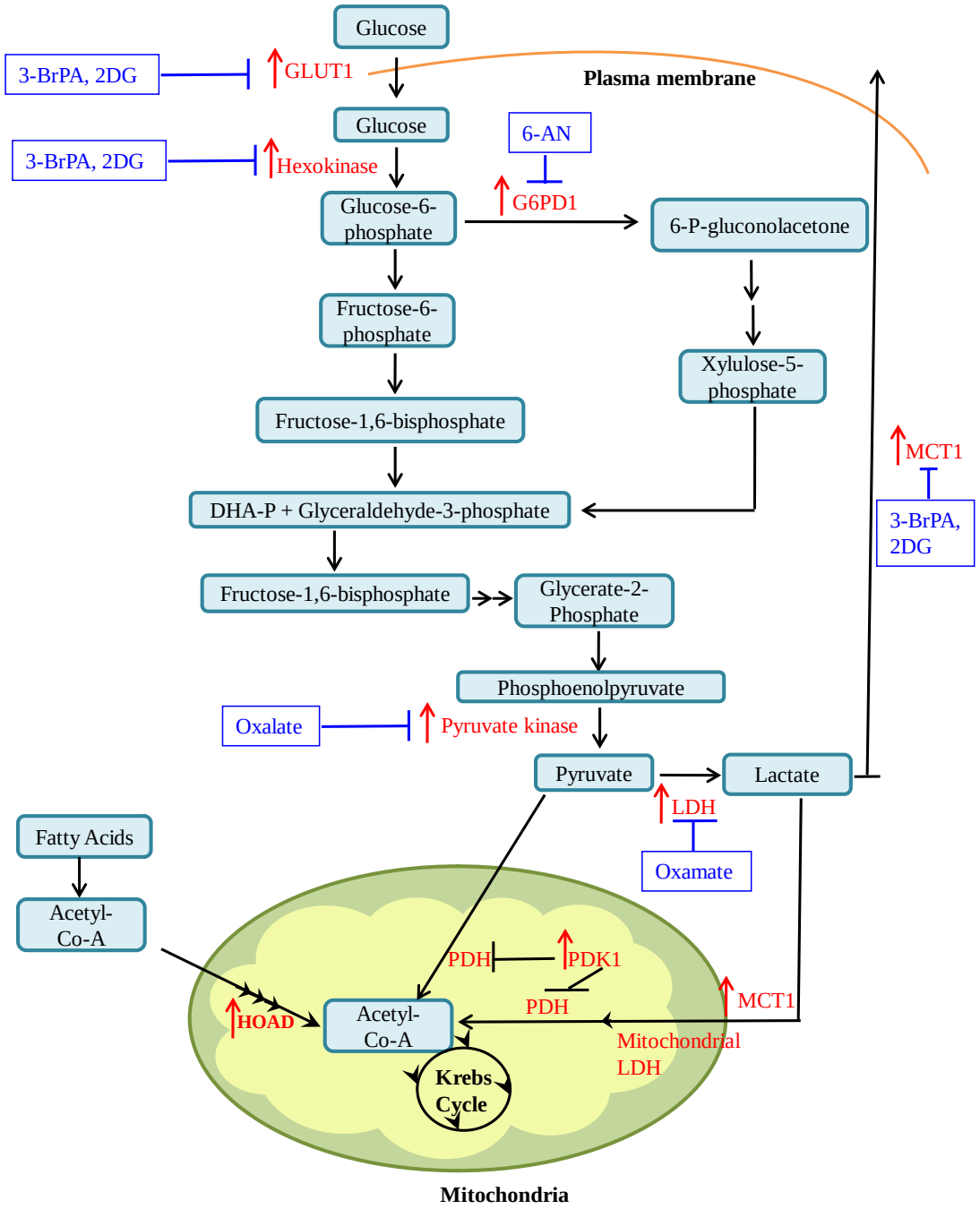

Figure 33. Glycolytic inhibitors may provide therapeutic targets for BHD patients FLCN-deficient cells exhibit increased levels of MCT1, G6PD1, GLUT1, PDK1, Pyruvate Kinase and Lactate dehydrogenase. Inhibition of these targets may provide therapeutic beneifit for BHD patients

Constitutive activation of mTOR signalling appears to be involved in upregulating HIF activity as well as mitochondrial biogenesis in the FLCN-deficient cells analysed, both of which appear to be required in order to meet the energy demands of these cells in response to mitochondrial dysfunction. Therefore it may be possible that inhibition of mTOR provides more of a therapeutic benefit for BHD patients than inhibition of HIF1 activity alone. Results from several studies have also shown that the antidiabetic drug metformin inhibits cancer cell viability through the inhibition of mTORC1. Metformin inhibits mTORC1 via increased expression of Redd1 in a p53-dependent manner (Sahra *et al.*, 2011). However, the data presented in chapters 2 and 3 as well as results from other studies suggest that inhibition of mTORC1 on its own in BHD deficient cells may not result in complete restoration of HIF activity (Knaup *et al.*, 2009) or mitochondrial biogenesis to normal levels. However, Metformin has been shown to activate AMPK and inhibit glucose phosphorylation and glycolysis in rat hepatocytes (Guigas *et al.*, 2006). 2-deoxyglucose, which also activates AMPK and inhibits glycolysis, has been shown to selectively inhibit the proliferation of BHD^- UOK257 cells by inhibiting glucose uptake (Preston *et al.*, 2011). It may be possible that a drug such as Metformin, which not only inhibits glycolysis and activates AMPK, but also inhibits mTORC1 signalling, may provide an effective potential therapeutic target for BHD patients.

Loss of functional FLCN has also been shown to result in increased levels of mTORC2 activity which in turn activates Akt and thus mTORC1 signalling (Baba *et al.*, 2006; Hasumi *et al.*, 2009). Kinase inhibitors which target mTORC1 and mTORC2 may therefore provide another viable solution (Evangilisti *et al.*, 2011). Reagents such as Torin inhibit both mTORC1 and mTORC2 by inhibiting the kinase activity of mTOR (Dufour, 2011). Further investigation would be required in order to determine whether treatment with inhibitors of

mTORC1, either individually or in combination with inhibitors of mTORC2 or other reagents, would provide an effective treatment for BHD patients.

In conclusion, it appears that endogenous FLCN is localised to both the nucleus and mitochondria within a cell. It may be possible that FLCN is involved in maintaining a level of communication between the nucleus and the mitochondria that could involve sensing ROS, DNA-damage repair, cell cycle check point control and energy homeostasis. Loss of function of FLCN results in increased production of ROS species such as H_2O_2. This leads to compromised mitochondrial membrane potential and decreased ATP production as a result of increased expression of uncoupling proteins in order to try and reduce the increased levels of ROS. FLCN is also phosphorylated at multiple residues by both mTORC1 and AMPK and activity of both mTORC1 and AMPK is increased in response loss of functional FLCN. This results in increased levels of mitochondrial biogenesis and increased levels of glycolytic activity via increased activation of HIFα proteins in order to compensate for this energy deficit. Furthermore, it appears that both mTORC1 and AMPK could drive HIF transcription and mitochondrial biogenesis through modulation of FLCN phosphorylation. ULK-mediated autophagy also appears to be upregulated upon loss of functional FLCN, possibly as a result of the increased levels of AMPK activation in order to provide a protection for these cells. This may be via catabolising of the dysfunctional mitochondria observed in cells upon loss of BHD, a process which may be exploited as a potential therapeutic target for BHD patients. However, further investigation is however required into FLCN's involvement in sensing ROS, DNA-damage repair and the exact method as to how FLCN modulates HIF activity and mitochondrial biogenesis. Investigations into these cellular processes may also provide clues to potential therapeutic targets for treatment of BHD patients (Figure 33B).

References

Abraham R (2004). PI 3-kinase related kinases: 'big' players in stress-induced signaling pathways. DNA Repair 3: 883-887.

Akao M, O'Rourke B, Kusuoka H, Teshima Y, Jones S, Marbán E (2003). Differential Actions of Cardioprotective Agents on the Mitochondrial Death Pathway. Circulation Research 92: 195-202.

Alexander A, Cai S-L, Kim J, Nanez A, Sahin M, MacLean K *et al.* (2010). ATM signals to TSC2 in the cytoplasm to regulate mTORC1 in response to ROS. PNAS 107: 4153-4158.

Alonso-Montes C, Castro M, Reguero J, Perrot A, Ozcelik C, Geier C *et al.* (2008). Mitochondrial transcription factors TFA, TFB1 and TFB2: a search for DNA variants/haplotypes and the risk of cardiac hypertrophy. Dis Markers 25: 131-139.

Amin M, Crotty T, Tickoo S, Farrow G (1997). Renal oncocytoma: a reappraisal of morphologic features with clinicopathologic findings in 80 cases. Am J Surg Pathol 21: 1-12.

Arico A, Petiot A, Bauvy C, Dubbelhuis P, Meijer A, Codogno P *et al.* (2001). The Tumor Suppressor PTEN Positively Regulates Macroautophagy by Inhibiting the Phosphatidylinositol 3-Kinase/Protein Kinase B Pathway. Journal of Biological Chemistry 276: 35243-35246.

Arico S, Petiot A, Bauvy C, Dubbelhuis P, Meijer A, Codogno P *et al.* (2001). The tumor suppressor PTEN positively regulates macroautophagy by inhibiting the phosphatidylinositol 3-kinase/protein kinase B pathway. Journal of Biological Chemistry 276: 35243-35246.

Arsham A, JJ H, Simon M (2003). A Novel Hypoxia-inducible Factor-independent Hypoxic response Regulating Mammalian Target of Rapamycin and its Targets. Journal of Biological Chemistry 278: 29655-29660.

Baba M, Hong S-B, Sharma N, Warren M, Nickerson M, Iwamatsu A *et al.* (2006). Folliculin encoded by the BHD gene interacts with a binding protein, FNIP1, and AMPK, and is involved in AMPK and mTOR signalling. P Natl Acad Sci USA 103: 15552–15557.

Baba M, M, Hong S-B, Tessarollo L, Haines D, Southon E, Patel V *et al.* (2008). Kidney-targeted Birt-Hogg-Dubé gene inactivation in a mouse model: Erk1/2 and Akt-mTOR activation, cell hyperproliferation, and polycystic kidneys. J Natl Cancer Inst 100: 140-154.

Belanger A, Lu H, Date T, Liu L, Vincent K, Akita G *et al.* (2002). Hypoxia Up-regulates Expression of Peroxisome Proliferator-activated Receptor γ Angiopoietin-related Gene (PGAR) in Cardiomyocytes: Role of Hypoxia Inducible Factor 1α. Journal of Molecular and Cellular Biology 34: 765-774.

Bellance N, Benard G, Furt F, Begueret H, Smolková K, Passerieux E *et al.* (2009). Bioenergetics of lung tumors: alteration of mitochondrial biogenesis and respiratory capacity. Int J Biochem Cell Biol 41: 2566-2577.

Bellot G, Garcia-Medina R, Gounon P, Chiche J, Roux D, Pouysségur J *et al.* (2009). Hypoxia-induced Autophagy is mediated through HIFinduction of BNIP3 and BNIP3L via their BH3-domains. Molecular and Cellular Biology.

Benhammou J, Vocke C, Santani A, Schmidt L, Baba M, Seyama K *et al.* (2011). Identification of intragenic deletions and duplication in the FLCN gene in Birt-Hogg-Dubé syndrome. Gneens Chromosomes Cancer 50: 466-477.

Birt A, Hogg G, Dubé W (1977). Hereditary multiple fibrofolliculomas with trichodiscomas and acrochordons. Arch Dermatol 113: 1674-1677.

Blank M, Mandel M, Keisari Y, Meruelo D, Lavie G. (2003). Enhanced ubiquitinylation of heat shock protein 90 as a potential mechanism for mitotic cell death in cancer cells induced with hypericin. Cancer Res 63(23): 8241-7.

Blokina O, Virolainen E, Fagerstedt KV (2003). Antioxidants, Oxidative Damage and Oxygen Deprivation Stress: a Review. Ann Bot 91 (2): 179-194.

Blommaart E, Luiken J, Blommaart P, van Woerkom G, Meijer A (1995). Phosphorylation of ribosomal protein S6 is inhibitory for autophagy in isolated rat hepatocytes. Journal of Biological Chemistry 270: 2320-2326.

Boehlke C, Kotsis F, Patel V, Braeg S, Voelker H, Bredt S *et al.* (2010). Primary cilia regulate mTORC1 activity and cell size through Lkb1. Nature Cell Biology 12: 1115-1122.

Bogacka I, Ukropcova B, McNeil M, Gimble J, Smith S (2005). Structural and functional consequences of mitochondrial biogenesis in human adipocytes in vitro. J Clin Endocrinol Metab 90: 6650-6656.

Bok J, Ishida K-I, Griffiths A (2003). Ultrastructural changes in Neurospora cells undergoing senescence induced by kalilo plasmids. Mycologia 95: 500-505.

Bonekamp N, Völkl A, Fahimi H, Schrader M (2009). Reactive oxygen species and peroxisomes: struggling for balance. Biofactors 35: 346-355.

Bonnet C, Aldred M, von Ruhland C, Harris R, Sandford Ra, Cheadle J (2009). Defects in cell polarity underlie TSC and ADPKD-associated cystogenesis. Hum Mol Genet 18: 2166-2176.

Bønsdorff T, Jansen J, Lingaas F (2008). Second hits in the FLCN gene in a hereditary renal cancer syndrome in dogs. Mamm Genome 19: 121-126.

Bønsdorff T, Jansen J, Thomassen R, Lingaas F (2009). Loss of heterozygosity at the FLCN locus in early renal cystic lesions in dogs with renal cystadenocarcinoma and nodular dermatofibrosis. Mamm Genome 20: 315-320.

Bratslavsky G, Sudarshan S, Neckers L, Linehan W (2007). Pseudohypoxic pathways in renal cell carcinoma. Clin Cancer Res 13: 4667-4671.

Brown E, Albers M, Shin T, Ichikawa K, Keith C, Lane W *et al.* (1994). A mammalian protein targeted by G1-arresting rapamycin-receptor complex. Nature 369: 756-758.

Brugarolas J, Vazquez F, Reddy A, Sellers W, Kaelin Jr W (2003). TSC2 regulates VEGF through mTOR-dependent and -independent pathways. Cancer Cell 4: 147-158.

Brugarolas J, Kaelin W (2004). Dysregulation of HIF and VEGF is a unifying feature of the familial hamartoma syndromes. Cancer Cell 6: 7-10.

Brul S, Wiemer E, Westerveld A, Strijland A, Wanders R, Schram A *et al.* (1988). Kinetics of the assembly of peroxisomes after fusion of complementary cell lines from patients with the cerebro-hepato-renal (Zellweger) syndrome and related disorders. Biochem Bioph Res Commun 152: 1083-1089.

Buc H, Demaugre F, Moncion A, Leroux J (1981). Metabolic consequences of pyruvate kinase inhibition by oxalate in intact rat hepatocytes. Biochimie 63: 595-602.

Budanov A, Karin M (2007). p53 target genes sestrin1 and sestrin2 connect genotoxic stress and mTOR signaling. Cell 134: 451-460.

Buller C, Loberg R, Fan M-H, Zhu Q, Park J, Vesely E *et al.* (2007). A GSK-3/TSC2/mTOR pathway regulates glucose uptake and GLUT1 glucose transporter expression. Am J Physiol Cell Physiol 295: 836-843.

Burton T, Eisenstat D, Gibson S (2009). BNIP3 (Bcl-2 19 kDa Interacting Protein) Acts as Transcriptional Repressor of Apoptosis-Inducing Factor Expression Preventing Cell Death in Human Malignant Gliomas. The Journal of Neuroscience 29: 4189-4199.

Byrne M, Mallipeddi R, Pichert G, Whittaker S (2011). Birt–Hogg–Dubé syndrome with a renal angiomyolipoma: Further evidence of a relationship between Birt–Hogg–Dubé syndrome and tuberous sclerosis complex. Australasian Journal of Dermatology.

Cantó C, Jiang L, Deshmukh A, Mataki C, Coste A, Lagouge M *et al.* (2010). Interdependence of AMPK and SIRT1 for metabolic adaptation to fasting and exercise in skeletal muscle. Cell Metabolism 11: 213-219.

Cash T, Gruber J, Hartman T, Henske E, Simon M (2011). Loss of the Birt–Hogg–Dube´ tumor suppressor results in apoptotic resistance due to aberrant TGFb-mediated transcription. Onocgene 30.

Castino R, Isidoro C, Murphy D (2005). Autophagy-dependent cell survival and cell death in an autosomal dominant familial neurohypophyseal diabetes insipidus in vitro model. The FASEB Journal 19: 1024-1026.

Chadha K, Khoury T, Yu J, Black J, Gibbs J, Kuvshinoff B *et al.* (2006). Activated Akt and Erk expression and survival after surgery in pancreatic carcinoma. Ann Surg Oncol 13: 933-999.

Chen J, Zheng X, Brown E, Schreiber S (1995). Identification of an 11-kDa FKBP12-rapamycin-binding domain within the 289-kDa FKBP12-rapamycin-associated protein and characterization of a critical serine residue. PNAS 92: 4947-4951.

Chen Z, Lu W, Garcia-Prieto C, Huang P (2007). The Warburg effect and its cancer therapeutic implications. J Bioenerg Biomembr 39: 267-274.

Chen J, Futami K, Petillo D, Peng J, Wang P, Knol J *et al.* (2008). Deficiency of FLCN in mouse kidney led to development of polycystic kidneys and renal neoplasia. PLoS One 3: 3581.

Chen C, Jeon S, Bhaskar P, Nogueira V, Sundararajan D, Tonic I *et al.* (2010). FoxOs inhibit mTORC1 and activate Akt by inducing the expression of Sestrin3 and Rictor. Dev Cell 18: 592-604.

Chen L, Xu B, Liu L, Luo Y, Zhou H, Chen W *et al.* (2011). Cadmium induction of reactive oxygen species activates the mTOR pathway, leading to neuronal cell death. Free Radical Biology and Medicine 50: 624-632.

Chhipa R, Wu Y, Ip C (2011). AMPK-mediated autophagy is a survival mechanism in androgen-dependent prostate cancer cells subjected to androgen deprivation and hypoxia. Cellular Signalling 23: 1466-1472.

Chiang G, Abraham RT (2007). Targeting the mTOR signaling network in cancer. Trends Mol Med 13: 433-442.

Cho M, Klanderman B, Litonjua A, Sparrow D, Silverman E, Raby B (2008). Folliculin mutations are not associated with severe COPD. BMC Med Genet 9: 120.

Christiensen S, Pedersen S, Satir P, Veland I, Schneider L (2008). The Primary Cilium Coordinates Signaling Pathways in Cell Cycle Control and Migration During Development and Tissue Repair. Curr Top Dev Biol 85: 261-301.

Clark P (2009). The role of VHL in clear-cell renal cell carcinoma and its relation to targeted therapy. Kidney Int 76: 939-945.

Cocciolone R, Crotty K, Andrews L, Haass N, Moloney F (2010). Multiple desmoplastic melanomas in Birt-Hogg-Dubé syndrome and a proposed signaling link between folliculin, the mTOR pathway, and melanoma susceptibility. Arch Dermatol 146: 1316-1318.

Connor K, Subbaram S, Regan K, Nelson K, Mazurkiewicz J, Bartholomew P *et al.* (2005). Mitochondrial H2O2 Regulates the Angiogenic Phenotype via PTEN Oxidation. Journal of Biological Chemistry 280: 16916-16924.

Corradetti M, Inoki K, Bardeesy N, DePinho R, Guan K (2004). Regulation of the TSC pathway by LKB1: evidence of a molecular link between tuberous sclerosis complex and Peutz-Jeghers syndrome. Genes and Development 18: 1533-1538.

Cunningham J, Rodgers J, Arlow D, Vazquez F, Mootha V, Puigserver P (2007). mTOR controls mitochondrial oxidative function through a YY1–PGC-1a transcriptional complex. nature 450: 736-741.

Dang CV (2008). The Interplay between MYC and HIF in the Warburg Effect. Ernst Shering Foundation Symposium Proceedings 4: 35-53

Degtyarev M, De Mazière A, Orr C, Lin J, Lee B, Tien J *et al.* (2008). Akt inhibition promotes autophagy and sensitizes PTEN-null tumors to lysosomotropic agents. J Cell Biol 183: 101-116.

Dufour M, Dormond-Meuwly A, Demartines N, Dormond A. (2011). Targeting the Mammalian Target of Rapamycin (mTOR) in Cancer Therapy: Lessons from Past and Future Perspectives. *Cancer 3*: 2478-2500

Dennis P, Jaeschke A, Saitoh M, Fowler B, Kozma S, Thomas G (2001). Mammalian TOR: a homeostatic ATP sensor. Science 294: 1102-1105.

Distel B, Erdmann R, Gould S, Blobel G, Crane D, Cregg J *et al.* (1996). A Unified Nomenclature for Peroxisome Biogenesis Factors. The Journal of Cell Biology 135: 1-3.

Dunlop E, Tee A (2009). Mammalian target of rapamycin complex 1: Signalling inputs, substrates and feedback mechanisms. Cellular Signalling 21: 827-835.

Dunlop E, Hunt D, Acosta-Jaquez H, Finger D, Tee A (2011). ULK1 inhibits mTORC1 signaling, promotes multisite Raptor phosphorylation and hinders substrate binding. Autophagy 7: 737-747.

Elfiky A, Aziz S, Conrad P, Siddiqui S, Hackl W, Maira M *et al.* (2011). Characterization and targeting of phosphatidylinositol-3 kinase (PI3K) and mammalian target of rapamycin (mTOR) in renal cell cancer. J Transl Med 11: 133.

El-Hashemite N, Walker V, Zhang H, Kwiatkowski D (2003). Loss of TSC1 or TSc2 induces vascular endothelial growth factor production through mammalian target of rapamycin. Cancer Research 63: 5173-5177.

Esposti M, De Vries S, Crimi M, Ghelli A, Patarnello T, Meyer A (1993). Mitochondrial cytochrome b: evolution and structure of the protein. Biochimica Et Biophysica Acta (BBA) - Bioenergetics 1143: 243-271.

Evangelisti C, Ricci F, Tazzari P, Tabellini G, Battistelli M, Falcieri E *et al.* (2011). Targeted inhibition of mTORC1 and mTORC2 by active-site mTOR inhibitors has cytotoxic effects in T-cell acute lymphoblastic leukemia. Leukemia 25: 781-791.

Facchinetti V, Ouyang W, Wei H, Soto N, Lazorchak A, Gould C *et al.* (2008). The mammalian target of rapamycin complex 2 controls folding and stability of Akt and protein kinase C. Embo Journal 27: 1932-1943.

Fang J, Quinones Q, Holman T-L, Morowitz M, Wang Q, Zhao H *et al.* (2006). The H+-Linked Monocarboxylate Transporter (MCT1/SLC16A1): A Potential Therapeutic Target for High-Risk Neuroblastoma. Molecular Pharmacology 70: 2108-2115.

Fernandes da Silva N, Gentle D, Hesson LB, Morton DG, Latif F, Maher ER. (2003). Analysis of the Birt-Hogg- Dubé (BHD) tumour suppressor gene in sporadic renal cell carcinoma and colorectal cancer. J Med Genet 40: 820-824.

Fosslien E (2008). Cancer Morphogenesis: Role of Mitochondrial Failure. Annals of Clinical & Laboratory Science 38: 307-330.

Fröhlich B, Zeitz C, Mátyás G, Alkadhi H, Tuor C, Berger W *et al.* (2008). Novel mutations in the folliculin gene associated with spontaneous pneumothorax. Eur Respir J 32: 1316-1320.

Fujii H, Jiang W, Matsumoto T, Miyai K, Sashara K, Ohtsuji N, Hino O. (2006). Birt-Hogg-Dubé gene mutations in human endometrial carcinomas with microsatellite instability. J Pathol 209: 328-335.

Gamboa J, Andrade F (2010). Mitochondrial content and distribution changes specific to mouse diaphragm after chronic normobaric hypoxia. AJP - Regu Physiol 298: 575-583.

Gao P, Tchernyshyov I, Chang T-C, Lee Y-S, Kita K, Ochi T *et al.* (2009). c-Myc suppression of miR-23a/b enhances mitochondrial glutaminase expression and glutamine metabolism. Nature 458: 762-765.

Garcia-Prieto C, Huang P (2007). The Warburg effect and its cancer therapeutic implications. J Bioenerg Biomembr 39: 267-274.

Geng Y, Kohli L, Klocke B, Roth K (2010). Chloroquine-induced autophagic vacuole accumulation and cell death in glioma cells is p53 independent. Neuro Oncol.

Goetz S, Anderson K (2010). The primary cilium: a signalling centre during vertebrate development. Nat Rev Genet 11: 331-344.

Gomez R, Sampson J, Whittemore V (1999). Tuberous sclerosis complex, 3 edn. Oxford University Press: Oxford.

Graham R, Nolasco M, Peterlin B, Garcia C (2005). Nonsense mutations in folliculinFLCN presenting as isolated familial spontaneous pneumothorax in adults. Am J Respir Crit Care Med 172: 39-44.

Green A, Johnson P, Yates J (1994). The tuberous sclerosis gene on chromosome 9q34 acts as a growth suppressor. Hum Mol Genet 3: 1833-1834.

Green A, Smith M, Yates J (1994). Loss of heterozygosity on chromosome 16p13.3 in hamartomas from tuberous sclerosis patients. Nat Genet 6: 193-196.

Guertin D, Sabatini D (2007). Defining the role of mTOR in cancer. Cancer Cell 12: 9-22.

Guigas B, Bertrand L, Taleux N, Foretz M, Wiernsperger N, Vertommen D *et al.* (2006). 5-Aminoimidazole-4-Carboxamide-1-β-d-Ribofuranoside and Metformin Inhibit Hepatic Glucose Phosphorylation by an AMP-Activated Protein Kinase–Independent Effect on Glucokinase Translocation. Diabetes 55: 865-874.

Gunji Y, Akiyoshi T, Sato T, Kurihara M, Tominaga S, Takahashi K *et al.* (2007). Mutations of the Birt Hogg Dube gene in patients with multiple lung cysts and recurrent pneumothorax. J Med Genet 44: 588-593.

Guo K, Searfoss G, Krolikowski D, Pagnoni M, Franks C, Clark K *et al.* (2001). Hypoxia induces the expression of the pro-apoptotic gene BNIP3. Cell Death Differ 8: 367-376.

Guo Z, Kozlov S, Lavin M, Person M, Paull T (2010). ATM Activation by Oxidative Stress. Science 330: 517-521.

Gwinn D, Shackelford D, Egan D, Mihaylova M, Mery A, Vasquez D *et al.* (2008). AMPK Phosphorylation of Raptor Mediates a Metabolic Checkpoint. Molecular Cell 30: 214-226.

Hamacher-Brady A, Brady N, Gottlieb R, Gustafsson A (2006). Autophagy as a Protective Response to Bnip3-Mediated Apoptotic Signaling in the Heart. Autophagy 2: 303-305.

Hands S, Proud C, Wyttenbach A (2009). Wyttenbach1 mTOR's role in ageing: protein synthesis or autophagy. Aging 1.

Hartman T, Liu D, Zilfou J, Robb V, Morrison T, Watnick T *et al.* (2009). The tuberous sclerosis proteins regulate formation of the primary cilium via a rapamycin-insensitive and polycystin 1-independent pathway. Hum Mol Genet 18: 151-163.

Hartman T, Nicolas E, Klein-Szanto A, Al-Saleem T, Cash T, Simon C *et al.* (2009). The Role of the Birt-Hogg-Dubé Protein in mTOR Activation and Renal Tumorigenesis. Oncogene 28: 1594-1604.

Hasumi Y, Baba M, Ailma R, Linehan W (2009). Homozygous loss of BHD causes early embryonic lethality and kidney tumour development with activation of mTORC1 and mTORC2. Proc Natl Acad Sci USA 106: 18722-18727.

Heath-Engel H, Shore G (2006). Mitochondrial membrane dynamics, cristae remodelling and apoptosis. Biochim Biophys Acta 1763: 549-560.

Hemminki A, Markie D, Tomlinson I, Avizienyte E, Roth S, Loukola A *et al.* (1998). A serine/threonine kinase gene defective in Peutz-Jeghers syndrome. Nature 391: 184-187.

Hildebrandt F, Benzing T, Katsanis N (2011). Ciliopathies. N Engl J Med 364: 1533-1543.

Hock M, Kralli A (2009). Transcriptional Control of Mitochondrial Biogenesis and Function. Annu Rev Physiol 71: 177-203.

Hong S, Oh H, Valera V, Stull J, Ngo D, Baba M *et al.* (2010a). Tumour suppressor FLCN inhibits tumorigenesis of a FLCN-null renal cancer cell line and regulates expression of key molecules in TGF-β signaling. Molecular Cancer 9: 1-13.

Hong S, Oh H, Valera V, Baba M, Schmidt L, Linehan W (2010b). Inactivation of the FLCN tumor suppressor gene induces TFE3 transcriptional activity by increasing its nuclear localization. PLoS One 5: 15793.

Hosokawa N, Hara T, Kaizuka T, Kishi C, Takamura A, Miura Y *et al.* (2009). Nutrient-dependent mTORC1 Association with the ULK1–Atg13–FIP200 Complex Required for Autophagy. Mol Biol Cell 20: 1981-1991.

Huang L, Arany Z, Livingston D, Bunn H (1996). Activation of Hypoxia-inducible Transcription Factor Depends Primarily upon Redox-sensitive Stabilization of Its α Subunit. Journal of Biological Chemistry 271: 32253-32259.

Hudon V, Sabourin S, Dydensborg A, Kottis V, Ghazi A, Paquet M *et al.* (2010). Renal tumour suppressor function of the Birt-Hogg-Dubé syndrome gene product folliculin. J Med Genet 47: 182-189.

Husseinzadeh H, Garcia J (2011). Therapeutic rationale for mTOR inhibition in advanced renal cell carcinoma. Curr Clin Pharmacol 6: 214-221.

Inoki K, Zhu Ta, Guan K (2003). TSC2 Mediates Cellular Energy Response to Control Cell Growth and Survival. Cell 115: 577-590.

Isaacs J, Jung Y, Mole D, Lee S, Torres-Cabala C, Chung Y *et al.* (2005). HIF overexpression correlates with biallelic loss of fumarate hydratase in renal cancer: novel role of fumarate in regulation of HIF stability. Cancer Cell 8: 143-153.

Iyer N, Leung S, Semenza G (1998). The Human Hypoxia-Inducible Factor 1α Gene:HIF1A Structure and Evolutionary Conservation. Genomics 52: 159-165.

Jefferies H, Reinhard C, Kozma S, Thomas G (1994). Rapamycin selectively represses translation of the "polypyrimidine tract" mRNA family. PNAS 91: 4441-4445.

Jiang W, Fujii H, Matsumoto T, Ohtsuji N, Tsurumaru M, Hino O (2007). Birt-Hogg-Dubé (BHD) gene mutations in human gastric cancer with high frequency microsatellite instability. Cancer Letters 248: 103-111.

Jiang B-H, Liu L-Z (2008). PI3K/PTEN signalling in tumorigenesis and angiogenesis. Biochim Biophys Acta 1784: 150-158.

Jin T, Nakatani H, Taguchi T, Nakano T, Okabayashi T, Sugimoto T *et al.* (2006). STI571 (Glivec) suppresses the expression of vascular endothelial growth factor in the gastrointestinal stromal tumor cell line, GIST-T1. World J Gastroenterol 12: 703-708.

Johannessen C, Reczek E, James M, Brems H, Legius E, Cichowski K (2005). The NF1 tumor suppressor critically regulates TSC2 and mTOR. PNASA 102: 8573-8578.

Jones R, Thompson C (2009). Tumor suppressors and cell metabolism: a recipe for cancer growth. Genes and Development 23: 537-548.

Kaelin W (2005). The von Hippel–Lindau protein, HIF hydroxylation, and oxygen sensing. Biochem Bioph Res Commun 338: 627-638.

Kang YJ, Lu M-K, Guan K-L. (2011). The TSC1 and TSC2 tumor suppressors are required for proper ER stress response and protect cells from ER stress-induced apoptosis. Cell Death Differ 18(1): 133–144.

Kelly D, Scarpulla R (2004). Transcriptional regulatory circuits controlling mitochondrial biogenesis and function. Genes and Development 18: 357-368.

Khoo S, Giraud S, Kahnoski K, Chen J, Motorna O, Nickolov R *et al.* (2002). Clinical and genetic studies of Birt-Hogg-Dubé syndrome. J Med Genet 39: 906-912.

Kim J, Chu S, Gramlich J, Pride Y, Babendreier E, Chauhan D *et al.* (2005). Activation of the PI3K/mTOR pathway by BCR-ABL contributes to increased production of reactive oxygen species. Blood 105: 1717-1723.

Kim J-W, Tchernyshyov I, Semenza G, Dang C (2006). HIF-1-mediated expression of pyruvate dehydrogenase kinase: A metabolic switch required for cellular adaptation to hypoxia. Cell Metabolism 3: 177-185.

Kim J, Kundu M, Viollet B, Guan K-L (2011). AMPK and mTOR regulate autophagy through direct phosphorylation of Ulk1. Nature Cell Biology 13: 132-141.

Kleymenova E, Ibraghimov-Beskrovnaya O, Kugoh H, Everitt J, Xu H, Kiguchi K *et al.* (2001). Tuberin-dependent membrane localization of polycystin-1: a functional link between polycystic kidney disease and the TSC2 tumor suppressor gene. Mol Cell 7: 823-832.

Kleymenova E, Ibraghimov-Beskrovnaya O, Kugoh H, Everitt J, Xu H, Kiguchi K *et al.* (2001). Tuberin-dependent membrane localization of polycystin-1: a functional link between polycystic kidney disease and the TSC2 tumor suppressor gene. Mol Cell 7: 823-832.

Knaup K, Jozefowski K, Schmidt R, Bernhardt W, Weidemann A, Juergensen J *et al.* (2009). Mutual Regulation of Hypoxia-Inducible Factor and Mammalian Target of Rapamycin as a Function of Oxygen Availability. Mol Cancer Res 7: 88-98.

Komori K, Takagi Y, Sanada M, Lim T, Nakatsu Y, Tsuzuki T *et al.* (2009). A novel protein, MAPO1, that functions in apoptosis triggered by O6-methylguanine mispair in DNA. Oncogene 28: 1142-1150.

Koukourakis M, Simopoulos C, Polychronidis A, Perente S, Botaitis S, Giatromanolaki A *et al.* (2003). The effect of trastuzumab/docatexel combination on breast cancer angiogenesis:

dichotomus effect predictable by the HIFI alpha/VEGF pre-treatment status. Anticancer Res 23: 1673-1680.

Krauß S, Foerster J, Schneider R, Schweiger S (2008). Protein Phosphatase 2A and Rapamycin Regulate the Nuclear Localization and Activity of the Transcription Factor GLI3. Cancer Research 68: 4658.

Krieg M, Haas R, Brauch H, Acker T, Flamme I, Plate K (2000). Up-regulation of hypoxia-inducible factors HIF-1 and HIF-2 under normoxic conditions in renal carcinoma cells by von Hippel-Lindau tumor suppressor gene loss of function. Oncogene 19: 5435-5443.

Kunogi M, Kurihara M, Ikegami T, Kobayashi T, Shindo N, Kumasaka T *et al.* (2010). Clinical and genetic spectrum of Birt-Hogg-Dube syndrome patients in whom pneumothorax and/or multiple lung cysts are the presenting feature. J Med Genetic 47: 281-187.

Kwiatkowski D, Zhang H, Bandura J, Heiberger K, Glogauer M, El-Hashemite N *et al.* (2002). A mouse model of TSC1 reveals sex-dependent lethality from liver hemangiomas, and up-regulation of p70S6 kinase activity in Tsc1 null cells. Hum Mol Genet 11: 525-534.

Land S, Tee A (2007). Hypoxia-inducible Factor 1α Is Regulated by the Mammalian Target of Rapamycin (mTOR) via an mTOR Signaling Motif. Journal of Biological Chemistry 282: 20534-20543.

Laughner E, Taghavi P, Chiles K, Mahon P, Semenza G (2001). HER2 (neu) Signaling Increases the Rate of Hypoxia-Inducible Factor 1α (HIF-1α) Synthesis: Novel Mechanism for HIF-1-Mediated Vascular Endothelial Growth Factor Expression Molecular and Cellular Biology 21: 3995-4004.

Lee M, Hwang J, Lee H, Jung S, Kang I, Chi S *et al.* (2003). AMP-activated protein kinase activity is critical for hypoxia-inducible factor-1 transcriptional activity and its target gene expression under hypoxic conditions in DU145 cells. Journal of Biological Chemistry 278: 39653-39661.

Lee K, Kim S, Park S, Park H, Min K, Jin S *et al.* (2006). Peroxisome proliferator activated receptor-gamma modulates reactive oxygen species generation and activation of nuclear factor-kappaB and hypoxia-inducible factor 1alpha in allergic airway disease of mice. J Allergy Clin Immunol 118: 120-127.

Lee J, Park S, Takahashi Y, Wang H-G (2010). The Association of AMPK with ULK1 Regulates Autophagy. PLoS One 5: 15394.

Lee W, KIm S (2010). AMPK-Dependent Metabolic Regulation by PPAR Agonists. PPAR Research 2010.

Li Y, Wang Y, Kim E, Beemiller P, Wang C-Y, Swanson J *et al.* (2007). Bnip3 Mediates the Hypoxia-induced Inhibition on Mammalian Target of Rapamycin by Interacting with Rheb. Journal of Biological Chemistry 282: 35803-35813.

Li Z, Bao S, Wu Q, Wang H, Eyler C, Sathornsumetee S *et al.* (2009). Hypoxia-inducible factors regulate tumourigenic capacity of glioma stem cells. Cancer Cell 15: 501-513.

Li M, Zhao L, Liu J, Liu A, Jia C, Ma D *et al.* (2010). Multi-mechanisms are involved in reactive oxygen species regulation of mTORC1 signaling. Cellular Signalling 22: 1469-1476.

Liang X, Jackson S, Seaman M, Brown K, Kempkes B, Hibshoosh H *et al.* (1999). Induction of autophagy and inhibition of tumorigenesis by beclin 1. Nature 402: 672-676.

Liang H, Ward W (2006). PGC-1α: a key regulator of energy metabolism. Adv Physiol Educ 30: 145-151.

Lingaas F, Comstock K, Kirkness E, Sørensen A, Aarskaug T, Hitte C *et al.* (2003). A mutation in the canine BHD gene is associated with hereditary multifocal renal cystadenocarcinoma and nodular dermatofibrosis in the German Shepherd dog. Hum Mol Genet 12: 3043-3053.

Liu M, Poellinger L, Walker C (2003). Up-regulation of hypoxiainducible factor 2 in renal cell carcinoma associated with loss of Tsc-2 tumour suppressor gene. Cancer Research 63: 2675-2680.

Liu H, Zang C, Schefe J, Schwarzlose-Schwarck S, Regierer A, Elstner E *et al.* (2011). The mTOR inhibitor RAD001 sensitizes tumor cells to the cytotoxic effect of carboplatin in breast cancer in vitro. Anticancer Res 31: 2713-2722.

Lowe S, Cepero E, Evan G (2004). Intrinsic tumour suppression. Nature 432: 307-315.

Luo Z, Saha A, Xiang X, Ruderman N (2005). AMPK, the metabolic syndrome and cancer. Trends Pharmacol Sci 26: 69-76.

Maehama T, Dixon J (1998). The Tumor Suppressor, PTEN/MMAC1, Dephosphorylates the Lipid Second Messenger, Phosphatidylinositol 3,4,5-Trisphosphate. The Journal of Biological Chemistry 273: 13375-13378.

Maiuri M, Tasdemir E, Criollo A, Morselli E, Vicencio J, Carnuccio R *et al.* (2009). Control of autophagy by oncogenes and tumor suppressor genes. Cell Death and Differentiation 16: 87-93.

Manning B, Cantley L (2006). AKT/PKB signalling: navigating downstream. Cell 129: 1261-1274.

Maxwell P (2005). The HIF pathway in cancer. Semin Cell Dev Biol 16: 523-530.

Meijer A, Codogno P (2004). Regulation and role of autophagy in mammalian cells. The International Journal of Biochemistry and Cell Biology 36: 2445-2462.

Melillo G (2010). Editorial: T cells, not “immune” from HIF. Journal of Leukocyte Biology 87: 359-361.

Minami, Tambe Y, Watanabe R, Isono T, Haneda M, Isobe K *et al.* (2007). Suppression of viral replication by stress-inducible GADD34 protein via the mammalian serine/threonine protein kinase mTOR pathway. J Virol 81: 11106-11115.

Moiseeva O, Bourdeau V, Roux A, Descheˆnes-Simard X, Ferbeyre G (2009). Mitochondrial Dysfunction Contributes to Oncogene-Induced Senescence. Molecular and Cellular Biology 29: 4495-4507.

Monastyrska I, Klionsky D (2006). Autophagy in organelle homeostasis: peroxisome turnover. Mol Aspects Med 27: 483-494.

Mortimore G, Schworer C (1998). Tor, a phosphatidylinositol kinase homologue, controls autophagy in yeast. Journal of Biological Chemistry 273: 3963-3966.

Munafó D, Colombo M (2001). A novel assay to study autophagy: regulation of autophagosome vacuole size by amino acid deprivation. J Cell Sci 114: 3619-3629.

Nahorski M, Lim D, Martin L, Gille J, McKay K, Rehal P *et al.* (2010). Investigation of the Birt-Hogg-Dube tumour suppressor gene (FLCN) in familial and sporadic colorectal cancer. J Med Genet 47: 385-390.

Nascimento E, Ouwens D (2009). PRAS40: target or modulator of mTORC1 signalling and insulin action? Arch Physiol Biochem 115: 163-175.

Noda T, Ohsumi Y (1998). Tor, a phosphatidylinositol kinase homologue, controls autophagy in yeast. Journal of Biological Chemistry 273: 3963-3966.

Nojima H, Tokunaga C, Eguchi S, Oshiro N, Hidayat S, Yoshino K *et al.* (2003). The Mammalian Target of Rapamycin (mTOR) Partner, Raptor, Binds the mTOR Substrates p70 S6 Kinase and 4E-BP1 through Their TOR Signaling (TOS) Motif. The Journal of Biological Chemistry 278: 15461-15464.

Ochsendorf F, Runne U (1991). Chloroquine and hydroxychloroquine: side effect profile of important therapeutic drugs. Hautarzt 42: 140-146.

Okimoto K, Sakurai J, Kobayashi T, Mitani H, Hirayama Y, Nickerson M *et al.* (2003). A germ-line insertion in the Birt–Hogg–Dube´ (BHD) gene gives rise to the Nihon rat model of inherited renal cancer. PNAS 101: 2023-2027.

Painter J, Tapanainen H, Somer M, Tukiainen P, Aittomäki K (2005). A 4-bp deletion in the Birt–Hogg–Dube gene (FLCN) causes dominantly inherited spontaneous pneumothorax. Am J Hum Genet 76: 522-527.

Palmirotta R, Donati P, Savonarola A, Cota C, Ferroni P, Guadagni F (2008). Birt-Hogg-Dubé (BHD) syndrome: report of two novel germline mutations in the folliculin (FLCN) gene. Eur J Dermatol 18: 382-386.

Park S, Lee T, Chang I (2011). Role of the mTOR Pathway in the Progression and Recurrence of Bladder Cancer: An Immunohistochemical Tissue Microarray Study. Korean J Urol 52: 466-473.

Parkhitko A, Myachina F, Morrison T, Hindi K, Auricchio N, Karbowniczek M *et al.* (2011). Tumorigenesis in tuberous sclerosis complex is autophagy and p62/sequestosome 1 (SQSTM1)-dependent. PNAS 108: 12455-12460.

Patane` G, Anello M, Piro S, Vigneri R, Purrello F, Rabuazzo A (2002). Role of ATP Production and Uncoupling Protein-2 in the Insulin Secretory Defect Induced by Chronic Exposure
to High Glucose or Free Fatty Acids and Effects of Peroxisome Proliferator–Activated Receptor-y Inhibition. Diabetes 51: 2749-2756.

Paumard P, Vaillier J, Coulary B, Schaeffer J, Soubannier V, Mueller D *et al.* (2002). The ATP synthase is involved in generating mitochondrial cristae morphology. The EMBO Journal 21: 221-230.

Pazour G, San Agustin J, Follit J, Rosenbaum J, Witman G (2002). Polycystin-2 localizes to kidney cilia and the ciliary level is elevated in orpk mice with polycystic kidney disease. Curr Biol 12: 378-380.

Peeters A, Fraisl P, van den Berg S, Ver Loren van Themaat E, Van Kampen A, Rider M *et al.* (2011). Carbohydrate metabolism is perturbed in peroxisome-deficient hepatocytes due to mitochondrial dysfunction, AMP-activated protein kinase (AMPK) activation, and peroxisome proliferator-activated receptor γ coactivator 1α (PGC-1α) suppression. Journal of Biological Chemistry 286: 162-179.

Peterson R, Desai B, Hardwick J, Schreiber S (1999). Protein phosphatase 2A interacts with the 70-kDa S6 kinase and is activated by inhibition of FKBP12-rapamycin-associated protein. Natl Acad Sci USA 96: 4438-4442.

Petiot A, Ogier-Denis E, Blommaart E, Meijer A, Codogno P (2000). Distinct classes of phosphatidylinositol 3'-kinases are involved in signaling pathways that control macroautophagy in HT-29 cells. Journal of Biological Chemistry 275: 992-998.

Piantadosi C, Suliman H (2006). Mitochondrial transcription factor A induction by redox activation of nuclear respiratory factor 1. Journal of Biological Chemistry 281: 324-333.

Piao X, Kobayashi T, Wang L, Shiono M, Takagi Y, Sun G *et al.* (2009). Regulation of folliculin (the BHD gene product) phosphorylation by Tsc2-mTOR pathway. Biochemical and Biophysical Research Communications 389: 16-21.

Plomp P, Gordon P, Meijer A, Høyvik H, Seglen P (1989). Energy dependence of different steps in the autophagic-lysosomal pathway. Journal of Biological Chemistry 264: 6699-6704.

Pollard P, Brie J, Alam N, Barwell J, Barclay E, Wortham N *et al.* (2005). Accumulation of Krebs cycle intermediates and over-expression of HIF1a in tumours which result from germline FH and SDH mutations. Hum Mol Genet 14: 2231-2239.

Pore N, Jiang Z, Shu H, Bernhard E, Kao G, Maity A (2006). Akt1 activation can augment hypoxia-inducible factor-1α expression by increasing protein translation through a mammalian target of rapamycin-independent pathway. Molecular Cancer Research 4: 471-479.

Pore N, Zibin, J, Gupta A, Cerniglia G, Kao G, Maity A (2006). EGFR Tyrosine Kinase Inhibitors Decrease VEGF Expression by Both Hypoxia-Inducible Factor (HIF)-1–Independent
and HIF-1–Dependent Mechanisms. Cancer Research 66: 3197-3204.

Preston R, Philp A, Claessens T, Gijezen L, Dydensborg A, Dunlop E *et al.* (2011). Absence of the Birt–Hogg–Dube´ gene product is associated with increased hypoxia-inducible factor transcriptional activity and a loss of metabolic flexibility. Oncogene 30: 1159-1173.

Rapisarda A, Uranchimeg B, Sordet O, Pommier Y, Shoemaker R, Melillo G (2004). Topoisomerase I-mediated inhibition of hypoxia-inducible factor 1: mechanism and therapeutic implications. Cancer Research 64: 1475-1482.

Ravikumar B, Sarkar S, Davies JE, Futter M, Garcia-Arencibia M, Green-Thompson Z *et al.* (2010). Regulation of Mammalian autophagy in Physiology and Pathophysiology. Physiol Rev 90(4): 1383-1435.

Ren Y, Huang F, Liu Y, Yang Y, Jiang Q, Xu C. Autophagy inhibition through PI3K/Akt increases apoptosis by sodium selenite in NB4 cells. BMB report: 599-604

Rikka S, Quinsay M, Thomas R, Kubli A, Zhang X, Murphy A *et al.* (2011). Bnip3 impairs mitochondrial bioenergetics and stimulates mitochondrial turnover. Cell Death and Differentiation 18: 721-731.

Roberts P, Der C (2007). Targeting the Raf-MEK-ERK mitogen-activated protein kinase cascade for the treatment of cancer. Oncogene 26: 3291-3310.

Robey R, Hay N (2009). Is Akt the "Warburg kinase"?-Akt-energy metabolism interactions and oncogenesis. Semin Cancer Biol 19: 25-31.

Rosner M, Hanneder M, Siegel N, Valli A, Fuchs C, Hengstschläger M (2008). The mTOR pathway and its role in human genetic diseases. Mutat Res 659: 284-292.

S B, Westerveld A, Strljland A, Wanders R, Schram A, Heymans H *et al.* (1988). Genetic heterogeneity in the cerebrohepatorenal (Zellweger) syndrome and other inherited disorders with a generalized impairment of peroxisomal functions. A study using complementation analysis. Journal of Clinical Investigation 81: 1710-1715.

Sabatini D (2006). mTOR and cancer: insights into a complex relationship. Nature Reviews Cancer 6: 729-734.

Sahra I, Regazzetti C, Robert G, Laurent K, Le Marchand-Brustel Y, Auberger P *et al.* (2011). Metformin, Independent of AMPK, Induces mTOR Inhibition and Cell-Cycle Arrest through REDD1. Cancer Research 71: 4366.

Salvemini F, Franze A, Iervolino A, Filosa S, Salzano S, Ursini M (1999). Enhanced glutathione levels and oxidoresistance mediated by increased glucose-6-phosphate dehydrogenase expression. Journal of Biological Chemistry 274: 2750-2757.

Sancak Y, Bar-Peled L, Zoncu R, Markhard A, Nada S, Sabatini D (2010). Ragulator-Rag complex targets mTORC1 to the lysosomal surface and is necessary for its activation by amino acids. Cell 141: 290-303.

Satir P, Pedersen L, Christiensen S (2010). The primary cilium at a glance. J Cell Sci 123: 499-503.

Schellens J, Vreeling-Sindelárová H, PJAM P, AJ M (1988). Schellens, H. Vreeling-Sindelárová, P.J.A.M. Plomp and A.J. Meijer, Hepatic autophagy and intracellular ATP. A morphometric study. Experimental Cell Research 177: 103-108.

Schlieman M, Fahy B, Ramsamooj R, Beckett L, Bold R (2003). Incidence, mechanism and prognostic value of activated AKT in pancreas cancer. Br J Cancer 89: 2110-2115.

Schmidt L, Duh F, Chen F, Kishida T, Glenn G, Choyke P *et al.* (1997). Germline and somatic mutations in the tyrosine kinase domain of the MET proto-oncogene in papillary renal carcinomas. Nat Genet 16: 68-73.

Schmidt L, Nickerson M, Warren M, Glenn G, Toro J, Merino M *et al.* (2005). Germline BHD-mutation spectrum and phenotype analysis of a large cohort of families with Birt-Hogg-Dubé syndrome. Am J Hum Genet 76: 1023-1033.

Schönthal A (2009). Endoplasmic reticulum stress and autophagy as targets for cancer therapy. Cancer Letters 275: 163-169.

Schrader M, Yoon Y (2007). Mitochondria and peroxisomes: are the ‘Big Brother’ and the ‘Little Sister’ closer than assumed? BioEssays 29: 1105-1114.

Semenza G (2003). Targeting HIF-1 for cancer therapy. Nature Reviews Cancer 3: 721-732.

Semenza G (2007). HIF-1 mediates the Warburg effect in clear cell renal carcinoma. J Bioenerg Biomembr 39: 231-234.

Semenza G (2008). Hypoxia-inducible factor 1 and cancer pathogenesis. IUBMB Life 60: 591-597.

Sengupta S, Peterson T, Sabatini D (2010). Regulation of the mTOR Complex 1 Pathway by Nutrients, Growth Factors, and Stress. Molecular Cell 40: 310-322.

Serpillon S, Floyd B, Gupte R, George S, Kozicky M, Neito V *et al.* (2009). Superoxide production by NAD(P)H oxidase and mitochondria is increased in genetically obese and

hyperglycemic rat heart and aorta before the development of cardiac dysfunction. The role of glucose-6-phosphate dehydrogenase-derived NADPH. Am J Physiol Heart Circ Physiol 297: 153-162.

Shadel G (2008). Expression and maintenance of mitochondrial DNA: new insights into human disease pathology. Am J Pathol 172: 1445-1456.

Shaw R, Cantley L (2006). Ras, PI(3)K and mTOR signalling controls tumour cell growth. Nature 441: 424-430.

Shillingford J, Murcia N, Larson C, Low S, Hedgepeth R, Brown N *et al.* (2006). The mTOR pathway is regulated by polycystin-1, and its inhibition reverses renal cystogenesis in polycystic kidney disease. PNAS 103: 5466-5471.

Shin HW, Cho CH, Kim TY, Park JW. (2010). Sunitanib deregulates tumour adaptation to hypoxia by inhibiting HIF1α synthesis in HT-29 Colon cancer cells. Biochem Biophys Res Commun 398(2): 205-11.

Shin J-H, Shin Y-K, Ku J-L, Jeong S-Y, Hong S-H, Park S-Y *et al.* (2003). Mutations of the Birt-Hogg-Dubé (BHD) gene in sporadic colorectal carcinomas and colorectal carcinoma cell lines with microsatellite instability. J Med Genet 40: 364-367.

Shoag J, Arany Z (2010). Regulation of hypoxia-inducible genes by PGC-1 alpha. Arterioscler Thromb Vasc Biol 30: 662-666.

Simonnet H, Demont J, Pfeiffer K, Guenaneche L, Bouvier R, Brandt U *et al.* (2003). Mitochondrial complex I is deficient in renal oncocytomas. Carcinogenesis 24: 1461-1466.

Simons M, Gloy J, Ganner A, Bullerkotte A, Bashkurov M, Krönig C *et al.* (2005). Inversin, the gene product mutated in nephronophthisis type II, functions as a molecular switch between Wnt signaling pathways. Nat Genet 37: 537-543.

Singh S, Zhen W, Zheng Z, Wang H, Oh S, Liu W *et al.* (2006). The Drosophila homolog of the human tumour suppressor gene BHD interacts with the JAK-STAT and Dpp signaling pathways in regulating male germline stem cell maintenance. Oncogene 25: 5933-5941.

Sonveaux P, Végran F, Schroeder T, Wergin M, Verrax J, Rabbani Z *et al.* (2008). Targeting lactate-fueled respiration selectively kills hypoxic tumor cells in mice. J Clin Invest 118: 3930-3942.

Stec R, Grala B, Maczewski M, Bodnar L, Szczylik C (2009). Chromophobe renal cell cancer--review of the literature and potential methods of treating metastatic disease. J Exp Clin Cancer Res 7: 134.

Steinberg S, Dodt G, Raymond G, Braverman N, AnMoser A, Moser H (2006). Peroxisome biogenesis disorders. Biochimica et Biophysica Acta (BBA) - Molecular Cell Research 1763: 1733-1748.

Störkel S, Eble J, Adlakha K, Amin M, Blute M, Bostwick D *et al.* (1997). Classification of renal cell carcinoma: Workgroup No. 1. Union Internationale Contre le Cancer (UICC) and the American Joint Committee on Cancer (AJCC). Cancer 80: 987-989.

St-Pierre J, Drori S, Uldry M, Silvaggi J, Rhee J, Jager S *et al.* (2006). Suppression of Reactive Oxygen Species and Neurodegeneration by the PGC-1 Transcriptional Coactivators. Cell 127: 397-408.

Sudarshan S, Shanmugasundaram K, Naylor S, Lin S, Livi C, O'Neill C *et al.* (2011). Reduced Expression of Fumarate Hydratase in Clear Cell Renal Cancer Mediates HIF-2α Accumulation and Promotes Migration and Invasion. PLoS One 6.

Sundaram S, Tasker A, Morrell M (2009). Familial spontaneous pneumothorax and lung cysts due to a Folliculin exon 10 mutation. Eur Respir J 33: 1510-1512.

Surpili M, Delben T, Kobarg J (2003). Identification of proteins that interact with the central coiled-coil region of the human protein kinase NEK1. Biochemistry 42: 15369-15376.

Tafani M, Schito L, Anwar T, Indelicato M, Sale P, Di Vito M *et al.* (2008). Induction of autophagic cell death by a novel molecule is increased by hypoxia. Autophagy 4: 1042-1053.

Takagi T, Kobayashi M, Shiono L, Wang X, Piao G, Sun D *et al.* (2008). Interaction of FLCN (Birt–Hogg–Dube gene product) with a novel Fnip1-like (FnipL/Fnip2) protein. Oncogene 27: 5339-5547.

Tanida I, Ueno T, Kominami E (2008). LC3 and Autophagy. Methods of Mol Biol 445: 77-88.

Tee A, Finger D, Manning B, Kwiatkowski D, Cantley L, Blenis J (2002). Tuberous sclerosis complex-1 and -2 gene products function together to inhibit mammalian target of rapamycin (mTOR)-mediated downstream signaling. Cell Biology 99: 13571-13576.

Thoma C, Frew I, Hoerner C, Montani M, Moch H, Krek W (2007). pVHL and GSK3β are components of a primary cilium-maintenance signalling network. Nature Cell Biology 9: 588-595.

Thornburg J, Nelson K, Clem B, Lane A, Arumugam S, Simmons A *et al.* (2008). Targeting aspartate aminotransferase in breast cancer. Breast Cancer Research 10: 1-12.

Togashi Y, Kobayashi T, Momose S, Ueda M, Okimoto K, Hino O (2006). Transgenic rescue from embryonic lethality and renal carcinogenesis in the Nihon rat model by introduction of a wild-type Bhd gene. Oncogene 25: 2885-2889.

Tolkovsky A (2009). Mitoautophagy. Biochim Biophys Acta 1793: 1508-1515.

Toro J, Glenn G, Duray P, Darling T, Weirich G, Zbar B, Linehan M, Turner M (1999). Birt-Hogg-Dube´ Syndrome: A Novel Marker of Kidney Neoplasia. Arch Dermatol 135: 1195-1202.

Toro J, Pautler S, Stewart L, Glenn G, Weinreich M, Toure O *et al.* (2007). Lung cysts, spontaneous pneumothorax, and genetic associations in 89 families with Birt-Hogg-Dubé syndrome. Am J Respir Crit Care Med 175: 1044-1053.

Toro J, Wei M, Glenn G, Weinreich M, Toure O, Vocke C *et al.* (2008). BHD mutations, clinical and molecular genetic investigations of Birt-Hogg-Dubé syndrome: a new series of 50 families and a review of published reports. J Med Genet 45: 321-331.

Torres V (2010). Treatment strategies and clinical trial design in ADPKD. Adv Chronic Kidney Dis 17: 190-204.

Tsutsumi S, Gotoh T, Tomisato W, Mima S, Hoshino T, Hwang H-J *et al.* (2004). Endoplasmic reticulum stress response is involved in nonsteroidal anti-inflammatory drug-induced apoptosis. Cell Death and Differentiation 11: 1009-1016.

Tuder R, Yoshida T, Fijalkowka I, Biswal S, Petrache I (2006). Role of Lung Maintenance Program in the Heterogeneity of Lung Destruction in Emphysema. Proc Am Thorac Soc 3: 673-679.

Turcotte S, Giaccia A (2010). Targeting cancer cells through autophagy for anticancer therapy. Curr Opin cell Biol 22: 246-251.

Valle I, lvarez-Barrientos A, Arza E, Lamas S, Monsalve M (2005). PGC-1a regulates the mitochondrial antioxidant defense system in vascular endothelial cells. Cardiovascular Research 66: 562-573.

Van der Heiden M, Cantley L, Thompson C (2009). Understanding the Warburg effect: the metabolic requirements of cell proliferation. Science 324: 1029-1033.

van Slegtenhorst M, Khabibullin D, Hartman T, Nicolas E, Kruger W, Henske E (2007). The Birt-Hogg-Dube and Tuberous Sclerosis Complex Homologs Have Opposing Roles in Amino Acid Homeostasis in Schizosaccharomyces pombe. The Journal of Biological Chemistry 282: 24583-24590.

Ventura-Clapier R, Garnier A, Veksler V (2008). Transcriptional control of mitochondrial biogenesis: the central role of PGC-1α. Cardiovasc Res 79: 208-217.

Verzola D, Bertolotto M, Villaggio B, Ottonello L, Dallegri F, Salvatore F *et al.* (2004). Oxidative Stress Mediates Apoptotic Changes Induced by Hyperglycemia in Human Tubular Kidney Cells. J Am Soc Nephrol 15: 85-87.

Vocke C, Yang Y, Pavlovich C, Schmidt L, Nickerson M, Torres-Cabala C *et al.* (2005). High frequency of somatic frameshift BHD gene mutations in Birt-Hogg-Dubé-associated renal tumors. J Natl Cancer Inst 97: 931-935.

Wakao S, Andre C, Benning C (2008). Functional Analyses of Cytosolic Glucose-6-Phosphate Dehydrogenases and Their Contribution to Seed Oil Accumulation in Arabidopsis. Plant Physiology 146: 277-288.

Wan X, Fan X, Chen M, Xiang J, Huang P, Guo L *et al.* (2010). Elevated Beclin 1 expression is correlated with HIF-1alpha in predicting poor prognosis of nasopharyngeal carcinoma. Autophagy 6: 395-404.

Wang Q, Ding Y, Kohtz S, Mizushima N, Cristea I, Rout M *et al.* (2006). Induction of Autophagy in Axonal Dystrophy and Degeneration Journal of Neuroscience 26: 8057-8068.

Wang L, Kobayashi T, Piao X, Shiono M, Takagi Y, Mineki R *et al.* (2010). Serine 62 is a phosphorylation site in folliculin, the Birt–Hogg–Dubé gene product. FEBS Letters 584: 39-43.

Warburg O (1956). The origin of cells. Science 123: 309-314.

Warren M, Torres-Cabala C, Turner M, Merino M, Matrosova V, Nickerson M *et al.* (2004). Expression of Birt-Hogg-Dubé gene mRNA in normal and neoplastic human tissues. Mod Pathol 17: 998–1011.

Watanabe R, Wei L, Huang J (2011). mTOR signaling, function, novel inhibitors, and therapeutic targets. J Nucl Med 52: 497-500.

Webber J, Tooze S (2010). Coordinated regulation of autophagy by p38α MAPK through mAtg9 and p38IP. The EMBO Journal 29: 27-40.

Wedel S, Hudak L, Seibel J, Juengel E, Tsaur I, Haferkamp A *et al.* (2011). Combined targeting of the VEGFr/EGFr and the mammalian target of rapamycin (mTOR) signaling pathway delays cell cycle progression and alters adhesion behavior of prostate carcinoma cells. Cancer Letters 301: 17-28.

Wigfield S, Winter S, Giatromanolaki A, Taylor J, Koukourakis M, Harris A (2008). PDK-1 regulates lactate production in hypoxia and is associated with poor prognosis in head and neck squamous cancer. Brit J Cancer 98: 1975-1984.

Woodward E, Ricketts C, Killick P, Gad S, Morris M, Kavalier F *et al.* (2008). Familial non-VHL clear cell (conventional) renal cell carcinoma: clinical features, segregation analysis, and mutation analysis of FLCN. Clin Cancer Res 14: 5925-5930.

Wu Z, Puigserver P, Andersson U, Zhang C, Adelmant G, Mootha V *et al.* (1999). Mechanisms Controlling Mitochondrial Biogenesis and Respiration through the Thermogenic Coactivator PGC-1. Cell 98: 115-124.

Wu C-H, Ho Y-S, Tsai C-Y, Wang Y-J, Tseng H, Wei P-L *et al.* (2009). In vitro and in vivo study of phloretin-induced apoptosis in human liver cancer cells involving inhibition of type II glucose transporter. Int J Cancer 124: 2210-2219.

Wullschleger S, Loewith R, Hall M (2006). TOR signaling in growth and metabolism. Cell 124: 471-484.

Wysocki P (2009). mTOR in renal cell cancer: modulator of tumor biology and therapeutic target. Expert Rev Mol Diagn 9: 231-241.

Xu G, O'Connell P, Viskochil D, Cawthon R, Robertson M, Culver M *et al.* (1990). The neurofibromatosis type 1 gene encodes a protein related to GAP. Cell 62: 599-608.

Xu R, Pelicano H, Zhang H, Giles F, Keating M, Huang P (2005). Synergistic effect of targeting mTOR by rapamycin and depleting ATP by inhibition of glycolysis in lymphoma and leukemia cells. Leukemia 19: 2153-2158.

Xu R, Pelicano H, Zhou Y, Carew J, Feng L, Bhalla K *et al.* (2005). Inhibition of glycolysis in cancer cells: a novel strategy to overcome drug resistance associated with mitochondrial respiratory defect and hypoxia. Cancer Research 65: 613-621.

Xu Y, Cui X, Sun S, Lee S, Li Y, Kwon J *et al.* (2011). Mitochondrial dysfunction influences apoptosis and autophagy in porcine parthenotes developing in vitro. J reprod Dev 57: 143-150.

Yang Y, Padilla-Nash H, Vira M, Abu-Asab M, Val D, Worrell R *et al.* (2008). The UOK 257 Cell Line – A Novel Model for Studies of the Human Birt-Hogg-Dubé Gene Pathway. Cancer Genet Cytogenet 180: 100-109.

Yoder B, Hou X, Guay-Woodford L (2002). The polycystic kidney disease proteins, polycystin-1, polycystin-2, polaris, and cystin, are co-localized in renal cilia. J Am Soc Nephrol 13: 2508-2516.

Yu P, Hong C, Sachidanandan C, Babitt J, Deng D, Hoyng S *et al*. (2008). Dorsomorphin inhibits BMP signals required for embryogenesis and iron metabolism. Nature Chemical Biology 4: 33-41.

Yun H, Lee M, Kim S-S, Ha J (2005). Glucose Deprivation Increases mRNA Stability of Vascular Endothelial Growth Factor through Activation of AMP-activated Protein Kinase in DU145 Prostate Carcinoma. Journal of Biological Chemistry 280: 9963-9972.

Z K, Michalopoulos G, Stolz D (2006). Peroxisomal localization of hypoxia-inducible factors and hypoxia-inducible factor regulatory hydroxylases in primary rat hepatocytes exposed to hypoxia-reoxygenation. Am J Pathol 169: 1251-1269.

Zhang H, Gao P, Fukuda R, Kumar G, Krishnamachary B, Zeller K *et al.* (2007). HIF-1 inhibits mitochondrial biogenesis and cellular respiration in VHL-deficient renal cell carcinoma by repression of C-MYC activity. Cancer Cell 11: 407-420.

Zong H, Ren J, Young L, Pypaert M, Mu J, Birnbaum M *et al.* (2002). AMP kinase is required for mitochondrial biogenesis in skeletal muscle in response to chronic energy deprivation. PNAS 99: 15983-15987.

Appendices

Appendix I Abbreviations

Abbreviation	Full form
2DG	2-Deoxyglucose
4E-BP1	Eukaryotic Translation Initiation Factor 4E Binding Protein
5-TOP	5’ tract of pyrimadines
ACC	Acetyl co-A Carboxylase
ADPKD	Autosomal dominant polycystic kidney disease
AIF	Apoptosis Inducing factor
AMPK	Adenosine monophosphate (AMP) -activated protein kinase
AraA	Adenine 9-β-D-arabinofuranoside
ATG	Autophagy related
ATM	Ataxia-telangiectasia mutated
BHD	Birt-Hogg-Dubé
BNIP3	BCL2/adenovirus E1B 19 kDa protein-interacting protein 3
CaMK	calcium/calmodulin dependant kinase
cAMP	Cyclic AMP
CCCP	Carbonyl cyanide m-chloro phenyl hydrazone
CCND1	Cell Cyclin D1
CDK	Cyclin Dependent kinases
DEPTOR	DEP domain containing MTOR-interacting protein
DMEM	Dulbecco's Modified Eagle Medium
DNA	Deoxyribonucleic acid
ERAD	Endoplasmic-reticulum-associated protein degradation
ERK	Extracellular Signal-Regulated Kinase
FAT	FRAP, ATM and TRRAP domains
FH	Fumarate Hydratase
FLCN	Folliculin
FNIP1	Folliculin Interacting Protein 1
FNIP2	Folliculin Interacting Protein 2
FRAP	FKBP-12-rapamycin associated protein
FRB	FKBP-12/rapamycin
G6PD1	Glucose-6-phosphate dehydrogenase
GAP	GTPase activating protein
GDP	Guanosine Diphosphate
GLUT1	Glucose transporter type 1
GSC	Germline Stem Cells
GTP	Guanosine tri phosphate
H2O2	Hydrogen Peroxide
HDAC	Histone deacetylase
HEAT	Huntington Elongaion factor 3, A subunit of protein phosphatase 2A and Tor1

HIF	Hypoxia inducible factor
HK	Hexokinase
HK2	Human Kidney 2
HLRCC	Hereditary Leiomyomatosis and Renal cell carcinoma
HOAD	3-hydroxy-acyl-CoA
HSCs	Hematopoeitic stem cells
IGF	Insulin like growth factor 1
Jak/Stat	Janus kinase/signal transducers and activators of transcription
LDH	Lactate Dehydrogenase
Liver kinase B1	Liver kinase B1
LST8	Lethal with sec13 protein 8
MCT1	Monocarboxylate transporter 1
MCT4	Monocarboxylate transporter 4
MEF	Mouse Embryonic Fibroblast
MEK	Mitogen-activated protein kinase kinase
MIDM2	Murine double minute 2
mTOR	Mammalian Target of Rapamycin
NF1	Neurofibromin 1
NRF1	Nuclear Respiritory Factor 1
NRF2	Nuclear Respiritory Factor 2
ODDD	Oxygen dependant degradation domain
PC1	Polycystin 1
PC2	Polycystin2
PDH	Pyruvate Dehydrogenase
PDK1	Pyruvate dehydrogenase kinase 1
PDK1	3-phosphoinositide-dependent protein kinase 1
PGC1α	Peroxisome proliferator-activated receptor gamma coactivator 1-alpha
PGC1β	Peroxisome proliferator-activated receptor gamma coactivator 1-beta
PI3K	Phosphoinositide-3-kinase
Pip2	Phosphatidylinositol (3,4,5)-triphosphate (PtdIns(3,4,5)P2)
Pip3	Phosphatidylinositol (3,4,5)-triphosphate (PtdIns(3,4,5)P3)
PKB	Protein Kinase B
PP1	Protein Phosphatase 1
PP2a	Protein Phosphatase 2A
PPAR	Peroxisome proliferator-activated receptor
PTEN	Phosphatase and Tensin Homolog
Raptor	Regulatory associated protein of MTOR
RCC	Renal Cell Carcinoma
RCND	Renal Cystadenocarcinoma and Nodular Dermatofibrosis
Rheb	Ras homolog enriched in brain
Rictor	Rapamycin-insensitive companion of Tor
RNA	Ribonucleic acid

ROS	Reactive Oxygen Species
RPL13	Ribosomal protein L13
rpS6	Ribosomal protein S6
RT	Real Time
RT	Reverse transcriptase
S6K1	P70-S6 Kinase 1
SERCA	Sarco/Endoplasmic Reticulum Ca2+-ATPase
Sh	Short hairpin
Si	Small interfering
Sin1	Stress-activated protein kinase-interacting protein 1
SOD2	Superoxide dismutase 2
STK11	Serine/threonine kinase 11
TFAM	Transcription factor A, mitochondrial
TFE3	Transcription factor E3
TFEB	Transcription factor EB
TH	Thyroid hormone
TOS	Tor Signalling
TRRAP	Transformation/transcription domain-associated protein
TSC	Tuberous Sclerosis Complex
UCP3	Uncoupling protein 3
ULK1	UNC 51-like kinase
UTR	Untranslated region
VEGF	Vascular Endothelial Growth Factor
VHL	Von Hippel Lindau
YY1	Ying-Yang 1

Appendix II. Materials and methods

Antibodies and Other Biochemicals

Dr Arnim Pause (McGill University, Canada) kindly provided the anti-Folliculin antibodies. Rapamycin was purchased from Calbiochem/Merck (Beeston, Nottingham, UK). 2-deoxyglucose was obtained from Sigma-Aldrich Company Ltd. (Dorset, UK). Dr. Laura S. Schmitt kindly provided the N-terminal Flag-tagged BHD vector was a kind gift from (Bethesda, MD USA, described in (Baba, 2006)). The PGC1a luciferase reporter construct was a kind gift from Dr. Kieth Barr (Davis, CA, USA). The PR4-CMV renilla control for luciferase assays was a kind gift from Prof. Maurice Van Steensel's lab (University of Maastricht, Netherlands). Anti-BNIP3, anti-β-actin, anti-VEGF-A, anti-GLUT1, anti-PDK1, and anti-UCP3 antibodies were purchased from Abcam (Cambridge, UK). Anti-phospho-rpS6 (Ser235/236), anti-rpS6, anti-phospho-Akt (Thr308, Ser476), anti-Akt antibodies, anti-acetyl choline carboxylase and anti-raptor and anti-phospho raptor (Ser792), anti-phospho acetyl choline carboxylase (Ser79), anti-AMPKa and phospho-AMPKa (Thr172), as well as anti-4E-BP1 and anti-phospho 4E-BP1 (Ser65) antibodies, were purchased from Cell Signalling Technology (Danvers, MA, USA). Anti-GLUT4, anti-MCT4, anti-MCT1, anti-PDH, and anti-phospho-PDH (Thr306, Ser473) antibodies were purchased from Santa Cruz Biotechnology (Santa Cruz, CA, USA). Anti-HIF1α and Anti-P62 ICK ligand antibodies were purchased from BD transduction laboratories (Oxford, UK). Anti-LC3 and anti-HIF2α antibodies used in western blot analyses were purchased from Novartis (Surrey, UK). Anti-Lamin/A/C was purchased from Millipore (Watford, UK). Anti-SOD2 was purchased from Genetex (Irvine, CA, USA). 3MA and Chloroquine diphosphate were purchased from Sigma-Aldrich Company Ltd. (Dorset, UK). Nelfinavir in the form of Viracept tablets was purchased from Pfizer, Inc (New York, USA).

Cell Culture

UOK257-2 and UOK257 cells that were a kind gift from Dr. Laura S. Schmitt (Bethesda, MD USA) were cultured in Dulbecco's Modified Eagle's Medium supplemented with 100 μg/ml streptomycin, 100 U/ml penicillin and 10 % (v/v) foetal calf serum (Gibco, Paisley, UK). UOK257-2 and UOK257 cells were incubated at either 1% or 21 % oxygen either with or without 50 nM rapamycin treatment as indicated. After 18 h, these cells were harvested.
CRUK HEK293 cells that were purchased from ATCC were cultured in Dulbecco's Modified Eagle's Medium supplemented with 100 μg/ml streptomycin 100 μg/ml streptomycin, 100 U/ml penicillin and 10 % (v/v) foetal calf serum (Gibco, Paisley, UK). UOK257-2 and were incubated at 21 % oxygen. These cells were harvested after 18 h.
Stable clones of Human Kidney 2 (HK2) cells expressing scrambled (HK2 G10) or BHD shRNA (HK2 5968 A5) were generated using mission shRNA constructs (purchased from -Aldrich Company Ltd. (Dorset, UK)) by Tijs Claessens (Maastricht, Netherlands). HK2 5968 A5 (BHD^-) and HK2 G10 (BHD^+) cells were incubated at either 1 % or 21 % oxygen as indicated. These cells were harvested after 18 h.

$BHD^{+/+}$ and $BHD^{-/-}$ Mouse Embryonic Fibroblast (MEF) cells that were a kind gift from Prof. Arnim Pause (Quebec, Canada) were cultured in Dulbecco's Modified Eagle's Medium supplemented with 10 % (v/v) foetal calf serum, 100 U/ml penicillin and 100 μg/ml streptomycin (Gibco, Paisley, UK). UOK257-2 and UOK257 cells were incubated at either 1 % or 21 % oxygen either with or without 50 nM rapamycin treatment as indicated. After 18 h, these cells were harvested.

DNA extraction

Phosphate buffered saline (PBS) was used to wash the cells before they were lysed from the 6 cm^2 plates using 0.5 ml PBS. DNA was extracted using a DNeasy Blood and Tissue kit (Qiagen, West Sussex, United Kingdom) as described in the manufacturers' protocol.

mRNA extraction and reverse transcription

Phosphate buffered saline (PBS) was used to wash the cells before, they were lysed from the 6 cm^2 plates using 0.5 ml RNAprotect® Cell Reagent (Qiagen, West Sussex, United Kingdom). The rNA extraction process was performed using a RNeasy Plus mini kit (Qiagen, West Sussex, United Kingdom). During the RNA extraction procedure, Qiashredder tubes were used to homogenize the cell lysates as described in the manufacturer's protocol. A Quantitect reverse transcription kit (Qiagen, West Sussex, United Kingdom) and a thermal cycler (Applied Biosystems, California, USA) was then used to transcribe the total RNA from each sample (1 μg) into cDNA.

Real Time Quantitative PCR

96 well plates were used to conduct Quantitative Real Time PCR reactions using 25ng DNA per reaction, Sybr Green PCR Master mix (Qiagen, West Sussex, United Kingdom) and appropriate primer assays. The following procedure was then used to perform the assays: initial denaturation step (95 ^oC, 15 min), 40 cycles of denaturation (94 ^oC, 15 sec), annealing step (55 ^oC, 30 sec (RPL13, Cytochrome b), 60 ^oC (NRF1, NRF2, TFAM) 59 ^oC (PGC1 β) 58 ^oC (PGC1 α)), extension step (72 ^oC, 40 sec). The sequences of the Cytochrome B primers used were Forward 5'-GCGTCCTTGCCCTATTACTATC-3'; Reverse 5'-CTTACTGGTTGTCCTCCGATTC -3'. The sequences of the RPL13 primers used were Forward 5'-CTCAAGGTCGTGCGTCGTCTG-3'; Reverse 5'-TGGCTTTCTCTTTCCTCTTCTC -3'. The sequences of the SOD2 primers used were Forward 5'-GCCTGCACTGAAGTTCAATG-3'; Reverse 5'-ATCTGTAAGCGACCTTGCTC-3'. The sequences of the UCP3 primers used were Forward 5'-GGATTTGTGCCCTCCTTTCTG-3'; Reverse 5'-AGATTCCCGCAGTACCTGGACT-3' The sequences of the PGC1β primers used were Forward 5'-GAACCCAACCAGTACAGCCCCGATG-3'; Reverse 5'-GCTGAGGTGCATGATAGAGCGTCTC-3'. The sequences of the PGC1α primers used were Forward 5'-CAAGATCAAGGTCTCCAGGCAGTAGATCC-3'; Reverse 5'-CGATATTCTTCCCTCTTCAGCCTCTCGTG-3'. The sequences of the NRF1 primers used were Forward 5'-GTCCAGATCCCTGTGAGCAT-3'; Reverse 5'-

CAATGTCACCACCTCCACAG-3'. The sequences of the NRF2/GABPA primers used were Forward 5'-ACCTTCATCACCAACCCAAG-3'; Reverse 5'-AGAAGCTCACCTGGGAACAG-3'. The sequences of the TFAM primers used were Forward 5'-TCCAAGAAGCTAAGGGTGATTC-3'; Reverse 5'-CGAGTTTCGTCCTCTTTAGCA-3'. The sequences of the human VEGF-A I–II primers used were Forward 5'-CTGCTGTCTTGGGTGCATTG-3'; Reverse 5'-TTCACAATTTGTTGTGCTGTAG-3', as described in Roland *et al*. (2000). The sequences of the mouse VEGF-A I–II primers used were Forward 5'-GGAGAGCAGAAGTCCCATGA-3'; Reverse 5'-ACTCCAGGGCTTCATCGTTA-3', as described in Garcia *et al*. (2009). All of the other primer sets were bought from Qiagen, who have to right to with hold primer sequence information. Quantification of the amplification products took place during the extension step in the 40th cycle. The results were then determined using the ddCT method, and normalised first to either RPL13 or β-Actin. I verified that only one PCR product was produced with each primer set and their specificity by performing a dissociation step. The correct amplicon length for each of the PCR products was also verified via resolution on a 2 % polyacrylamide gel. The expected size of the amplified products was approximately 77 bp for GLUT1 catalogue number (QT00068957), 70 bp for human VEGF-A, 104 bp for human b-actin (Catalogue number QT01680476), 73 bp for human BNIP3 (Catalogue number QT00024178), 96 bp for CCND1 (Catalogue number QT00495285), 91 bp for G6PD1 (Catalogue number QT00071596), 104 bp for HIF1α (Catalogue number QT00083664), 127 bp for HIF2α (Catalogue number QT00069587), 196 bp for Cytochrome B, 250 bp for RPL13, 170 bp for human PGC1β, 196 bp for human PGC1α, 250 bp for TFAM, 73 bp for UCP3, 102 bp for NRF1, 89 bp for NRF2, 82 bp for SOD2, 63 bp for mouse PGC1α (Catalogue number QT00156303), 61 bp for mouse ATP5G1 (Catalogue number QT01038198), 77 bp for mouse β-actin (Catalogue number QT01136772), 67 bp for mouse BNIP3 (Catalogue number QT00100233), 117 bp for mouse VEGF-A, 68 bp for human ULK1 (Catalogue number QT00009884), 85 bp for human ULK2 (Catalogue number QT00031381), 107 bp for mouse ULK1 (Catalogue number QT01759513) and for 150 bp for Beclin 1 (Catalogue number QT00004221). The information given is in accordance to the minimum information for publication of real time quantitative PCR data (Bustin *et al*., 2009).

Western Blotting

PBS was used to was the cells before lysis buffer (20 mM Tris, 135 mM NaCl, 5 % (v/v) glycerol, 50 mM NaF and 0.1 % (v/v) triton X-100, pH 7.5 supplemented with complete mini protease inhibitor cocktail (Roche Diagnostics Ltd. Burgess Hill, United Kingdom) and 1 mM Dithiothreitol (DTT)) was used to lyse them from the 6 cm^2 plates using at 4 ^{o}C. After centrifugation at 13,000 rpm for 8 min at 4 ^{o}C the samples were boiled at 70 °C for 10 min with x4 NuPAGE® LDS Sample buffer (Invitrogen, Paisley, United Kingdom) and 25 mM DTT and. For preparation of HIF2α and HIF1α protein samples, cells were lysed with 62.5 mM Tris-HCl (pH 6.8), 2 % (w/v) SDS, 10 % (v/v) glycerol, 50 mM DTT, and 0.1 (w/v)

bromophenol blue followed by pulse sonication before being boiled at 95 ^{o}C for 5 min. Samples were then separated by electrophoresis using the NuPAGE® gel system (Invitrogen, Paisley, United Kingdom) according to manufacturers' protocol. Proteins were transferred to Polyvinylidene Difluoride membranes (Millipore, South West, United Kingdom), blocked in 5 % (w/v) dry milk powder in Tris buffered saline (TBS-T) (2.42 g Tris base, 8 g NaCl, 1 l H_2O_2 pH 7.6, 1 ml Tween 20). The required primary antibody and Horse Radish Peroxidse-conjugated secondary antibody in TBST were then used to probe for each particular protein. Enhanced Chemiluminescent solution and Hyperfilm (both from GE Healthcare, Buckinghamshire, United Kingdom) were then used to visualise the proteins and each film was developed using a Konica Minolta SRX101A developer. Densitometry analyses were performed where indicated using Image J software. For larger gels; the samples were run for 5 h and transferred overnight using omniPage maxi vertical electrophoresis according to manufacturers' protocol using Running buffer (1.44.07 g glycine, 30.285 g Tris base, 10 g SDS made up to 1 l with dH_2O).

HIF Luciferase assay

UOK257 cells and BHD$^{-/-}$ MEF cells were transfected with either Flag-tagged BHD or pRK7 empty vector alongside a firefly luciferase reporter pGL2-TK-HRE plasmid (a gift from G Melillo (National Cancer Institute at Frederick, Maryland, USA) along with 1 µl 1mM PR4-CMV renilla control using Lipofectamine 2000 transfection reagent (Invitrogen, Paisley, UK) according to the manufacturer's protocol. BHD- and BHD^{+} HK2 cells were transfected with the firefly luciferase reporter pGL2-TK-HRE plasmid (a gift from G Melillo (National Cancer Institute at Frederick, Maryland, USA)) along with 1 µl 1 mM PR4-CMV renilla control using Lipofectamine 2000 transfection reagent (Invitrogen, Paisley, UK) according to the manufacturer's protocol. The pGL2-TK-HRE plasmid was generated using the protocol described by Rapisarda *et al.* (Rapisarda *et al.*, 2002). 4 h post transfection, the medium was changed on cells and cells were incubated at 21 % oxygen either with or without 50 nM rapamycin treatment as indicated. The cells were washed in phosphate-buffered saline after 24 h post transfection, before being lysed in lysis buffer (20 mM Tris, 135mM NaCl, 5% (v/v) glycerol, 50mM NaF and 0.1% (v/v) triton X-100, pH 7.5, which had been supplemented with complete mini-protease inhibitor cocktail (Roche Diagnostics Ltd) and 1mM DTT) at 4 ^{o}C. Renilla and firefly luciferase levels were analysed in 80 µg of protein lysate combined with 20 µg lysis buffer using a dual luciferase assay kit (Promega UK, Southampton, UK) and a luminometer 2 s and 10 s after initial injection according to manufacturers' protocol.

PGC1α Luciferase Assay

UOK257 cells and BHD$^{-/-}$ MEF cells were transfected with either Flag-tagged BHD or pRK7 empty vector alonside the PGC1α firefly luciferase reporter (a kind gift from Kieth Barr,

University of California, USA) and 1 µl 1 mM PR4-CMV vector as a renilla control using Lipofectamine 2000 transfection reagent (Invitrogen, Paisley, United Kingdom) according to the manufacturer's protocol. 4 h post-transfection, the medium was changed on cells and cells were incubated at 21 % oxygen either with or without 50 nM rapamycin treatment as indicated. The cells were washed in PBS after 24 h post transfection before being lysed in lysis buffer (20 mM Tris, 135 mM NaCl, 5 % (v/v) glycerol, 50 mM NaF and 0.1 % (v/v) triton X-100, pH 7.5 which was supplemented with complete mini protease inhibitor cocktail (Roche Diagnostics Ltd. Burgess Hill, United Kingdom) and 1 mM DTT) at 4 ^{o}C. After centrifuging the samples at 13,000 rpm for 8 minutes at 4 ^{o}C, 80 µg of protein lysate in 20 µl lysis buffer was combined with a dual luciferase assay kit (Promega UK, Southampton, UK) and analysed for renilla and firefly luciferase levels via a luminometer 2 s and 10 s after the first injection according to manufacturers' protocol

CellTitre-glo cell viability assay

UOK257 cells and UOK257-2 cells were transferred to a 96 well tissue culture plate (2 wells per cell line, 10000 cells per well). DMEM was then used to make up each well to 150 µl. 150 µl CellTiter-Glo Reagent from a CellTiter-Glo Luminescent Cell Viability Assay (Promega UK. Southhampton, UK) was then placed into each well. The reactions were then incubated at room temperature for 1 h before the plate was placed in a luminometer and the luminescence was read

CyQUANT (R) cell proliferation assay.

After counting, cells were plated onto a black 96-well plate (10,000 cells per well). In total, 10, 20, 30 and 40 µM Nelfinavir, 5 mM 3MA, and 100 µM Chloroquine were added where indicated 24 h after cells were plated and the plates were incubated at 37 ^{o}C for 24 h. Medium was removed from the cells at the required time point, before the 96 well plates were frozen at 80 ^{o}C. After thawing, each well had 200 ml CyQUANT (R) mix, prepared as described in the CyQUANT (R) Cell Proliferation Assay (Invitrogen, Paisley, UK) manufacturer's protocol, added to it. A fluorometer was then used to measure fluoresence at 485 and 520 nm.

L-Lactate assay

Cells were counted and 10,000 were plated per well of a black 96-well plate and grown in DMEM for 6 hours**.** 20 µl of DMEM was then taken from these cells and incubated with 80 µl working reagent prepared using the EnzyChrom L-Lactate Assay Kit manufacturers' protocol (Universal Biologicals LTD, Cambridge, UK). Standards were also prepared according to manufacturers' protocol and incubated with 80 µl working reagent. Absorbance levels were then read at 565 nm using a fluorometer. Levels of L-lactate within the samples

were determined by comparing to the standard curve generated by measuring the absorbance of the standards prepared.

Hydrogen Peroxide (H_20_2) assay

UOK257 and UOK257-2 cells growing in DMEM were washed with Krebs ringer buffer before being incubated in Krebs ringer buffer for 30 minutes in normoxia (21 %). Media was then taken from the cells and incubated with Amplex red reagent as described in the Amplex red hydrogen peroxide assay (Invitrogen, Paisley, UK) manufacturer's instructions. Standards were also prepared according to manufacturers' protocol before fluorescence was then measured using a fluorometer at 530-560 nm excitation and 590 nm emission. Levels of H_2O_2 within the samples were determined by comparing to the standard curve generated by measuring the fluorescence of the standards prepared.

Cell fractionation.

UOK257-2, UOK257, and HEK 293 cells were grown to full confluency in 150 mm tissue culture plates. Cells were then washed and scraped into phosphate buffered saline. Mitochondrial and cytosolic fractions were then generated using a mitochondrial cell fractionation kit (Active motif, La Hulpe, Belgium) according to manufacturer's protocol. Nuclear fractions were generated by centrifuging the cells down at 13000 rpm for 10 s before removing the phosphate buffered saline and adding 400µl hypotonic solution (100 mM HEPES pH 7.9, 1.5mM $MgCl_2$, 10 mM KCl, 0.5 mM DTT, 0.2 mM PMSF**)**. The cells were pulse vortexed and incubated on ice for 10 minutes. The cells were then centrifuged at 13000 rpm for 10 s before removing the hypotonic buffer and adding 100 µl hypertonic buffer (20 mM HEPES, 25 % glycerol, 420 mM NaCl, 1.5 mM $MgCl_2$, 0.2 mM EDTA, 0.5 mM DTT, 0.2 mM PMSF). The cells were then pulse vortexed before being incubated on ice for 20 minutes. The cells were then centrifuged for 2 minutes at 13000 rpm at 4 ^oC.

Cell death assay

Cells were counted and 10,000 cells were plated per well of a black 96-well plate. In total, 20 µM, and 30µM Nelfinavir and 50 µM and 100 µM Chloroquine, and 50nm rapamycin were added, where indicated, 24 h after cells were grown in 10 % FBS. Cell death assays were then conducted using a Cell death detection elisa assay (Roche, Hertfordshire, UK**)** according to manufacturers' protocol. Absorbance was then measured using a fluorometer at 405 nm.

Electron Microscopy work.

$BHD^{-/-}$ and $BHD^{+/+}$ MEF cells were maintained in 35 mm plates in DMEM and grown to full confluency on EM grids. The cells were then fixed in 1 % glutaraldehyde and Transmission Electron microscopy work was conducted in order to obtain images of the mitochondria within these cells. The surface area of the inner mitochondrial membrane of the mitochondria in the images obtained from these cells was then measured and the ratio of surface area of inner membrane/total area of mitochondria was determined. (Work carried out by Mr. Chris Von Ruhland). Image J 1.45 was used on overlay outlines of mitochondrial cristae to measure mitochondrial surface area as well as their total volume.

Appendix III. Statistical Analyses

A Shapiro-Wilk test was used to determine normal distribution (Sample size <50) where appropriate. If 2 groups were of normal distribution an Independent t-test was conducted.

If there were more than 2 groups and they were of normal distribution, a One-way independent-measures ANOVA was conducted.

Table 1 ANOVA analysis of BNIP3 mRNA levels in UOK257 cells

Multiple Comparisons Dependent variable BNIP3 Tukey HSD

(I) BHD			(J) BHD			Mean Difference (I-J)	Std. Error	Sig.	95% Confidence Interval	
O_2 (%)	BHD	Rapamycin	O_2 (%)	BHD	Rapamycin				Lower Bound	Upper Bound
21	+	-	21	+	+	.00115	.26111	1.000	-.9029	.9051
			21	-	-	-.98922*	.26111	.027	-1.8932	-.0852
			21	-	+	-.35940	.26111	.855	-1.2634	.5446
			1	+	-	-.16371	.26111	.998	-1.0677	.7403
			1	+	+	-.10106	.26111	1.000	-1.0051	.8029
			1	-	-	-2.38276*	.26111	.000	-3.2868	-1.4788
			1	-	+	-.37249	.26111	.833	-1.2765	.5315
21	+	+	21	+	-	-.00115	.26111	1.000	-.9051	.9029
			21	-	-	-.99037*	.26111	.027	-1.8944	-.0864
			21	-	+	-.36054	.26111	.853	-1.2645	.5435
			1	+	-	-.16486	.26111	.998	-1.0689	.7391
			1	+	+	-.10221	.26111	1.000	-1.0062	.8018

			1	-	-	-2.38391*	.26111	.000	-3.2879	-1.4799
			1	-	+	-.37363	.26111	.831	-1.2776	.5304
21	-	-	21	+	-	.98922*	.26111	.027	.0852	1.8932
			21	+	+	.99037*	.26111	.027	.0864	1.8944
			21	-	+	.62983	.26111	.299	-.2742	1.5338
			1	+	-	.82551	.26111	.087	-.0785	1.7295
			1	+	+	.88816	.26111	.056	-.0158	1.7922
			1	-	-	-1.39354*	.26111	.001	-2.2975	-.4895
			1	-	+	.61674	.26111	.321	-.2873	1.5207
21	-	+	21	+	-	.35940	.26111	.855	-.5446	1.2634
			21	+	+	.36054	.26111	.853	-.5435	1.2645
			21	-	-	-.62983	.26111	.299	-1.5338	.2742
			1	+	-	.19568	.26111	.994	-.7083	1.0997
			1	+	+	.25833	.26111	.970	-.6457	1.1623
			1	-	-	-2.02336*	.26111	.000	-2.9274	-1.1194
			1	-	+	-.01309	.26111	1.000	-.9171	.8909
1	+	-	21	+	-	.16371	.26111	.998	-.7403	1.0677
			21	+	+	.16486	.26111	.998	-.7391	1.0689
			21	-	-	-.82551	.26111	.087	-1.7295	.0785
			21	-	+	-.19568	.26111	.994	-1.0997	.7083
			1	+	+	.06265	.26111	1.000	-.8413	.9667
			1	-	-	-2.21904*	.26111	.000	-3.1230	-1.3150
			1	-	+	-.20877	.26111	.991	-1.1128	.6952
1	+	+	21	+	-	.10106	.26111	1.000	-.8029	1.0051
			21	+	+	.10221	.26111	1.000	-.8018	1.0062
			21	-	-	-.88816	.26111	.056	-1.7922	.0158
			21	-	+	-.25833	.26111	.970	-1.1623	.6457
			1	+	-	-.06265	.26111	1.000	-.9667	.8413
			1	-	-	-2.28170*	.26111	.000	-3.1857	-1.3777
			1	-	+	-.27142	.26111	.961	-1.1754	.6326
1	-	-	21	+	-	2.38276*	.26111	.000	1.4788	3.2868
			21	+	+	2.38391*	.26111	.000	1.4799	3.2879
			21	-	-	1.39354*	.26111	.001	.4895	2.2975
			21	-	+	2.02336*	.26111	.000	1.1194	2.9274

			1	+	-	2.21904*	.26111	.000	1.3150	3.1230
			1	+	+	2.28170*	.26111	.000	1.3777	3.1857
			1	-	+	2.01027*	.26111	.000	1.1063	2.9143
1	-	+	21	+	-	.37249	.26111	.833	-.5315	1.2765
			21	+	+	.37363	.26111	.831	-.5304	1.2776
			21	-	-	-.61674	.26111	.321	-1.5207	.2873
			21	-	+	.01309	.26111	1.000	-.8909	.9171
			1	+	-	.20877	.26111	.991	-.6952	1.1128
			1	+	+	.27142	.26111	.961	-.6326	1.1754
			1	-	-	-2.01027*	.26111	.000	-2.9143	-1.1063

*. The mean difference is significant at the 0.05 level.

Table 2. ANOVA analysis of CCND1 mRNA levels in UOK257 cells

Multiple Comparisons

Dependent variable CCND1

Tukey HSD

(I) BHD			(J) BHD			Mean Difference (I-J)	Std. Error	Sig.	95% Confidence Interval	
O_2 (%)	BHD	Rapamycin	O_2 (%)	BHD	Rapamycin				Lower Bound	Upper Bound
21	+	-	21	+	+	-.00017	.14615	1.000	-.5062	.5058
			21	-	-	-.99940*	.14615	.000	-1.5054	-.4934
			21	-	+	-.73795*	.14615	.002	-1.2439	-.2320
			1	+	-	-.00280	.14615	1.000	-.5088	.5032
			1	+	+	-.00164	.14615	1.000	-.5076	.5043
			1	-	-	-1.84585*	.14615	.000	-2.3518	-1.3399
			1	-	+	-.29444	.14615	.502	-.8004	.2116
21	+	+	21	+	-	.00017	.14615	1.000	-.5058	.5062
			21	-	-	-.99923*	.14615	.000	-1.5052	-.4932
			21	-	+	-.73778*	.14615	.002	-1.2438	-.2318
			1	+	-	-.00263	.14615	1.000	-.5086	.5034
			1	+	+	-.00147	.14615	1.000	-.5075	.5045

			1	-	-	-1.84569*	.14615	.000	-2.3517	-1.3397
			1	-	+	-.29427	.14615	.503	-.8003	.2117
21	-	-	21	+	-	.99940*	.14615	.000	.4934	1.5054
			21	+	+	.99923*	.14615	.000	.4932	1.5052
			21	-	+	.26145	.14615	.635	-.2445	.7674
			1	+	-	.99660*	.14615	.000	.4906	1.5026
			1	+	+	.99776*	.14615	.000	.4918	1.5038
			1	-	-	-.84645*	.14615	.001	-1.3524	-.3405
			1	-	+	.70497*	.14615	.004	.1990	1.2110
21	-	+	21	+	-	.73795*	.14615	.002	.2320	1.2439
			21	+	+	.73778*	.14615	.002	.2318	1.2438
			21	-	-	-.26145	.14615	.635	-.7674	.2445
			1	+	-	.73515*	.14615	.002	.2292	1.2411
			1	+	+	.73631*	.14615	.002	.2303	1.2423
			1	-	-	-1.10790*	.14615	.000	-1.6139	-.6019
			1	-	+	.44351	.14615	.109	-.0625	.9495
1	+	-	21	+	-	.00280	.14615	1.000	-.5032	.5088
			21	+	+	.00263	.14615	1.000	-.5034	.5086
			21	-	-	-.99660*	.14615	.000	-1.5026	-.4906
			21	-	+	-.73515*	.14615	.002	-1.2411	-.2292
			1	+	+	.00116	.14615	1.000	-.5048	.5071
			1	-	-	-1.84306*	.14615	.000	-2.3490	-1.3371
			1	-	+	-.29164	.14615	.513	-.7976	.2144
1	+	+	21	+	-	.00164	.14615	1.000	-.5043	.5076
			21	+	+	.00147	.14615	1.000	-.5045	.5075
			21	-	-	-.99776*	.14615	.000	-1.5038	-.4918
			21	-	+	-.73631*	.14615	.002	-1.2423	-.2303
			1	+	-	-.00116	.14615	1.000	-.5071	.5048
			1	-	-	-1.84421*	.14615	.000	-2.3502	-1.3382
			1	-	+	-.29280	.14615	.509	-.7988	.2132
1	-	-	21	+	-	1.84585*	.14615	.000	1.3399	2.3518
			21	+	+	1.84569*	.14615	.000	1.3397	2.3517
			21	-	-	.84645*	.14615	.001	.3405	1.3524
			21	-	+	1.10790*	.14615	.000	.6019	1.6139

			1	+	-	1.84306*	.14615	.000	1.3371	2.3490
			1	+	+	1.84421*	.14615	.000	1.3382	2.3502
			1	-	+	1.55142*	.14615	.000	1.0454	2.0574
1	-	+	21	+	-	.29444	.14615	.502	-.2116	.8004
			21	+	+	.29427	.14615	.503	-.2117	.8003
			21	-	-	-.70497*	.14615	.004	-1.2110	-.1990
			21	-	+	-.44351	.14615	.109	-.9495	.0625
			1	+	-	.29164	.14615	.513	-.2144	.7976
			1	+	+	.29280	.14615	.509	-.2132	.7988
			1	-	-	-1.55142*	.14615	.000	-2.0574	-1.0454

*. The mean difference is significant at the 0.05 level.

Table 3. ANOVA analysis of G6PD1 mRNA levels in UOK257 cells

Multiple Comparisons

Dependent variable G6PD1

Tukey HSD

(I) BHD			(J) BHD			Mean Difference (I-J)	Std. Error	Sig.	95% Confidence Interval	
O_2 (%)	BHD	Rapamycin	O_2 (%)	BHD	Rapamycin				Lower Bound	Upper Bound
21	+	-	21	+	+	.05290	.18869	1.000	-.6129	.7187
			21	-	-	-.84233*	.16877	.004	-1.4379	-.2468
			21	-	+	-.59629*	.16877	.050	-1.1918	-.0008
			1	+	-	.09569	.18869	.999	-.5701	.7615
			1	+	+	.11135	.16877	.997	-.4842	.7069
			1	-	-	-.92428*	.16877	.002	-1.5198	-.3288
			1	-	+	-.29848	.16877	.648	-.8940	.2970
21	+	+	21	+	-	-.05290	.18869	1.000	-.7187	.6129
			21	-	-	-.89523*	.18869	.006	-1.5610	-.2294
			21	-	+	-.64918	.18869	.058	-1.3150	.0166
			1	+	-	.04280	.20669	1.000	-.6866	.7722
			1	+	+	.05846	.18869	1.000	-.6074	.7243

			1	-	-	-.97717*	.18869	.003	-1.6430	-.3114
			1	-	+	-.35138	.18869	.594	-1.0172	.3144
21	-	-	21	+	-	.84233*	.16877	.004	.2468	1.4379
			21	+	+	.89523*	.18869	.006	.2294	1.5610
			21	-	+	.24605	.16877	.816	-.3495	.8416
			1	+	-	.93803*	.18869	.004	.2722	1.6038
			1	+	+	.95368*	.16877	.001	.3582	1.5492
			1	-	-	-.08194	.16877	1.000	-.6775	.5136
			1	-	+	.54385	.16877	.085	-.0517	1.1394
21	-	+	21	+	-	.59629*	.16877	.050	.0008	1.1918
			21	+	+	.64918	.18869	.058	-.0166	1.3150
			21	-	-	-.24605	.16877	.816	-.8416	.3495
			1	+	-	.69198*	.18869	.039	.0262	1.3578
			1	+	+	.70764*	.16877	.015	.1121	1.3032
			1	-	-	-.32799	.16877	.546	-.9235	.2675
			1	-	+	.29781	.16877	.650	-.2977	.8933
1	+	-	21	+	-	-.09569	.18869	.999	-.7615	.5701
			21	+	+	-.04280	.20669	1.000	-.7722	.6866
			21	-	-	-.93803*	.18869	.004	-1.6038	-.2722
			21	-	+	-.69198*	.18869	.039	-1.3578	-.0262
			1	+	+	.01566	.18869	1.000	-.6502	.6815
			1	-	-	-1.01997*	.18869	.002	-1.6858	-.3542
			1	-	+	-.39417	.18869	.465	-1.0600	.2716
1	+	+	21	+	-	-.11135	.16877	.997	-.7069	.4842
			21	+	+	-.05846	.18869	1.000	-.7243	.6074
			21	-	-	-.95368*	.16877	.001	-1.5492	-.3582
			21	-	+	-.70764*	.16877	.015	-1.3032	-.1121
			1	+	-	-.01566	.18869	1.000	-.6815	.6502
			1	-	-	-1.03563*	.16877	.001	-1.6311	-.4401
			1	-	+	-.40983	.16877	.299	-1.0053	.1857
1	-	-	21	+	-	.92428*	.16877	.002	.3288	1.5198
			21	+	+	.97717*	.18869	.003	.3114	1.6430
			21	-	-	.08194	.16877	1.000	-.5136	.6775
			21	-	+	.32799	.16877	.546	-.2675	.9235

			1	+	-	1.01997*	.18869	.002	.3542	1.6858
			1	+	+	1.03563*	.16877	.001	.4401	1.6311
			1	-	+	.62580*	.16877	.036	.0303	1.2213
1	-	+	21	+	-	.29848	.16877	.648	-.2970	.8940
			21	+	+	.35138	.18869	.594	-.3144	1.0172
			21	-	-	-.54385	.16877	.085	-1.1394	.0517
			21	-	+	-.29781	.16877	.650	-.8933	.2977
			1	+	-	.39417	.18869	.465	-.2716	1.0600
			1	+	+	.40983	.16877	.299	-.1857	1.0053
			1	-	-	-.62580*	.16877	.036	-1.2213	-.0303

*. The mean difference is significant at the 0.05 level.

Table 4. ANOVA analyses of GLUT1 mRNA levels UOK257 cells

Multiple Comparisons

Dependent variable GLUT1

Tukey HSD

(I) BHD			(J) BHD			Mean Difference (I-J)	Std. Error	Sig.	95% Confidence Interval	
O_2 (%)	BHD	Rapamycin	O_2 (%)	BHD	Rapamycin				Lower Bound	Upper Bound
21	+	-	21	+	+	.03263	2.52805	1.000	-8.8880	8.9533
			21	-	-	-.56509	2.52805	1.000	-9.4858	8.3556
			21	-	+	-.07946	2.82645	1.000	-10.0531	9.8941
			1	+	-	-7.92092	2.52805	.099	-16.8416	.9997
			1	+	+	-4.79107	2.52805	.574	-13.7117	4.1296
			1	-	-	-16.97599*	2.82645	.001	-26.9496	-7.0024
			1	-	+	-9.51713*	2.52805	.033	-18.4378	-.5965
21	+	+	21	+	-	-.03263	2.52805	1.000	-8.9533	8.8880
			21	-	-	-.59773	2.52805	1.000	-9.5184	8.3229
			21	-	+	-.11209	2.82645	1.000	-10.0857	9.8615
			1	+	-	-7.95355	2.52805	.097	-16.8742	.9671
			1	+	+	-4.82371	2.52805	.567	-13.7444	4.0970

			1	-	-	-17.00863*	2.82645	.001	-26.9822	-7.0350
			1	-	+	-9.54976*	2.52805	.032	-18.4704	-.6291
21	-	-	21	+	-	.56509	2.52805	1.000	-8.3556	9.4858
			21	+	+	.59773	2.52805	1.000	-8.3229	9.5184
			21	-	+	.48564	2.82645	1.000	-9.4880	10.4592
			1	+	-	-7.35583	2.52805	.144	-16.2765	1.5648
			1	+	+	-4.22598	2.52805	.704	-13.1466	4.6947
			1	-	-	-16.41090*	2.82645	.001	-26.3845	-6.4373
			1	-	+	-8.95204*	2.52805	.049	-17.8727	-.0314
21	-	+	21	+	-	.07946	2.82645	1.000	-9.8941	10.0531
			21	+	+	.11209	2.82645	1.000	-9.8615	10.0857
			21	-	-	-.48564	2.82645	1.000	-10.4592	9.4880
			1	+	-	-7.84146	2.82645	.178	-17.8151	2.1321
			1	+	+	-4.71162	2.82645	.706	-14.6852	5.2620
			1	-	-	-16.89654*	3.09622	.002	-27.8221	-5.9710
			1	-	+	-9.43767	2.82645	.070	-19.4113	.5359
1	+	-	21	+	-	7.92092	2.52805	.099	-.9997	16.8416
			21	+	+	7.95355	2.52805	.097	-.9671	16.8742
			21	-	-	7.35583	2.52805	.144	-1.5648	16.2765
			21	-	+	7.84146	2.82645	.178	-2.1321	17.8151
			1	+	+	3.12984	2.52805	.907	-5.7908	12.0505
			1	-	-	-9.05508	2.82645	.088	-19.0287	.9185
			1	-	+	-1.59621	2.52805	.998	-10.5169	7.3245
1	+	+	21	+	-	4.79107	2.52805	.574	-4.1296	13.7117
			21	+	+	4.82371	2.52805	.567	-4.0970	13.7444
			21	-	-	4.22598	2.52805	.704	-4.6947	13.1466
			21	-	+	4.71162	2.82645	.706	-5.2620	14.6852
			1	+	-	-3.12984	2.52805	.907	-12.0505	5.7908
			1	-	-	-12.18492*	2.82645	.012	-22.1585	-2.2113
			1	-	+	-4.72605	2.52805	.589	-13.6467	4.1946
1	-	-	21	+	-	16.97599*	2.82645	.001	7.0024	26.9496
			21	+	+	17.00863*	2.82645	.001	7.0350	26.9822
			21	-	-	16.41090*	2.82645	.001	6.4373	26.3845
			21	-	+	16.89654*	3.09622	.002	5.9710	27.8221

			1	+	-	9.05508	2.82645	.088	-.9185	19.0287
			1	+	+	12.18492*	2.82645	.012	2.2113	22.1585
			1	-	+	7.45887	2.82645	.220	-2.5147	17.4325
1	-	+	21	+	-	9.51713*	2.52805	.033	.5965	18.4378
			21	+	+	9.54976*	2.52805	.032	.6291	18.4704
			21	-	-	8.95204*	2.52805	.049	.0314	17.8727
			21	-	+	9.43767	2.82645	.070	-.5359	19.4113
			1	+	-	1.59621	2.52805	.998	-7.3245	10.5169
			1	+	+	4.72605	2.52805	.589	-4.1946	13.6467
			1	-	-	-7.45887	2.82645	.220	-17.4325	2.5147

*. The mean difference is significant at the 0.05 level.

Table 5. ANOVA analysis of VEGF-A mRNA levels in UOK257 cells

Multiple Comparisons

Dependent variable VEGF

Tukey HSD

(I) BHD			(J) BHD			Mean Difference (I-J)	Std. Error	Sig.	95% Confidence Interval	
O_2 (%)	BHD	Rapamycin	O_2 (%)	BHD	Rapamycin				Lower Bound	Upper Bound
21	+	-	21	+	+	.00594	.37774	1.000	-1.3018	1.3137
			21	-	-	-.99200	.37774	.216	-2.2998	.3158
			21	-	+	-.45278	.37774	.921	-1.7606	.8550
			1	+	-	-.05030	.37774	1.000	-1.3581	1.2575
			1	+	+	-.00609	.37774	1.000	-1.3139	1.3017
			1	-	-	-2.84558*	.37774	.000	-4.1534	-1.5378
			1	-	+	-3.75703*	.37774	.000	-5.0648	-2.4492
21	+	+	21	+	-	-.00594	.37774	1.000	-1.3137	1.3018
			21	-	-	-.99794	.37774	.211	-2.3057	.3098
			21	-	+	-.45872	.37774	.916	-1.7665	.8491
			1	+	-	-.05624	.37774	1.000	-1.3640	1.2515

			1	+	+	-.01203	.37774	1.000	-1.3198	1.2958
			1	-	-	-2.85152*	.37774	.000	-4.1593	-1.5437
			1	-	+	-3.76297*	.37774	.000	-5.0707	-2.4552
21	-	-	21	+	-	.99200	.37774	.216	-.3158	2.2998
			21	+	+	.99794	.37774	.211	-.3098	2.3057
			21	-	+	.53922	.37774	.832	-.7686	1.8470
			1	+	-	.94170	.37774	.265	-.3661	2.2495
			1	+	+	.98591	.37774	.221	-.3219	2.2937
			1	-	-	-1.85359*	.37774	.003	-3.1614	-.5458
			1	-	+	-2.76503*	.37774	.000	-4.0728	-1.4572
21	-	+	21	+	-	.45278	.37774	.921	-.8550	1.7606
			21	+	+	.45872	.37774	.916	-.8491	1.7665
			21	-	-	-.53922	.37774	.832	-1.8470	.7686
			1	+	-	.40248	.37774	.955	-.9053	1.7103
			1	+	+	.44669	.37774	.926	-.8611	1.7545
			1	-	-	-2.39280*	.37774	.000	-3.7006	-1.0850
			1	-	+	-3.30424*	.37774	.000	-4.6120	-1.9965
1	+	-	21	+	-	.05030	.37774	1.000	-1.2575	1.3581
			21	+	+	.05624	.37774	1.000	-1.2515	1.3640
			21	-	-	-.94170	.37774	.265	-2.2495	.3661
			21	-	+	-.40248	.37774	.955	-1.7103	.9053
			1	+	+	.04421	.37774	1.000	-1.2636	1.3520
			1	-	-	-2.79528*	.37774	.000	-4.1031	-1.4875
			1	-	+	-3.70673*	.37774	.000	-5.0145	-2.3989
1	+	+	21	+	-	.00609	.37774	1.000	-1.3017	1.3139
			21	+	+	.01203	.37774	1.000	-1.2958	1.3198
			21	-	-	-.98591	.37774	.221	-2.2937	.3219
			21	-	+	-.44669	.37774	.926	-1.7545	.8611
			1	+	-	-.04421	.37774	1.000	-1.3520	1.2636
			1	-	-	-2.83949*	.37774	.000	-4.1473	-1.5317
			1	-	+	-3.75094*	.37774	.000	-5.0587	-2.4432
1	-	-	21	+	-	2.84558*	.37774	.000	1.5378	4.1534
			21	+	+	2.85152*	.37774	.000	1.5437	4.1593
			21	-	-	1.85359*	.37774	.003	.5458	3.1614

			21	-	+	2.39280*	.37774	.000	1.0850	3.7006
			1	+	-	2.79528*	.37774	.000	1.4875	4.1031
			1	+	+	2.83949*	.37774	.000	1.5317	4.1473
			1	-	+	-.91144	.37774	.298	-2.2192	.3963
1	-	+	21	+	-	3.75703*	.37774	.000	2.4492	5.0648
			21	+	+	3.76297*	.37774	.000	2.4552	5.0707
			21	-	-	2.76503*	.37774	.000	1.4572	4.0728
			21	-	+	3.30424*	.37774	.000	1.9965	4.6120
			1	+	-	3.70673*	.37774	.000	2.3989	5.0145
			1	+	+	3.75094*	.37774	.000	2.4432	5.0587
			1	-	-	.91144	.37774	.298	-.3963	2.2192

*. The mean difference is significant at the 0.05 level.

Table 6. ANOVA analysis of HIF1α mRNA levels in UOK257 cells

Multiple Comparisons

HIF1

Tukey HSD

(I) BHD		(J) BHD		Mean Difference (I-J)	Std. Error	Sig.	95% Confidence Interval	
0_2 (%)	BHD	O_2(%)	BHD				Lower Bound	Upper Bound
21	+	21	-	-.99200	.33142	.067	-2.0533	.0693
		1	+	-.05030	.33142	.999	-1.1116	1.0110
		1	-	-2.84558*	.33142	.000	-3.9069	-1.7842
21	-	21	+	.99200	.33142	.067	-.0693	2.0533
		1	+	.94170	.33142	.083	-.1196	2.0030
		1	-	-1.85359*	.33142	.002	-2.9149	-.7922
1	+	21	+	.05030	.33142	.999	-1.0110	1.1116

		21	-	-.94170	.33142	.083	-2.0030	.1196
		1	-	-2.79528*	.33142	.000	-3.8566	-1.7339
1	-	21	+	2.84558*	.33142	.000	1.7842	3.9069
		21	-	1.85359*	.33142	.002	.7922	2.9149
		1	+	2.79528*	.33142	.000	1.7339	3.8566

*. The mean difference is significant at the 0.05 level.

Table 7. ANOVA analysis of HIF2α mRNA levels in UOK257 cells

Multiple Comparisons

HIF2

Tukey HSD

(I) BHD		(J) BHD		Mean Difference (I-J)	Std. Error	Sig.	95% Confidence Interval	
0_2 (%)	BHD	O_2(%)	BHD				Lower Bound	Upper Bound
21	+	21	-	-.14733	1.20395	.999	-4.0028	3.7081
		1	+	-4.60856*	1.20395	.021	-8.4640	-.7531
		1	-	-4.23750*	1.20395	.032	-8.0930	-.3820
21	-	21	+	.14733	1.20395	.999	-3.7081	4.0028
		1	+	-4.46123*	1.20395	.025	-8.3167	-.6058
		1	-	-4.09017*	1.20395	.038	-7.9456	-.2347
1	+	21	+	4.60856*	1.20395	.021	.7531	8.4640
		21	-	4.46123*	1.20395	.025	.6058	8.3167
		1	-	.37106	1.20395	.989	-3.4844	4.2265

1	-	21	+	4.23750*	1.20395	.032	.3820	8.0930
		21	-	4.09017*	1.20395	.038	.2347	7.9456
		1	+	-.37106	1.20395	.989	-4.2265	3.4844

*. The mean difference is significant at the 0.05 level.

Table 8. ANOVA analysis of HIF luciferase assay in UOK257 cells

Multiple Comparisons

HIF_lucif

Tukey HSD

(I) BHD		(J) BHD		Mean Difference (I-J)	Std. Error	Sig.	95% Confidence Interval	
BHD	Rapamycin	BHD	Rapamycin				Lower Bound	Upper Bound
+	-	+	+	18.18182	5.54242	.052	-.1645	36.5281
		-	-	-52.77778*	6.19662	.000	-73.2896	-32.2660
		-	+	-22.72727*	5.54242	.019	-41.0736	-4.3810
+	+	+	-	-18.18182	5.54242	.052	-36.5281	.1645
		-	-	-70.95960*	6.19662	.000	-91.4714	-50.4478
		-	+	-40.90909*	5.54242	.001	-59.2554	-22.5628
-	-	+	-	52.77778*	6.19662	.000	32.2660	73.2896
		-	+	70.95960*	6.19662	.000	50.4478	91.4714
		-	+	30.05051*	6.19662	.008	9.5387	50.5623
-	+	+	-	22.72727*	5.54242	.019	4.3810	41.0736
		+	+	40.90909*	5.54242	.001	22.5628	59.2554

		-	-	-30.05051*	6.19662	.008	-50.5623	-9.5387

*. The mean difference is significant at the 0.05 level.

Table 9. ANOVA analysis of HIF luciferase assay in ACHN cells

Multiple Comparisons

HIF_lucif

Tukey HSD

(I) BHD		(J) BHD		Mean Difference (I-J)	Std. Error	Sig.	95% Confidence Interval	
0_2 (%)	BHD	O_2(%)	BHD				Lower Bound	Upper Bound
21	+	21	-	-8.83508	3.94384	.192	-21.4647	3.7945
		1	+	-25.39267*	3.94384	.001	-38.0222	-12.7631
		1	-	-92.01571*	3.94384	.000	-104.6453	-79.3861
21	-	21	+	8.83508	3.94384	.192	-3.7945	21.4647
		1	+	-16.55759*	3.94384	.013	-29.1872	-3.9280
		1	-	-83.18063*	3.94384	.000	-95.8102	-70.5511
1	+	21	+	25.39267*	3.94384	.001	12.7631	38.0222
		21	-	16.55759*	3.94384	.013	3.9280	29.1872
		1	-	-66.62304*	3.94384	.000	-79.2526	-53.9935
1	-	21	+	92.01571*	3.94384	.000	79.3861	104.6453
		21	-	83.18063*	3.94384	.000	70.5511	95.8102
		1	+	66.62304*	3.94384	.000	53.9935	79.2526

*. The mean difference is significant at the 0.05 level.

Table 10. ANOVA analysis of VEGF-A mRNA levels in ACHN cells

Multiple Comparisons

Dependent variable VEGF

Tukey HSD

(I) BHD			(J) BHD			Mean Difference (I-J)	Std. Error	Sig.	95% Confidence Interval	
O_2 (%)	BHD	Rapamycin	O_2 (%)	BHD	Rapamycin				Lower Bound	Upper Bound
21	+	-	21	+	+	.13030	1.45726	1.000	-4.9150	5.1755
			21	-	-	-.56529	1.45726	1.000	-5.6105	4.4800
			21	-	+	.00308	1.45726	1.000	-5.0422	5.0483
			1	+	-	-.92704	1.45726	.998	-5.9723	4.1182
			1	+	+	-.68332	1.45726	1.000	-5.7286	4.3619
			1	-	-	-5.11544*	1.45726	.046	-10.1607	-.0702
			1	-	+	-2.07503	1.45726	.834	-7.1203	2.9702
21	+	+	21	+	-	-.13030	1.45726	1.000	-5.1755	4.9150
			21	-	-	-.69559	1.45726	1.000	-5.7408	4.3497
			21	-	+	-.12722	1.45726	1.000	-5.1725	4.9180
			1	+	-	-1.05734	1.45726	.995	-6.1026	3.9879
			1	+	+	-.81362	1.45726	.999	-5.8589	4.2316
			1	-	-	-5.24574*	1.45726	.039	-10.2910	-.2005
			1	-	+	-2.20533	1.45726	.790	-7.2506	2.8399
21	-	-	21	+	-	.56529	1.45726	1.000	-4.4800	5.6105
			21	+	+	.69559	1.45726	1.000	-4.3497	5.7408
			21	-	+	.56837	1.45726	1.000	-4.4769	5.6136
			1	+	-	-.36175	1.45726	1.000	-5.4070	4.6835
			1	+	+	-.11803	1.45726	1.000	-5.1633	4.9272
			1	-	-	-4.55015	1.45726	.093	-9.5954	.4951

			1	-	+	-1.50974	1.45726	.961	-6.5550	3.5355
21	-	+	21	+	-	-.00308	1.45726	1.000	-5.0483	5.0422
			21	+	+	.12722	1.45726	1.000	-4.9180	5.1725
			21	-	-	-.56837	1.45726	1.000	-5.6136	4.4769
			1	+	-	-.93012	1.45726	.998	-5.9754	4.1151
			1	+	+	-.68640	1.45726	1.000	-5.7316	4.3589
			1	-	-	-5.11852*	1.45726	.045	-10.1638	-.0733
			1	-	+	-2.07811	1.45726	.833	-7.1234	2.9671
1	+	-	21	+	-	.92704	1.45726	.998	-4.1182	5.9723
			21	+	+	1.05734	1.45726	.995	-3.9879	6.1026
			21	-	-	.36175	1.45726	1.000	-4.6835	5.4070
			21	-	+	.93012	1.45726	.998	-4.1151	5.9754
			1	+	+	.24372	1.45726	1.000	-4.8015	5.2890
			1	-	-	-4.18840	1.45726	.144	-9.2336	.8569
			1	-	+	-1.14799	1.45726	.991	-6.1932	3.8973
1	+	+	21	+	-	.68332	1.45726	1.000	-4.3619	5.7286
			21	+	+	.81362	1.45726	.999	-4.2316	5.8589
			21	-	-	.11803	1.45726	1.000	-4.9272	5.1633
			21	-	+	.68640	1.45726	1.000	-4.3589	5.7316
			1	+	-	-.24372	1.45726	1.000	-5.2890	4.8015
			1	-	-	-4.43212	1.45726	.108	-9.4774	.6131
			1	-	+	-1.39171	1.45726	.975	-6.4370	3.6535
1	-	-	21	+	-	5.11544*	1.45726	.046	.0702	10.1607
			21	+	+	5.24574*	1.45726	.039	.2005	10.2910
			21	-	-	4.55015	1.45726	.093	-.4951	9.5954
			21	-	+	5.11852*	1.45726	.045	.0733	10.1638
			1	+	-	4.18840	1.45726	.144	-.8569	9.2336
			1	+	+	4.43212	1.45726	.108	-.6131	9.4774
			1	-	+	3.04041	1.45726	.462	-2.0048	8.0857
1	-	+	21	+	-	2.07503	1.45726	.834	-2.9702	7.1203
			21	+	+	2.20533	1.45726	.790	-2.8399	7.2506
			21	-	-	1.50974	1.45726	.961	-3.5355	6.5550
			21	-	+	2.07811	1.45726	.833	-2.9671	7.1234
			1	+	-	1.14799	1.45726	.991	-3.8973	6.1932

			1	+	+	1.39171	1.45726	.975	-3.6535	6.4370
			1	-	-	-3.04041	1.45726	.462	-8.0857	2.0048

*. The mean difference is significant at the 0.05 level.

Table 11. Anova analysis of HIF luciferase assay in BHD MEF cells

Multiple Comparisons

HIF_lucif
Tukey HSD

(I) BHD		(J) BHD		Mean Difference (I-J)	Std. Error	Sig.	95% Confidence Interval	
BHD	Rapamycin	BHD	Rapamycin				Lower Bound	Upper Bound
+	-	+	+	9.76444	8.28955	.656	-16.7816	36.3105
		-	-	-89.10161*	8.28955	.000	-115.6477	-62.5556
		-	+	-19.92904	8.28955	.154	-46.4751	6.6170
+	+	+	-	-9.76444	8.28955	.656	-36.3105	16.7816
		-	-	-98.86604*	8.28955	.000	-125.4121	-72.3200
		-	+	-29.69347*	8.28955	.029	-56.2395	-3.1474
-	-	+	-	89.10161*	8.28955	.000	62.5556	115.6477
		-	+	98.86604*	8.28955	.000	72.3200	125.4121
		-	+	69.17257*	8.28955	.000	42.6265	95.7186
-	+	+	-	19.92904	8.28955	.154	-6.6170	46.4751
		+	+	29.69347*	8.28955	.029	3.1474	56.2395
		-	-	-69.17257*	8.28955	.000	-95.7186	-42.6265

*. The mean difference is significant at the 0.05 level.

Table 12. T-test analysis of BNIP3 mRNA levels in BHD MEF cells

T-test

Independent Samples Test

		Levene's Test for Equality of Variances		t-test for Equality of Means						
									95% Confidence Interval of the Difference	
		F	Sig.	t	df	Sig. (2-tailed)	Mean Difference	Std. Error Difference	Lower	Upper
BNIP3	Equal variances assumed	14.838	.018	-16.644	4	.000	-.78088	.04692	-.91114	-.65062
	Equal variances not assumed			-16.644	2.000	.004	-.78088	.04692	-.98275	-.57901

Table 13. ANOVA analysis of HIF luciferase assay in HK2 cells

Multiple Comparisons

HIF_lucif

Tukey HSD

(I) BHD		(J) BHD		Mean Difference (I-J)	Std. Error	Sig.	95% Confidence Interval	
BHD	Rapamycin	BHD	Rapamycin				Lower Bound	Upper Bound
+	-	+	+	17.71995	9.25812	.295	-11.9278	47.3677
		-	-	-60.17348*	9.25812	.001	-89.8213	-30.5257
		-	+	-19.75217	9.25812	.222	-49.3999	9.8956
+	+	+	-	-17.71995	9.25812	.295	-47.3677	11.9278
		-	-	-77.89343*	9.25812	.000	-107.5412	-48.2457
		-	+	-37.47212*	9.25812	.016	-67.1199	-7.8244
-	-	+	-	60.17348*	9.25812	.001	30.5257	89.8213
		-	+	77.89343*	9.25812	.000	48.2457	107.5412

		-	+	40.42131*	9.25812	.010	10.7735	70.0691
-	+	+	-	19.75217	9.25812	.222	-9.8956	49.3999
		+	+	37.47212*	9.25812	.016	7.8244	67.1199
		-	-	-40.42131*	9.25812	.010	-70.0691	-10.7735

*. The mean difference is significant at the 0.05 level.

Table 14. T-test analysis of L-Lactate assay in UOK257 cells

T-test

Independent Samples Test

		Levene's Test for Equality of Variances		t-test for Equality of Means						
									95% Confidence Interval of the Difference	
		F	Sig.	t	df	Sig. (2-tailed)	Mean Difference	Std. Error Difference	Lower	Upper
L_lactate	Equal variances assumed	1.225E16	.000	-1.332	2	.314	-.16748	.12575	-.70855	.37360
	Equal variances not assumed			-1.332	1.262	.374	-.16748	.12575	-1.16076	.82581

Table 15. ANOVA analysis of Mitochondrial vs genomic DNA in UOK257 cells

Multiple Comparisons

Dependent variable mtDNA

Tukey HSD

(I) BHD			(J) BHD			Mean Difference (I-J)	Std. Error	Sig.	95% Confidence Interval	
O_2 (%)	BHD	Rapamycin	O_2 (%)	BHD	Rapamycin				Lower Bound	Upper Bound
21	+	-	21	+	+	.41186	.50947	.990	-1.3520	2.1757
			21	-	-	-4.40037*	.50947	.000	-6.1642	-2.6365
			21	-	+	-1.55536	.50947	.105	-3.3192	.2085
			1	+	-	.31936	.50947	.998	-1.4445	2.0832
			1	+	+	.53928	.50947	.957	-1.2246	2.3031
			1	-	-	-.98708	.50947	.547	-2.7509	.7768
			1	-	+	-.65926	.50947	.888	-2.4231	1.1046
21	+	+	21	+	-	-.41186	.50947	.990	-2.1757	1.3520

			21	-	-	-4.81223*	.50947	.000	-6.5761	-3.0484
			21	-	+	-1.96722*	.50947	.023	-3.7311	-.2034
			1	+	-	-.09250	.50947	1.000	-1.8564	1.6714
			1	+	+	.12742	.50947	1.000	-1.6364	1.8913
			1	-	-	-1.39894	.50947	.178	-3.1628	.3649
			1	-	+	-1.07112	.50947	.453	-2.8350	.6927
21	-	-	21	+	-	4.40037*	.50947	.000	2.6365	6.1642
			21	+	+	4.81223*	.50947	.000	3.0484	6.5761
			21	-	+	2.84501*	.50947	.001	1.0812	4.6089
			1	+	-	4.71973*	.50947	.000	2.9559	6.4836
			1	+	+	4.93965*	.50947	.000	3.1758	6.7035
			1	-	-	3.41328*	.50947	.000	1.6494	5.1771
			1	-	+	3.74111*	.50947	.000	1.9773	5.5050
21	-	+	21	+	-	1.55536	.50947	.105	-.2085	3.3192
			21	+	+	1.96722*	.50947	.023	.2034	3.7311
			21	-	-	-2.84501*	.50947	.001	-4.6089	-1.0812
			1	+	-	1.87472*	.50947	.033	.1109	3.6386
			1	+	+	2.09464*	.50947	.014	.3308	3.8585
			1	-	-	.56828	.50947	.944	-1.1956	2.3321
			1	-	+	.89610	.50947	.653	-.8678	2.6600
1	+	-	21	+	-	-.31936	.50947	.998	-2.0832	1.4445
			21	+	+	.09250	.50947	1.000	-1.6714	1.8564
			21	-	-	-4.71973*	.50947	.000	-6.4836	-2.9559
			21	-	+	-1.87472*	.50947	.033	-3.6386	-.1109
			1	+	+	.21992	.50947	1.000	-1.5439	1.9838
			1	-	-	-1.30644	.50947	.238	-3.0703	.4574
			1	-	+	-.97862	.50947	.557	-2.7425	.7852
1	+	+	21	+	-	-.53928	.50947	.957	-2.3031	1.2246
			21	+	+	-.12742	.50947	1.000	-1.8913	1.6364
			21	-	-	-4.93965*	.50947	.000	-6.7035	-3.1758
			21	-	+	-2.09464*	.50947	.014	-3.8585	-.3308
			1	+	-	-.21992	.50947	1.000	-1.9838	1.5439
			1	-	-	-1.52636	.50947	.117	-3.2902	.2375
			1	-	+	-1.19854	.50947	.325	-2.9624	.5653

1	-	-	21	+	-	.98708	.50947	.547	-.7768	2.7509
			21	+	+	1.39894	.50947	.178	-.3649	3.1628
			21	-	-	-3.41328*	.50947	.000	-5.1771	-1.6494
			21	-	+	-.56828	.50947	.944	-2.3321	1.1956
			1	+	-	1.30644	.50947	.238	-.4574	3.0703
			1	+	+	1.52636	.50947	.117	-.2375	3.2902
			1	-	+	.32782	.50947	.997	-1.4360	2.0917
1	-	+	21	+	-	.65926	.50947	.888	-1.1046	2.4231
			21	+	+	1.07112	.50947	.453	-.6927	2.8350
			21	-	-	-3.74111*	.50947	.000	-5.5050	-1.9773
			21	-	+	-.89610	.50947	.653	-2.6600	.8678
			1	+	-	.97862	.50947	.557	-.7852	2.7425
			1	+	+	1.19854	.50947	.325	-.5653	2.9624
			1	-	-	-.32782	.50947	.997	-2.0917	1.4360

*. The mean difference is significant at the 0.05 level.

Table 16. T-test analysis of UCP3 mRNA data for UOK257 cell line

Independent Samples Test

		Levene's Test for Equality of Variances		t-test for Equality of Means						
									95% Confidence Interval of the Difference	
		F	Sig.	t	df	Sig. (2-tailed)	Mean Difference	Std. Error Difference	Lower	Upper
UCP3	Equal variances assumed	13.333	.022	-11.714	4	.000	-2163.61649	184.71085	-2676.45603	-1650.77695
	Equal variances not assumed			-11.714	2.000	.007	-2163.61649	184.71085	-2958.36314	-1368.86984

If the resulting p-value of a Levene's test is less than typically 0.05 there is a difference between the variances in the groups tested.

Equal variances not assumed (Sig=0.022 therefore <0.05 for Levene's test) therefore P=0.007

Table 17. T-test analysis of SOD2 mRNA data for UOK257 cell line

Independent Samples Test

		Levene's Test for Equality of Variances		t-test for Equality of Means						
									95% Confidence Interval of the Difference	
		F	Sig.	t	df	Sig. (2-tailed)	Mean Difference	Std. Error Difference	Lower	Upper
SOD2	Equal variances assumed	7.155	.056	-10.474	4	.000	-1.08609E7	1.03697E6	-1.37400E7	-7.98181E6
	Equal variances not assumed			-10.474	2.000	.009	-1.08609E7	1.03697E6	-1.53226E7	-6.39917E6

If the resulting p-value of a Levene's test is less than typically 0.05 there is a difference between the variances in the groups tested.

.

Equal variances assumed (Sig=0.056 therefore > 0.05 for Levene’s test) therefore P=0.000

Table 18. T-test analysis of PGC1β mRNA data for UOK257 cell line

Independent Samples Test

		Levene's Test for Equality of Variances		t-test for Equality of Means						
									95% Confidence Interval of the Difference	
		F	Sig.	t	df	Sig. (2-tailed)	Mean Difference	Std. Error Difference	Lower	Upper
Pgc1b	Equal variances assumed	11.336	.028	-5.611	4	.005	-1.77001	.31546	-2.64586	-.89417
	Equal variances not assumed			-5.611	2.000	.030	-1.77001	.31546	-3.12731	-.41272

If the resulting p-value of a Levene's test is less than typically 0.05 there is a difference between the variances in the groups tested.

Equal variances not assumed (Sig=0.028 therefore < 0.05 for Levene’s test) therefore P=0.005

Table 19. T-test analysis of NRF1 mRNA data for UOK257 cell line

Independent Samples Test

		Levene's Test for Equality of Variances		t-test for Equality of Means						
									95% Confidence Interval of the Difference	
		F	Sig.	t	df	Sig. (2-tailed)	Mean Difference	Std. Error Difference	Lower	Upper
NRF1	Equal variances assumed	5.916	.072	-5.419	4	.006	-132.99571	24.54394	-201.14060	-64.85082
	Equal variances not assumed			-5.419	2.000	.032	-132.99571	24.54394	-238.59975	-27.39167

If the resulting p-value of a Levene's test is less than typically 0.05 there is a difference between the variances in the groups tested.

Equal variances assumed (Sig=0.072 therefore > 0.05 for Levene's test) therefore P=0.006

Table 20. T-test analysis of NRF2 mRNA data for UOK257 cell line

Independent Samples Test

		Levene's Test for Equality of Variances		t-test for Equality of Means						
									95% Confidence Interval of the Difference	
		F	Sig.	t	df	Sig. (2-tailed)	Mean Difference	Std. Error Difference	Lower	Upper
NFR2	Equal variances assumed	15.690	.017	-5.254	4	.006	-6.32785	1.20428	-9.67148	-2.98422
	Equal variances not assumed			-5.254	2.000	.034	-6.32785	1.20428	-11.50947	-1.14624

If the resulting p-value of a Levene's test is less than typically 0.05 there is a difference between the variances in the groups tested.

Equal variances not assumed (Sig=0.017 therefore < 0.05 for Levene's test) therefore P=0.034

Table 21. T-test analysis of TFAM mRNA data for UOK257 cell line

Independent Samples Test

		Levene's Test for Equality of Variances		t-test for Equality of Means						
									95% Confidence Interval of the Difference	
		F	Sig.	t	df	Sig. (2-tailed)	Mean Difference	Std. Error Difference	Lower	Upper
TFAM	Equal variances assumed	13.453	.021	-.624	4	.567	-.07877	.12626	-.42934	.27179
	Equal variances not assumed			-.624	2.000	.596	-.07877	.12626	-.62204	.46450

If the resulting p-value of a Levene's test is less than typically 0.05 there is a difference between the variances in the groups tested.

Equal variances not assumed (Sig=0.021 therefore < 0.05 for Levene’s test) therefore P=0.596

Table 23. T-test analysis of ATP5G1 mRNA data for BHD MEF cell line

Independent Samples Test

		Levene's Test for Equality of Variances		t-test for Equality of Means						
									95% Confidence Interval of the Difference	
		F	Sig.	t	df	Sig. (2-tailed)	Mean Difference	Std. Error Difference	Lower	Upper
ATP5G1	Equal variances assumed	11.140	.029	-4.327	4	.012	-12.53896	2.89779	-20.58451	-4.49341
	Equal variances not assumed			-4.327	2.000	.049	-12.53896	2.89779	-25.00713	-.07079

If the resulting p-value of a Levene's test is less than typically 0.05 there is a difference between the variances in the groups tested.

Equal variances not assumed (Sig=0.029 therefore < 0.05 for Levene’s test) therefore P=0.049

Table 24. T-test analysis of PGC1a mRNA data for BHD MEF cell line

Independent Samples Test

		Levene's Test for Equality of Variances		t-test for Equality of Means						
									95% Confidence Interval of the Difference	
		F	Sig.	t	df	Sig. (2-tailed)	Mean Difference	Std. Error Difference	Lower	Upper
PGC1a	Equal variances assumed	11.023	.029	-4.501	4	.011	-2.50202	.55585	-4.04530	-.95873
	Equal variances not assumed			-4.501	2.000	.046	-2.50202	.55585	-4.89365	-.11039

If the resulting p-value of a Levene's test is less than typically 0.05 there is a difference between the variances in the groups tested.

Equal variances not assumed (Sig=0.029 therefore < 0.05 for Levene’s test) therefore P=0.046

Table 25. T-test analysis of PGC1α mRNA data for HK2 cell line

Independent Samples Test

		Levene's Test for Equality of Variances		t-test for Equality of Means						
									95% Confidence Interval of the Difference	
		F	Sig.	t	df	Sig. (2-tailed)	Mean Difference	Std. Error Difference	Lower	Upper
PGC1a	Equal variances assumed	5.213E16	.000	-17.976	2	.003	-1.11092	.06180	-1.37683	-.84500
	Equal variances not assumed			-17.976	1.000	.035	-1.11092	.06180	-1.89618	-.32565

If the resulting p-value of a Levene's test is less than typically 0.05 there is a difference between the variances in the groups tested.

Equal variances not assumed (Sig=0.000 therefore < 0.05 for Levene's test) therefore P=0.035

Table 26. PGC1b mRNA data for HK2 cell line

Independent Samples Test

		Levene's Test for Equality of Variances		t-test for Equality of Means						
									95% Confidence Interval of the Difference	
		F	Sig.	t	df	Sig. (2-tailed)	Mean Difference	Std. Error Difference	Lower	Upper
PGC1b	Equal variances assumed	.	.	-17.418	2	.003	-20.20249	1.15986	-25.19297	-15.21202
	Equal variances not assumed			-17.418	1.000	.037	-20.20249	1.15986	-34.93991	-5.46507

If the resulting p-value of a Levene's test is less than typically 0.05 there is a difference between the variances in the groups tested.

Equal variances not assumed (Sig=0.000 therefore < 0.05 for Levene's test) therefore P=0.101

Table 27. T-test for ATP levels in UOK257 cells

Independent Samples Test

		Levene's Test for Equality of Variances		t-test for Equality of Means						
									95% Confidence Interval of the Difference	
		F	Sig.	t	df	Sig. (2-tailed)	Mean Difference	Std. Error Difference	Lower	Upper
ATP level	Equal variances assumed	2.956	.116	7.018	10	.000	34.75845	4.95306	23.72235	45.79455
	Equal variances not assumed			7.018	7.146	.000	34.75845	4.95306	23.09461	46.42230

If the resulting p-value of a Levene's test is less than typically 0.05 there is a difference between the variances in the groups tested.

Equal variances assumed (Sig=0.116 therefore > 0.05 for Levene's test) therefore P=0.000

Table 28. ANOVA analysis of PGC1α Luciferase assay in UOK257 cells

Multiple Comparisons

PGC1a_lucif

Tukey HSD

(I) BHD		(J) BHD		Mean Difference (I-J)	Std. Error	Sig.	95% Confidence Interval	
0_2 (%)	BHD	O_2(%)	BHD				Lower Bound	Upper Bound
21	+	21	-	-53.36538*	1.98044	.000	-59.7074	-47.0233
		1	+	31.49038*	1.98044	.000	25.1483	37.8324
		1	-	18.87019*	1.98044	.000	12.5281	25.2123
21	-	21	+	53.36538*	1.98044	.000	47.0233	59.7074
		1	+	84.85577*	1.98044	.000	78.5137	91.1978
		1	-	72.23558*	1.98044	.000	65.8935	78.5776
1	+	21	+	-31.49038*	1.98044	.000	-37.8324	-25.1483
		21	-	-84.85577*	1.98044	.000	-91.1978	-78.5137
		1	-	-12.62019*	1.98044	.001	-18.9623	-6.2781
1	-	21	+	-18.87019*	1.98044	.000	-25.2123	-12.5281
		21	-	-72.23558*	1.98044	.000	-78.5776	-65.8935
		1	+	12.62019*	1.98044	.001	6.2781	18.9623

Multiple Comparisons

PGC1a_lucif
Tukey HSD

(I) BHD		(J) BHD		Mean Difference (I-J)	Std. Error	Sig.	95% Confidence Interval	
0_2 (%)	BHD	O_2(%)	BHD				Lower Bound	Upper Bound
21	+	21	-	-53.36538*	1.98044	.000	-59.7074	-47.0233
		1	+	31.49038*	1.98044	.000	25.1483	37.8324
		1	-	18.87019*	1.98044	.000	12.5281	25.2123
21	-	21	+	53.36538*	1.98044	.000	47.0233	59.7074
		1	+	84.85577*	1.98044	.000	78.5137	91.1978
		1	-	72.23558*	1.98044	.000	65.8935	78.5776
1	+	21	+	-31.49038*	1.98044	.000	-37.8324	-25.1483
		21	-	-84.85577*	1.98044	.000	-91.1978	-78.5137
		1	-	-12.62019*	1.98044	.001	-18.9623	-6.2781
1	-	21	+	-18.87019*	1.98044	.000	-25.2123	-12.5281
		21	-	-72.23558*	1.98044	.000	-78.5776	-65.8935
		1	+	12.62019*	1.98044	.001	6.2781	18.9623

*. The mean difference is significant at the 0.05 level.

Table 29. ANOVA analysis of PGC1a Luciferase assay in BHD MEF cells

Multiple Comparisons

PGC1a_lucif

Tukey HSD

(I) BHD		(J) BHD		Mean Difference (I-J)	Std. Error	Sig.	95% Confidence Interval	
BHD	Rapamycin	BHD	Rapamycin				Lower Bound	Upper Bound
+	-	21	-	2.14856	6.79974	.988	-19.6266	23.9237
		1	+	-45.31694*	6.79974	.001	-67.0921	-23.5418
		1	-	-21.57602	6.79974	.052	-43.3512	.1991
+	+	21	+	-2.14856	6.79974	.988	-23.9237	19.6266
		1	+	-47.46551*	6.79974	.001	-69.2407	-25.6903
		1	-	-23.72458*	6.79974	.033	-45.4997	-1.9494
	+	21	+	45.31694*	6.79974	.001	23.5418	67.0921
		21	-	47.46551*	6.79974	.001	25.6903	69.2407
		1	-	23.74093*	6.79974	.033	1.9658	45.5161
1	-	21	+	21.57602	6.79974	.052	-.1991	43.3512
		21	-	23.72458*	6.79974	.033	1.9494	45.4997
		1	+	-23.74093*	6.79974	.033	-45.5161	-1.9658

*. The mean difference is significant at the 0.05 level.

Table 30. T-test analysis of H_2O_2 assay in UOK257 cells

T-Test

Independent Samples Test

		Levene's Test for Equality of Variances		t-test for Equality of Means						
									95% Confidence Interval of the Difference	
		F	Sig.	t	df	Sig. (2-tailed)	Mean Difference	Std. Error Difference	Lower	Upper
H2O2	Equal variances assumed	2.074	.245	-8.556	3	.003	-2.82819	.33053	-3.88010	-1.77629
	Equal variances not assumed			-10.879	2.184	.006	-2.82819	.25997	-3.86122	-1.79517

If the resulting p-value of a Levene's test is less than typically 0.05 there is a difference between the variances in the groups tested.

Equal variances assumed (Sig=0.245 therefore > 0.05 for Levene's test) therefore P=0.006

Table 31. T-test analysis of PGC1α mRNA levels in HK2 cells

Independent Samples Test

		Levene's Test for Equality of Variances		t-test for Equality of Means						
									95% Confidence Interval of the Difference	
		F	Sig.	t	df	Sig. (2-tailed)	Mean Difference	Std. Error Difference	Lower	Upper
PGC1a	Equal variances assumed	5.213E16	.000	-17.976	2	.003	-1.11092	.06180	-1.37683	-.84500
	Equal variances not assumed			-17.976	1.000	.035	-1.11092	.06180	-1.89618	-.32565

Table 32. T-test analysis of PGC1β mRNA levels in HK2 cells

Independent Samples Test

		Levene's Test for Equality of Variances		t-test for Equality of Means						
									95% Confidence Interval of the Difference	
		F	Sig.	t	df	Sig. (2-tailed)	Mean Difference	Std. Error Difference	Lower	Upper
Pgc1b	Equal variances assumed	.	.	-17.418	2	.003	-20.20249	1.15986	-25.19297	-15.21202
	Equal variances not assumed			-17.418	1.000	.037	-20.20249	1.15986	-34.93991	-5.46507

Table 33. T-test analysis of the surface area of cristae to total area of mitochondria ratio in BHD MEF cells.

Independent Samples Test

		Levene's Test for Equality of Variances		t-test for Equality of Means						
									95% Confidence Interval of the Difference	
		F	Sig.	t	df	Sig. (2-tailed)	Mean Difference	Std. Error Difference	Lower	Upper
surfacearea	Equal variances assumed	.261	.612	-8.784	39	.000	-2.11876	.24122	-2.60667	-1.63085
	Equal variances not assumed			-8.749	37.462	.000	-2.11876	.24217	-2.60924	-1.62828

If the resulting p-value of a Levene's test is less than typically 0.05 there is a difference between the variances in the groups tested.

Equal variances assumed (Sig=0.612 therefore > 0.05 for Levene's test) therefore P=0.000

Table 34. T-test analysis of ULK1 mRNA data for UOK257 cell line

Independent Samples Test

		Levene's Test for Equality of Variances		t-test for Equality of Means						
									95% Confidence Interval of the Difference	
		F	Sig.	t	df	Sig. (2-tailed)	Mean Difference	Std. Error Difference	Lower	Upper
ULK1	Equal variances assumed	4.454	.102	-5.314	4	.006	-149.68090	28.16688	-227.88470	-71.47709
	Equal variances not assumed			-5.314	2.000	.034	-149.68090	28.16688	-270.87322	-28.48857

If the resulting p-value of a Levene's test is less than typically 0.05 there is a difference between the variances in the groups tested.

Equal variances not assumed (Sig=0.102 therefore >0.05 for Levene's test) therefore P=0.006

Table 35. T-test analysis of ULK2 mRNA data for UOK257 cell line

Independent Samples Test

		Levene's Test for Equality of Variances		t-test for Equality of Means						
									95% Confidence Interval of the Difference	
		F	Sig.	t	df	Sig. (2-tailed)	Mean Difference	Std. Error Difference	Lower	Upper
ULK2	Equal variances assumed	4.512	.101	-3.308	4	.030	-10.19764	3.08298	-18.75737	-1.63792
	Equal variances not assumed			-3.308	2.000	.081	-10.19764	3.08298	-23.46264	3.06735

If the resulting p-value of a Levene's test is less than typically 0.05 there is a difference between the variances in the groups tested.

Equal variances assumed (Sig=0.101 therefore > 0.05 for Levene's test) therefore P=0.030

Table 36. T-test analysis of ULK1 mRNA data for BHD MEF cells

Independent Samples Test

		Levene's Test for Equality of Variances		t-test for Equality of Means						
									95% Confidence Interval of the Difference	
		F	Sig.	t	df	Sig. (2-tailed)	Mean Difference	Std. Error Difference	Lower	Upper
ULK1	Equal variances assumed	5.784	.074	-8.406	4	.001	-1.50744	.17934	-2.00537	-1.00951
	Equal variances not assumed			-8.406	2.000	.014	-1.50744	.17934	-2.27908	-.73580

If the resulting p-value of a Levene's test is less than typically 0.05 there is a difference between the variances in the groups tested.

Equal variances assumed (Sig=0.074 therefore > 0.05 for Levene's test) therefore P=0.001

Table 37. ANOVA analysis of CyQUANT (R) Cell Proliferation assay in BHD MEF cells (3MA (5nM) and Nelfinavir (50μM))

Multiple Comparisons

Dependent Variable:Proliferation

Tukey HSD Post-Hoc Test

(I) BHD			(J) BHD			Mean Difference (I-J)	Std. Error	Sig.	95% Confidence Interval	
BHD	3MA (nM)	Nelfinavir (μM)	BHD	3MA (nM)	Nelfinavir (μM)				Lower Bound	Upper Bound
+	0	0	-	0	0	.00000	2.43300	1.000	-9.6314	9.6314
			+	5	0	6.79184	2.43300	.255	-2.8396	16.4233
			-	5	0	-.02325	2.43300	1.000	-9.6547	9.6082
			+	5	20	36.30740*	2.43300	.000	26.6760	45.9388
			-	5	20	25.54937*	2.43300	.000	15.9179	35.1808
			+	5	30	23.44575*	2.43300	.000	13.8143	33.0772
			-	5	30	36.90504*	2.43300	.000	27.2736	46.5365
			+	5	40	46.26332*	2.43300	.000	36.6319	55.8947
			-	5	40	46.76552*	2.43300	.000	37.1341	56.3969
-	0	0	+	0	0	.00000	2.43300	1.000	-9.6314	9.6314

			+	5	0	6.79184	2.43300	.255	-2.8396	16.4233
			-	5	0	-.02325	2.43300	1.000	-9.6547	9.6082
			+	5	20	36.30740*	2.43300	.000	26.6760	45.9388
			-	5	20	25.54937*	2.43300	.000	15.9179	35.1808
			+	5	30	23.44575*	2.43300	.000	13.8143	33.0772
			-	5	30	36.90504*	2.43300	.000	27.2736	46.5365
			+	5	40	46.26332*	2.43300	.000	36.6319	55.8947
			-	5	40	46.76552*	2.43300	.000	37.1341	56.3969
+	5	0	+	0	0	-6.79184	2.43300	.255	-16.4233	2.8396
			-	0	0	-6.79184	2.43300	.255	-16.4233	2.8396
			-	5	0	-6.81509	2.43300	.251	-16.4465	2.8163
			+	5	20	29.51557*	2.43300	.000	19.8841	39.1470
			-	5	20	18.75753*	2.43300	.000	9.1261	28.3890
			+	5	30	16.65391*	2.43300	.001	7.0225	26.2853
			-	5	30	30.11320*	2.43300	.000	20.4818	39.7446
			+	5	40	39.47148*	2.43300	.000	29.8401	49.1029
			-	5	40	39.97369*	2.43300	.000	30.3423	49.6051
-	5	0	+	0	0	.02325	2.43300	1.000	-9.6082	9.6547
			-	0	0	.02325	2.43300	1.000	-9.6082	9.6547
			+	5	0	6.81509	2.43300	.251	-2.8163	16.4465

			+	5	20	36.33066*	2.43300	.000	26.6992	45.9621
			-	5	20	25.57262*	2.43300	.000	15.9412	35.2040
			+	5	30	23.46900*	2.43300	.000	13.8376	33.1004
			-	5	30	36.92829*	2.43300	.000	27.2969	46.5597
			+	5	40	46.28657*	2.43300	.000	36.6551	55.9180
			-	5	40	46.78878*	2.43300	.000	37.1574	56.4202
+	5	20	+	0	0	-36.30740*	2.43300	.000	-45.9388	-26.6760
			-	0	0	-36.30740*	2.43300	.000	-45.9388	-26.6760
			+	5	0	-29.51557*	2.43300	.000	-39.1470	-19.8841
			-	5	0	-36.33066*	2.43300	.000	-45.9621	-26.6992
			-	5	20	-10.75803*	2.43300	.026	-20.3895	-1.1266
			+	5	30	-12.86166*	2.43300	.008	-22.4931	-3.2302
			-	5	30	.59763	2.43300	1.000	-9.0338	10.2291
			+	5	40	9.95591*	2.43300	.041	.3245	19.5873
			-	5	40	10.45812*	2.43300	.031	.8267	20.0895
-	5	20	+	0	0	-25.54937*	2.43300	.000	-35.1808	-15.9179

			-	0	0	-25.54937*	2.43300	.000	-35.1808	-15.9179
			+	5	0	-18.75753*	2.43300	.000	-28.3890	-9.1261
			-	5	0	-25.57262*	2.43300	.000	-35.2040	-15.9412
			+	5	20	10.75803*	2.43300	.026	1.1266	20.3895
			+	5	30	-2.10362	2.43300	.994	-11.7350	7.5278
			-	5	30	11.35566*	2.43300	.018	1.7242	20.9871
			+	5	40	20.71395*	2.43300	.000	11.0825	30.3454
			-	5	40	21.21615*	2.43300	.000	11.5847	30.8476
+	5	30	+	0	0	-23.44575*	2.43300	.000	-33.0772	-13.8143
			-	0	0	-23.44575*	2.43300	.000	-33.0772	-13.8143
			+	5	0	-16.65391*	2.43300	.001	-26.2853	-7.0225
			-	5	0	-23.46900*	2.43300	.000	-33.1004	-13.8376
			+	5	20	12.86166*	2.43300	.008	3.2302	22.4931
			-	5	20	2.10362	2.43300	.994	-7.5278	11.7350
			-	5	30	13.45929*	2.43300	.006	3.8279	23.0907
			+	5	40	22.81757*	2.43300	.000	13.1861	32.4490

			-	5	40	23.31977*	2.43300	.000	13.6883	32.9512
-	5	30	+	0	0	-36.90504*	2.43300	.000	-46.5365	-27.2736
			-	0	0	-36.90504*	2.43300	.000	-46.5365	-27.2736
			+	5	0	-30.11320*	2.43300	.000	-39.7446	-20.4818
			-	5	0	-36.92829*	2.43300	.000	-46.5597	-27.2969
			+	5	20	-.59763	2.43300	1.000	-10.2291	9.0338
			-	5	20	-11.35566*	2.43300	.018	-20.9871	-1.7242
			+	5	30	-13.45929*	2.43300	.006	-23.0907	-3.8279
			+	5	40	9.35828	2.43300	.059	-.2731	18.9897
			-	5	40	9.86049*	2.43300	.044	.2291	19.4919
+	5	40	+	0	0	-46.26332*	2.43300	.000	-55.8947	-36.6319
			-	0	0	-46.26332*	2.43300	.000	-55.8947	-36.6319
			+	5	0	-39.47148*	2.43300	.000	-49.1029	-29.8401
			-	5	0	-46.28657*	2.43300	.000	-55.9180	-36.6551
			+	5	20	-9.95591*	2.43300	.041	-19.5873	-.3245

			-	5	20	-20.71395*	2.43300	.000	-30.3454	-11.0825
			+	5	30	-22.81757*	2.43300	.000	-32.4490	-13.1861
			-	5	30	-9.35828	2.43300	.059	-18.9897	.2731
			-	5	40	.50220	2.43300	1.000	-9.1292	10.1336
-	5	40	+	0	0	-46.76552*	2.43300	.000	-56.3969	-37.1341
			-	0	0	-46.76552*	2.43300	.000	-56.3969	-37.1341
			+	5	0	-39.97369*	2.43300	.000	-49.6051	-30.3423
			-	5	0	-46.78878*	2.43300	.000	-56.4202	-37.1574
			+	5	20	-10.45812*	2.43300	.031	-20.0895	-.8267
			-	5	20	-21.21615*	2.43300	.000	-30.8476	-11.5847
			+	5	30	-23.31977*	2.43300	.000	-32.9512	-13.6883
			-	5	30	-9.86049*	2.43300	.044	-19.4919	-.2291
			+	5	40	-.50220	2.43300	1.000	-10.1336	9.1292

*. The mean difference is significant at the 0.05 level.

Table 38. ANOVA analysis of CyQUANT (R) Cell Proliferation assay in BHD MEF cells (Chloroquine (100µM) and Nelfinavir (50µM))

One-Way ANOVA with Tukey Post-Hoc Test

Multiple Comparisons

Dependent Variable:Proliferation

Tukey HSD Post-Hoc Test

(I) BHD			(J) BHD			Mean Difference (I-J)	Std. Error	Sig.	95% Confidence Interval	
BHD	Chloroquine (µM)	Nelfinavir (µM)	BHD	Chloroquine (µM)	Nelfinavir (µM)				Lower Bound	Upper Bound
+	0	0	-	0	0	.00000	8.06980	1.000	-29.9235	29.9235
			+	0	10	.91972	8.06980	1.000	-29.0038	30.8432
			-	0	10	-8.15727	8.06980	1.000	-38.0808	21.7663
			+	0	20	3.79277	8.06980	1.000	-26.1308	33.7163
			-	0	20	24.14979	8.06980	.227	-5.7737	54.0733
			+	0	30	4.64539	8.06980	1.000	-25.2781	34.5689
			-	0	30	47.51020*	8.06980	.000	17.5867	77.4337
			+	100	0	8.13381	8.06980	1.000	-21.7897	38.0573
			-	100	0	42.68454*	8.06980	.001	12.7610	72.6081
			+	100	10	23.21007	8.06980	.280	-6.7134	53.1336
			-	100	10	70.29501*	8.06980	.000	40.3715	100.2185
			+	100	20	27.38033	8.06980	.102	-2.5432	57.3038
			-	100	20	83.58616*	8.06980	.000	53.6626	113.5097
			+	100	30	45.87329*	8.06980	.000	15.9498	75.7968
			-	100	30	90.01174*	8.06980	.000	60.0882	119.9353

-	0	0	+	0	0	.00000	8.06980	1.000	-29.9235	29.9235
			+	0	10	.91973	8.06980	1.000	-29.0038	30.8432
			-	0	10	-8.15727	8.06980	1.000	-38.0808	21.7663
			+	0	20	3.79277	8.06980	1.000	-26.1308	33.7163
			-	0	20	24.14979	8.06980	.227	-5.7737	54.0733
			+	0	30	4.64539	8.06980	1.000	-25.2781	34.5689
			-	0	30	47.51021*	8.06980	.000	17.5867	77.4337
			+	100	0	8.13381	8.06980	1.000	-21.7897	38.0573
			-	100	0	42.68454*	8.06980	.001	12.7610	72.6081
			+	100	10	23.21008	8.06980	.280	-6.7134	53.1336
			-	100	10	70.29501*	8.06980	.000	40.3715	100.2185
			+	100	20	27.38033	8.06980	.102	-2.5432	57.3039
			-	100	20	83.58616*	8.06980	.000	53.6626	113.5097
			+	100	30	45.87329*	8.06980	.000	15.9498	75.7968
			-	100	30	90.01175*	8.06980	.000	60.0882	119.9353
+	0	10	+	0	0	-.91972	8.06980	1.000	-30.8432	29.0038
			-	0	0	-.91973	8.06980	1.000	-30.8432	29.0038
			-	0	10	-9.07699	8.06980	.998	-39.0005	20.8465
			+	0	20	2.87304	8.06980	1.000	-27.0505	32.7966
			-	0	20	23.23007	8.06980	.279	-6.6935	53.1536
			+	0	30	3.72566	8.06980	1.000	-26.1979	33.6492
			-	0	30	46.59048*	8.06980	.000	16.6670	76.5140
			+	100	0	7.21408	8.06980	1.000	-22.7094	37.1376

			-	100	0	41.76481*	8.06980	.001	11.8413	71.6883
			+	100	10	22.29035	8.06980	.338	-7.6332	52.2139
			-	100	10	69.37529*	8.06980	.000	39.4518	99.2988
			+	100	20	26.46060	8.06980	.130	-3.4629	56.3841
			-	100	20	82.66643*	8.06980	.000	52.7429	112.5900
			+	100	30	44.95356*	8.06980	.000	15.0300	74.8771
			-	100	30	89.09202*	8.06980	.000	59.1685	119.0155
-	0	10	+	0	0	8.15727	8.06980	1.000	-21.7663	38.0808
			-	0	0	8.15727	8.06980	1.000	-21.7663	38.0808
			+	0	10	9.07699	8.06980	.998	-20.8465	39.0005
			+	0	20	11.95003	8.06980	.977	-17.9735	41.8736
			-	0	20	32.30706*	8.06980	.024	2.3835	62.2306
			+	0	30	12.80265	8.06980	.960	-17.1209	42.7262
			-	0	30	55.66747*	8.06980	.000	25.7439	85.5910
			+	100	0	16.29107	8.06980	.798	-13.6324	46.2146
			-	100	0	50.84180*	8.06980	.000	20.9183	80.7653
			+	100	10	31.36734*	8.06980	.033	1.4438	61.2909
			-	100	10	78.45228*	8.06980	.000	48.5288	108.3758
			+	100	20	35.53759*	8.06980	.009	5.6141	65.4611

			-	100	20	91.74342*	8.06980	.000	61.8199	121.6669
			+	100	30	54.03055*	8.06980	.000	24.1070	83.9541
			-	100	30	98.16901*	8.06980	.000	68.2455	128.0925
+	0	20	+	0	0	-3.79277	8.06980	1.000	-33.7163	26.1308
			-	0	0	-3.79277	8.06980	1.000	-33.7163	26.1308
			+	0	10	-2.87304	8.06980	1.000	-32.7966	27.0505
			-	0	10	-11.95003	8.06980	.977	-41.8736	17.9735
			-	0	20	20.35703	8.06980	.481	-9.5665	50.2805
			+	0	30	.85262	8.06980	1.000	-29.0709	30.7761
			-	0	30	43.71744*	8.06980	.001	13.7939	73.6410
			+	100	0	4.34104	8.06980	1.000	-25.5825	34.2646
			-	100	0	38.89177*	8.06980	.003	8.9682	68.8153
			+	100	10	19.41731	8.06980	.556	-10.5062	49.3408
			-	100	10	66.50225*	8.06980	.000	36.5787	96.4258
			+	100	20	23.58756	8.06980	.258	-6.3360	53.5111
			-	100	20	79.79339*	8.06980	.000	49.8699	109.7169
			+	100	30	42.08052*	8.06980	.001	12.1570	72.0040
			-	100	30	86.21898*	8.06980	.000	56.2955	116.1425
-	0	20	+	0	0	-24.14979	8.06980	.227	-54.0733	5.7737

			-	0	0	-24.14979	8.06980	.227	-54.0733	5.7737
			+	0	10	-23.23007	8.06980	.279	-53.1536	6.6935
			-	0	10	-32.30706*	8.06980	.024	-62.2306	-2.3835
			+	0	20	-20.35703	8.06980	.481	-50.2805	9.5665
			+	0	30	-19.50441	8.06980	.549	-49.4279	10.4191
			-	0	30	23.36041	8.06980	.271	-6.5631	53.2839
			+	100	0	-16.01598	8.06980	.816	-45.9395	13.9075
			-	100	0	18.53474	8.06980	.628	-11.3888	48.4583
			+	100	10	-.93972	8.06980	1.000	-30.8632	28.9838
			-	100	10	46.14522*	8.06980	.000	16.2217	76.0687
			+	100	20	3.23054	8.06980	1.000	-26.6930	33.1541
			-	100	20	59.43636*	8.06980	.000	29.5128	89.3599
			+	100	30	21.72349	8.06980	.377	-8.2000	51.6470
			-	100	30	65.86195*	8.06980	.000	35.9384	95.7855
+	0	30	+	0	0	-4.64539	8.06980	1.000	-34.5689	25.2781
			-	0	0	-4.64539	8.06980	1.000	-34.5689	25.2781
			+	0	10	-3.72566	8.06980	1.000	-33.6492	26.1979

			-	0	10	-12.80265	8.06980	.960	-42.7262	17.1209
			+	0	20	-.85262	8.06980	1.000	-30.7761	29.0709
			-	0	20	19.50441	8.06980	.549	-10.4191	49.4279
			-	0	30	42.86482*	8.06980	.001	12.9413	72.7883
			+	100	0	3.48842	8.06980	1.000	-26.4351	33.4119
			-	100	0	38.03915*	8.06980	.004	8.1156	67.9627
			+	100	10	18.56469	8.06980	.626	-11.3588	48.4882
			-	100	10	65.64963*	8.06980	.000	35.7261	95.5731
			+	100	20	22.73494	8.06980	.309	-7.1886	52.6585
			-	100	20	78.94077*	8.06980	.000	49.0172	108.8643
			+	100	30	41.22790*	8.06980	.001	11.3044	71.1514
			-	100	30	85.36636*	8.06980	.000	55.4428	115.2899
-	0	30	+	0	0	-47.51020*	8.06980	.000	-77.4337	-17.5867
			-	0	0	-47.51021*	8.06980	.000	-77.4337	-17.5867
			+	0	10	-46.59048*	8.06980	.000	-76.5140	-16.6670
			-	0	10	-55.66747*	8.06980	.000	-85.5910	-25.7439

			+	0	20	-43.71744*	8.06980	.001	-73.6410	-13.7939
			-	0	20	-23.36041	8.06980	.271	-53.2839	6.5631
			+	0	30	-42.86482*	8.06980	.001	-72.7883	-12.9413
			+	100	0	-39.37640*	8.06980	.002	-69.2999	-9.4529
			-	100	0	-4.82567	8.06980	1.000	-34.7492	25.0979
			+	100	10	-24.30013	8.06980	.220	-54.2237	5.6234
			-	100	10	22.78481	8.06980	.306	-7.1387	52.7083
			+	100	20	-20.12988	8.06980	.499	-50.0534	9.7936
			-	100	20	36.07595*	8.06980	.007	6.1524	65.9995
			+	100	30	-1.63692	8.06980	1.000	-31.5604	28.2866
			-	100	30	42.50154*	8.06980	.001	12.5780	72.4251
+	100	0	+	0	0	-8.13381	8.06980	1.000	-38.0573	21.7897
			-	0	0	-8.13381	8.06980	1.000	-38.0573	21.7897
			+	0	10	-7.21408	8.06980	1.000	-37.1376	22.7094
			-	0	10	-16.29107	8.06980	.798	-46.2146	13.6324
			+	0	20	-4.34104	8.06980	1.000	-34.2646	25.5825
			-	0	20	16.01598	8.06980	.816	-13.9075	45.9395
			+	0	30	-3.48842	8.06980	1.000	-33.4119	26.4351

			-	0	30	39.37640*	8.06980	.002	9.4529	69.2999
			-	100	0	34.55073*	8.06980	.012	4.6272	64.4743
			+	100	10	15.07627	8.06980	.871	-14.8473	44.9998
			-	100	10	62.16121*	8.06980	.000	32.2377	92.0847
			+	100	20	19.24652	8.06980	.570	-10.6770	49.1700
			-	100	20	75.45235*	8.06980	.000	45.5288	105.3759
			+	100	30	37.73948*	8.06980	.004	7.8160	67.6630
			-	100	30	81.87794*	8.06980	.000	51.9544	111.8015
-	100	0	+	0	0	-42.68454*	8.06980	.001	-72.6081	-12.7610
			-	0	0	-42.68454*	8.06980	.001	-72.6081	-12.7610
			+	0	10	-41.76481*	8.06980	.001	-71.6883	-11.8413
			-	0	10	-50.84180*	8.06980	.000	-80.7653	-20.9183
			+	0	20	-38.89177*	8.06980	.003	-68.8153	-8.9682
			-	0	20	-18.53474	8.06980	.628	-48.4583	11.3888
			+	0	30	-38.03915*	8.06980	.004	-67.9627	-8.1156
			-	0	30	4.82567	8.06980	1.000	-25.0979	34.7492

			+	100	0	-34.55073*	8.06980	.012	-64.4743	-4.6272
			+	100	10	-19.47446	8.06980	.552	-49.3980	10.4491
			-	100	10	27.61048	8.06980	.096	-2.3130	57.5340
			+	100	20	-15.30421	8.06980	.859	-45.2277	14.6193
			-	100	20	40.90162*	8.06980	.001	10.9781	70.8251
			+	100	30	3.18875	8.06980	1.000	-26.7348	33.1123
			-	100	30	47.32721*	8.06980	.000	17.4037	77.2507
+	100	10	+	0	0	-23.21007	8.06980	.280	-53.1336	6.7134
			-	0	0	-23.21008	8.06980	.280	-53.1336	6.7134
			+	0	10	-22.29035	8.06980	.338	-52.2139	7.6332
			-	0	10	-31.36734*	8.06980	.033	-61.2909	-1.4438
			+	0	20	-19.41731	8.06980	.556	-49.3408	10.5062
			-	0	20	.93972	8.06980	1.000	-28.9838	30.8632
			+	0	30	-18.56469	8.06980	.626	-48.4882	11.3588
			-	0	30	24.30013	8.06980	.220	-5.6234	54.2237

			+	100	0	-15.07627	8.06980	.871	-44.9998	14.8473
			-	100	0	19.47446	8.06980	.552	-10.4491	49.3980
			-	100	10	47.08494*	8.06980	.000	17.1614	77.0085
			+	100	20	4.17025	8.06980	1.000	-25.7533	34.0938
			-	100	20	60.37608*	8.06980	.000	30.4526	90.2996
			+	100	30	22.66321	8.06980	.314	-7.2603	52.5867
			-	100	30	66.80167*	8.06980	.000	36.8781	96.7252
-	100	10	+	0	0	-70.29501*	8.06980	.000	-100.2185	-40.3715
			-	0	0	-70.29501*	8.06980	.000	-100.2185	-40.3715
			+	0	10	-69.37529*	8.06980	.000	-99.2988	-39.4518
			-	0	10	-78.45228*	8.06980	.000	-108.3758	-48.5288
			+	0	20	-66.50225*	8.06980	.000	-96.4258	-36.5787
			-	0	20	-46.14522*	8.06980	.000	-76.0687	-16.2217
			+	0	30	-65.64963*	8.06980	.000	-95.5731	-35.7261
			-	0	30	-22.78481	8.06980	.306	-52.7083	7.1387

			+	100	0	-62.16121*	8.06980	.000	-92.0847	-32.2377
			-	100	0	-27.61048	8.06980	.096	-57.5340	2.3130
			+	100	10	-47.08494*	8.06980	.000	-77.0085	-17.1614
			+	100	20	-42.91469*	8.06980	.001	-72.8382	-12.9912
			-	100	20	13.29114	8.06980	.946	-16.6324	43.2147
			+	100	30	-24.42173	8.06980	.214	-54.3452	5.5018
			-	100	30	19.71673	8.06980	.532	-10.2068	49.6403
+	100	20	+	0	0	-27.38033	8.06980	.102	-57.3038	2.5432
			-	0	0	-27.38033	8.06980	.102	-57.3039	2.5432
			+	0	10	-26.46060	8.06980	.130	-56.3841	3.4629
			-	0	10	-35.53759*	8.06980	.009	-65.4611	-5.6141
			+	0	20	-23.58756	8.06980	.258	-53.5111	6.3360
			-	0	20	-3.23054	8.06980	1.000	-33.1541	26.6930
			+	0	30	-22.73494	8.06980	.309	-52.6585	7.1886

			-	0	30	20.12988	8.06980	.499	-9.7936	50.0534
			+	100	0	-19.24652	8.06980	.570	-49.1700	10.6770
			-	100	0	15.30421	8.06980	.859	-14.6193	45.2277
			+	100	10	-4.17025	8.06980	1.000	-34.0938	25.7533
			-	100	10	42.91469*	8.06980	.001	12.9912	72.8382
			-	100	20	56.20583*	8.06980	.000	26.2823	86.1294
			+	100	30	18.49296	8.06980	.632	-11.4306	48.4165
			-	100	30	62.63142*	8.06980	.000	32.7079	92.5549
-	100	20	+	0	0	-83.58616*	8.06980	.000	-113.5097	-53.6626
			-	0	0	-83.58616*	8.06980	.000	-113.5097	-53.6626
			+	0	10	-82.66643*	8.06980	.000	-112.5900	-52.7429
			-	0	10	-91.74342*	8.06980	.000	-121.6669	-61.8199
			+	0	20	-79.79339*	8.06980	.000	-109.7169	-49.8699
			-	0	20	-59.43636*	8.06980	.000	-89.3599	-29.5128
			+	0	30	-78.94077*	8.06980	.000	-108.8643	-49.0172

			-	0	30	-36.07595*	8.06980	.007	-65.9995	-6.1524
			+	100	0	-75.45235*	8.06980	.000	-105.3759	-45.5288
			-	100	0	-40.90162*	8.06980	.001	-70.8251	-10.9781
			+	100	10	-60.37608*	8.06980	.000	-90.2996	-30.4526
			-	100	10	-13.29114	8.06980	.946	-43.2147	16.6324
			+	100	20	-56.20583*	8.06980	.000	-86.1294	-26.2823
			+	100	30	-37.71287*	8.06980	.004	-67.6364	-7.7893
			-	100	30	6.42559	8.06980	1.000	-23.4979	36.3491
+	100	30	+	0	0	-45.87329*	8.06980	.000	-75.7968	-15.9498
			-	0	0	-45.87329*	8.06980	.000	-75.7968	-15.9498
			+	0	10	-44.95356*	8.06980	.000	-74.8771	-15.0300
			-	0	10	-54.03055*	8.06980	.000	-83.9541	-24.1070
			+	0	20	-42.08052*	8.06980	.001	-72.0040	-12.1570

			-	0	20	-21.72349	8.06980	.377	-51.6470	8.2000
			+	0	30	-41.22790*	8.06980	.001	-71.1514	-11.3044
			-	0	30	1.63692	8.06980	1.000	-28.2866	31.5604
			+	100	0	-37.73948*	8.06980	.004	-67.6630	-7.8160
			-	100	0	-3.18875	8.06980	1.000	-33.1123	26.7348
			+	100	10	-22.66321	8.06980	.314	-52.5867	7.2603
			-	100	10	24.42173	8.06980	.214	-5.5018	54.3452
			+	100	20	-18.49296	8.06980	.632	-48.4165	11.4306
			-	100	20	37.71287*	8.06980	.004	7.7893	67.6364
			-	100	30	44.13846*	8.06980	.000	14.2149	74.0620
-	100	30	+	0	0	-90.011744*	8.06980	.000	-119.9353	-60.0882
			-	0	0	-90.011755*	8.06980	.000	-119.9353	-60.0882
			+	0	10	-89.09202*	8.06980	.000	-119.0155	-59.1685
			-	0	10	-98.16901*	8.06980	.000	-128.0925	-68.2455
			+	0	20	-86.21898*	8.06980	.000	-116.1425	-56.2955

			-	0	20	-65.86195*	8.06980	.000	-95.7855	-35.9384
			+	0	30	-85.36636*	8.06980	.000	-115.2899	-55.4428
			-	0	30	-42.50154*	8.06980	.001	-72.4251	-12.5780
			+	100	0	-81.87794*	8.06980	.000	-111.8015	-51.9544
			-	100	0	-47.32721*	8.06980	.000	-77.2507	-17.4037
			+	100	10	-66.80167*	8.06980	.000	-96.7252	-36.8781
			-	100	10	-19.71673	8.06980	.532	-49.6403	10.2068
			+	100	20	-62.63142*	8.06980	.000	-92.5549	-32.7079
			-	100	20	-6.42559	8.06980	1.000	-36.3491	23.4979
			+	100	30	-44.13846*	8.06980	.000	-74.0620	-14.2149

*. The mean difference is significant at the 0.05 level.

Table 39. ANOVA analysis of Cell death Elisa assay on BHD MEF cells (Nelfinavir 30µM, Chloroquine 100µM)

One-Way ANOVA with Tukey Post-Hoc Test

Multiple Comparisons

Dependent Variable:Proliferation

Tukey HSD Post-Hoc Test

(I) BHD			(J) BHD			Mean Difference (I-J)	Std. Error	Sig.	95% Confidence Interval	
BHD	Chloroquine (µM)	Nelfinavir (µM)	BHD	Chloroquine (µM)	Nelfinavir (µM)				Lower Bound	Upper Bound
+	0	0	-	0	0	.00000	.49343	1.000	-1.7083	1.7083
			+	0	30	.01815	.49343	1.000	-1.6902	1.7265
			-	0	30	-3.57810*	.49343	.000	-5.2864	-1.8698
			+	100	0	.00330	.49343	1.000	-1.7050	1.7116
			-	100	0	-2.52613*	.49343	.002	-4.2345	-.8178
			+	100	30	-.13303	.49343	1.000	-1.8414	1.5753
			-	100	30	-2.64121*	.49343	.001	-4.3495	-.9329
-	0	0	+	0	0	.00000	.49343	1.000	-1.7083	1.7083
			+	0	30	.01815	.49343	1.000	-1.6902	1.7265
			-	0	30	-3.57810*	.49343	.000	-5.2864	-1.8698
			+	100	0	.00330	.49343	1.000	-1.7050	1.7116
			-	100	0	-2.52613*	.49343	.002	-4.2345	-.8178
			+	100	30	-.13303	.49343	1.000	-1.8414	1.5753
			-	100	30	-2.64121*	.49343	.001	-4.3495	-.9329
+	0	30	+	0	0	-.01815	.49343	1.000	-1.7265	1.6902
			-	0	0	-.01815	.49343	1.000	-1.7265	1.6902

			-	0	30	-3.59625*	.49343	.000	-5.3046	-1.8879
			+	100	0	-.01486	.49343	1.000	-1.7232	1.6935
			-	100	0	-2.54428*	.49343	.002	-4.2526	-.8360
			+	100	30	-.15119	.49343	1.000	-1.8595	1.5571
			-	100	30	-2.65936*	.49343	.001	-4.3677	-.9510
-	0	30	+	0	0	3.57810*	.49343	.000	1.8698	5.2864
			-	0	0	3.57810*	.49343	.000	1.8698	5.2864
			+	0	30	3.59625*	.49343	.000	1.8879	5.3046
			+	100	0	3.58139*	.49343	.000	1.8731	5.2897
			-	100	0	1.05197	.49343	.436	-.6564	2.7603
			+	100	30	3.44506*	.49343	.000	1.7367	5.1534
			-	100	30	.93689	.49343	.570	-.7714	2.6452
+	100	0	+	0	0	-.00330	.49343	1.000	-1.7116	1.7050
			-	0	0	-.00330	.49343	1.000	-1.7116	1.7050
			+	0	30	.01486	.49343	1.000	-1.6935	1.7232
			-	0	30	-3.58139*	.49343	.000	-5.2897	-1.8731
			-	100	0	-2.52943*	.49343	.002	-4.2378	-.8211
			+	100	30	-.13633	.49343	1.000	-1.8447	1.5720

			-	100	30	-2.64451*	.49343	.001	-4.3528	-.9362
-	100	0	+	0	0	2.52613*	.49343	.002	.8178	4.2345
			-	0	0	2.52613*	.49343	.002	.8178	4.2345
			+	0	30	2.54428*	.49343	.002	.8360	4.2526
			-	0	30	-1.05197	.49343	.436	-2.7603	.6564
			+	100	0	2.52943*	.49343	.002	.8211	4.2378
			+	100	30	2.39310*	.49343	.003	.6848	4.1014
			-	100	30	-.11508	.49343	1.000	-1.8234	1.5932
+	100	30	+	0	0	.13303	.49343	1.000	-1.5753	1.8414
			-	0	0	.13303	.49343	1.000	-1.5753	1.8414
			+	0	30	.15119	.49343	1.000	-1.5571	1.8595
			-	0	30	-3.44506*	.49343	.000	-5.1534	-1.7367
			+	100	0	.13633	.49343	1.000	-1.5720	1.8447
			-	100	0	-2.39310*	.49343	.003	-4.1014	-.6848
			-	100	30	-2.50818*	.49343	.002	-4.2165	-.7999
-	100	30	+	0	0	2.64121*	.49343	.001	.9329	4.3495
			-	0	0	2.64121*	.49343	.001	.9329	4.3495
			+	0	30	2.65936*	.49343	.001	.9510	4.3677
			-	0	30	-.93689	.49343	.570	-2.6452	.7714

			+	100	0	2.64451*	.49343	.001	.9362	4.3528
			-	100	0	.11508	.49343	1.000	-1.5932	1.8234
			+	100	30	2.50818*	.49343	.002	.7999	4.2165

*. The mean difference is significant at the 0.05 level.

Table 40. ANOVA analysis of Cell death Elisa assay on BHD MEF cells (Chloroquine 50µM, Nelfinavir 20µM, Rapamycin 50nm)

Multiple Comparisons

Dependent Variable:Proliferation

Tukey HSD Post-Hoc Test

(I) BHD				(J) BHD				Mean Difference (I-J)	Std. Error	Sig.	95% Confidence Interval	
BHD	Chloroquine (µM)	Nelfinavir (µM)	Rapamycin (nM)	BHD	Chloroquine (µM)	Nelfinavir (µM)	Rapamycin (nM)				Lower Bound	Upper Bound
1+	0	0	0	-	0	0	0	.00000	.46891	1.000	-1.6907	1.6907
				+	0	30	0	-.29249	.46891	1.000	-1.9832	1.3982
				-	0	30	0	-.95573	.46891	.666	-2.6465	.7350
				+	100	0	0	-.16115	.46891	1.000	-1.8519	1.5296
				-	100	0	0	-.28516	.46891	1.000	-1.9759	1.4056

				+	100	30	0	-1.86203*	.46891	.022	-3.5528	-.1713
				-	100	30	0	-3.70182*	.46891	.000	-5.3926	-2.0111
				+	0	0	50	-.02649	.46891	1.000	-1.7172	1.6642
				-	0	0	50	-.92969	.46891	.700	-2.6204	.7610
				+	100	0	50	-1.20199	.46891	.351	-2.8927	.4887
				-	100	0	50	-2.86458*	.46891	.000	-4.5553	-1.1739
2-	0	0	0	+	0	0	0	.00000	.46891	1.000	-1.6907	1.6907
				+	0	30	0	-.29249	.46891	1.000	-1.9832	1.3982
				-	0	30	0	-.95573	.46891	.666	-2.6465	.7350
				+	100	0	0	-.16115	.46891	1.000	-1.8519	1.5296
				-	100	0	0	-.28516	.46891	1.000	-1.9759	1.4056
				+	100	30	0	-1.86203*	.46891	.022	-3.5528	-.1713
				-	100	30	0	-3.70182*	.46891	.000	-5.3926	-2.0111

				+	0	0	50	-.02649	.46891	1.000	-1.7172	1.6642
				-	0	0	50	-.92969	.46891	.700	-2.6204	.7610
				+	100	0	50	-1.20199	.46891	.351	-2.8927	.4887
				-	100	0	50	-2.86458*	.46891	.000	-4.5553	-1.1739
3+	0	30	0	+	0	0	0	.29249	.46891	1.000	-1.3982	1.9832
				-	0	0	0	.29249	.46891	1.000	-1.3982	1.9832
				-	0	30	0	-.66323	.46891	.949	-2.3540	1.0275
				+	100	0	0	.13135	.46891	1.000	-1.5594	1.8221
				-	100	0	0	.00734	.46891	1.000	-1.6834	1.6981
				+	100	30	0	-1.56954	.46891	.086	-3.2603	.1212
				-	100	30	0	-3.40933*	.46891	.000	-5.1001	-1.7186
				+	0	0	50	.26600	.46891	1.000	-1.4247	1.9567
				-	0	0	50	-.63719	.46891	.961	-2.3279	1.0535

				+	100	0	50	-.90949	.46891	.725	-2.6002	.7812
				-	100	0	50	-2.57209*	.46891	.001	-4.2628	-.8814
4-	0	30	0	+	0	0	0	.95573	.46891	.666	-.7350	2.6465
				-	0	0	0	.95573	.46891	.666	-.7350	2.6465
				+	0	30	0	.66323	.46891	.949	-1.0275	2.3540
				+	100	0	0	.79458	.46891	.854	-.8962	2.4853
				-	100	0	0	.67057	.46891	.945	-1.0202	2.3613
				+	100	30	0	-.90630	.46891	.729	-2.5970	.7844
				-	100	30	0	-2.74609*	.46891	.000	-4.4368	-1.0554
				+	0	0	50	.92924	.46891	.700	-.7615	2.6200
				-	0	0	50	.02604	.46891	1.000	-1.6647	1.7168
				+	100	0	50	-.24626	.46891	1.000	-1.9370	1.4445
				-	100	0	50	-1.90885*	.46891	.018	-3.5996	-.2181
5+	100	0	0	+	0	0	0	.16115	.46891	1.000	-1.5296	1.8519

				-	0	0	0	.16115	.46891	1.000	-1.5296	1.8519
				+	0	30	0	-.13135	.46891	1.000	-1.8221	1.5594
				-	0	30	0	-.79458	.46891	.854	-2.4853	.8962
				-	100	0	0	-.12401	.46891	1.000	-1.8147	1.5667
				+	100	30	0	-1.70088*	.46891	.048	-3.3916	-.0102
				-	100	30	0	-3.54068*	.46891	.000	-5.2314	-1.8499
				+	0	0	50	.13466	.46891	1.000	-1.5561	1.8254
				-	0	0	50	-.76854	.46891	.878	-2.4593	.9222
				+	100	0	50	-1.04084	.46891	.552	-2.7316	.6499
				-	100	0	50	-2.70344*	.46891	.000	-4.3942	-1.0127
6-	100	0	0	+	0	0	0	.28516	.46891	1.000	-1.4056	1.9759
				-	0	0	0	.28516	.46891	1.000	-1.4056	1.9759
				+	0	30	0	-.00734	.46891	1.000	-1.6981	1.6834

				-	0	30	0	-.67057	.46891	.945	-2.3613	1.0202
				+	100	0	0	.12401	.46891	1.000	-1.5667	1.8147
				+	100	30	0	-1.57687	.46891	.083	-3.2676	.1139
				-	100	30	0	-3.41667*	.46891	.000	-5.1074	-1.7259
				+	0	0	50	.25867	.46891	1.000	-1.4321	1.9494
				-	0	0	50	-.64453	.46891	.958	-2.3353	1.0462
				+	100	0	50	-.91683	.46891	.716	-2.6076	.7739
				-	100	0	50	-2.57943*	.46891	.001	-4.2702	-.8887
7+	100	30	0	+	0	0	0	1.86203*	.46891	.022	.1713	3.5528
				-	0	0	0	1.86203*	.46891	.022	.1713	3.5528
				+	0	30	0	1.56954	.46891	.086	-.1212	3.2603
				-	0	30	0	.90630	.46891	.729	-.7844	2.5970
				+	100	0	0	1.70088*	.46891	.048	.0102	3.3916
				-	100	0	0	1.57687	.46891	.083	-.1139	3.2676

				-	100	30	0	-1.83979*	.46891	.025	-3.5305	-.1491
				+	0	0	50	1.83554*	.46891	.025	.1448	3.5263
				-	0	0	50	.93234	.46891	.696	-.7584	2.6231
				+	100	0	50	.66004	.46891	.951	-1.0307	2.3508
				-	100	0	50	-1.00255	.46891	.604	-2.6933	.6882
8-	100	30	0	+	0	0	0	3.70182*	.46891	.000	2.0111	5.3926
				-	0	0	0	3.70182*	.46891	.000	2.0111	5.3926
				+	0	30	0	3.40933*	.46891	.000	1.7186	5.1001
				-	0	30	0	2.74609*	.46891	.000	1.0554	4.4368
				+	100	0	0	3.54068*	.46891	.000	1.8499	5.2314
				-	100	0	0	3.41667*	.46891	.000	1.7259	5.1074
				+	100	30	0	1.83979*	.46891	.025	.1491	3.5305
				+	0	0	50	3.67533*	.46891	.000	1.9846	5.3661
				-	0	0	50	2.77214*	.46891	.000	1.0814	4.4629
				+	100	0	50	2.49984*	.46891	.001	.8091	4.1906
				-	100	0	50	.83724	.46891	.810	-.8535	2.5280
9+	0	0	50	+	0	0	0	.02649	.46891	1.000	-1.6642	1.7172

				-	0	0	0	.02649	.46891	1.000	-1.6642	1.7172
				+	0	30	0	-.26600	.46891	1.000	-1.9567	1.4247
				-	0	30	0	-.92924	.46891	.700	-2.6200	.7615
				+	100	0	0	-.13466	.46891	1.000	-1.8254	1.5561
				-	100	0	0	-.25867	.46891	1.000	-1.9494	1.4321
				+	100	30	0	-1.83554*	.46891	.025	-3.5263	-.1448
				-	100	30	0	-3.67533*	.46891	.000	-5.3661	-1.9846
				-	0	0	50	-.90320	.46891	.733	-2.5939	.7875
				+	100	0	50	-1.17550	.46891	.381	-2.8662	.5152
				-	100	0	50	-2.83809*	.46891	.000	-4.5288	-1.1474
-	0	0	50	+	0	0	0	.92969	.46891	.700	-.7610	2.6204
				-	0	0	0	.92969	.46891	.700	-.7610	2.6204
				+	0	30	0	.63719	.46891	.961	-1.0535	2.3279

				-	0	30	0	-.02604	.46891	1.000	-1.7168	1.6647
				+	100	0	0	.76854	.46891	.878	-.9222	2.4593
				-	100	0	0	.64453	.46891	.958	-1.0462	2.3353
				+	100	30	0	-.93234	.46891	.696	-2.6231	.7584
				-	100	30	0	-2.77214*	.46891	.000	-4.4629	-1.0814
				+	0	0	50	.90320	.46891	.733	-.7875	2.5939
				+	100	0	50	-.27230	.46891	1.000	-1.9630	1.4184
				-	100	0	50	-1.93490*	.46891	.016	-3.6256	-.2442
+	100	0	50	+	0	0	0	1.20199	.46891	.351	-.4887	2.8927
				-	0	0	0	1.20199	.46891	.351	-.4887	2.8927
				+	0	30	0	.90949	.46891	.725	-.7812	2.6002
				-	0	30	0	.24626	.46891	1.000	-1.4445	1.9370
				+	100	0	0	1.04084	.46891	.552	-.6499	2.7316
				-	100	0	0	.91683	.46891	.716	-.7739	2.6076
				+	100	30	0	-.66004	.46891	.951	-2.3508	1.0307

				-	100	30	0	-2.49984*	.46891	.001	-4.1906	-.8091
				+	0	0	50	1.17550	.46891	.381	-.5152	2.8662
				-	0	0	50	.27230	.46891	1.000	-1.4184	1.9630
				-	100	0	50	-1.66260	.46891	.057	-3.3533	.0281
-	100	0	50	+	0	0	0	2.86458*	.46891	.000	1.1739	4.5553
				-	0	0	0	2.86458*	.46891	.000	1.1739	4.5553
				+	0	30	0	2.57209*	.46891	.001	.8814	4.2628
				-	0	30	0	1.90885*	.46891	.018	.2181	3.5996
				+	100	0	0	2.70344*	.46891	.000	1.0127	4.3942
				-	100	0	0	2.57943*	.46891	.001	.8887	4.2702
				+	100	30	0	1.00255	.46891	.604	-.6882	2.6933
				-	100	30	0	-.83724	.46891	.810	-2.5280	.8535
				+	0	0	50	2.83809*	.46891	.000	1.1474	4.5288
				-	0	0	50	1.93490*	.46891	.016	.2442	3.6256
				+	100	0	50	1.66260	.46891	.057	-.0281	3.3533

*. The mean difference is significant at the 0.05 level.

Table 41. T-test analysis of Beclin mRNA data in UOK257 cells

Independent Samples Test

		Levene's Test for Equality of Variances		t-test for Equality of Means						
									95% Confidence Interval of the Difference	
		F	Sig.	t	df	Sig. (2-tailed)	Mean Difference	Std. Error Difference	Lower	Upper
Beclin	Equal variances assumed	6.887	.059	-2.013	4	.114	-.024	.012	-.056	.009
	Equal variances not assumed			-2.013	2.000	.182	-.024	.012	-.074	.027

If the resulting p-value of a Levene's test is less than typically 0.05 there is a difference between the variances in the groups tested.

Equal variances assumed (Sig=0.059 therefore > 0.05 for Levene's test) therefore P=0.114

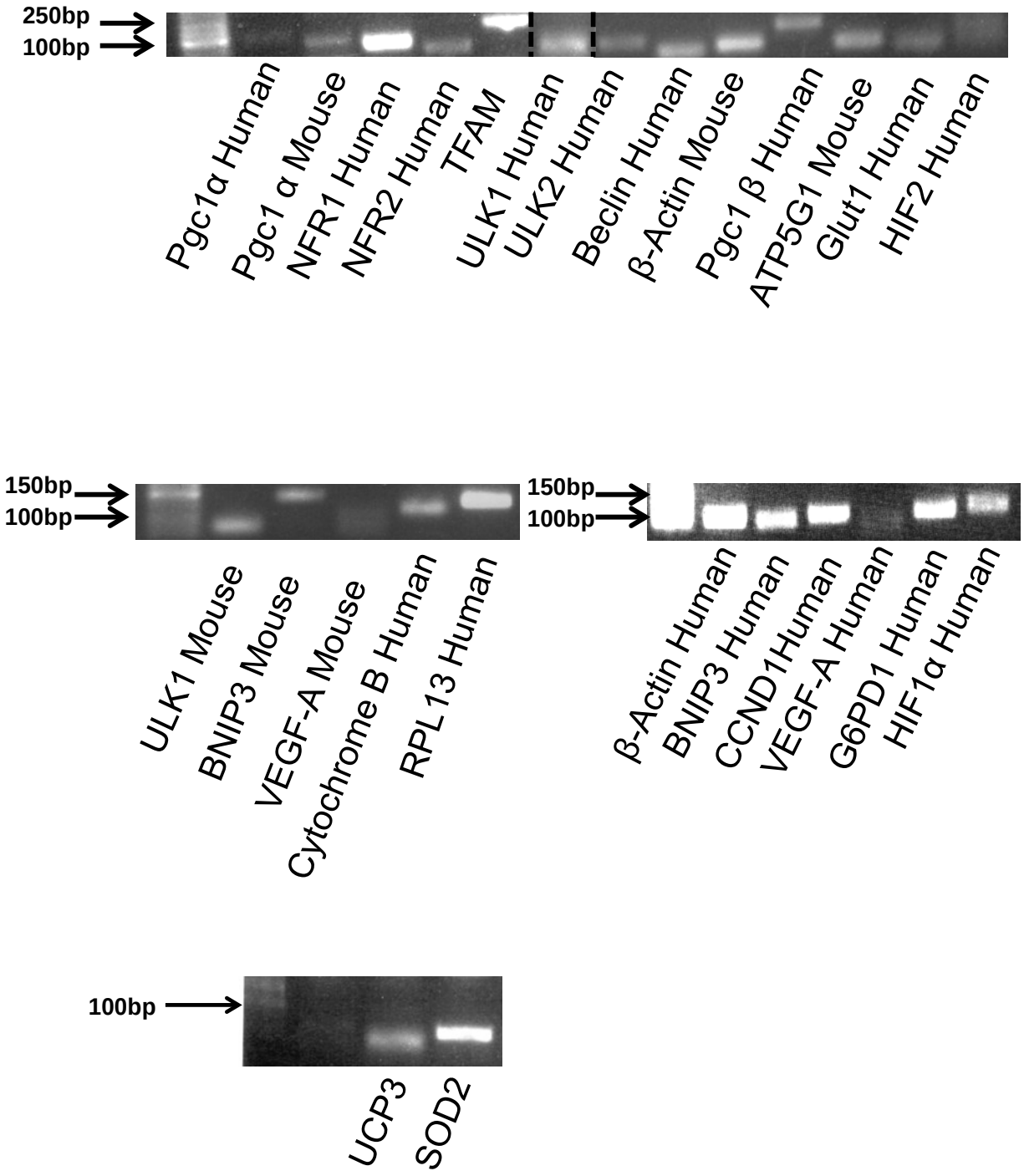

Figure 34. Electrophoresis gel showing amplicon length for RT-PCR primers

Appendicies V. Standard curvesand R-values for RT-PCR Primer assays

Mouse β-actin standard curve

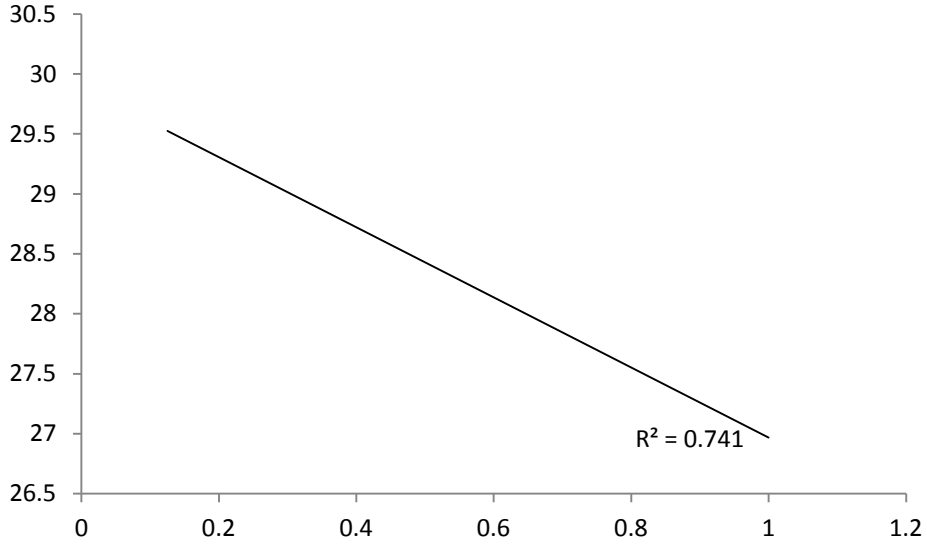

Mouse ATP5G1 standard curve

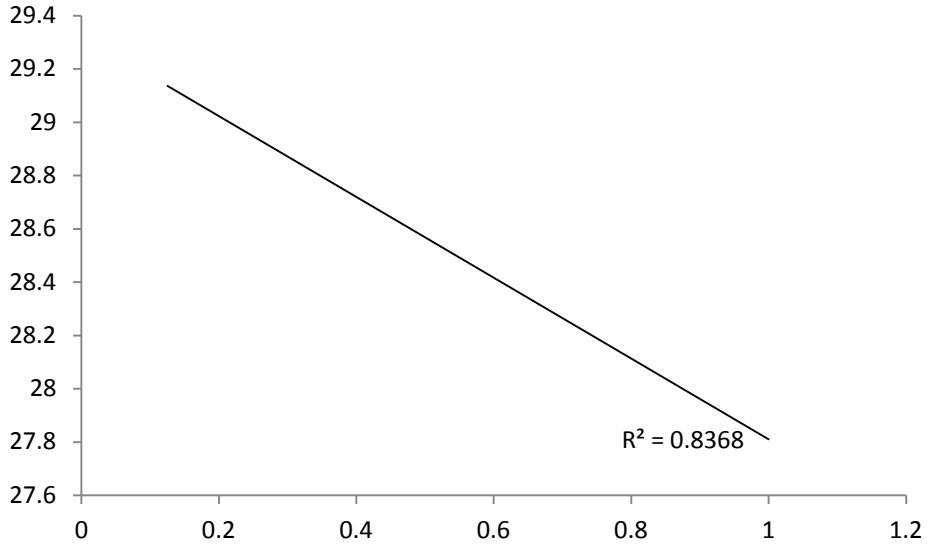

Mouse BNIP3 standard curve

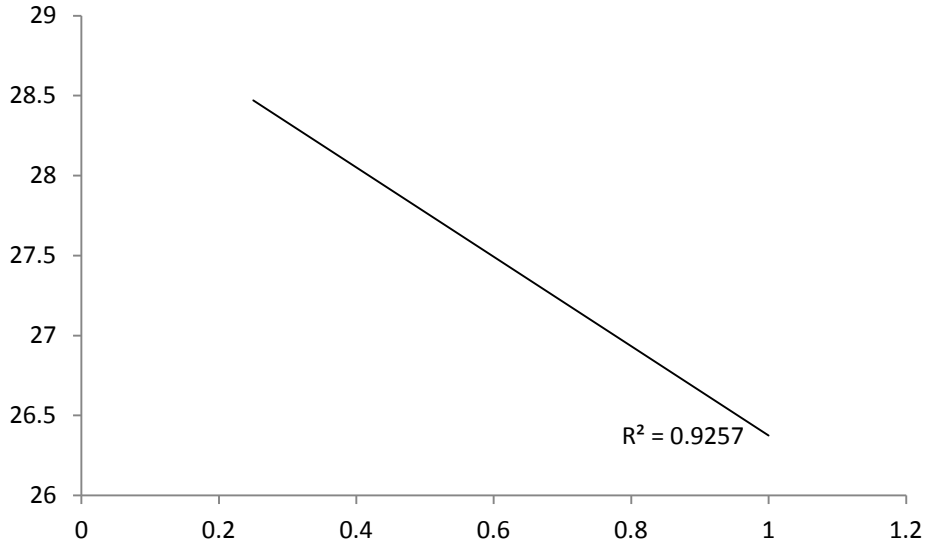

Human Cytochrome b standard curve

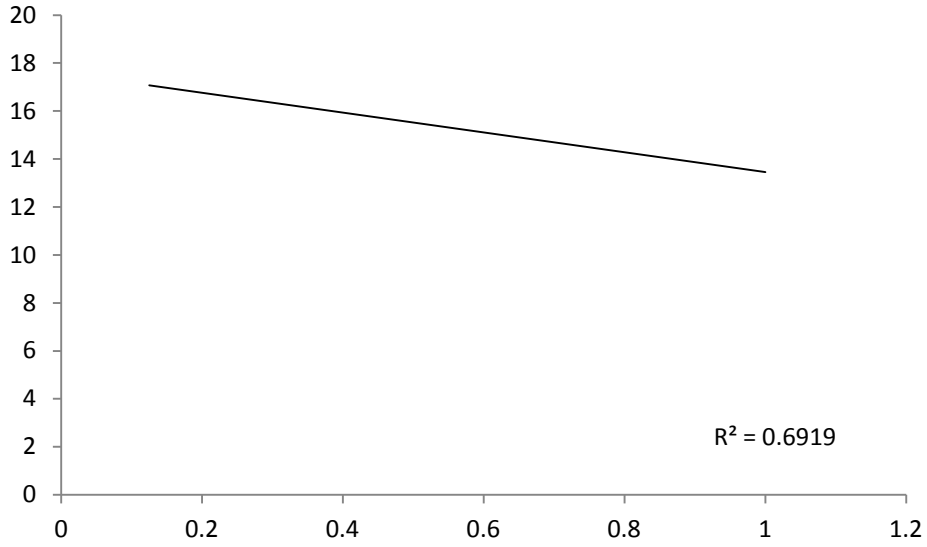

Human NRF2 standard curve

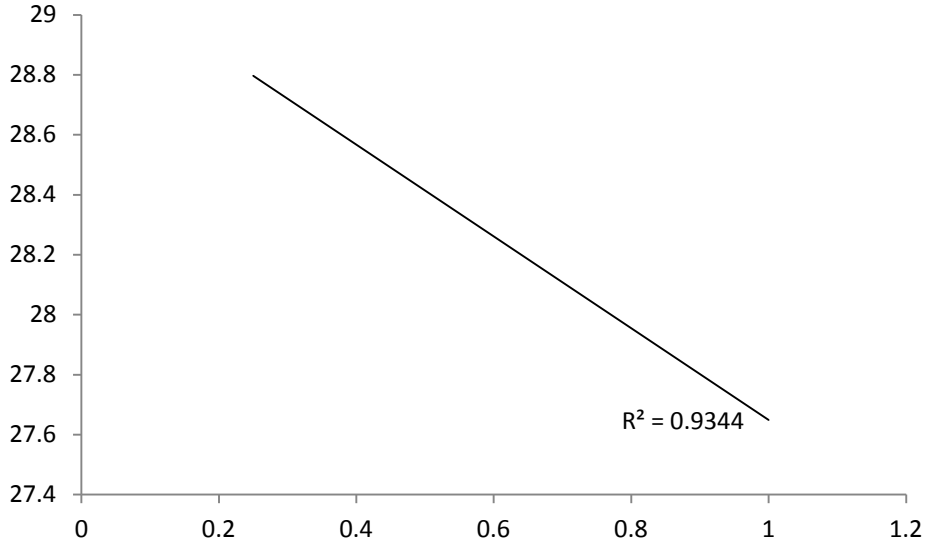

Human NRF1 standard curve

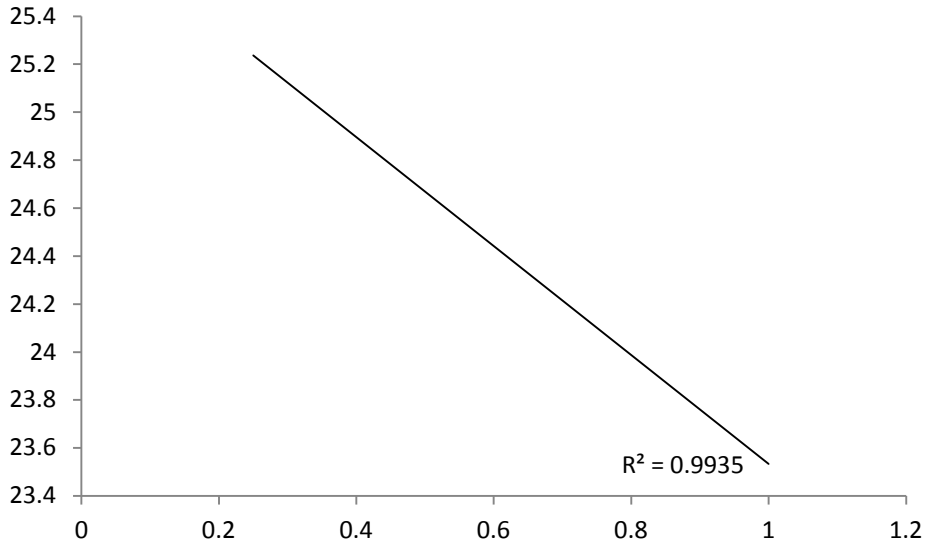

Human PGC1β standard curve

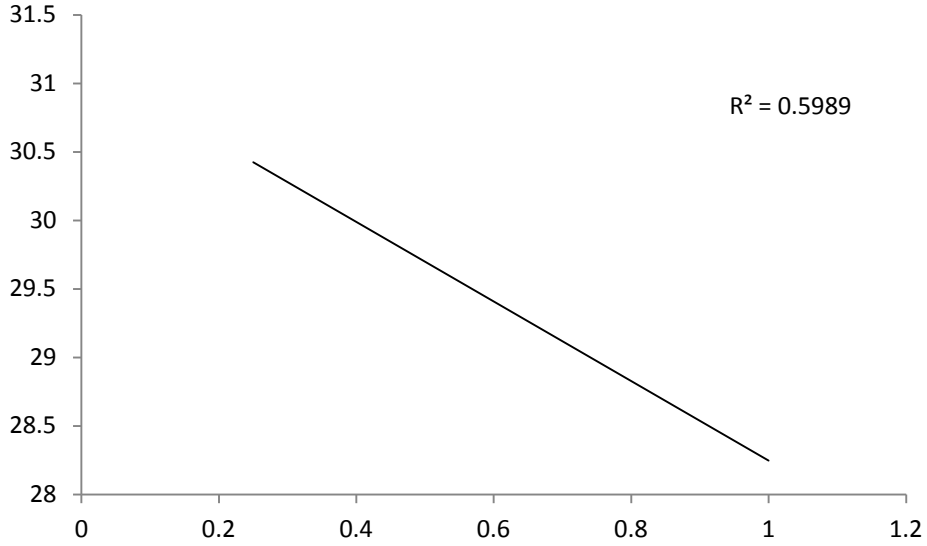

Human PGC1α standard curve

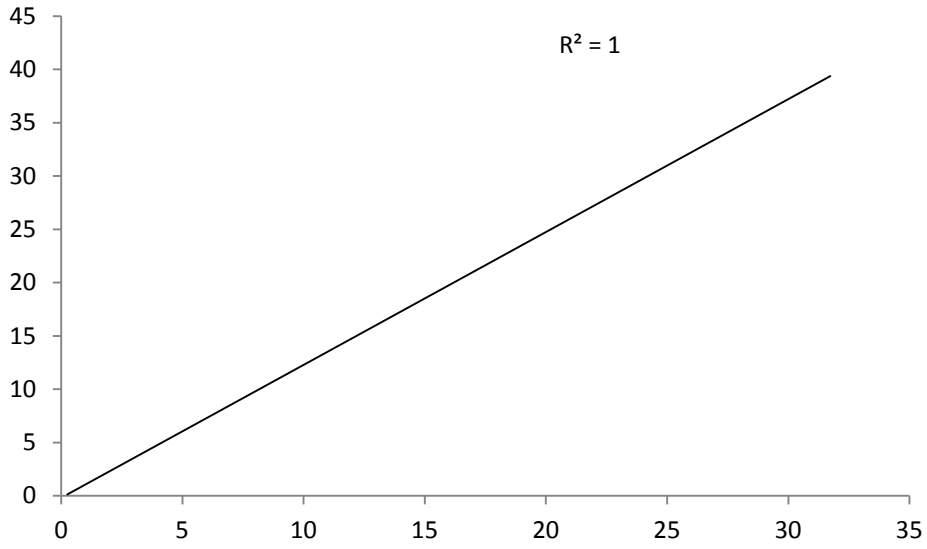

Mouse PGC1α standard curve

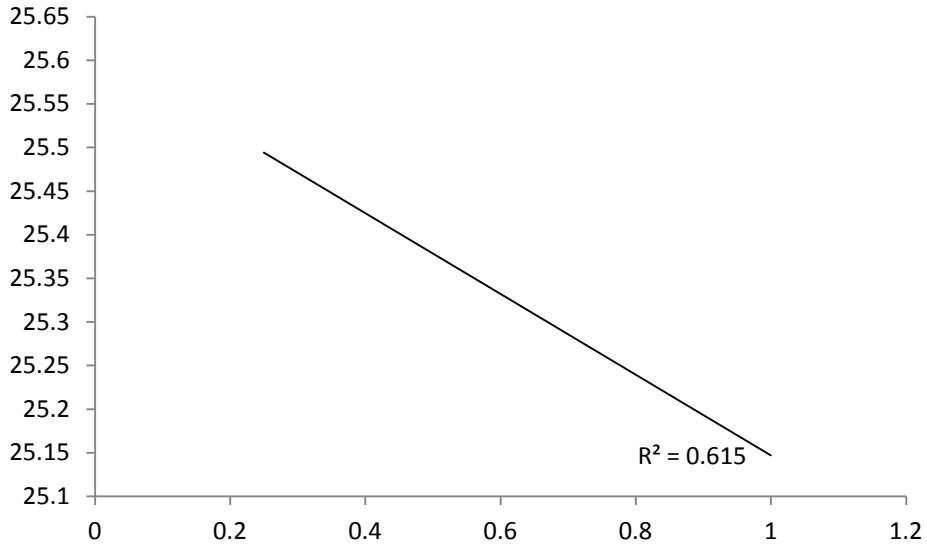

Human RPL13 standard curve

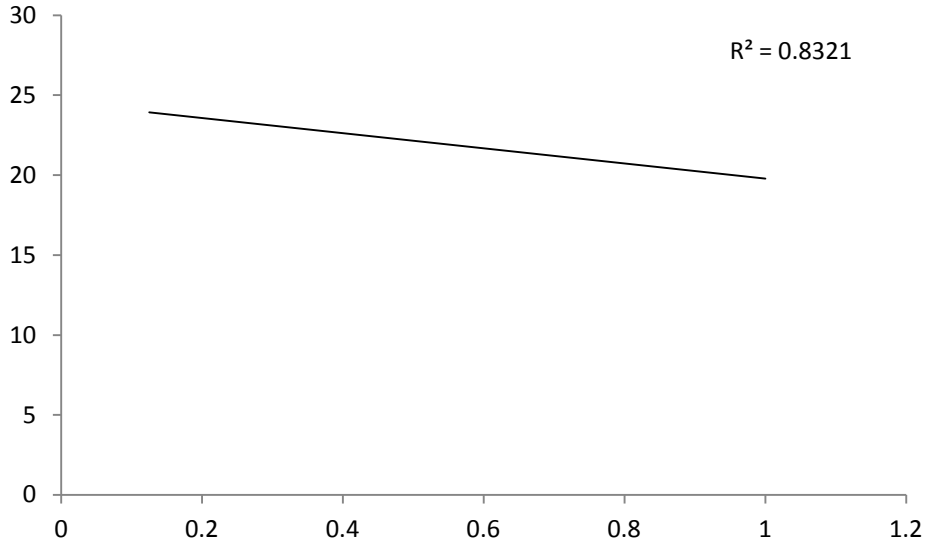

Human SOD2 standard curve

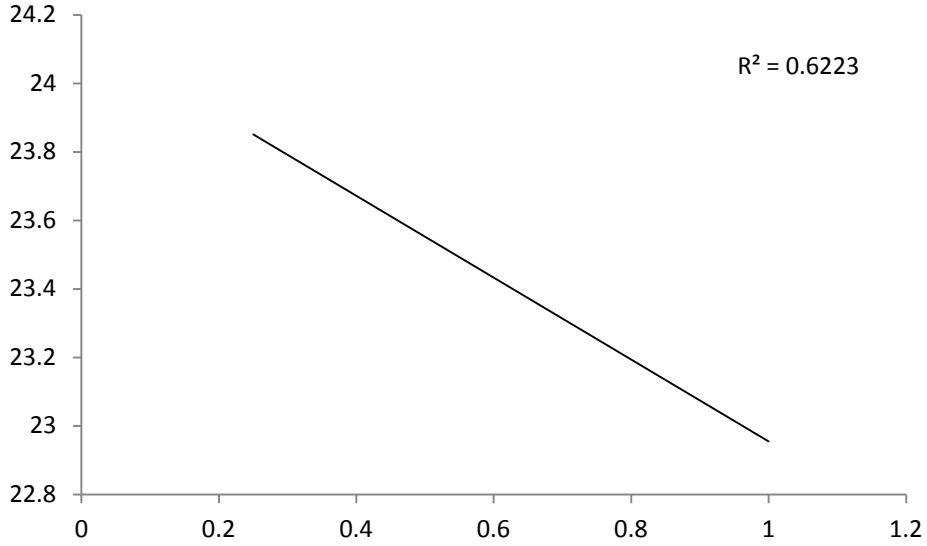

Human TFAM standard curve

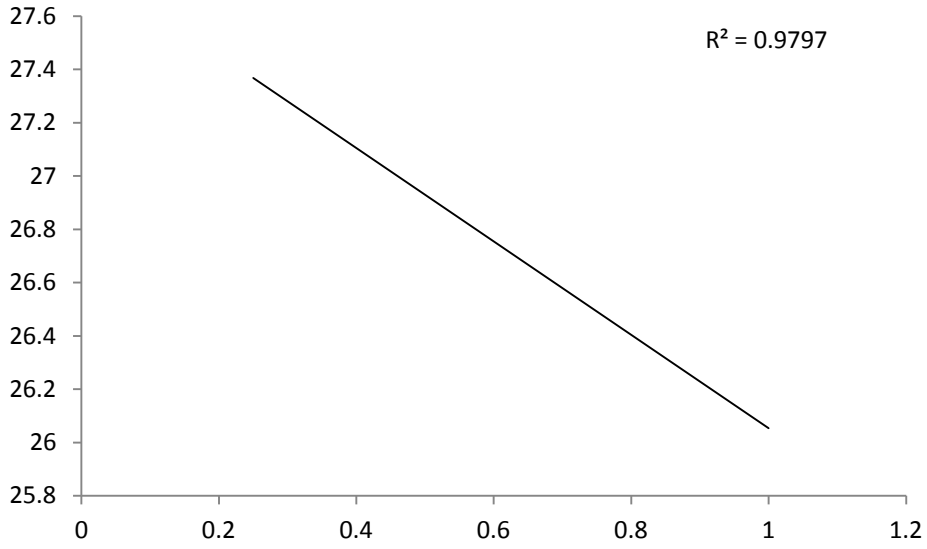

Human UCP3 standard curve

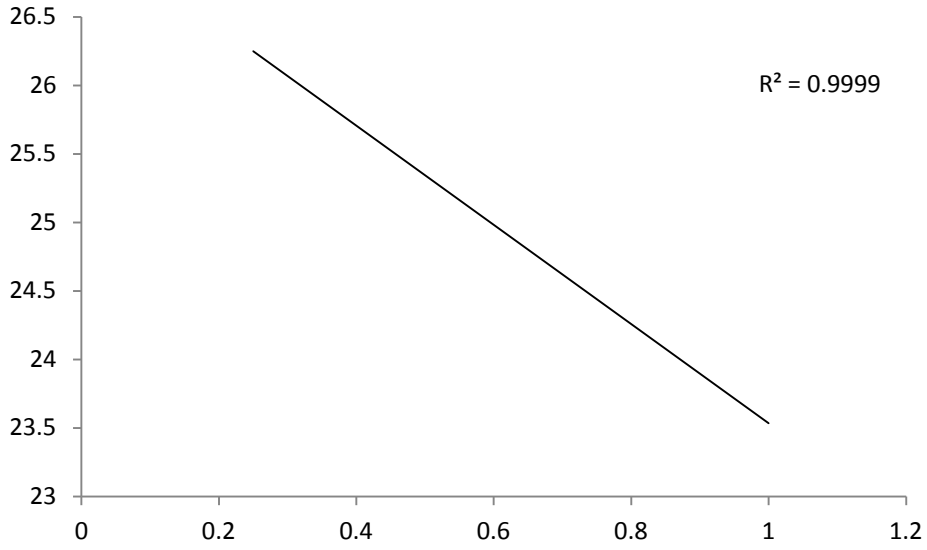

Human ULK 1standard curve

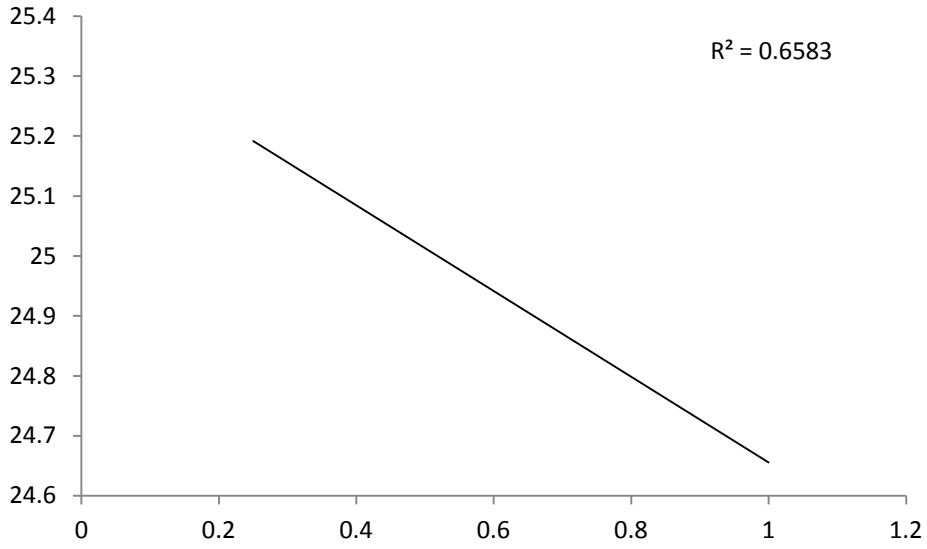

Mouse ULK1standard curve

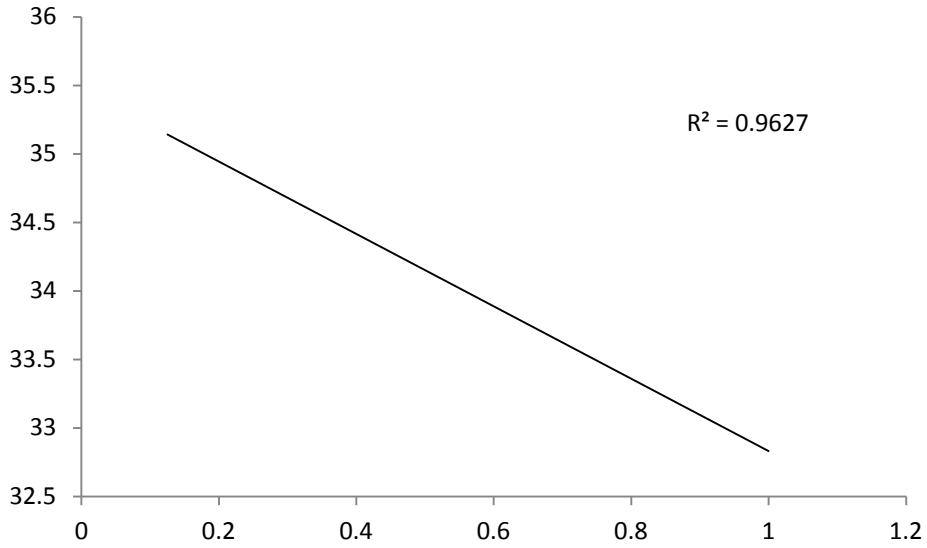

Human ULK2 standard curve

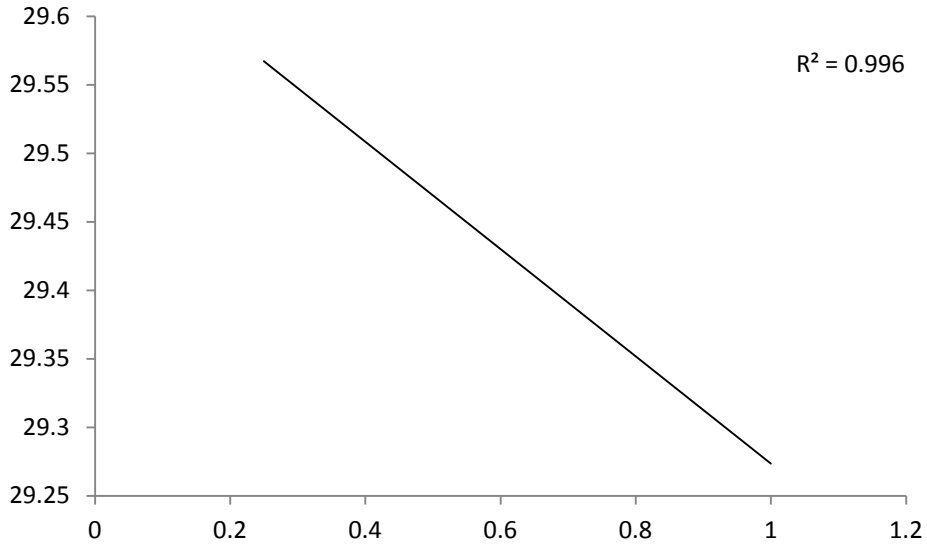

Mouse VEGF-A standard curve

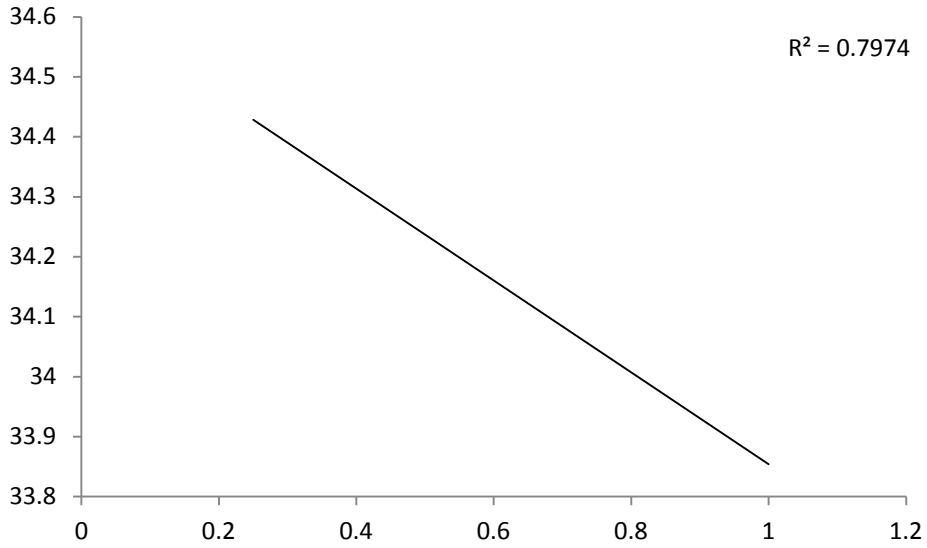

Human B-Actin standard curve

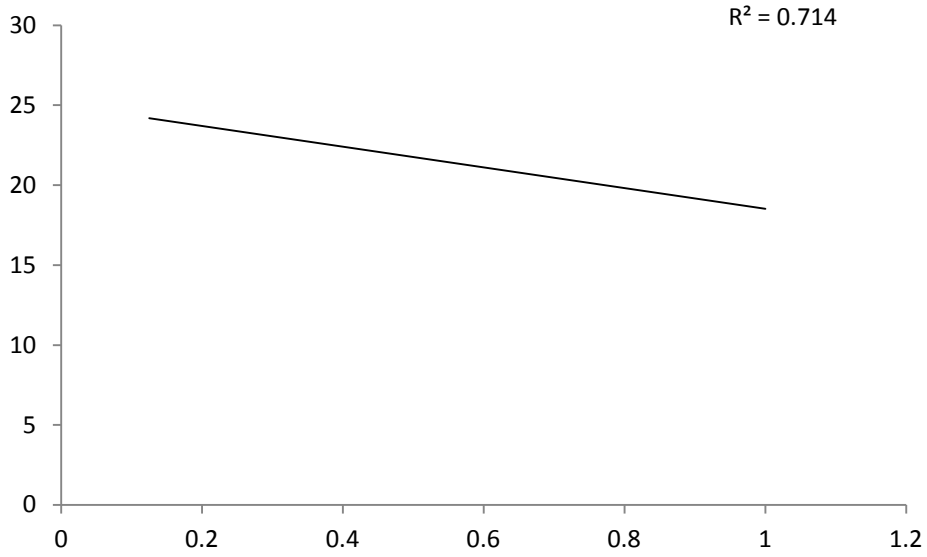

Human BNIP3standard curve

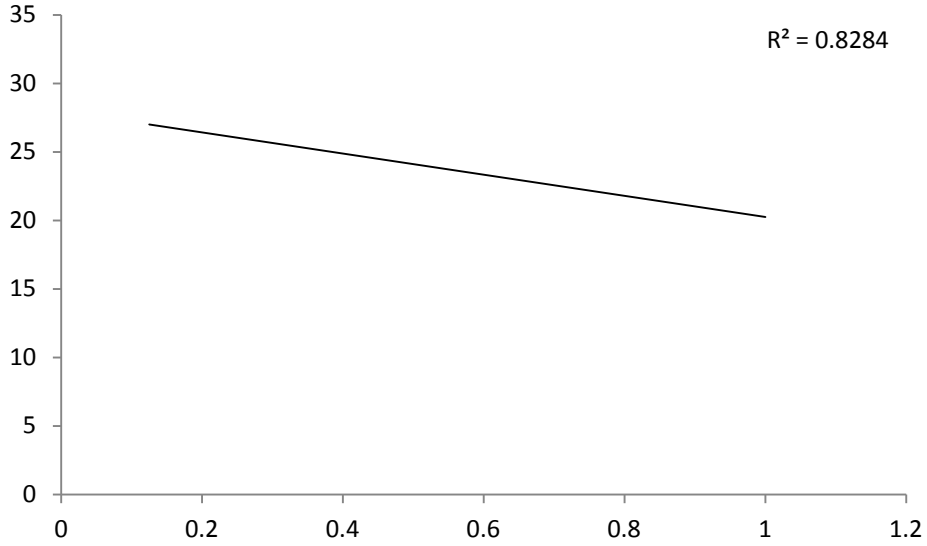

Human CCND1 standard curve

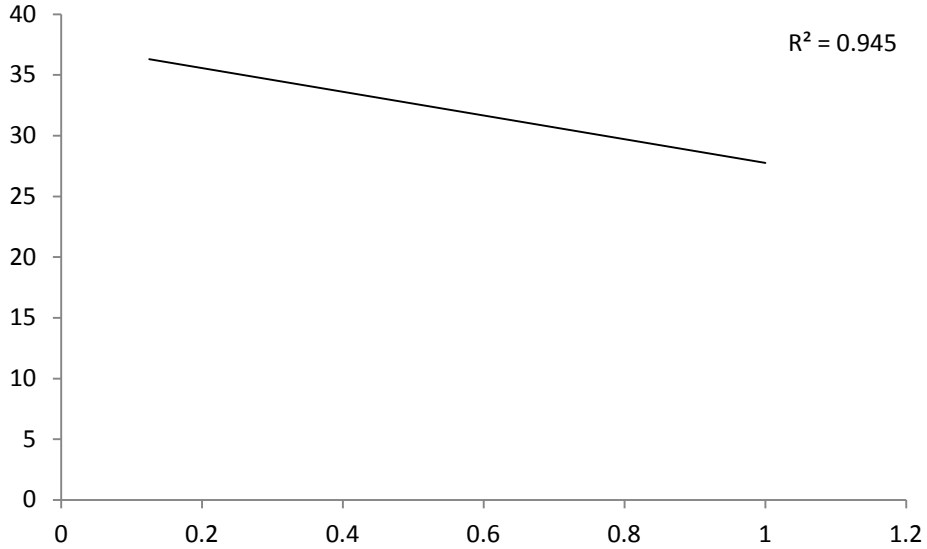

Human G6PD1standard curve

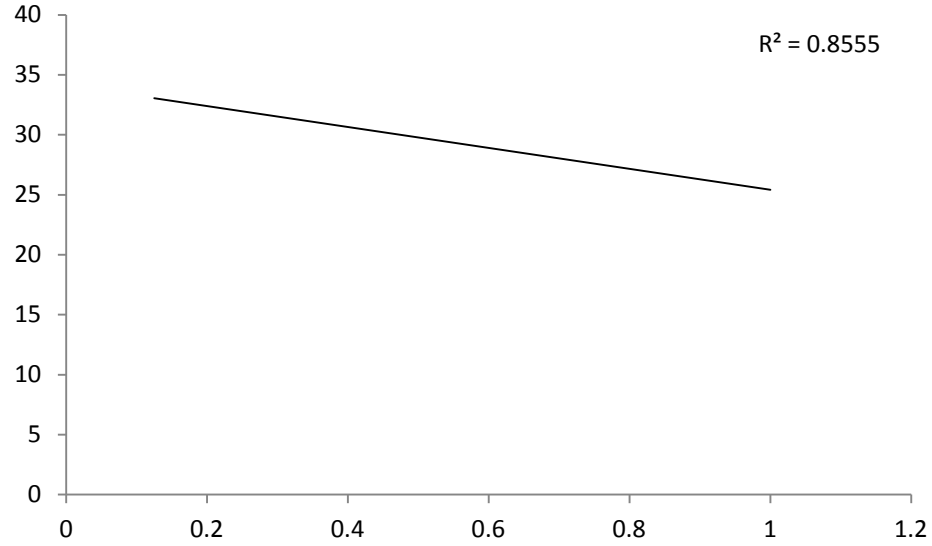

Human HIF1α standard curve

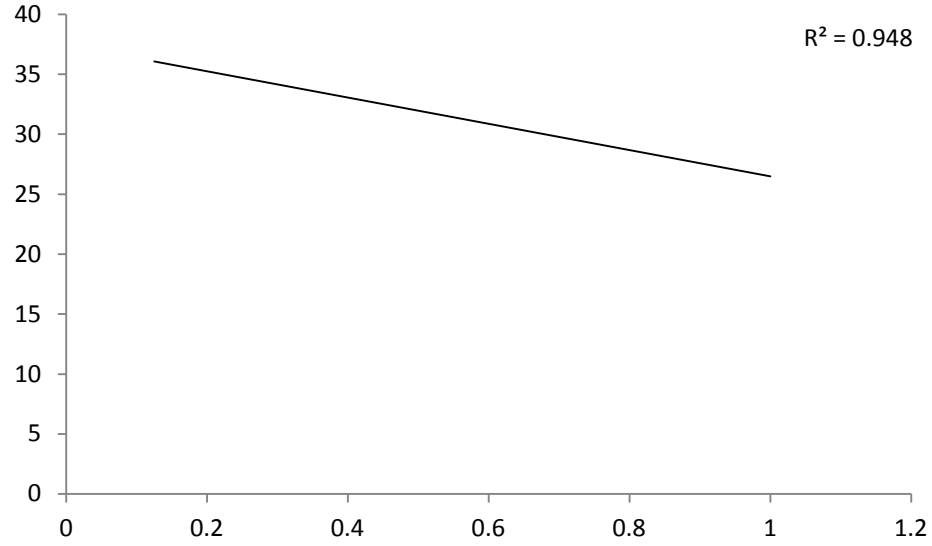

Human VEGF-A standard curve

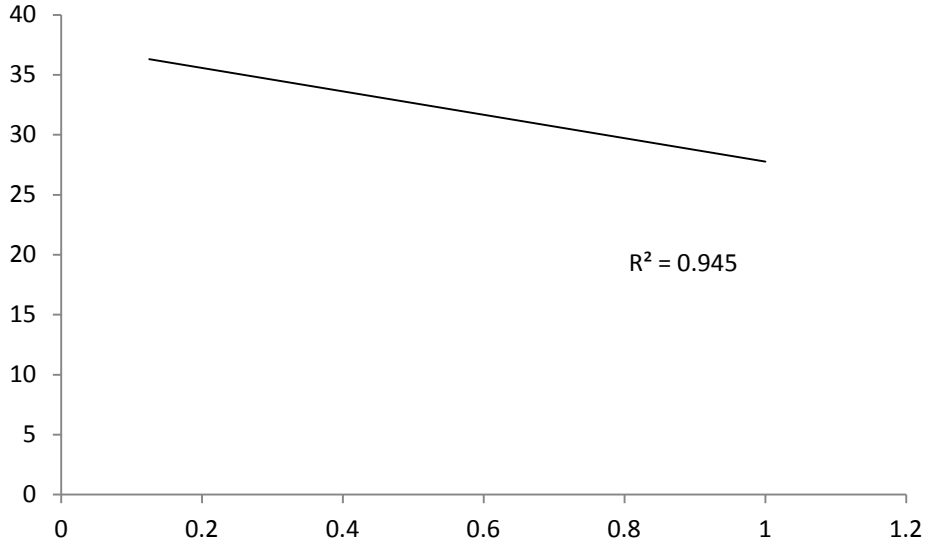

Human GLUT1 standard curve

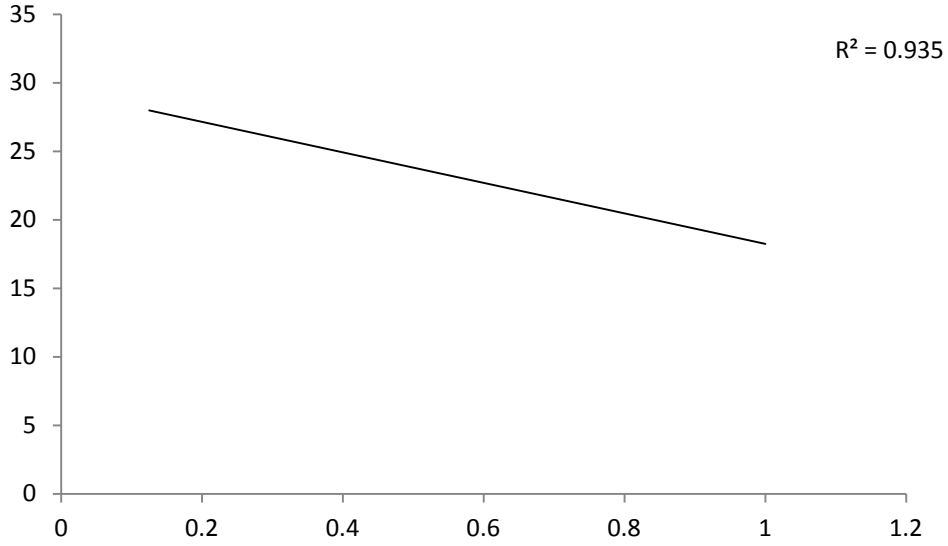

Human HIF2α standard curve

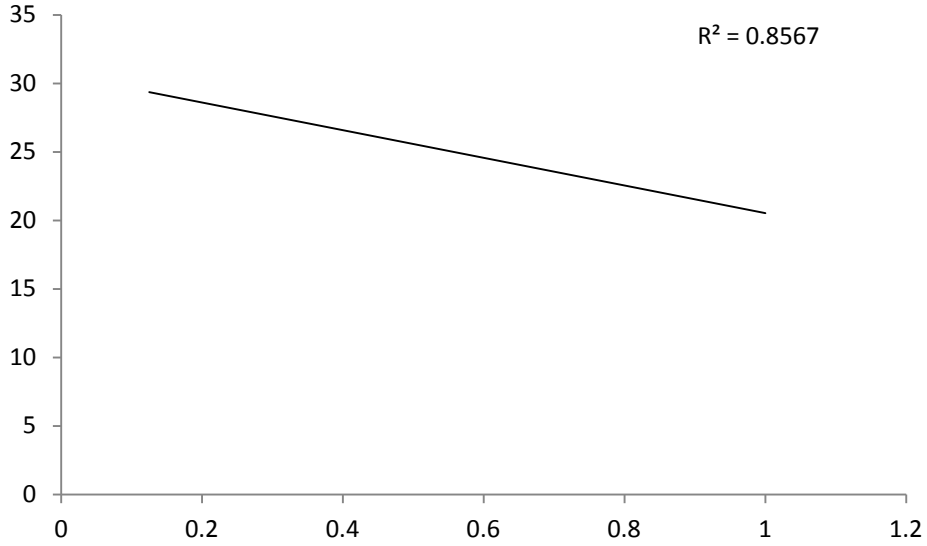

Beclin1 standard curve